Inflammatory Macrophages and Renal Tubular Epithelial Cell Apoptosis.

Tiina Marika Johanna Kipari

Thesis presented for the degree of Ph.D
The University of Edinburgh
2007

Abstract

Macrophages (Mϕ) play a key role in renal inflammation and may be cytotoxic to resident cells within tissues. I began this thesis by examining the effect of Mϕ upon the level of apoptosis and proliferation in tubular epithelial cells *in vitro*. I used a microscopically quantifiable co-culture assay to determine whether inflammatory Mϕ modulated apoptosis and proliferation of (i) Madine-Darby canine kidney (MDCK) cells and (ii) primary murine tubular epithelial cells. Bone marrow-derived Mϕ and target tubular cells were differentially labeled with fluorochromes and interacted for 24 hrs. Apoptosis and proliferation was quantified by fluorescent microscopy after fixation and Hoechst staining. Quiescent non-activated Mϕ did not induce significant apoptosis of tubular cells whilst cytokine activated (LPS/IFN-γ) Mϕ induced marked apoptosis of both MDKC and primary tubular cells. Pharmacological inhibition of nitric oxide (NO) production with L-NAME or inclusion of cytokine activated Mϕ derived from inducible nitric oxide synthase (iNOS) knockout (KO) mice reduced apoptosis in both MDKC and primary tubular cells. MDCK cell proliferation was significantly suppressed by both non-activated and activated Mϕ from iNOS WT and iNOS KO mice indicating that it was an NO-independent effect. In contrast, no effect upon primary tubular cell proliferation was evident.

I then went on to examine the role of NO *in vivo* in the murine model of unilateral ureteric obstruction (UUO) characterised by tubular cell apoptosis and interstitial fibrosis. Initially UUO was performed in iNOS KO and wild-type mice but iNOS KO mice exhibited significantly increased Mϕ infiltration. Therefore, the

specific iNOS inhibitor L-NIL (control D-NIL) was administered between days 5 to 7 following UUO. Mice were sacrificed at day 7 and the obstructed kidney removed for histological analysis. L-NIL treatment did not affect Mϕ infiltration but did reduce both tubular and interstitial cell apoptosis. Proliferation of tubular cells and interstitial cells was unaffected. Although myofibroblast accumulation was unaffected, interstitial fibrosis was significantly increased by L-NIL treatment.

I also investigated the effect of conditional Mϕ ablation in the UUO model. The conditional Mϕ ablation mice used in these studies are transgenic for the human diphtheria toxin receptor (DTR) under the CD11b promoter (CD11b-DTR mice). Intraperitoneal (*i.p*) administration of diphtheria toxin (DT) to DTR mice results in the rapid and specific depletion of monocytes and Mϕ. DTR mice underwent UUO at day 0 and either DT or PBS was administered *i.p* on days 5, 6 and 7. Mice were sacrificed at day 7 and the obstructed kidney removed for histological analysis. Administration of DT resulted in a 3-fold reduction in interstitial Mϕ accumulation in obstructed kidneys. However, Mϕ depletion had no effect upon proximal or distal tubular cell proliferation or apoptosis. Interestingly, Mϕ depletion had no effect upon the accumulation of myofibroblasts but attenuated interstitial fibrosis.

Dedicated to Perra
and my family.

Acknowledgements

First and foremost, I would like to thank my supervisor Dr. Jeremy Hughes. It was his inspirational research ideas and unfailing enthusiastic guidance that made this thesis possible. Thank you for your tremendous support and patience during the past years!

I am also very grateful to Professor John Savill for bringing me into his research group as a research assistant and also giving me the opportunity to undertake a PhD. Thank you for providing me with this truly excellent research opportunity.

I wish to express my gratitude and appreciation to all my colleagues, past or present, who helped me during this work. In particular I wish to acknowledge the following people: Experimental Surgeon Spike Clay for performing all the *in vivo* surgery and for his help with all the *in vivo* work, Shonna Johnston for helping me with flow cytometry and microscopy, Sarah Farnworth and Dr. Alison MacKinnon for performing Real-time PCR, Aili Zhang for technical advice, Bob Morris and Susan Harvey for histology assistance and Professor Richard Lang's group that generated the CD11b-DTR mice.

Special thanks are also due to Dr. Jean-Fraincois Cailhier, David Ferenbach, Kristian Houlberg, Dr. Paul Hartley, Dr. Mark Lucas and Simon Watson, for all the useful discussions we had both inside the lab and outside the lab.

My warmest thanks goes to all my friends and family in Sweden and special thanks to Linda Wetterstrand. Finally this thesis could not have been completed without the support and love from my boyfriend Per-Ragnar Iverstrand.

Declaration

I, Tiina Marika Johanna Kipari, declare that this thesis was composed myself and the work contained herein is my own and was done by myself with the technical help of people I have acknowledged in the appropriate section, and this work has not been submitted for any other degree or professional qualification except as specified.

Table of Contents

Index of Figures

Index of Tables

Abbreviations

%	:	percentage
°C	:	degrees celcius
A	:	absorbance
ABAM	:	antibiotic antimycotic
AIF	:	apoptosis inducing factor
AOP-RANTES	:	amino oxypentane RANTES
Apaf-1	:	apoptosis protease activating factor 1
APC	:	allophycocyanin
α-SMA	:	alpha smooth muscle actin
ATP	:	adenosine triphosphate
BH domain	:	Bcl-2 homology domain
BH4	:	tetrahydrobiopterine
BMDM	:	bone marrow derived Mϕ
BMP-7	:	bone morphogenic protein 7
Bp	:	base pairs
BSA	:	bovine serum albumin
BW	:	body weight
cAMP	:	cyclic adenosine monophosphate
CD40L	:	CD40 ligand
CDK	:	cyclin-dependent kinases
c-FLIP	:	cellular FLICE inhibitor protein
CKI	:	cyclin kinase inhibitor
CO_2	:	carbon dioxide
CSF-1	:	colony stimulating factor 1
cyt c	:	cytochrome c
DAB	:	diaminobenzidine
DABCO	:	1-4-diazabicyclo-2-2-2-octane
dATP	:	deoxyadenosine 5´-triphosphate
DC	:	dendritic cell
DD	:	death domain
DEA/NO	:	diethylamine NONOate
DED	:	death effector domain
DIABLO	:	direct inhibitor of apoptosis binding protein with a low isoelectric point
DISC	:	death-inducing signalling complex
DMEM/F12	:	dulbecco's modified eagle medium with F12
DMSO	:	dimethylsulphoxide
D-NAME		N^G-nitro-D-arginine-methyl ester
D-NIL	:	D-N6-(1-iminoethyl)-lysine

DT	:	diphtheria toxin
ECM	:	extracellular matrix
EDTA	:	ethylenediaminetetraacetic acid
EFG	:	epidermal growth factor
EMT	:	epithelial mesenchymal transition
eNOS	:	endothelial NOS
EtOH	:	ethanol
FACS	:	fluorescence-activated cell sorter
FAD	:	flavin adenine dinucleotide
FADD	:	fas associated death domain
FasL	:	fas ligand
FCS	:	foetal calf serum
FGF-2	:	basic fibroblast growth factor 2
FITC	:	fluorescein isothiocyanate
FMN	:	flavin mononucleotide
FSP-1	:	fibroblast-specific protein 1
H_2O_2	:	hydrogen peroxide
hbEGF	:	heparin binding epidermal growth factor
HBSS	:	hanks balanced salt solution
HFG	:	hepatocyte growth factor
HK-2	:	human kidney-2
Hpf	:	high power field
HRP	:	horse radish peroxidase
HtrA2	:	high temperature requirement protein
i.p	:	intraperitoneally
I/R	:	ischemia reperfusion
IAP	:	inhibitor of apoptosis protein
ICAM-1	:	intercellular adhesion molecule 1
IFN-g	:	inteferon gamma
Ig	:	immunoglobulin
IL	:	interleukin
iNOS	:	inducible NOS
KO	:	knockout
LFA-1	:	leukocyte functional antigen 1
L-NAME	:	N^G-nitro-L-arginine-methyl ester
L-NIL	:	L-N-imino-ethyl lysine
L-NMMA	:	N^G-mono-methyl-L-arginine
LPS	:	lipopolysaccaride
LTAg	:	large T antigen
MCP-1	:	monocyte chemoattractant protein l
MDCK	:	madin darby canine kidney

MEM	:	minimal essential medium
MeOH	:	methanol
MET	:	mesenchymal to epithelial transition
Mϕ	:	macrophage
MHC	:	Major histocompatibility complex
Min	:	minute
MIP-1α	:	Mϕ-inflammatory protein 1 alpha
MMP	:	matrix metalloproteinase
MOMP	:	mitochondrial outer membrane permeabilisation
N_2O_3	:	dinitrogen trioxide
N_2O_4	:	dinitrogen tetraoxide
NaCl	:	sodium cloride
NADPH	:	nicotinamide adenine dinucleotide phosphate
nNOS	:	neuronal NOS
NO	:	niric oxide
NO_2	:	nitrogen dioxide
NO_2^-	:	nitrite
NONOates	:	diazeniumdiolates
NOS	:	NO synthase
NTN		nephrotoxic nephritis
$ONOO^-$	:	peroxynitrite
PAI-1	:	plasminogen activator inhibitor
PAS	:	periodic acid Schiff
PBS	:	phosphate buffered saline
PBS -/-	:	PBS without calcium and magnesium
PCNA	:	proliferating cell nuclear antigen
PE	:	phycoerythrin
PECAM-1	:	platelet endothelial cell adhesion molecule 1
PMN	:	neutrophil
PS	:	phosphatidylserine
PTE	:	primary tubular epithelial
PTH		parathyroid hormone
RANTES	:	regulated upon activation normal T cell expressed and secreted
RNOS	:	reactive nitrogen oxide species
RT	:	room temperature
Smac	:	second mitochondria-derived activator of caspases
SNP	:	sodium nitroprusside
O_2^-		superoxide anion
SOD	:	superoxide dismutases
Spermine/NO	:	spermine NONOate
$t_{1/2}$	:	half life

TAE	:	tris EDTA acetate
TBM		tubular basement membrane
TBS	:	tris buffered saline
T_c	:	cytotoxic T cell
TCI	:	tissue culture insert
TE	:	tris EDTA
TEC		tubular epithelial cell
TGF-β	:	transforming growth factor beta
T_h	:	T helper cells
TIFF	:	tagged image file format
TIMP	:	tissue inhibitor of MMP
TNF-α	:	tumour necrosis factor alpha
TNFR	:	tumour necrosis factor receptor
tPA	:	tissue-type plasminogen activator
TUNEL	:	terminal deoxynucleotidyl transferase-mediated dUTP nick-end labeling
uPA	:	urokinase-type plasminogen activator
uPAR	:	uPA receptor
UUO		unilateral ureteric obtrucion
VCAM-1	:	vascular cell adhesion molecule 1
vs		versus
VLA-4	:	very late activation antigen 4
WT	:	wild-type

Chapter 1.

Introduction

1.1 THE KIDNEYS

The main functions of the kidneys are the production of urine, the secretion of hormones, blood pressure control and the regulation of water, electrolyte and acid-base balance. Two important functional regions of the kidney are the outer cortex and the inner medulla (Figure 1-1). The functional units of the kidneys are the nephrons (Figure 1-2) consisting of the glomerulus, an organised sieve-like structure of capillary loops surrounded by the Bowman's capsule, and the associated tubules. The major regions of the tubule are the proximal convoluted tube, the descending and ascending limbs of the loops of Henle and the distal convoluted tube. The distal convoluted tubule drains into the collecting duct, which serves many other nephrons. The interstitium comprises the area between the tubules and contains the critically important peritubular capillaries that provide the metabolically active tubules with oxygen and nutrients. The interstitium also contains extracellular matrix that acts as a supporting structure and a population of resident macrophages (Mϕ), dendritic cells (DC) and fibroblasts. Urine filtrate is produced in the glomerulus by filtration of the plasma and the urine is modified by re-absorption and secretion as it passes along the nephron tubules. The filtered urine continues in the collecting duct, drains into the renal pelvis and subsequently via the ureter into the urinary bladder.

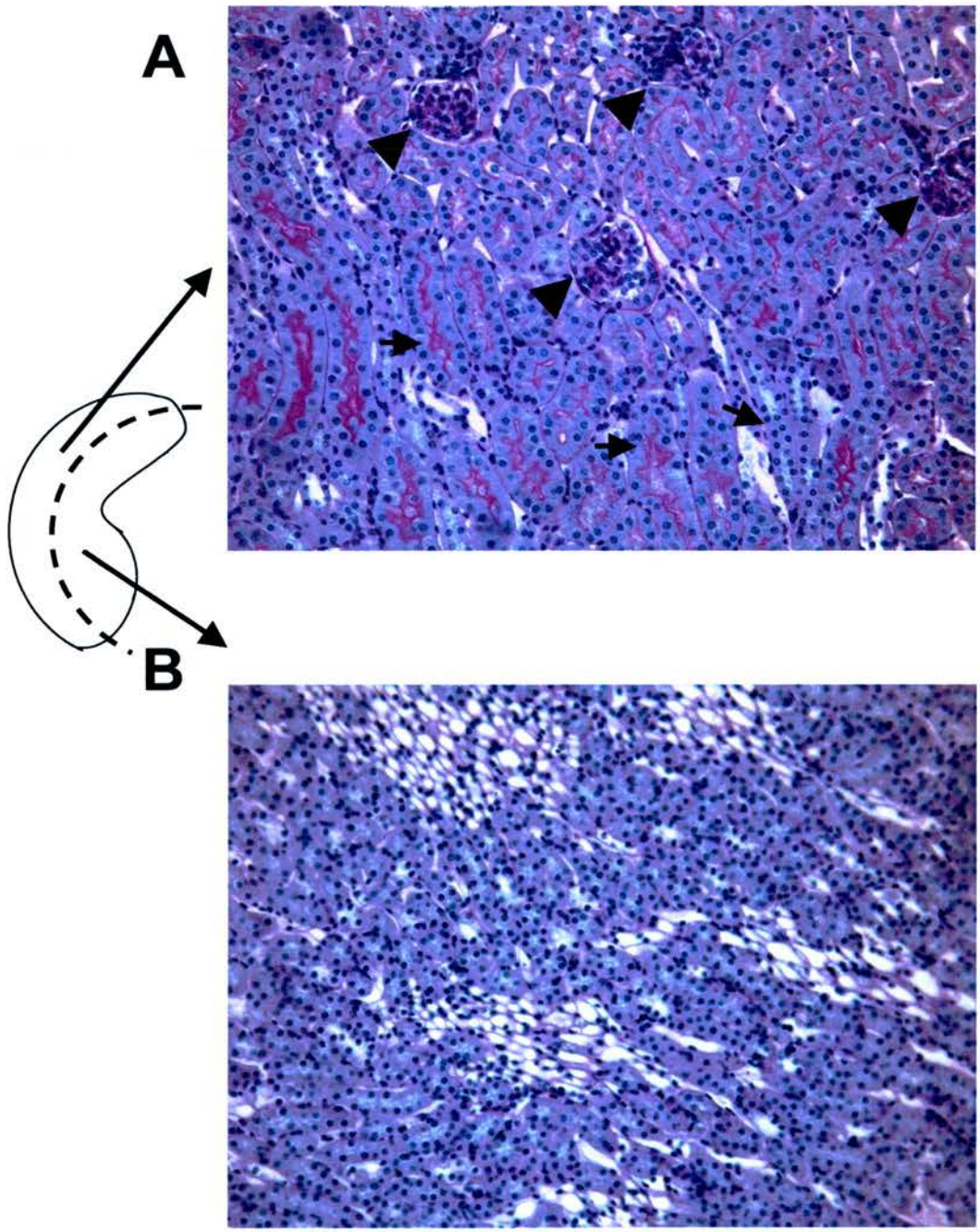

Figure 1- 1 Photomicrographs of normal mouse kidney after Periodic acid Schiff (PAS) staining demonstrating cortex and medulla.
The cortex has glomeruli (big arrow heads) and tubules (small arrow heads) (**A**). Medulla is shown in (**B**). (x100 magnification).

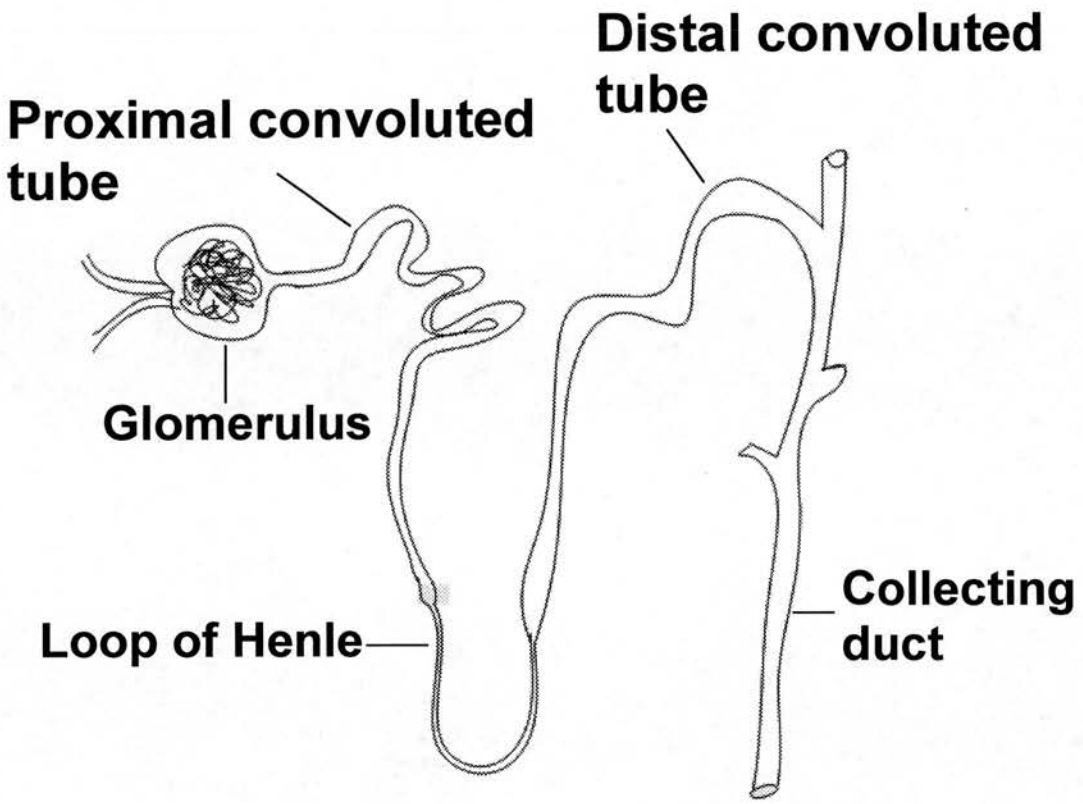

Figure 1- 2 Schematic diagram chart of a nephron within a kidney.

1.2 TUBULAR EPITHELIAL CELLS

Tubular epithelial cells are the predominant cells in the renal tubulointerstitium and are critically important resident renal cells. Proximal tubules consist of cuboidal epithelial cells that are very metabolically active and have microvilli that form an extensive brush border on their free apical surface. The microvilli increase the surface area exposed to the glomerular filtrate and enhance the reabsorprtion of substances such as filtered electrolytes as well as low molecular proteins. The epithelial cells of the distal tubules are also cuboidal but lack microvilli. Proximal tubular epithelial cells can easily be distinguished from distal tubular epithelial cells by periodic acid Schiff (PAS) staining, as proximal tubular cells exhibit a characteristic PAS-positive luminal brush border (Hughes et al., 1999) (Figure 1-3). Proximal and distal tubular epithelial cells can further be characterised by the differential expression of specific antigens, enzyme profiles, transport function studies and hormonal responsiveness – these differences are summarised in Table 1-1.

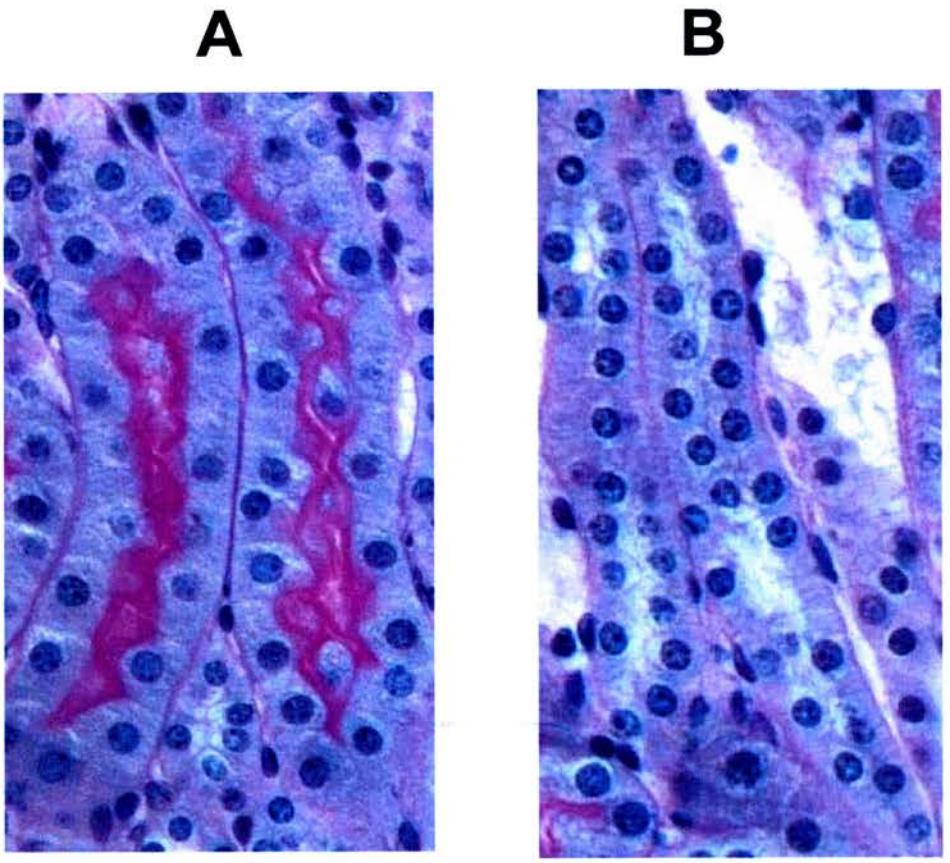

Figure 1- 3 Photomicrographs of normal mouse kidney after PAS staining showing distal and proximal tubules.
Proximal tubules (**A**) are distinguished from the distal tubules (**B**) by their characteristic pink brush border (x400 original magnification).

Table 1- 1 Surface antigens and characteristic features for distinguishing proximal and distal tubular epithelial cells.

PROXIMAL TUBULAR EPITHELIAL CELL	DISTAL TUBULAR EPITHELIAL CELL
Surface antigens:	**Surface antigens:**
N-cadherin (Nouwen et al., 1993)	E-cadherin (Nouwen et al., 1993)
Gamma-glytamyl transferase (Briere et al., 1985)	Tamm Horsfall protein (Baer et al., 2006)
Intestinal alkaline phosphatase (Briere et al., 1985)	
Alanine aminopeptidase (Toutain et al., 1991)	
Dipeptidyl peptidase IV (Mentzel et al., 1996)	
Leucine aminopeptidase (Elliget and Trump, 1991)	
Aquaporin-1 (Bedford et al., 2003)	Aquaporin-2 (Bedford et al., 2003)
Hormone responsiveness	**Hormone responsiveness**
Parathyroid hormone (PTH) stimulated cyclic adenosine monophosphate (cAMP) synthesis (Morel, 1981)	Vasopressin stimulated cAMP synthesis (Morel, 1981)
Transport studies	**Transport studies:**
Sodium dependent α-methylglucoside transport (Chung et al., 1982)	

1.2.1 Primary tubular epithelial cell culture

In vitro cell culture of primary tubular epithelial (PTE) cells provides an excellent means of studying specific cellular interactions in contrast to more complicated *in vivo* experiments. A potential disadvantage of primary cell cultures is that the cells have been directly removed from the *in vivo* condition and this may induce a change in the phenotype of the cell from that which is evident *in vivo*.

Despite this potential confounding factor, much has been learned about the function of various cell types in primary culture. Primary cell culture protocols have been developed for the growth of tubular epithelial cells from various species including human (Detrisac et al., 1984), mouse (Taub and Sato, 1980), rat (Elliget and Trump, 1991) and rabbit (Chung et al., 1982). The culture method for PTE cells (Harrison et al., 2006) that I used in this thesis is described in detail in Chapter 2.2. Other methods are based on separation techniques such as differential sieving, centrifugation using Percoll gradient (Gesek et al., 1987) or staining for specific tubular epithelial cell markers surface makers followed by cell sorting using magnetic beads (Baer et al., 1997) or FACS (Fluorescence-Activated Cell Sorter) (Helbert et al., 2001).

1.2.2 Tubular epithelial cell lines

There are a number of well established immortalised (transformed) tubular epithelial cell lines which can be used for *in vitro* studies. Commonly used tubular epithelial cell lines include:

(i) murine proximal PKSV-PR cells derived from the transgenic mouse carrying the SV40 large T antigen (LTAg) gene under the control of the L-type pyruvate kinase promoter (Lacave et al., 1993),

(ii) proximal MCT cells harvested from the cortex of SJL mice and then transformed using the SV40 LTAg (Haverty et al., 1988),

(iii) distal MDCK (Madin Darby Canine Kidney) cells that were derived from a female cocker spaniel in 1958 by S. H. Madin and N. B. Darby,

(iv) proximal porcine LLC-PK_1 cells harvested from juvenile male Hamshire pig (Hull et al., 1976) and

(v) proximal HK-2 (Human Kidney-2) cell harvested from normal adult human kidney and then transformed with the human papilloma E6/E7 gene (Ryan et al., 1994).

1.3 INFLAMMATION

1.3.1 History of inflammation

Over 2000 years ago, the Greek physician Celsius (30BC-38AD) documented the four cardinal signs of inflammation: *rubor* (redness), *tumor* (swelling), *calor* (heat) and *dolor* (pain). Virchow (1799-1879) described the fifth cardinal sign of *function laesa* (loss of function) in 1871. Although Galen (129–201 AD) proposed that inflammation was an essential part of the response to injury, inflammation was very much regarded as a 'disease' until the late 18^{th} century. John Hunter (1728-1793) was the first to realise that inflammation was generally beneficial to the host despite the fact that it was a response to tissue injury.

Later Cohnheim (1839-1884), a former student of Virchow, described the emigration of white blood cells though the walls of small blood vessels during inflammation. Metchnikoff (1845-1916) described the process of phagocytosis in 1882. He inserted rose thorns into the larvae of starfish and demonstrated that mesenchymal cells migrated and accumulated around the puncture site. He described the phagocytic actions of these cells and named the big cells 'macrophagocytes' and the smaller cells 'microphagocytes'. These cells are now known as Mϕ and neutrophils (PMN) (Segal, 2005).

Inflammation is now regarded as a protective response of the host to tissue injury and infection. The prime purpose of inflammation is to localise, neutralise and remove pathogens from the tissues whilst limiting tissue injury and setting the scene for subsequent tissue repair (Henson, 2005). The inflammatory response results in vasodilatation and an increased permeability of the microcirculation that facilitates the emigration of leukocytes to the site of inflammation (Chapter 1.16).

1.3.2 The neutrophil (PMN)

PMN are the first cells to appear at the site of inflammation during acute inflammation and are followed by monocytes which subsequently differentiate into tissue Mϕ (Serhan and Savill, 2005). The rapidly recruited PMN plays an important role in host defense against bacterial infection as activated PMN generate antimicrobial proteins and can undergo a 'respiratory burst', which produces large amounts of reactive oxygen radicals and hydrogen peroxide. PMN generate proteases that can degrade extracellular matrix that can damage host tissues (so-called 'friendly fire'). Thus, the multiple effects of activated PMN during acute inflammation can

result in significant tissue injury. The PMN has important phagocytic actions and may also release cytokines and chemokines, which recruit more leukocytes to the site of inflammation such that the inflammatory response is exacerbated.

1.3.3 The lymphocytes

PMN and Mϕ are the first line of defense and comprise key facets of the innate immune system. The second line of defense is the adaptive immune system, which is composed of DC and lymphocytes. DC are 'professional antigen presenting cells' and play a crucial role in the initiation of immune responses against pathogens. Activated DC migrate to lymphoid tissues and present antigens to naïve lymphocytes and initiate an immune response.

T and B lymphocytes are the main effector cells of the adaptive immune system. B and T cells have antigen specific receptors such that an encounter with specific antigen induces lymphocyte activation and clonal expansion.

T lymphocytes are divided into $CD8^+$ cytotoxic T cells (T_c) and $CD4^+$ T helper (T_h) cells and the T_h cells are further dived into T_{h1} and T_{h2} according to the pattern of cytokines they produce (Mosmann et al., 1986) T_c lymphocytes recognise antigens, which have been processed into peptides and are presented on major histocompatibility complex (MHC) class I bearing cells. T_h lymphocytes recognise peptides presented by MHC class II on antigen presenting cells such as Mϕ, DC and B cells. The interaction with the MHC molecule/peptide complex is mediated by the T cell receptor and associated co-stimulatory molecules such CD80 and CD86. T cells become anergic or undergo apoptosis in the absence of the co-stimulatory

signal. T_c lymphocytes use perforin and granzyme B to induce the lysis of target cells.

B cells can recognise, process and present antigens in association with their own MHC II molecules. T_h lymphocytes can recognise B cells (CD40 on the B cell and CD40 ligand [CD40L] on the T_h cell) and support B cell proliferation via the production of cytokines that may also influence antibody class switching. In addition, cytokines released from T_h lymphocytes are also important in modulating Mϕ activation as discussed later (Chapter 1.5). Normal naïve T and B cells mainly traffic within the lymphoid tissues but effector T cells migrate to the site of inflammation where they are involved in tissue injury.

1.4 MONOCYTE DIFFERENTIATION

All normal non-inflamed tissues contain a population of resident Mϕ although these cells may exhibit different phenotypes in different organs e.g. Kupffer cells in the liver, microglia in the central nervous system. During inflammation, it was initially thought that infiltrating monocytes were recruited from a single pool of circulating monocytes. However, recent work by Geismann and colleagues have demonstrated the existence of two principal subsets of blood monocytes with distinct migratory properties that may be distinguished by various surface markers including CC chemokine receptor 2 (CCR2) (the receptor for CC chemokine ligand 2 [CCL2], also known as monocyte chemoattractant protein 1 [MCP-1]), fractalkine receptor (CX_3CR1), Ly6C (subepitope for GR1) and CD62L (also known as L-selectin). Monocytes with the profile $CCR2^+$ $CX_3CR1^{low}CD62L^+GR1^+$ were rapidly recruited to injured tissues and developed into inflammatory Mϕ - these monocytes represent

the 'inflammatory monocyte subset'. In contrast, monocytes with the profile $CCR2^{-}$ $CX_3CR1^{hi}GR1^{-}$ were selectively recruited to normal, non-inflamed tissues and differentiated into resident tissue Mϕ - these monocytes represent the 'resident monocyte subset'. Both subsets were found to have the potential of differentiating into DC (Geissmann et al., 2003).

It is currently unclear which developmental pathway and precursor cells are involved in generating these two monocyte populations (Gordon and Taylor, 2005; Taylor and Gordon, 2003). Interestingly, however, Fogg et al recently demonstrated that Mϕ and DC can arise from a common progenitor cell, which can give rise to resident Mϕ in the brain, resident splenic DC and inflammatory Mϕ and DC (Fogg et al., 2006).

1.5 Mϕ ACTIVATION

The Mϕ is a remarkably versatile cell and plays an important role in the initiation, progression and resolution of inflammation (Cailhier et al., 2006; Duffield et al., 2005b; Kluth et al., 2004). The outcome of inflammation is dependent upon many factors but the nature of the Mϕ activating signals and the local microenvironment at the inflamed tissue will be important modulating factors. Mϕ can adopt various phenotypes, with different effector functions. Although somewhat simplistic, various Mϕ activation states have been defined *in vitro* including:

(i) classical activation,

(ii) alternative activation,

(iii) type II activation and

(iv) activation following the phagocytosis of apoptotic cells.

1.5.1 Classically activated Mϕ

The classically activated Mϕ phenotype can be induced by exposing Mϕ to interferon gamma (IFN-γ), (provided *in vivo* by T_h lymphocytes or natural killer cells), followed by stimulation with microbial products that engage Toll like receptors (e.g. lipopolysaccharide [LPS]). Classically activated Mϕ produce pro-inflammatory cytokines such as tumour necrosis factor alpha (TNF-α) and interleukin (IL) 12 (IL-12) as well as nitric oxide (NO) and this phenotype is associated with significant microbicidal activity. Classically activated Mϕ express high levels of MHC class II and CD86, (Mosser, 2003) but reduced mannose receptor expression. They also have been reported to have a reduced capacity to phagocytose apoptotic cells (Erwig et al., 1998).

1.5.2 Alternatively activated Mϕ

Alternative activation follows Mϕ activation with IL-4, IL-13 or glucocorticoids. Such treatment results in the expression of high levels of mannose receptors, scavenger receptors and the IL-1 receptor antagonist. Alternatively activated Mϕ do not generate significant amounts of NO and are therefore relatively ineffective at killing intracellular organisms. Alternatively activated Mϕ are more associated with tissue repair. Additional markers for alternatively activated Mϕ include FIZZI and YM1 (Edwards et al., 2006; Gordon, 2003).

1.5.3 TYPE II activated Mϕ

TYPE II activated Mϕ were first described by Mosser and colleagues (Anderson and Mosser, 2002). They exposed Mϕ to CD40L in the presence of immunoglobulin (Ig) G immune complexes and noted that these Mϕ were anti-inflammatory as they produced enhanced levels of IL-10 and reduced levels of IL-12. Type II activated Mϕ promote the development of a T_{h2} adaptive immune response with increased T cell IL-4 and IgG class switching in B cells (Mosser, 2003).

1.5.4 Mϕ activation following the uptake of apoptotic cells

Cells may undergo apoptosis (Chapter 1.6) during normal tissue homeostasis as well as during inflammation and the resultant apoptotic corpses must be cleared. Apoptotic cells are avidly ingested by Mϕ and may profoundly affect the Mϕ phenotype by inducing an anti-inflammatory Mϕ phenotype characterised by increased production of transforming growth factor-beta (TGF-β) and prostaglandin E2 as well as decreased production of IL-1, IL-6, TNF-α and Mϕ-inflammatory protein 1 alpha (MIP-1α) (Fadok et al., 1998; Voll et al., 1997). Apoptotic cells can modulate the response of Mϕ to other stimuli. For example, the exposure of Mϕ to LPS after the uptake of apoptotic cells leads to an increased production of IL-10 and a reduced production of IL-12. In addition, the simultaneous exposure of Mϕ to both apoptotic cells and LPS modulates the Mϕ response and results in increased early production of TNF-α whilst increasing the later generation of TGF-β (Lucas et al., 2003). It can therefore be appreciated that Mϕ ingestion of apoptotic cells may

induce a switch in the phenotype from an injurious pro-inflammatory Mϕ to a reparative anti-inflammatory Mϕ and it is highly likely that this Mϕ phenotype is very important during the resolution phase of inflammation (Savill et al., 2002; Serhan and Savill, 2005).

1.6 APOPTOSIS

Apoptosis, (programmed cell death) is an evolutionary conserved physiological process and plays a central role in embryogenesis, the maintenance of tissue homeostasis, host defense as well as the resolution phase of inflammation. Apoptosis can be triggered a variety of stimuli such as growth factor deprivation, UV damage or by the release of 'apoptosis inducing ligands' from cells of the immune system. Regardless of the inducer of the apoptotic process, there are a series of characteristic events that may occur that eventually leads to the demise of the cell.

In early seminal studies, apoptosis was described by morphological alterations of the cell (Kerr et al., 1972) including cell shrinkage, cytoplasmic condensation and vacuolation, chromatin condensation, cytoplasmic blebbing and eventual fragmentation of the cell into membrane-bound apoptotic bodies. The integrity of the plasma membrane and intracellular organelles remains intact during apoptosis. Apoptotic cells represent a source of autoantigens (Casciola-Rosen et al., 1994) and are therefore swiftly recognised and cleared by Mϕ (Ren and Savill, 1998; Savill, 1997; Savill et al., 2002; Savill and Fadok, 2000; Savill et al., 1989). It should be noted, however, that apoptotic cell may also be phagocytosed by semi-professional phagocytes such as mesangial cells and fibroblasts (Hall et al., 1994; Hughes et al., 1997; Savill et al., 1992).

In contrast to apoptosis, necrosis is characterised by widespread disruption of cell integrity and the release of intracellular contents (Kanduc et al., 2002; Wyllie, 1980). Necrosis typically results from severe cellular injury such as severe ischemia, sustained hyperthermia or high doses of toxic agents. Necrotic cell death mainly affects groups or contiguous fields of adjacent cells, whereas apoptosis can affect discrete cells within otherwise healthy and viable cell populations. Necrotic cells display dramatic membrane dysfunction and disruption of organelles such that the cell swells and eventually disintegrates. The internal homeostasis of the cell is lost and cellular constituents are released into the microenvironment where they typically evoke an inflammatory response.

1.7 DETECTION OF APOPTOTIC CELLS

The morphological criteria described by Kerr in 1972 still represent the 'gold standard' for identifying apoptotic cells in tissue sections. Additional methods of identifying apoptotic cells in tissue sections include the terminal deoxynucleotidyl transferase-mediated dUTP nick-end labeling (TUNEL) assay (Gavrieli et al., 1992) for the identification of DNA fragmentation – a typical feature of the majority of apoptotic cells. Other methods may be used for cells induced to undergo apoptosis *in vitro*. For example, during apoptosis, the DNA is cleaved into discrete fragments of multiples of 180 base pairs (bp) and a characteristic DNA ladder can be seen after electrophoresis (Wyllie, 1980; Wyllie et al., 1980). The detection of apoptosis-induced phosphatidylserine (PS) exposure (Fadok et al., 1992a; Fadok et al., 1992b) by Annexin V binding is a common flow cytometric method for determining and quantifying the level of apoptosis in cell populations (Koopman et al., 1994).

Apoptotic cells are rapidly phagocytosed *in vivo* (Barres et al., 1992; Coles et al., 1993; Parnaik et al., 2000) by neighbouring Mϕ as well as other resident parenchymal cells. The level of apoptosis is typically very low in normal tissues but is increased during tissue injury and inflammation (Baker et al., 1994).

1.8 APOPTOTIC PATHWAYS AND EFFECTORS

1.8.1 Caspases

Caspases (cysteinyl aspartate proteases) are intracellular proteolytic enzymes containing a cysteine at the active site and cleave substrates after an aspartic acid residue. Caspases are highly conserved through evolution and are common to multicellular organisms. The caspases can be divided into three families. Caspases 1, 4, 5, 11 and 12 (in vertebrates) are involved in the proteolytic processing of the precursors of the inflammatory cytokines such as IL-1 and IL-18 (Martinon and Tschopp, 2004). The remaining caspases are mainly involved in apoptosis and are divided into:

'Initiator caspases' such as caspase 2, 8, 9 and 10 (note, caspase-10 is not present in the mouse) (Siegel, 2006), that are involved in the early events of the apoptosis process. They further activate the caspase cascade leading to the activation of the 'effector caspases'

The effector or 'executioner' caspase group includes caspase 3, 6 and 7 and are involved in the final stages of the apoptosis process where they are responsible for the proteolysis of many intracellular proteins.

Two distinct pathways leading to the activation of initiator caspases can be distinguished (Hengartner, 2000). The first pathway is triggered by ligands that directly bind to death receptors expressed at the cell surface and this is called the 'extrinsic' apoptosis pathway (Walczak and Krammer, 2000). The second pathway involves the mitochondria with caspase activation resulting from the release of mitochondrial products (Green and Reed, 1998). This second pathway is called the' intrinsic' apoptotic pathway (Green and Kroemer, 2004).

1.8.2 The extrinsic pathway of apoptosis

The extrinsic apoptotic pathway is triggered by ligand binding of death receptors on the plasma membrane. The death receptors belong to the tumour necrosis factor receptor (TNFR) superfamily and the best characterised are Fas (also known as CD95) and TNFR1, for review see (Wallach et al., 1999). The death receptors are activated after ligand-induced trimerisation. The extracellular domain of the receptors contains one to five cysteine rich repeats whilst a death domain (DD) is located in the cytoplasmic tail. Ligand binding of the death receptor results in conformational changes. The resultant protein-protein interactions and resultant caspase activation is based on close 'proximity induced activation' that is regulated by DDs and death effector domains (DEDs) (Hengartner, 2000). Usually death receptors activate caspase-8, which then leads to the activation of the caspase 3-effector pathway. However, death receptor ligation can also activate caspase-2 and 10 (Jin and El-Deiry, 2005).

1.8.2.1 **Fas mediated apoptosis**

The Fas death receptor is expressed by many cell types including T cells (Krammer, 2000), and tubular epithelial cells (Du et al., 2004) Fas ligand (FasL) is mainly expressed on leukocytes (especially T cells and Mϕ) (Brown and Savill, 1999; Liles et al., 1996; Suda et al., 1995) but may also be expressed by parenchymal cells such as tubular epithelial cells (Lorz et al., 2000).

Ligation of the Fas death receptor results in trimerisation of the receptor and binding of the DD of the cytoplasmic portion of the trimerised Fas receptor to a cytoplasmic adaptor protein called FADD (Fas associated death domain) (Chinnaiyan et al., 1995) by DD-DD interactions. FADD recruits procaspase-8 by homologous interaction of the DED domain of FADD and the DED of procaspase-8 and this generates a protein complex called the death-inducing signalling complex (DISC) (Peter and Krammer, 2003). Caspase-8 is activated by autoproteolysis (proximity induced activation) (Hengartner, 2000) and released from the DISC into the cytoplasm. Active caspase-8 is able to activate various members of the caspase family especially caspase-3, which completes the cell death programme and leads to apoptosis of the cell. A simplified schema of the events involved in this process is shown in Figure 1-4.

The activity of active caspase-8 can also be amplified via interactions with the mitochondria ('a way for crosstalking between extrinsic and the intrinsic pathway'). Activated caspase-8 can cleave cytosolic Bid (a pro-apoptotic member of the Bcl-2 family). Truncated Bid is then translocated to the mitochondria and stimulates the release of cytochrome c (Cyt c) (Luo et al., 1998) and other pro-apoptotic factors (Figure 1-4). An additional level of regulation of the above events

is represented by cellular FLICE inhibitor protein (c-FLIP) (Irmler et al., 1997). c-FLIP is an inactive caspase homologue and binds to both FADD and pro-caspase-8 to inhibit the formation of active caspase-8 and inhibiting apoptosis (Tschopp et al., 1998) (Figure 1-4).

1.8.3 The intrinsic pathway of apoptosis

The intrinsic pathway of apoptosis involves the mitochondria and can be triggered by insults such as DNA damage (UV-induced) and cell 'stress' induced by hypoxia, cytotoxic drugs, free radicals, growth factor withdrawal etc. A pivotal event in the mitochondrial pathway is mitochondrial outer membrane permeabilisation (MOMP). This leads to mitochondrial dysfunction characterised by a fall in the mitochondrial membrane potential, swelling of the mitochondrial matrix and finally rupture of the outer membrane resulting in the release of cyt c into the cytoplasm (the mechanism of cyt c release is reviewed elsewhere (Garrido et al., 2006)). In the presence of deoxyadenosine 5′-triphosphate (dATP), cyt C interacts with apoptosis protease activating factor 1 (Apaf-1) which is activated via heptamerisation following a conformational change. This complex then combines with pro-caspase 9 to form the apoptosome complex, which results in caspase-9 activation (Acehan et al., 2002). Downstream activation of the 'effector' caspases follows which leads to apoptosis (Figure 1-4). These events are regulated by several heat shock proteins and by inhibitor of apoptosis proteins (IAPs). IAPs are potent intracellular inhibitors of caspases (caspase 3 and 9) and can prevent cell death (Salvesen and Duckett, 2002).

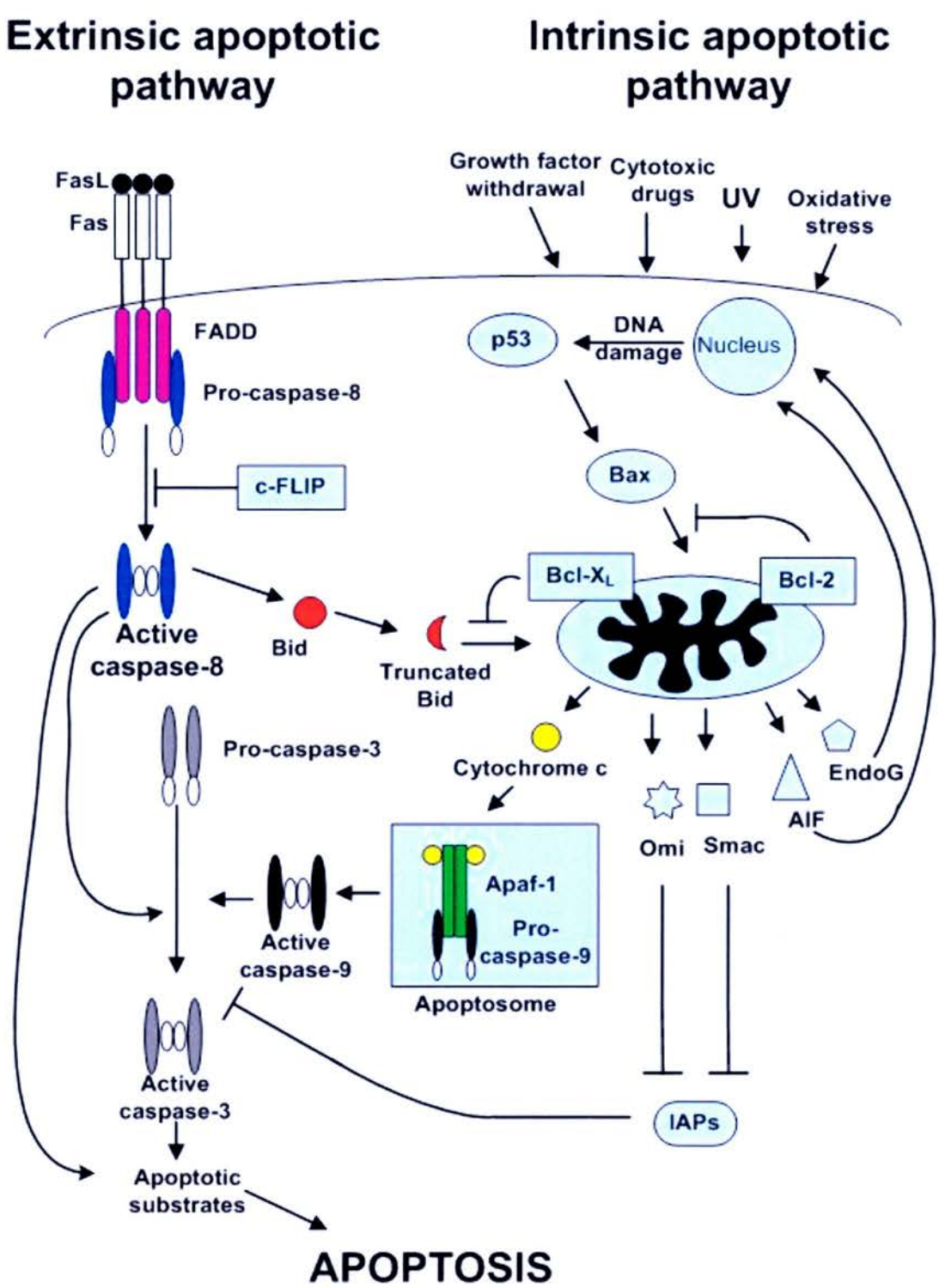

Figure 1- 4 Diagram of the extrinsic and intrinsic apoptotic pathways. The extrinsic pathway is exampled with Fas-induced apoptosis, see text for details. (Modified from (Hengartner, 2000)).

The activity of IAP can be neutralised by Smac/DIABLO (second mitochondria-derived activator of caspases/direct inhibitor of apoptosis binding protein with a low isoelectric point), or by HtrA2 (high temperature requirement protein also know as Omi). Both Smac/DIABLO and HtrA2 are released from the mitochondria during activation of the intrinsic pathway – an action that attempts to ensure that apoptosis proceeds (Figure 1.4). Other pro-apoptotic proteins released from the mitochondria include apoptosis inducing factor (AIF) and endoG (a sequence unspecific *DNase*) These can translocate into the nucleus and mediate caspase independent apoptotic cell death (Figure 1-4). The role of mitochondrial released pro-apoptotic proteins in the apoptotic process is reviewed (Antonsson, 2004; van Loo et al., 2002).

1.8.4 Bcl-2 family

The Bcl-2 family consists of several members that may inhibit or induce death. Many proteins of the Bcl-2 family are located in the outer mitochondrial membrane and regulate MOMP and cyt c release from the mitochondria (Figure 1-4). The Bcl-2 family members are divided into three main groups based on their conserved Bcl-2 homology (BH) domains. Anti-apoptotic members such as Bcl-2 and Bcl-X_L contain four BH domains (BH1-BH4). Pro-apoptotic multidomain members such as Bax and Bak possess three BH domains. Lastly, the pro-apoptotic members of the third group share only homology in the BH3 domain and examples are Bad, Bid and Bik (Hengartner, 2000). Bcl-2 can inhibit the recruitment of the pro-apoptotic member Bax to the mitochondria and Bcl-X_L inhibits the translocation of truncated bid to the mitochondria (Figure 1-4).

1.9 FasL/FAS IN THE KIDNEY

Although FasL may be expressed by mesangial cells, renal fibroblasts and tubular epithelial cells it is mostly expressed by leukocytes such as lymphocytes, and monocytes/Mϕ (Lorz et al., 2000; Ortiz et al., 1997; Ortiz-Arduan et al., 1996). *In vitro* Fas ligation often induces apoptosis in various cells such as leukocytes, fibroblasts and mesangial cells (Gonzalez-Cuadrado et al., 1997; Ortiz et al., 1997) although it is of interest that tubular epithelial cells require cytokine priming (Ortiz-Arduan et al., 1996). Increased FasL expression has been noted in rat proliferative glomerulonephritis (Lorz et al., 2000) as well as human renal transplant patients with chronic allograft nephropathy (Sharma et al., 1996). Increased Fas expression is evident in murine ischemia-reperfusion injury (Nogae et al., 1998), murine LPS endotoxaemia (Ortiz-Arduan et al., 1996), the remnant kidney model in the rat (Hattori et al., 1998) and in human proliferative glomerulonephritis (Takemura et al., 1995). Gonzalez-Cuadrado et al induced apoptosis of mesangial cells by treating mice with an agonistic Fas antibody although there was little tubular cell apoptosis evident in this study (Gonzalez-Cuadrado et al., 1997).

1.9.1 Apoptosis of MDCK cells

The situation may be complicated in certain situations. For example, MDCK cells undergo apoptosis following partial ATP (adenosine triphosphate) depletion induced by 'chemical hypoxia', exhibit a marked increase in caspase-8 activity and are rescued by treatment with caspase inhibitors (Feldenberg et al., 1999). Activation of caspase-3 is evident during ATP depletion or hypoxia and was accompanied by

cyt c release from the mitochondria (Saikumar et al., 1998). However, although such a stimulus would be predicted to act predominantly via the intrinsic or mitochondrial pathway, the ATP-depleted cells upregulated the expression of Fas, FasL and FADD. Thus, partial ATP depletion appears to induce Fas-mediated apoptosis that is amplified by the mitochondrial pathway in MDCK cells. Treatment with exogenous agonistic anti-Fas monoclonal antibodies also induces apoptosis of MDCK cells in non-ischemic conditions indicating that MDCK cells retain a Fas-dependent pathway of apoptosis.

1.9.2 Compartmentalisation of FasL/Fas in MDCK cells

An added level of complexity is that cells may exhibit compartmentalisation of Fas and FasL which is believed to prevent auto-paracrine apoptosis in tubular epithelial cells (Tan and Hunziker, 2003). Fas and FasL exist within different cellular compartments and are thus segregated from each other. Fas is expressed at the basolateral surface whilst FasL is expressed in the intracellular compartment (Tan and Hunziker, 2003).

1.10 APOPTOSIS IS IMPORTANT IN THE RESOLUTION OF INFLAMMATION

Apoptosis is very much a double-edged sword. The efficient deletion of excessive, damaged or non-functioning renal cells as well as infiltrating inflammatory cells by apoptosis is undoubtedly beneficial for the resolution of glomerulonephritis (Savill, 1994). For example, the anti-thy 1.1 model of glomerulonephritis in the rat is characterised by an initial wave of mesangial cell

death followed by marked proliferation that results in glomerular hypercellularity (Jefferson and Johnson, 1999). Over time, however, the glomeruli are remodelled and normocellularity is restored. Elegant work by Baker et al demonstrated that the hypercellular glomeruli exhibited high levels of mesangial cell apoptosis and a careful kinetic analysis indicated that apoptosis could account for the loss of mesangial cells during the remodelling phase (Baker et al., 1994). Thus, in this context, apoptosis represents a beneficial cell clearance mechanism to counterbalance excessive levels of cell proliferation. In contrast, the seminal work of Gobe et al demonstrated that tubular epithelial cell apoptosis was a key factor in the development of renal tubular atrophy in experimental hydronephrosis, induced by unilateral ureteric obstruction (UUO), (Gobe and Axelsen, 1987).

1.11 CELL PROLIFERATION AND ITS REGULATION

1.11.1 The cell cycle

The cell cycle comprises a series of tightly controlled events that drive cell proliferation. In response to mitotic signals, quiescent cells in G_0 enter the cell cycle at early G_1. In the absence of mitogenic stimuli, the cells may undergo differentiation, apoptosis or revert to G_0. In late G_1 there is a so-called 'restriction point'. Once the cell has past this point, it becomes unresponsive to external stimuli and the cell is committed to complete the cell cycle, regardless of the presence or absence of mitogens. DNA is replicated and synthesised during the S phase and the cell undergoes mitosis in the M phase, resulting in two daughter cells. There are two

'checkpoints' where cell cycle progression can be arrested - one at the G_1/S transition and one at the G_2/M transition (Figure 1-5).

1.11.1.1 **Positive cell cycle regulators**

Cyclin-dependent kinases (CDKs) and cyclins act as positive regulators of cell cycle progression. CKDs are serine-threonine protein kinases which are constitutively expressed during the cell cycle. The activity of CKDs requires binding to cyclins with the level of expression and activity of cyclins varying according to the phase of the cell cycle. Formation of cyclin/CDK complexes results in phosphorylation and activation of the CDKs and these complexes target substrates that are involved in the transition between the cell cycle phases. The cell cycle starts when cyclin D (there are three D1, D2, D3) binds their catalytic partners CDK4/6. This cyclin/CDK complex is essential for entry into G_1 phase. The progression from G_1/S phase is regulated by the cyclin E/CDK2 complex whilst the cyclin A/CDK2 complex is required for DNA synthesis during S phase. The checkpoint at the G_2/M transition is controlled by the cyclin B/CDK1 complex with mitosis occurring thereafter (Shankland and Wolf, 2000).

1.11.1.2 **Negative cell cycle regulator**

Cyclin kinase inhibitor (CKIs) inhibit the cell cycle at multiple checkpoints via inactivation of the cyclin/CDK complexes. There are two families of CKIs - INK and Cip/Kip (reviewed by (Sherr and Roberts, 1999)). Members of the INK family

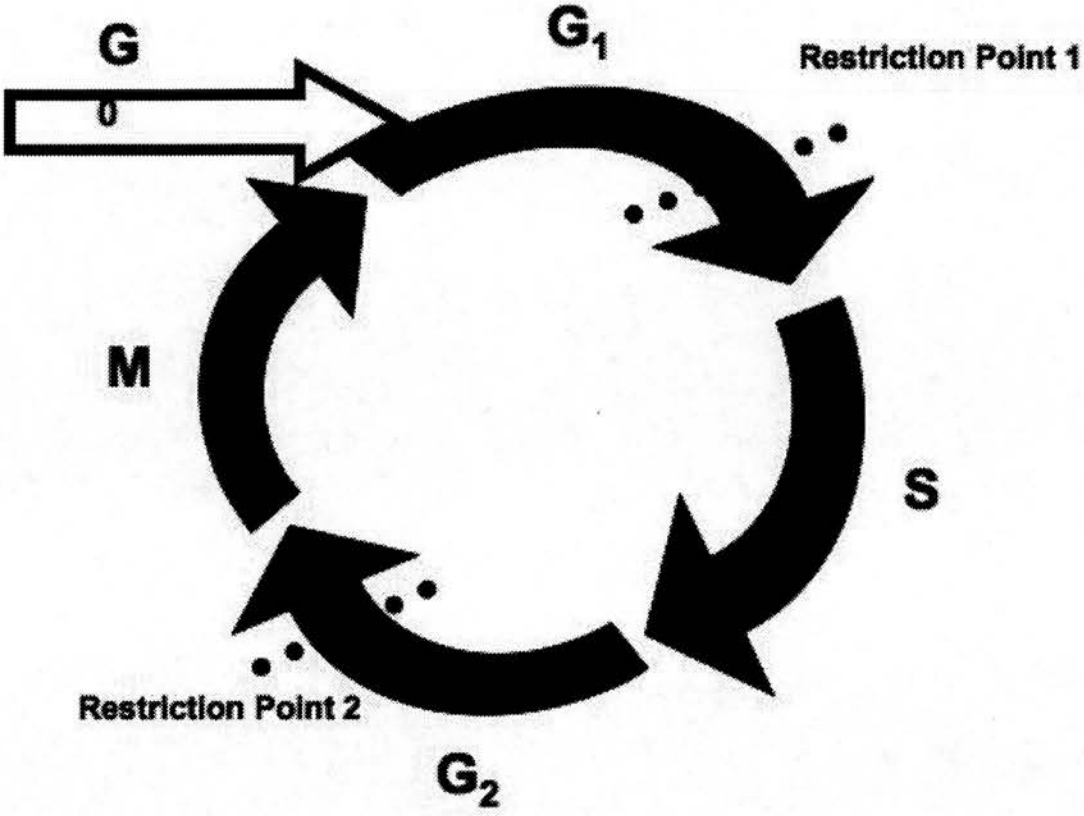

Figure 1- 5 The cell cycle.
Simple illustration of the cell cycle. Quiescent cells enter the cell cycle at early G_1, followed by S phase (DNA synthesis), (G_2) and finally mitosis (M).

includes $p15^{INK4b}$, $p16^{INK4a}$, $p18^{INK4c}$ and $p19^{INK4d}$ which inhibit the cyclin/CDK complexes in G_1. The second family includes $p21^{Cip}$, $p27^{Cip2}$ and $p57^{Kip}$ which inhibit cyclin-CDK complexes during both G_1 and S phase of the cell cycle. However, p21 can also inhibit DNA synthesis and repair by inhibiting the proliferating cell nuclear antigen (PCNA) (Luo et al., 1995). In response to DNA damage, p21 can be transcriptionally activated by p53 and acts to induce arrest in G_1 phase (Brugarolas et al., 1995).

1.11.2 p53 and apoptosis

The cell cycle regulator p53 is a nuclear protein and has been called the 'guardian of the genome' as it is strongly upregulated following DNA damage secondary to irradiation, genotoxic drugs, free radicals, etc. p53 induces cell cycle arrest at G_1/S via upregulation of p21 as described earlier, thus allowing the cells to undergo DNA repair and preventing the replication of cells which have damaged DNA. If the DNA damage is severe and irreparable, then p53 induces apoptosis of the cells (Figure 1-4), which may involve translocation of Fas to the cell surface (Bennett et al., 1998).

1.11.3 Cell cycle proteins and renal disease

The role of cell cycle and cell cycle regulatory proteins in renal disease has been investigated by members of Stuart Shankland's group (reviewed in (Griffin et al., 2003a; Griffin et al., 2003b; Marshall and Shankland, 2006; Shankland and Wolf, 2000). Work from this group investigated the role of the CKI p27 upon renal cell

apoptosis in nephrotoxic nephritis (NTN) and UUO. Mice targeted for the deletion of p27 exhibited increased tubular epithelial cell apoptosis in both models (Ophascharoensuk et al., 1998). No role for p21 in tubular epithelial cell apoptosis was found in UUO (Hughes and Shankland, 1999).

The level of p53 is increased in UUO (Morrissey et al., 1996). The absence of p53 provides partial protection of tubular epithelial cells from apoptosis in UUO as homozygous (p53 -/-) mice exhibited a 50% reduction in the level of tubular epithelial cell and interstitital cell apoptosis compared to control (p53+/+) mice (Choi et al., 2001). This suggest that renal cell apoptosis in obstructed kidneys involves both p53-dependent and p53-independent pathways.

1.12 TUBULOINTERSTITIAL FIBROSIS

Tubulointerstitial fibrosis is characterised by the excessive accumulation and deposition of ECM components, which eventually leads to tissue damage and scarring and associated renal impairment. Fibroblasts and myofibroblasts are the major ECM producing cells in the diseased tubulointerstitium and produce excess ECM such as collagens (type I, III, IV). The pathogenesis and mechanism of tubulointerstitial fibrosis has been reviewed in detail elsewhere (Eddy, 2000; Iwano and Neilson, 2004; Liu, 2006; Okada and Kalluri, 2005; Zeisberg et al., 2001).

1.12.1 Description of fibroblasts and myofibroblasts

Cortical fibroblasts and associated ECM provide structural support for the normal kidney interstitium. Normal renal fibroblasts typically display a spindle shaped elongated 'fusiform' phenotype and are quiescent (low proliferation/turnover). They may, however, proliferate in response to a variety of stimuli. Cultured 'normal' fibroblasts can be phenotyped according to their expression of fibroblast-specific protein 1 (FSP-1, also known as S100A4), vimentin and CD90 and lack of expression of desmin and cytokeratin (Grupp and Muller, 1999; Strutz et al., 1995). During renal inflammation, activated fibroblasts proliferate, adopt a myofibroblastic phenotype and produce abundant ECM. Myofibroblasts express alpha smooth muscle actin (α-SMA) and the presence and abundance of α-SMA positive cells is associated with the progression of renal disease (Badid et al., 2001; Roberts et al., 1997).

The origin of fibroblasts and myofibroblasts in diseased kidneys remains controversial. Fibroblasts may originate from the resident fibroblast population or by recruitment from bone marrow-derived stem cells (Abe et al., 2001). Also, myofibroblasts may be derived from these sources as well as from tubular epithelial cells by a process known as epithelial mesenchymal transition (EMT) (Iwano et al., 2002).

1.12.2 Epithelial to mesenchymal transition

EMT in renal fibrosis was first described by Strutz et al, when they showed that tubular epithelial cells could express the fibroblast marker FSP-1 in a mouse

model of anti-tubular basement membrane disease (Strutz et al., 1995). Currently, EMT is generally recognised as providing a significant contribution to the generation of interstitial myofibroblasts in renal fibrosis (reviewed by (Kalluri and Neilson, 2003; Lee et al., 2006)). Yang et al has suggested 4 key steps in the process of EMT: (1) loss of epithelial cell adhesion; (2) *de novo* α-SMA expression and actin re-organisation; (3) disruption of the tubular basement membrane (TBM) and (4) enhanced cell migration and invasion (Yang and Liu, 2001).

EMT has been observed in human renal biopsies (Rastaldi et al., 2002), human kidney transplants (Vongwiwatana et al., 2005) and in various animal models of renal fibrosis (reviewed in (Liu, 2004)).

1.13 DESCRIPTION OF MEDIATORS INVOLVED IN TUBULOINTERSTITAL FIBROSIS

The accumulation of ECM during tubulointerstitial fibrosis may be a consequence of excessive synthesis coupled with impaired ECM degradation. Proteolytic enzymes involved in ECM degradation are matrix metalloproteinases (MMPs), connective tissue proteases and components of the plasminogen system (plasminogen, plasminogen activators, and plasmin). MMP activity is regulated by tissue inhibitors of MMPs (TIMPs) and the plasminogen system is regulated by plasminogen activator inhibitor (PAI-1).

Various inflammatory mediators such as cytokines, NO and different growth factors are also involved in the regulation and accumulation of ECM in the tubulointerstitium. Examples of pro-fibrotic factors are TGF-β, connective tissue growth factor, angiotensin II and platelet-derived growth factor. In contrast,

hepatocyte growth factor (HGF) and bone morphogenic protein 7 (BMP-7) are anti-fibrotic.

1.13.1 Matrix metalloproteinases

Most MMPs are initially secreted as pro-enzymes that are proteolytically activated. MMP expression can be induced by various factors (inflammatory cytokines, growth factors and cell-ECM interactions), while their activity is inhibited by TIMPs (Nagase and Woessner, 1999). MMPs are subdivided into groups according to their domain structure and substrate preference: collagenases (MMP-1, 8 and 13), gelatinases (MMP-2 and 9), stromelysins (MMP-3, 10 and 11), matrilysins (MMP-7 and 26), membrane type (MT)-MMPs (MT-MMP 14, 15, 16, 17, 24 and 25) etc. (reviewed by (Nagase et al., 2006)).

During renal inflammation and scarring MMPs can be produced by infiltrating inflammatory Mϕ, fibroblasts, myofibroblasts and tubular epithelial cells and undoubtedly play a role in disease (reviewed by (Catania et al., 2007)). For example, MMP-2 can be involved in degradation of TBM, as transgenic mice overexpressing MMP-2 in proximal tubular epithelial cells developed spontaneous EMT and peritubular fibrosis (Cheng et al., 2006).

Metalloelastase (MMP-12) is expressed mainly by Mϕ and digests elastin and other ECM molecules. It allows Mϕ to invade tissue and degrade ECM (Shipley et al., 1996). Mϕ can also release collagenases (MMP-1 and 13) and regulate the activity of gelatinases (MMP-2 and 9) (Gibbs et al., 1999) and matrilysin (MMP-7) (Song et al., 2000). Human monocytes can also express matrilysins (Busiek et al., 1995). It can therefore be appreciated that Mϕ are capable of modulating the fibrotic process.

1.13.2 Tissue inhibitors of matrix metalloproteinases (TIMP)

There are four TIMPs (TIMP-1, 2, 3 and 4) and they inhibit MMP activity. TIMP-2 and 3 are normally expressed in the kidney while the expression of TIMP-1 has been shown to increase in human and animal models of renal fibrosis (Catania et al., 2007; Duymelinck et al., 2000).

Genetic deficiency of TIMP-1 fails to attenuate tissue fibrosis in the UUO model or in mice with overload proteinuria (Eddy et al., 2000; Kim et al., 2001a) indicating that TIMP-1 dependent inhibition of MMP is not critical in interstitial fibrosis and this may represent compensation by other TIMPs.

1.13.3 Plasminogen system

Plasmin is a serine protease and is generated from its pro-enzyme plasminogen by either urokinase-type plasminogen activator (uPA) or tissue-type plasminogen activator (tPA). Plasmin can degrade various components of ECM and is also involved in activating pro-MMPs .

Edgtton et al demonstrated that plasminogen is not protective in the UUO model since the obstructed kidneys of plasminogen deficient mice exhibited less fibrosis than wild-type (WT) control mice (Edgtton et al., 2004). Plasminogen deficient mice exhibited reduced Mϕ infiltration but comparable myofibroblast accumulation. Expression of TGF-β and MMP-2 was lower in the plasminogen deficient mice while MMP-9 activity was unchanged.

When UUO was induced in uPA receptor (uPAR) knockout (KO) mice, the activity of uPA, and tPA was reduced and these mice had more fibrosis compared to

WT control mice. The uPAR KO mice also had reduced HGF expression compared to WT controls (Zhang et al., 2003).

Yang et al induced UUO in mice lacking tPA and found reduced fibrosis, reduced TBM damage and reduced EMT in these mice compared to WT controls (Yang et al., 2002).

PAI-1 inhibits the plasminogen activators and is therefore likely to promote fibrosis. Indeed, the obstructed kidneys of transgenic mice overexpressing PAI-1 exhibit increased fibrosis compared to control mice (Matsuo et al., 2005). The transgenic mice exhibited increased Mϕ infiltration, increased myofibroblast accumulation and reduced uPA activity. The pro-fibrotic effect of PAI-1 was also demonstrated by Oda et al as PAI-1 KO mice were protected from fibrosis following UUO (Oda et al., 2001). PA1-1 KO mice exhibited reduced Mϕ infiltration and myofibroblast accumulation, but the activity of plasminogen activators and plasmin were unaffected. These two studies suggest that the pro-fibrotic action of PAI-1 is via an increase in Mϕ infiltration and that its effect as an inhibitor of serine proteases is less important.

1.13.4 TGF-β

In mammals there are three TGF-β isoforms (TGF-β1, TGF-β2, and TGF-β3). TGF-β plays important role in tissue development, inflammation, immune responses, wound healing, tissue repair and the progression of fibrosis. TGF-β is both an inhibitor and a stimulator of cell proliferation in a variety of cells.

The role of TGF-β in renal fibrosis has been thoroughly investigated including the various signaling pathways involved (reviewed in (Bottinger and Bitzer, 2002; Wang et al., 2005).

TGF-β promotes ECM accumulation in tubulointerstitial fibrosis by stimulating the production of interstitial proteins from both fibroblasts and myofibroblasts. In addition TGF-β can reduce the expression of MMPs and stimulate the production of TIMPs and PAI-1 thereby inhibiting the degradation of ECM and promoting fibrosis. TGF-β has also been shown to play an important role in the induction of EMT.

Strutz et al demonstrated that TGF-β1 induced proliferation of human renal fibroblasts - a process dependent on the action of basic fibroblast growth factor -2 (FGF-2) (Strutz et al., 2001). Interestingly, tubular epithelial cells can produce TFG-β and are able to stimulate fibroblast proliferation (Johnson et al., 1998). TGF-β also stimulates tubular epithelial cells to undergo EMT *in vitro* (Forino et al., 2006).

TGF-β expression is increased in experimental models of renal fibrosis (Downer et al., 1988; Fukuda et al., 2001; Wright et al., 1996). The key role of TGF-β in the induction of renal scarring was demonstrated by study of transgenic mice expressing TGF-β under the control of the murine albumin promoter. These mice exhibited increased levels of circulating TGF-β and marked tubulointerstitial fibrosis and glomerulosclerosis (Kopp et al., 1996). Several studies have demonstrated that inhibition of the expression or action of TGF-β is protective in experimental models of renal scarring (Hwang et al., 2006; Isaka et al., 2000; Lan et al., 2003; Miyajima et al., 2000; Moon et al., 2006).

1.13.5 HGF and BMP-7

HGF and BMP-7 are anti-fibrotic growth factors that can inhibit the development of fibrosis. Studies have demonstrated that HGF gene therapy or the administration of recombinant HGF, ameliorates fibrosis in the UUO model (Gao et al., 2002; Mizuno et al., 2001; Yang and Liu, 2003). The administration of either HGF or BMP-7 can prevent TGF-β induced EMT of tubular epithelial cells (Yang et al., 2005; Zeisberg et al., 2003), whilst the administration of BMP-7 to mice with UUO or NTN reversed EMT, repaired damaged tubular epithelial cells and improved renal function (Morrissey et al., 2002; Zeisberg et al., 2003). BMP-7 can also induce mesenchymal to epithelial transition (MET) in adult renal fibroblasts and facilitates regeneration of the injured kidney (Zeisberg et al., 2005).

1.14 Mϕ INDUCTION OF TUBULOINTERSTIAL FIBROSIS

A significant body of data suggests that Mϕ may play an important role in the development of tubulointerstitial fibrosis. The degree of Mϕ infiltration correlates with the severity of the renal fibrosis, whilst blocking chemokines or adhesion molecules involved in Mϕ infiltration reduces fibrosis in experimental models (Anders et al., 2002; Cheng et al., 2000; Kitagawa et al., 2004; Lloyd et al., 1997; Panzer et al., 1999; Wada et al., 2004). Also experiments using animals deficient in genes encoding proteins involved in Mϕ recruitment to inflamed sites have demonstrated protection from scarring (Kitagawa et al., 2004; Lange-Sperandio et al., 2002; Lange-Sperandio et al., 2006).

Mϕ generate many pro-inflammatory mediators at inflamed sites such as cytokines, reactive oxygen species, and NO but may also produce pro-fibrotic mediators such as TGF-β, epidermal growth factor (EGF) and FGF-2 (Eddy, 2000).

These pro-fibrotic mediators stimulate the proliferation of fibroblasts and myofibroblasts and these cells may produce chemokines, that amplifies the inflammatory response. The fibroblasts and myofibroblasts produce increased amounts of interstitial collagens and ECM accumulation occurs. Mϕ production of these pro-fibrotic mediators may also induce EMT of tubular epithelial cells (Strutz et al., 2002). Mϕ can also affect the activation and production MMPs that degrade ECM and the expression of TIMPS. Thus, the Mϕ is likely to play a key role in renal fibrosis and scarring.

1.15 THE MODEL OF EXPERIMENTAL HYDRONEPHROSIS

The model of experimental hydronephrosis is induced by ligation of one of the ureters and is also known as unilateral ureteric obstruction (UUO). UUO results in tubulointerstitial fibrosis and the model was pioneered by Klahr and colleagues (Klahr, 1991). UUO in rodents is a useful model of renal inflammation and scarring as it a robust, reliable and reproducible model that induces disease in all murine strains (Diamond et al., 1998). UUO is regarded as a non-immune model of renal inflammation as disease is lymphocyte independent (Shappell et al., 1998). Obstructed kidneys do not exhibit PMN infiltration but develop a prominent tubulointerstitial Mϕ infiltrate and this model therefore facilitates the study of Mϕ function during tubulointerstitial inflammation.

Mϕ infiltrate the cortical tubulointerstitium just hours after the induction of UUO and continue to accumulate with time (Diamond, 1995). Interstitial myofibroblasts and tubular epithelial cells proliferate early in the course of the disease (Diamond et al., 1995). Over time, however, continued ongoing apoptosis of tubular epithelial cells and myofibroblast accumulation results in progressive renal tubular atrophy and hypocellular interstitial scarring (Bascands and Schanstra, 2005; Gobe and Axelsen, 1987; Truong et al., 1998). There are similarities between UUO in rodents and the features of human obstructive uropathy although the rodent disease has a markedly accelerated course (Klahr, 1998).

I have used the experimental model of UUO model to study the mechanism underlying Mϕ induction of tubular epithelial cell apoptosis and the role of Mϕ in tubulointerstitial inflammation.

1.16 DESCRIPTION OF FACTORS INVOLVED IN Mϕ LOCALISATION IN TUBULOINTERSTITIAL INFLAMMATION

Mϕ within an inflamed kidney may either be directly derived from the circulation or result from Mϕ proliferation *in situ.* Work by Tesch et al suggested that significant Mϕ proliferation may occur within inflamed kidneys with the Mϕ growth factor CSF-1 (colony stimulating factor-1) being a key driver of this process (Le Meur et al., 2002). In contrast, recent studies in murine NTN suggest that Mϕ infiltration is predominantly the result of monocyte recruitment from the circulation (Duffield et al., 2005a).

Recruitment of leukocytes to inflamed sites involves a series of interdependent and closely regulated adhesive interactions between leukocytes and

the endothelium (reviewed by (Luster et al., 2005; Sean Eardley and Cockwell, 2005; Springer, 1994)).The circulating monocyte localises to sites of inflammation in response to a gradient of released chemoattractants or chemokines with all intrinsic renal cells being capable of secreting chemokines in response to injury (Segerer, 2003). The monocytes adhere to the activated endothelium and subsequently transmigrate via a typical leukocyte cascade involving rolling, firm adhesion and transendothelial migration. Selectins and their ligands mediate the initial contact between circulating leukocytes and the endothelium resulting in capture and rolling of the leukocytes along the vessel wall. The leukocyte becomes exposed to chemoattractants/chemokines and activating stimuli expressed on the endothelial surface and this leads to firm adhesion mediated by integrins and their ligands. The last step involves transendothelial migration of the leukocyte by diapedesis which is mediated by interactions between the integrins, PECAM-1 (platelet endothelial cell adhesion molecule 1) and members of the junctional adhesion molecule family.

1.16.1 Selectins

Selectins are carbohydrate-binding transmembrane proteins and there are three closely related members within the selectin family: E-selectin, L-selectin and P-selectin, which are named according to the cell type on which they were originally identified (i.e. endothelium, leukocytes and platelets respectively). E- and P-selectin are expressed on activated endothelial cells and bind to carbohydrate ligands, which are constitutively expressed on monocytes. L-selectin is constitutively expressed on most leukocytes and plays an important role in capturing leukocytes to the endothelial cell surface.

Lange-Sperandio et al performed UUO in neonatal triple selecting deficient (EPL-/-) and WT mice and demonstrated reduced Mϕ infiltration in EPL-/- mice compared to WT control mice thereby indicating a role for selectins in Mϕ recruitment to the tubulointerstium (Lange-Sperandio et al., 2002).

1.16.2 Integrins and adhesion molecules

Integrins are heterodimeric receptors consisting of non-covalently associated α and β subunits. The integrins on the rolling leukocytes must be activated and undergo a conformational change before they can bind to their specific endothelial ligands to establish firm adhesion to the endothelial surface.

The major integrins expressed on monocytes are the β_1 integrin very late activation antigen 4 (VLA-4, also known as CD49d/CD29 or $\alpha_4\beta_1$) and the two β_2 integrins, leukocyte functional antigen 1 (LFA-1, also known as CD11a/CD18 or $\alpha_L\beta_2$) and Mac-1 (also known as CD11b/CD18 or $\alpha_M\beta_2$) (Lange-Sperandio et al., 2006). Firm adhesion of monocytes involves the adhesive interaction between integrins and members of the immunoglobulin superfamily on endothelial cells e.g. intercellular adhesion molecule-1 (ICAM-1) and vascular cell adhesion molecule 1 (VCAM-1). Finally, the transendothelial migration and diapedesis of monocytes is mediated by interactions between PECAM-1 ((Muller and Randolph, 1999) and members of the junctional adhesion molecule family (Aurrand-Lions et al., 2002).

Recent work by Lange-Sperandio et al investigated the role of β_2 integrins in Mϕ recruitment in experimental hydronephrosis performed in neonatal mice. UUO was induced in 2 day old neonatal mice targeted for the deletion of either Mac-1 or LFA-1. Mac-1 KO mice displayed reduced Mϕ infiltration at days 1, 5 and 12 after

UUO while LFA-1 KO mice exhibited reduced levels at days 1 and 5 but at day 12 the Mϕ infiltration was comparable to WT control mice. Tubular epithelial cell apoptosis, tubular atrophy and tubulointerstitial fibrosis was reduced in Mac-1 KO mice but not in LFA-1 KO mice (Hughes, 2006; Lange-Sperandio et al., 2006).

The role of ICAM-1 in the murine UUO model was studied by Cheng et al by the administration of antisense oligonucleotides against ICAM-1. This resultant reduction in tubular epithelial cell expression of ICAM-1 was associated with diminished Mϕ infiltration and reduced extracellular matrix deposition (Cheng et al., 2000).

1.16.3 Chemokines

Chemokines (an abbreviation of 'chemotactic cytokines') are proteins that both stimulate leukocyte movement (chemokinesis) and direct movement (chemotaxis). Chemokines generate chemokine gradients that provide directional cues for the migration of leukocytes. Chemokines are important in leukocyte maturation in the bone marrow, lymphocyte trafficking and the replenishment of circulating leukocytes. Chemokines play an essential role during inflammation in the multi-step adhesion cascade as they activate integrins and thereby induce firm adhesion of leukocytes to endothelial cells (Luster, 1998; Moser et al., 2004). In addition chemokines exert other functions such as modulation of angiogenesis and involvement in lymphoid organ development. Some chemokines can also activate leukocytes and stimulate degranulation or the release of pro-inflammatory mediators. (Mackay, 2001; Rossi and Zlotnik, 2000).

Chemokines are structurally divided into four families (C, CC, CXC and CX_3C) according to the position of conserved cysteine residues in their primary sequence. Individual chemokines are named using the acronyms of the structural class they belong to, followed by an L (for ligand) and their gene number (Zlotnik and Yoshie, 2000). The nomenclature of the chemokine receptors is analogous to that of chemokines, using the family acronym followed by an R (for receptor) (CR, CCR, CXCR and CX_3CR) and a number that corresponds to the order of its discovery (Murphy et al., 2000). Many chemokines can bind to several different receptors within a subfamily and some chemokine receptors bind multiple chemokines (Rossi and Zlotnik, 2000; Zlotnik and Yoshie, 2000).

The largest family is the CC chemokines in which the cysteine residues lie next to each other. CC chemokines play important roles in recruiting mononuclear cells to sites of inflammation. CCL2 (MCP-1) belongs to this family. CCL2 mainly attracts monocytes but is also a chemoattractant for PMN, DC and T cells. CCL2 binds to the receptor CCR2 and CCL2 plays an important role in the recruitment of Mϕ to the inflamed tubulointerstitium (Sean Eardley and Cockwell, 2005). Other CC chemokines include CCL3 (MIP-1α), CCL4 (Mϕ inflammatory protein-β, MIP-1β) and CCL5 (also called RANTES [regulated upon activation normal T cell expressed and secreted]). CCL5, CCL4 and CCL3 bind to the chemokine receptor CCR1.

The role of CCL2 and its receptor CCR2 in tubulointerstitial inflammation has been extensively studied by using CCL2 or CCR2 deficient mice or function blocking antibodies (Sean Eardley and Cockwell, 2005). Tesch et al induced NTN in CCL2 KO mice and demonstrated that these mice exhibited comparable glomerular Mϕ infiltration injury but significantly less tubulointerstitial Mϕ infiltration, thereby

suggesting that CCL2 mainly directed Mϕ recruitment to the interstitium in this model (Tesch et al., 1999). Wada et al used anti-CCL2 gene therapy in the UUO model and demonstrated reduced numbers of infiltrating CCR2 positive Mϕ associated with diminished tubulointerstitial fibrosis (Wada et al., 2004).

CCR2 blockade during UUO or the use of CCR2 KO mice has demonstrated that the absence of CCR2 ameliorates tubulointerstitial fibrosis (Kitagawa et al., 2004). In contrast, NTN induced in CCR2 KO mice resulted in more severe disease compared to WT control mice despite the reduction in Mϕ infiltration (Bird et al., 2000).

Eis et al demonstrated that CCR1 but not CCR5 mediates leukocyte recruitment and tubulointerstitial fibrosis in the UUO model (Eis et al., 2004). Blockade of CCR1 with the CCR1 antagonist BX471 during UUO also resulted in diminished Mϕ recruitment and reduced tubulointerstitial fibrosis (Anders et al., 2002). In contrast, Topham et al, induced NTN in CCR1 deficient mice and demonstrated that absence of CCR1 resulted in increased Mϕ and T cell infiltration, an enhanced T_{h1} response and more severe glomerulonephritis (Topham et al., 1999).

Lloyd et al administered neutralising antibodies against CCL5 or CCL2 in mice with NTN (Lloyd et al., 1997). Although both antibodies reduced glomerular Mϕ infiltration, only neutralisation of CCL2 reduced glomerular crescent formation and collagen I deposition (Lloyd et al., 1997). The effect of the CCL5 antagonist amino-oxypentane RANTES (AOP-RANTES) in the rat model of anti-Thy 1.1 model of glomerulonephritis was studied by Panzer et al (Panzer et al., 1999). Administration of AOP-RANTES attenuated Mϕ infiltration and reduced collagen IV deposition. In contrast, administration of the RANTES antagonists (AOP-RANTES

or Met-RANTES) in murine immune complex glomerulonephritis resulted in more severe glomerulonephritis despite the diminished glomerular Mϕ infiltration (Anders et al., 2003).

Other monocyte chemoattractants are CXCL8 (IL-8) and CX_3CL1 (fractalkine). Fractalkine is attached directly to the cell membrane via a mucin stalk and the membrane bound protein must be cleaved before it can function as a soluble chemoattractant. In addition, membrane bound fractalkine can function as an adhesion molecule and arrest leukocytes directly upon the endothelial cell surface.

1.16.4 Cytokines

Cytokines are secreted proteins and they exert their actions by both autocrine and paracrine mechanisms. They are a multifunctional proteins involved in activation, immunity, inflammation, cell differentiation and cell growth (Feldmann et al., 1996). Cytokines can either increase or inhibit production of cytokines or other proteins such as chemokines (Gouwy et al., 2005). The main Mϕ-derived cytokines involved in tubulointerstitial inflammation are listed in Table 1-2.

Table 1- 2 Typical Mϕ released cytokines

Pro-inflammatory	Anti-inflammatory	Pro-fibrotic
TNF-α	IL-6	TGF-β
IL-1β	IL-10	
IL-6	TGF-β	
IL-8		
IL-12		
CSF-1		

1.17 Mϕ AND TUBOLINTERSTITIAL INFLAMMATION

Mϕ play a critical role in renal inflammation (Duffield et al., 2005a; Lange-Sperandio et al., 2002; Lange-Sperandio et al., 2006; Sean Eardley and Cockwell, 2005; Tesch et al., 1999) and infiltrate both the glomerular and tubulointerstitial compartments. The tubulointerstitium of the kidney, however, plays an important role in the progression of renal disease in humans irrespective of the initial trigger or site of injury (Bohle et al., 1994; Risdon et al., 1968). The degree of leukocyte infiltration and the severity of tubulointerstitial inflammation correlates with loss of renal function and predicts the risk for progression to end stage renal failure (Bohle et al., 1996; Bohle et al., 1992). Tubulointerstitial disease is characterised by all of the hallmarks of inflammation including leukocyte infiltration, cellular apoptosis and proliferation and the deposition of extracellular matrix. Although renal inflammation may resolve successfully, human disease as well as a number of animal models of renal disease may be characterised by ongoing unchecked apoptosis. This may lead to the excessive loss of key resident renal cells and the eventual development of hypocellular fibrotic scarring characterised by renal tubular atrophy and interstitial fibrosis (Diamond, 1995; Diamond et al., 1998; Gobe and Axelsen, 1987).

A small number of resident Mϕ are present within the normal kidney and prominent Mϕ infiltration is a striking feature of all forms of inflammatory renal disease. Examples of animal models of renal disease characterised by Mϕ infiltration include both immune mediated such as nephrotoxic nephritis (NTN) (Schreiner et al., 1978) and Thy 1 nephritis (Bagchus et al., 1990) and non-immune models such as UUO and renal ablation (Van Goor et al., 1994). Similarly, Mϕ infiltration is a

feature of a range of human diseases including lupus glomerulonephritis, IgA nephropathy and diabetic nephropathy (Schreiner, 1991).

Previous work has examined the role of Mϕ in NTN. Huang et al used micro-encapsulated clodronate to deplete infiltrating renal Mϕ and significantly diminished proteinuria (Huang et al., 1997). Also, clodronate-mediated Mϕ depletion in Thy 1 glomerulonephritis was associated with diminished production of mesangial cell matrix (Westerhuis et al., 2000). These studies indicate that infiltrating Mϕ play a key role in mediating renal inflammation and scarring.

1.18 Mϕ EFFECTORS AND TUBULAR EPITHELIAL CELL INJURY/APOPTOSIS

Mϕ are armed with multiple potentials mechanism to injure and kill pathogens and these are important during infection. In addition, Mϕ may also induce apoptosis of tumour cells (Cui et al., 1994) and various host cells. Elegant studies by Professor Richard Lang's group demonstrated that Mϕ can trigger microvascular endothelial cell apoptosis during the developmental deletion of intraocular vessels in the rodent eye (Diez-Roux et al., 1999; Lang et al., 1994; Lang and Bishop, 1993). Previous work from Duffield et al indicates that Mϕ may induce mesangial cell apoptosis *in vitro* (Duffield et al., 2000; Duffield et al., 2001). In addition, Mϕ may induce apoptosis of vascular smooth muscle cells *in vitro* and this is believed to be potentially important in atheromatous disease (Boyle et al., 2001; Boyle et al., 2002; Boyle et al., 2003).

The mechanism by which Mϕ induce apoptosis in various cell types has been investigated. Inflammatory Mϕ produce myriad pro-apoptotic mediators such as

NO, TNF-α as well as FasL. NO and TNF-a play a role in the induction of apoptosis in both mesangial cells and vascular smooth muscle (Boyle et al., 2002; Boyle et al., 2003; Duffield et al., 2000; Duffield et al., 2001). In addition, Mϕ can produce MMPs capable of degrading ECM and this may disrupt key survival signals imparted to renal cells by ECM (Mooney et al., 1999). Indeed, the degradation of ECM by Mϕ-derived MMPs may indirectly influence the fate of renal cells since tubular cell apoptosis may result from the ECM disruption evident in a murine model of Alport's syndrome (Rodgers et al., 2003).

An accumulating body of data indicate that Mϕ may induce tubular cell apoptosis in both immunological and non-immunological tubulointerstitial inflammation (Duffield et al., 2005a; Lange-Sperandio et al., 2002; Lenda et al., 2003; Tesch et al., 1999). As indicated previously, Tesch et al (Tesch et al., 1999) induced NTN in CCL2 KO mice and demonstrated a significantly reduced tubulointerstitial Mϕ infiltrate that was associated with reduced tubular cell apoptosis. This suggested that CCL2 promoted Mϕ-mediated tubular injury in this model. Although Tesch et al examined the interaction between Mϕ and tubular epithelial cells *in vitro*, they were unable to determine the mechanism underlying the cytotoxic effect of Mϕ but thought that a soluble factor was involved.

The concept that Mϕ may induce renal cell death *in vivo* was additionally supported by recent work in the Centre for Inflammation Research, University of Edinburgh. Duffield et al employed conditional Mϕ ablation to deplete Mϕ numbers in a model of progressive murine NTN (Duffield et al., 2005a). Mϕ ablation was associated with a significant reduction in the level of tubular cell apoptosis. In

addition, Mϕ ablation resulted in diminished proteinuria, improved renal function and diminished tubulointerstitial scarring.

Other researchers have studied the role of Mϕ in the 'non-immunological' model of UUO. Lenda et al induced UUO in CSF-1 deficient mice that exhibit reduced levels of Mϕ infiltration and activation (Lenda et al., 2003). Analysis of the obstructed kidneys of the CSF-1 deficient mice demonstrated a reduced interstitial Mϕ infiltrate that was associated with a reduced level of tubular cell apoptosis. Lange-Sperandio et al obstructed the kidneys of triple E-, P- and L-selectin KO mice and WT control mice within the first 48 hours after birth (Lange-Sperandio et al., 2002). As predicted, triple selectin KO mice exhibited a diminished level of tubulointerstitial Mϕ infiltration and this was associated with reduced levels of tubular cell apoptosis compared to control mice. These combined data strongly suggest that Mϕ play a role in modulating the level of tubular cell apoptosis in the inflamed tubulointerstitium of the kidney (Duffield et al., 2005a; Lange-Sperandio et al., 2002; Lenda et al., 2003). In addition, a striking correlation was found between the severity of the tubulointerstitial Mϕ infiltration and the level of tubular epithelial cell apoptosis (Duffield et al., 2005a; Lange-Sperandio et al., 2002; Lenda et al., 2003).

When I was undertaking the studies described in this thesis, there was very little data available regarding the mechanism involved in Mϕ-directed tubular cell death. Although *in vitro* studies attempting to dissect these mechanisms had been performed there was no clear Mϕ-derived death effector. Lange-Sperandio et al co-cultured cytokine activated J774 Mϕ (a murine Mϕ cell line) with PKSV-PR cells (a murine proximal tubular cell line) and demonstrated that cytokine activated Mϕ

induced significant tubular cell apoptosis (Lange-Sperandio et al., 2003). This study, however, and the previous more limited work by Tesch et al (Tesch et al., 1999) was unable to determine the nature of the Mϕ death effector which remained an undefined soluble mediator. It is pertinent, however, that Lange-Sperandio was unable to demonstrate a role for TNF-α, FasL or TGF-β (Lange-Sperandio et al., 2003).

1.19 CONDITIONAL Mϕ ABLATION MODEL

Identification of the human receptor for diphtheria toxin (DT) (also known as heparin-binding epidermal growth factor (hbEGF) (Naglich et al., 1992), or referred to as DTR for diphtheria toxin receptor) created an opportunity for a unique ablation strategy. The murine form of hbEGF binds DT poorly, but murine cells can be rendered sensitive through transgenic expression of human hbEGF or DTR. Richard Lang's group generated transgenic mice expressing human hbEGF lineage specifically under the CD11b promoter (CD11b-DTR) and demonstrated that cell ablation results from toxin injection (Cailhier et al., 2005). In addition, since DT is a protein synthesis inhibitor this strategy results in the induction of death in both mitotic and terminally differentiated cells. The death mechanism is apoptosis as 65% of the F4/80 positive peritoneal Mϕ are Annexin-V positive 6 hours after DT administration (Cailhier et al., 2005) The generation of CD11b-DTR transgenic mice used in this study have also been used to demonstrate the importance of Mϕ in progressive renal inflammation (Duffield et al., 2005a) and the progression of liver injury and subsequent resolution of fibrosis (Duffield et al., 2005b). This strategy has

also been used to generate transgenic mice in which hepatocytes (Saito et al., 2001) or DC (Jung et al., 2002) may be conditionally ablated.

1.20 NITRIC OXIDE

NO was first discovered as an endogenous vasodilator released from the endothelium to regulate vascular tone (Furchgott and Zawadzki, 1980). Since then knowledge of the biology of NO has increased enormously. NO plays an important role in the regulation of a wide range of physiological processes including angiogenesis, neurotransmission, platelet aggregation, host defense and immunity and modulation of inflammatory responses (Clancy et al., 1998; Moncada and Higgs, 2006; Quinn et al., 1995).

NO is enzymatically generated by NO synthases (NOS), which catalyse the oxidation of the amino acid L-arginine to NO and L-citrulline (Moncada et al., 1989; Palmer et al., 1988). This reaction is dependent on nicotinamide adenine dinucleotide phosphate (NADPH) as co-substrate, calmodulin, flavin mononucleotide (FMN), flavin adenine dinucleotide (FAD) and tetrahydrobiopterine (BH4) as co-factors.

Three different isoforms of NOS in mammals have been isolated. The neuronal NOS (nNOS also called NOS I) is expressed predominantly in neurons in the brain and peripheral nervous system. Endothelial NOS (eNOS, also called NOS III) is mainly expressed by endothelial cells. Both nNOS and eNOS are constitutively expressed and their activity is triggered by calcium binding to calmodulin. The constitutive NOS isoforms generate NO at physiological concentrations. The third isoform of the NOS family is inducible NOS (iNOS, also called NOS II). The iNOS isoform is not detectable in resting quiescent cells but

expression of iNOS can be induced by pro-inflammatory mediators such as cytokines and microbial products. iNOS is expressed in various cell types including Mϕ hepatocytes, chondrocytes, epithelial cells, mesangial cells and smooth muscle cells. Following the induction of iNOS expression, large amounts of NO may be generated over a prolonged period of time. iNOS binds tightly to calmodulin and its enzyme activity is independent of intracellular calcium concentrations. All NOS isoforms contain binding sites for FAD, FMN, calmodulin, heme and BH4.

1.21 Reactive nitrogen oxide species (RNOS)

High concentrations of NO generated by iNOS, can rapidly be oxidised to reactive nitrogen oxide species (RNOS) such as nitrogen dioxide (NO_2), dinitrogen trioxide (N_20_3) and dinitrogen tetraoxide (N_2O_4). N_2O_3 is the active species in biological systems. N_2O_3 can nitrosate (add an NO+ group to) thiols (S-nitrosation) or amines (N-nitrosation) and N_2O_3 can also be excreted as nitrite (NO_2^-) after hydrolysis (Brown and Borutaite, 2006). Under conditions of high NO and oxidative stress, superoxide anion (O_2^-) rapidly reacts with NO to produce the potent peroxynitrite ($ONOO^-$), which is a powerful oxidant. The most severe cytotoxic effects of NO are thought to be mediated by peroxynitrite. Peroxynitrite can trigger DNA breakage, inhibit DNA repair enzymes, cause protein oxidation and nitration and initiate lipid peroxidation (Pacher et al., 2007).

The major thiol in the cells is the reduced form of the cysteine-containing tripepetide gluthathione, and it plays an important role in protecting cells against oxidative stress (Meister and Anderson, 1983). The formation of peroxynitrite can be

inhibited by the removal of superoxide by scavenging enzymes called superoxide dismutases (SOD).

1.22 INHIBITION OF NO AND INOS KO MICE

iNOS mediated NO production can be inhibited by arginine analogues such as N^G-mono-methyl-L-arginine (L-NMMA) and N^G-nitro-L-arginine-methyl ester (L-NAME). These compounds act as competitive non-specific inhibitors of iNOS. Selective inhibitors of iNOS include L-N-imino-ethyl lysine (L-NIL), 1400W, GW5140 and aminoguanidine.

Protective effects of iNOS inhibition by these compounds upon injury and inflammation have been shown in various models of disease: collagen induced arthritis (Cuzzocrea et al., 2002), experimental ischemia-reperfusion injury (I/R) in rats and mice (Chatterjee et al., 2002; Chatterjee et al., 2003; Mark et al., 2005). There is controversy in the literature regarding the participation of iNOS derived NO in experimental glomerulonephritis (reviewed (Cattell, 2002; Trachtman, 2004), where renoprotective effects were demonstrated in some studies (Narita et al., 1995; Ogawa et al., 2002; Satriano et al., 2005), whereas other studies showed increased injury following iNOS inhibition (Weinberg et al., 1994; Westenfeld et al., 2002). Chronic iNOS inhibition by L-NIL and aminoguanidine has been shown to attenuate renal injury in 5/6 nephrectomised rats (Bautista-Garcia et al., 2006), whereas chronic NOS inhibition by L-NAME resulted in aggravated glomerular injury in rats with subtotal nephrectomy (Fujihara et al., 1995). NO production plays an important role in the pathogenesis of adriamycin nephropathy as administration of the iNOS inhibitor aminoguanidine suppressed proteinuria, interstitial cell infiltration and

apoptosis in animals with adriamycin nephropathy (Ozen et al., 2001). Furthermore studies have shown that systemic inhibition of iNOS reduces acute tubulointerstitial injury in rat renal allograft rejection (Vos et al., 2000).

To study the role of iNOS derived NO, mice targeted for the deletion of the *iNOS* gene has been generated (Wei et al., 1995). Work by Wei et al demonstrated that iNOS KO mice were more susceptible to the parasite infection Leishmania major than control iNOS WT mice. Further studies have demonstrated that iNOS KO mice are resistant to to LPS induced septic shock (Wei et al., 1995) , have impaired wound healing (Shi et al., 2001; Yamasaki et al., 1998), and exhibit resistance to bleomycin induce lung injury (Genovese et al., 2005). Hochberg et al induced UUO in iNOS KO mice and demonstrated that these mice developed increased tubulointerstitial fibrosis compared with iNOS WT control mice (Hochberg et al., 2000). In addition a later study from the same group demonstrated that the obstructed kidneys of iNOS KO mice at 7 day exhibited significantly more apoptotic tubular epithelial cells than compared with WT control mice (Miyajima et al., 2001).

1.23 NO DONORS

NO releasing compounds (NO-donors) can be used to study the effects of NO upon apoptosis. Sodium nitroprusside (SNP) is a stable NO-donor, and does not release NO spontaneously (unless exposed to light). SNP requires complex metabolism to generate intracellular NO and membrane-bound proteins are thought to have a role in NO generation (Butler and Megson, 2002). Diazeniumdiolates (also known as 'NONOates') are a group of NO donors, which have an NO dimer linked to a nucleophilic molecule via a nitrogen atom (Maragos et al., 1991). The

NONOates release NO spontaneously in aqueous solutions and examples of these are diethylamine NONOate (DEA/NO) and spermine NONOate (spermine/NO). These NO-donors have clearly defined rates of NO release and range over prolonged periods (first-order kinetics): DEA/NO (half-life [$t_{1/2}$]= 9 minutes) and Spermine/NO ($t_{1/2}$= 39min).

1.24 NITRIC OXIDE AND APOPTOSIS

The generation of high levels of NO can trigger both necrotic and apoptotic cell death. As is often the case for key biological mediators, NO represents a 'double edged sword' and NO has been described as a "Jekyll and Hyde" molecule as evidence indicates that NO possesses both pro and anti-apoptotic properties (reviewed by (Brune, 2003; Choi et al., 2002; Chung et al., 2001; Dimmeler and Zeiher, 1997; Kim et al., 2001b; Liu and Stamler, 1999).

NO generated at low concentrations (picomolar to nanoomolar) by the constitutive isoforms have beneficial and protective effects. However, at high concentrations of NO produced when iNOS is activated and during condition of oxidative stress, NO reacts with superoxide anion to produce peroxynitrite. NO may be highly cytotoxic under these conditions and drive cell death.

The pro-apoptotic signalling cascade of NO is attuned with the apoptotic pathway involving mitochondria (Bosca and Hortelano, 1999; Brown, 1999; Pacher et al., 2007). The RNOS formed from NO can damage DNA directly, and inhibit DNA repair enzymes (Wink et al., 1996). NO evoked upregulation of the tumour suppressor protein p53 has also been described (Messmer et al., 1994).

1.25 AIMS OF THIS WORK

The aim of my studies was to identify the mechanism whereby inflammatory Mϕ modulate renal inflammation by regulating the level of proliferation and apoptosis of tubular epithelial cells. This project therefore involved examining the effect of inflammatory Mϕ upon tubular epithelial cell apoptosis and proliferation *in vitro* and *in vivo*. The main aim was to determine the nature of the Mϕ-derived mediators. My aims were as follows:

1) To use a co-culture strategy to determine whether inflammatory Mϕ modulate renal tubular epithelial cell proliferation and apoptosis *in vitro.*

2) To define the mechanism by which inflammatory Mϕ induced renal tubular epithelial cells apoptosis *in vitro* and to test the *in vivo* relevance of the findings in the model of UUO.

3) To investigate the effect of conditional Mϕ ablation on tubulointerstitial injury and the modulation of tubular cell death *in vivo* in the model of UUO.

Chapter 2.

Methods

2.1 CELL CULTURE

The tissue culture reagents were from Life Technologies and tissue culture plastics were obtained from Costar Ltd or from BD Falcon. All other reagents used in this thesis were from Sigma-Aldrich Company Ltd (unless otherwise stated).

2.1.1 MDCK cells

MDCK cells are a distal tubular epithelial cell line originally derived from canine renal cortex. The MDCK cells were a gift from Jamie Davies (Dept of Physiology, University of Edinburgh, UK).

2.1.1.1 Thawing and passaging cells

A cryovial of frozen cells (MDCK cells or L929 cells, Chapter 2.1.2), which had been stored at liquid nitrogen (-196°C), was placed on dry ice and transported to the tissue-culture laboratory. Cells were thawed by agitating the vial by hand in a 37°C water bath after which the contents were transferred by pipette to a 15ml Falcon tube (BD Falcon, UK) containing 10ml of pre-warmed hanks balanced salt solution (HBSS) in a pre-cleaned tissue culture hood (10% Decon Neutracon with water, Decon Laboratories Ltd, UK), followed by 70% ethanol [EtOH] with water). All work carried out in the tissue-culture hood employed general sterile tissue-culture techniques. The cells were mixed by aspirating and releasing the cells by a pipette and the suspension was centrifuged at 210*g* for 5 minutes (min) at room temperature (RT). Without disturbing the cell pellet, the supernatant was gently aspirated in order to remove the storage solution from the thawed cells. The cells

were then resuspended in 5-10ml of Eagle's minimum essential medium (MEM) containing 1% non-essential amino acids, 100U/ml penicillin, 100μg/ml streptomycin and 10% heat-inactivated foetal calf serum (FCS). The cell suspension was added by pipette to a Costar culture flask containing the above pre-warmed medium (5ml medium for T25cm^2 flask, 10ml for T75cm^2, or 30ml for T162cm^2) and placed inside a 37°C incubator with humidified atmosphere of 5% carbon dioxide (CO_2). The growing cells were maintained in culture by passaging the cells when they were 80-90% confluent. The MDCK cells adopted a cobble stone appearance when confluent and this is a typical morphological pattern for tubular epithelial cells. To passage the MDCK cells, the old media was removed from the culture flask with a sterile pipette and the cells were washed twice with 5-10ml of sterile phosphate buffered saline (PBS) without calcium and magnesium (PBS-/-), to remove divalent cations and serum. The cells were enzymatically digested by adding sterile 1x trypsin- Ethylene-diamine-tetra acetic acid (EDTA) [50 units/ml trypsin and 5mM EDTA] solution (0.5ml for T25cm^2, 1ml for T75 cm^2 and 2ml for T162cm^2 culture flask). The flask was placed in the 37°C incubator for 2-5min, until the cells were detached. Detachment of cells was carefully monitored under the light microscope. Sometimes the flask was gently tapped in order to loosen all the cells. Trypsin was inactivated by adding fresh medium containing 10% FCS (4.5ml for T25cm^2, 9ml for T75cm^2 and 18ml for T162cm^2 flask) and the cell suspension was resuspended. The cells were then split 1:5 or 1:10 by adding an aliquot of the cell suspension to a new culture flask containing fresh pre-warmed medium. The flask was placed in the 37°C incubator so that the cells could adhere. The media was

changed every 2-3 days by aspirating and discharging the old media and replacing with fresh pre-warmed media.

2.1.1.2 **Freezing and storage of cells**

For long-time storage, 80-95% confluent MDCK cells (or L929 cells, Chapter 2.1.2) were detached with trypsin/EDTA and cell number was determined by microscopical counting using a haemocytometer after the trypsin inactivation step. The cells were then centrifuged at 210*g* for 5min at RT and the pellet was resuspended at $2x10^6$ cells/ml in freezing medium, which consisted of 20% dimethylsulphoxide (DMSO) in FCS. The cell suspension was transferred to a cryovial and immediately positioned inside a 'cell-freezing container', which contained iso-propanol, and then placed inside the -80°C freezer. After couple of days the vials were transferred to liquid nitrogen for long-term storage. This freezing procedure ensured gradual freezing of the cells.

2.1.2 L929 cells

L929 cells are a murine malignant fibrosarcoma cell line, which spontaneously secrete Mϕ colony stimulating factor (M-CSF), into the culture supernatant. The L929 conditioned supernatant is used for culturing bone-marrow derived Mϕ (BMDM) (Chapter 2.3). These L-929 cells were maintained in Dulbecco's modified Eagle medium with F12 (DMEM/12) containing glutamax (a stable replacement for L-glutamine) supplemented with 10% FCS, penicillin (100U/ml) and streptomycin (100µg/ml). Cells were grown in Costar T162cm^2 flasks

in 25ml medium and were split 1:30 as described for MDCK cells (Chapter 2.1.1.1) when confluent. The supernatant was harvested, filtered through a 0.45μm filter, aliquoted into 15ml Falcon tubes and stored at -80°C.

2.2 PREPARATION OF PTE CELLS

PTE cells were derived from kidneys of several strains of mice including C57BL/6 and FVB/N mice. The mouse was killed by cervical dislocation (Schedule 1 killing). The animal's coat was washed with 70% EtOH to limit contamination by fur and dander. Using autoclaved instruments, a lateral incision was made in the skin about midway down the abdomen and the skin was removed. The peritoneum was opened carefully and the left and right kidneys were removed and immediately placed in ice cold HBSS containing ABAM (antibiotic antimycotic solution; 100U/ml penicillin, 100μg/ml streptomycin and 250ng/ml amphotericin B). The kidneys could be stored on ice for up to 5 hours, but higher yields of PTE cells were obtained if the kidneys were processed immediately in a sterile pre-cleaned tissue culture hood. The kidneys were decapsulated, bisected and the medulla was removed using autoclaved scalpel and forceps on a sterile petri dish containing fresh pre-warmed HBSS. The kidneys were then transferred to a fresh petri dish containing fresh HBSS and the cortices were finely chopped into pieces that were approximately $1mm^3$ in size. Excess HBSS was gently removed with a sterile pasteur pipette. The chopped tissue was transferred to a Universal tube containing 9ml of sterile filtered digestion mixture, which contained 0.5mg/ml Collagenase type IV and 10μg/ml *DNase I* (Roche Molecular Biochemicals, UK) in HBSS. The mixture was incubated in a 37°C water bath and every 5-10min the mixture was resuspended, in order to

assist the digestion of the kidney pieces. After 20min incubation at 37°C, the mixture was resuspended and then allowed to settle. A 0.5ml sample of the supernatant was removed and transferred to a petri dish. The presence of tubules was observed under the light microscope if the enzymic digestion was adequate. If no tubules were present (or only short stumpy pieces) the kidneys were returned to the water bath for further digestion. Once dispersed long tubular segments pieces were present (Figure 2.1a), the supernatant was transferred to a new Universal tube and the digestion mixture and 10ml of HBSS was added and the tube was placed on ice. After 20min the tubules had settled to the bottom of the Universal tube. The HBSS was gently removed and the tubules were washed with 20ml of fresh HBSS and returned to ice for a further 20min to allow the tubules to settle again. After gentle aspiration of HBSS, the tubules were resuspended in pre-warmed PTE cell medium. This consisted of serum-free DMEM/12 containing 100U/ml penicillin, 100µg/ml streptomycin, 10µg/ml insulin, 5.5µg/ml transferrin, 5ng/ml selenium, 36ng/ml dexamethasone and 25ng/ml EGF. Two digested kidneys were resuspended in a total volume of 12ml PTE cell medium and plated in four Falcon T25cm^2 flasks (3ml cell suspension/flask). The cells were incubated in a humidified atmosphere of 5% CO_2 at 37°C and the media was changed every 2-3 days. After 2 days of culture, a cobble stone morphology characteristic of tubular epithelial cells started to appear (Figure 2.1 b). This typical cobble stone morphology was more apparent in confluent monolayers (after 7-10 days of culture) without evidence of fibroblast contamination (Figure 2.1c).

There was a potential for other cells to grow in the PTE cell cultures since the tubules were digested from whole kidney cortex. However, the selection of PTE

cell growth is favoured by the serum-free conditions and the specific media supplements used. To ensure that the cells maintained their primary cell phenotype and to minimise the risk of EMT (Chapter 1.12.2) the PTE cells were only trypsinised once. After the trypsin inactivation step, the cells were pelleted by centrifugation at 210*g* for 5min at RT. The supernatant was carefully aspirated and cells were washed with 10ml HBSS to ensure that excess FCS was removed. This was repeated once more and the cells were finally resuspended in serum-free PTE medium. Instead of passaging them to new flasks, they were directly seeded into the wells of Costar tissue-culture plates. If the PTE cells were trypsinised beyond the second passage they began to adopt a fibroblast like appearance and this may have been caused by growth factors present in FCS (especially TGF-β) since serum containing medium was used to inactivate the trypsin.

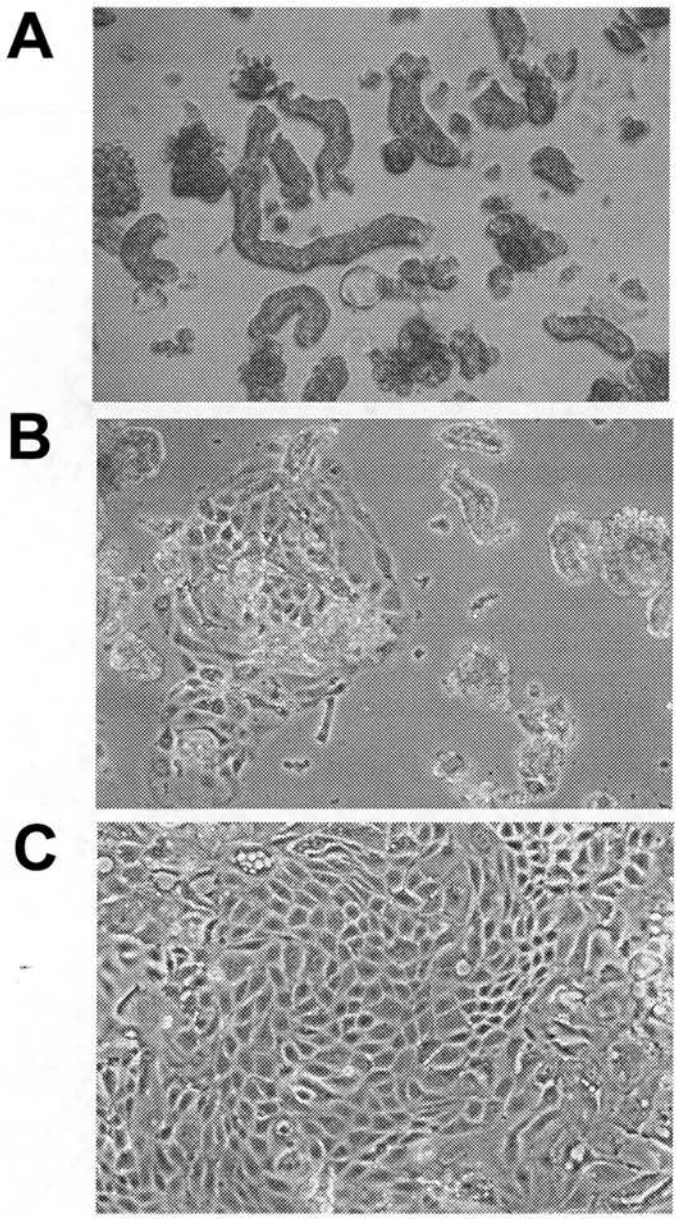

Figure 2- 1 Light photomicrographs showing PTE cell cultures at day 0, day 2 and day 10.
Tubules are visible at day 0 of culture (**A**) and islands of PTE cells start to form after 2 days of culture (**B**). A confluent monolayer of PTE cells is evident after 10 days of culture and exhibits a characteristic cobble stoned morphology, typical of tubular epithelial cells (**C**). (x400 magnification).

2.2.1 Characterisation of PTE cells

The PTE cells were characterised for a tubular epithelial cell phenotype morphologically by inspection under the light microscope, as confluent PTE cells exhibited a cobble stone appearance (Figure 2.2c). They were also characterised immunohistochemically after staining for cytokeratin, vimentin and α-SMA. Tubular epithelial cells should stain positively for cytokeratin, since this is a specific epithelial cell surface marker, while no staining should be observed for vimentin (fibroblast marker) or α-SMA (myofibroblast marker) (Chapter 1.121). Sterile autoclaved glass-cover slips were placed inside the wells of a Costar 24-well plate and 0.5ml of PTE medium added per well. The PTE cells were trypsinised and $1x10^5$ cells/ml were seeded onto the glass-cover slips. The cells were left to grow until they were 70-80% confluent. Unbound cells were washed off with HBSS and the cultures were fixed by adding a mixture of ice-cold methanol (MeOH) and acetone (50:50) solution. After 10min of fixation, the fixative was removed and the coverslips were left to air-dry. Non-specific binding was blocked by incubating the coverslips in a blocking solution consisting of PBS -/- with 2% normal goat serum and 0.1% Triton x100 for 30min at RT. This was achieved by placing a small amount of blocking solution onto a sheet of parafilm and the cover-slips were then inverted, so their cell-containing surface was in contact with the blocking solution. All subsequent incubations steps were performed in this manner. Primary antibodies included monoclonal anti-pan cytokeratin (IgG1 and IgG2a), monoclonal anti-vimentin (clone VIM 13.2, IgM) and monoclonal anti-α-SMA (IgG) or their respective isotype controls. Antibodies were diluted in the above blocking solution (cytokeratin 1/50, vimentin 1/100 and anti-α SMA 1/1000) and incubated overnight at 4°C. The next

day cells were washed x3 with blocking solution and incubated with their appropriate secondary antibodies: FITC conjugated goat-anti-mouse (IgM, 1/100) or Rhodamine red-conjugated goat-anti-mouse (IgG1, 1/100; Jackson ImmunoResearch Europe Ltd, UK). Following 45min incubation at RT the cells were washed x3 with PBS. Finally the coverslips were mounted onto glass-slides with Vectashield containing DAPI (Vector Laboratories, UK). Positive control cells included primary renal fibroblasts (kindly prepared by my colleague Madeleine Vernon). The cells were characterised by fluorescent microscopy. PTE cells did not express α-SMA (data not shown). However the cells stained positive for the tubular epithelial cell marker cytokeratin, (Figure 2-3a) and were negative for the fibroblast marker vimentin (Figure 2-3b). It is likely that the PTE cells were of a mixed tubular origin, since the cells were prepared by digestion of the whole kidney cortex. The tubular segment of the nephron consists of different parts (proximal, distal and collecting duct) and the PTE preparation method that I used did not allow the separation of these different cell types. For the purposes of this thesis, the PTE cells were not characterised for the different tubular origins. Proximal and distal tubular epithelial cell markers are discussed in the introduction (Chapter 1.2).

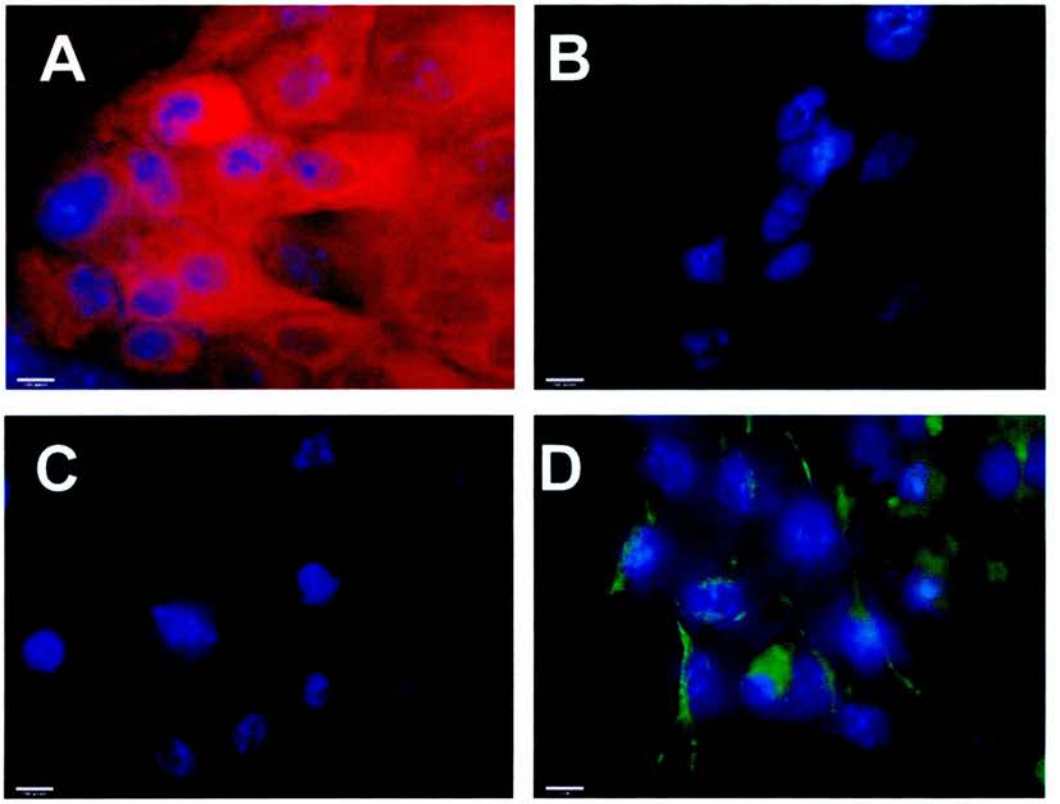

Figure 2- 2 Fluorescent photomicrographs of cytokeratin positive and vimentin negative PTE cells.
PTE cells were prepared and labeled according to Chapter 2.2.1. PTE cells stained positive for the specific epithelial cell marker cytokeratin (**A**) and were negative for the fibroblast marker vimentin (**B**). The specificity of the staining was checked by staining murine primary renal fibroblasts (cytokeratin **C**, vimentin **D**). Isotype control antibodies were negative (data not shown). (x1000 magnification).

2.3 PREPARATION OF BMDM

BMDM were prepared from the femurs of FVB/N or C57BL/6 mice. A 20-25g mouse was killed by cervical dislocation (Schedule 1 killing). The animal's coat was washed with 70% EtOH to limit contamination by fur and dander. Using autoclaved instruments, a lateral incision was made in the skin about midway down the abdomen and the skin was removed from the lower abdomen and legs. The femur was then revealed by dividing the muscles surrounding the bone and removing the tissue surrounding the hip joint. Finally the limb was excised by cutting through the knee joint and the hip joint. The limbs were rinsed with 70% EtOH and placed on ice in a container with HBSS containing 100U/ml penicillin, 100μg/ml streptomycin and transported to a sterile pre-cleaned tissue culture hood. The femurs were placed in a petri-dish containing 70% EtOH and tissue from the bones was removed with a sterile scalpel. Any remaining connective tissue was removed with disinfectant wipes. The femurs were washed in 70% EtOH and transferred to a fresh petri-dish containing 1ml of DMEM/F12. 10ml of DMEM/F12 supplemented with 20% conditioned L929 medium was drawn into a 10ml syringe and connected to a green 25 gauge needle. Using the scalpel blade and holding the femur close to the proximal end, the proximal 2mm of bone was removed. The bone was now held using sterile forceps over a clean Universal container and the needle inserted into the shaft of the bone from its proximal end. By applying gentle pressure medium was passed into the marrow cavity to flush out the marrow cells and the process was repeated for the other bone. The bone became translucent as the red bone marrow was flushed out. The cells were resuspended through a wide 19 gauge needle and cell number was assessed by microscopical counting using a haemocytometer. Typically one mouse

yielded 30-50x10^6 BMDM. The cells from one femur were placed into one 60ml 'non-adherent' Teflon pot (RVetter, Germany) and matured for seven days in a total volume of 40ml of DMEM/F12 medium with 20% conditioned L929 medium, to stimulate differentiation and maturation of Mϕ. 10ml of the medium was replenished every second day with fresh medium.

2.3.1 Characterisation of BMDM

2.3.1.1 Cytospin followed by Diff-quik staining

The maturation and purity of day 7 BMDM was assessed by examination of a cytospin following Diff-quik staining. 100-200μl of a suspension of BMDM (1x10^6 BMDM/ml) was added to the well of a 'cytospin holder' and the cells were cytocentrifuged at 300*g* for 3min in a Shandon Cytospin II (Shandon, UK). The cells were then fixed with 100% MeOH for 2min, followed by staining in the Diff-quik Red solution for 1min and Diff-quik Blue solution (both from Gamidor Ltd, UK) for 1min. All steps were performed at RT. The slides were rinsed with distilled water, left to air-dry overnight and finally coverslipped and mounted (Figure 2-3).

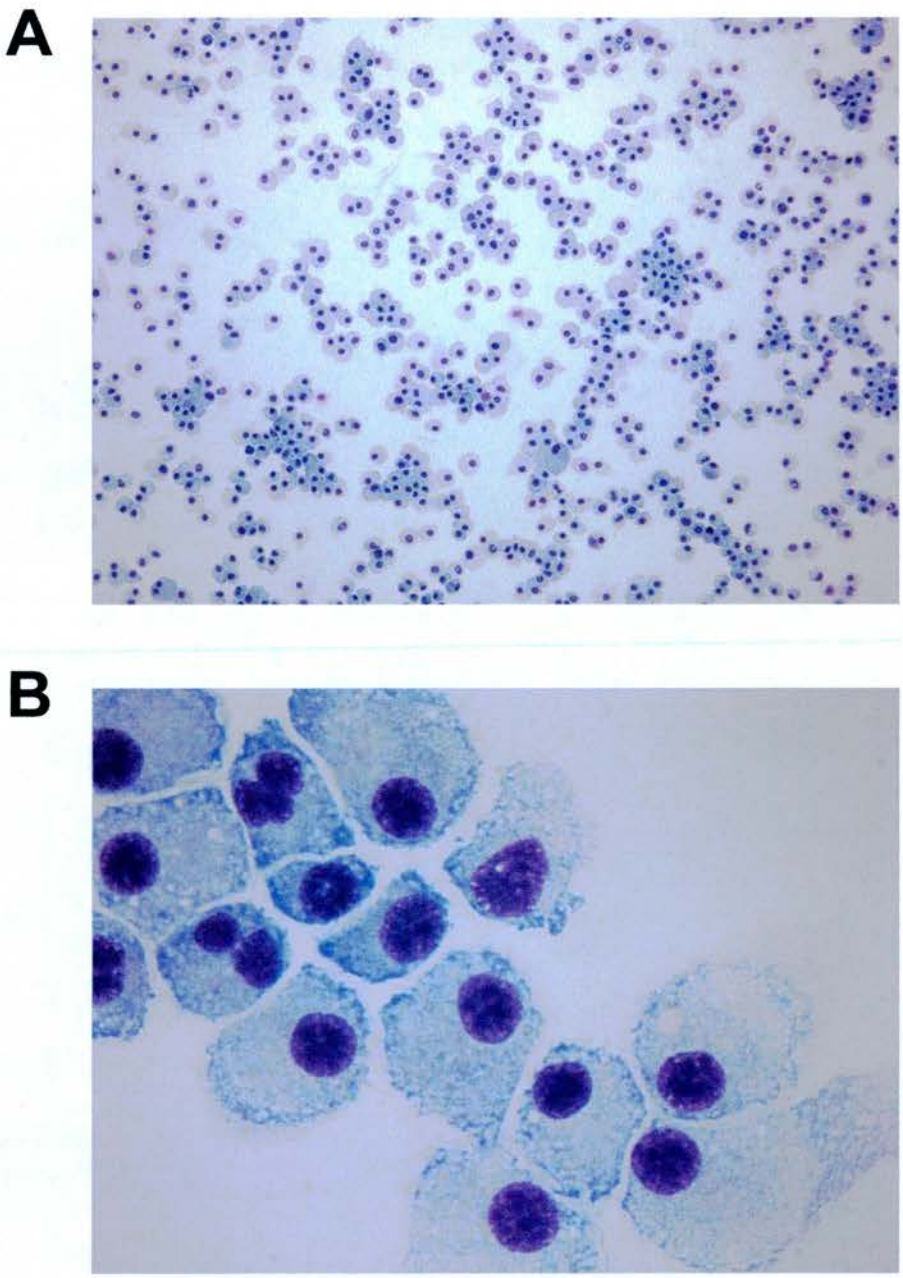

Figure 2- 3 Phenotyping day 7 BMDM morphologically after Diff Quik staining.

Maturation of day 7 BMDM was checked by cytopsin followed by Diff Quik staining. The cells were stained as described in Chapter 2.3.1.1. A low power view (x100 magnification) of many mature BMDM, without any contaminating cells such as PMN (**A**) and a high power view (x1000 magnification) indicating the features of BMDM (**B**).

2.3.1.2 **Flow cytometry**

Mature BMDM were also characterised by flow-cytometric analysis for their expression of F4/80 (a murine Mϕ restricted cell surface glycoprotein) (McKnight et al., 1996). BMDM were also analysed for CD11b, which is expressed by both monocytes and Mϕ. Double labelling with F4/80 and CD11b enables the identification of mature Mϕ, which are $F4/80^{high}/Cd11b^{high}$, in contrast to monocytes which should only express CD11b.

Day 7 Mϕ were harvested from the Teflon pots into chilled polystyrene FACS tubes (BD Falcon, UK) and centrifuged at 300*g* x 5min at 4˚C. The supernatant was carefully discarded and the cells were washed by adding 2ml of cold PBS -/-, followed by centrifugation at 300*g* x 5min at 4˚C. After discarding the supernatant, cells were resuspended ($2x10^5$cells/ml per FACS tube) in 100µl blocking solution (PBS -/- containing 10% mouse serum) and incubated for 30min on ice. Allophycocyanin (APC) conjugated monoclonal rat-anti-mouse F4/80 (IgG2aκ, Caltag Laboratories,UK) and fluorescein isothiocyanate (FITC) conjugated rat-anti-mouse CD11b (IgG2bκ, eBiosciences, UK), both diluted 1/100 in blocking solution, or their respective isotype controls were then added. The cells were mixed gently and incubated on ice for 30min in the dark. Before undergoing flow cytometric analysis, the cells were washed with cold PBS -/- and resuspended in 200-300µl of PBS -/-. Analyses were performed using a FACScan instrument (Becton Dickinson, UK) and the results were analysed with Cell Quest software (Becton Dickinson, UK) or FlowJo software (Treestar, USA). Flow cytometric analysis of day 7 BMDM after staining for F4/80 and CD11b is shown in Figure 2-4.

BMDM derived from iNOS WT and iNOS KO mice were also characterised by flow cytometry for their expression of iNOS. Mature BMDM were placed inside small 5ml Teflon pots ($5x10^5$/pot) and cultured for 24h in the presence or absence of LPS (1μg/ml) and murine IFN-γ (100 U/ml, Peprotech, UK). The BMDM were then harvested and stained for flow cytometry as described in the previous sections with the following modifications. Non-specific binding and permeabilistaion of the cells was achieved by incubating with blocking solution (10% goat serum, 1% Triton X-100, diluted in PBS) for 30min. Primary antibody (polyclonal rabbit-anti-human iNOS which also detects murine iNOS, Transduction Laboratories, UK) or isotype control (rabbit IgG) was diluted 1/100 in 2% goat serum (in PBS-/-) and incubated overnight at 4°C. Following two washes with cold in PBS -/-, the cells were incubated for 30min at RT with secondary antibody (Alexa Fluor®-488 conjugated goat-anti-rabbit IgG (H+L, Molecular Probes, USA, 1/100 dilution in 2% goat serum in PBS-/-). Finally the cells were washed twice with cold PBS-/- and analysed by flow cytometry.

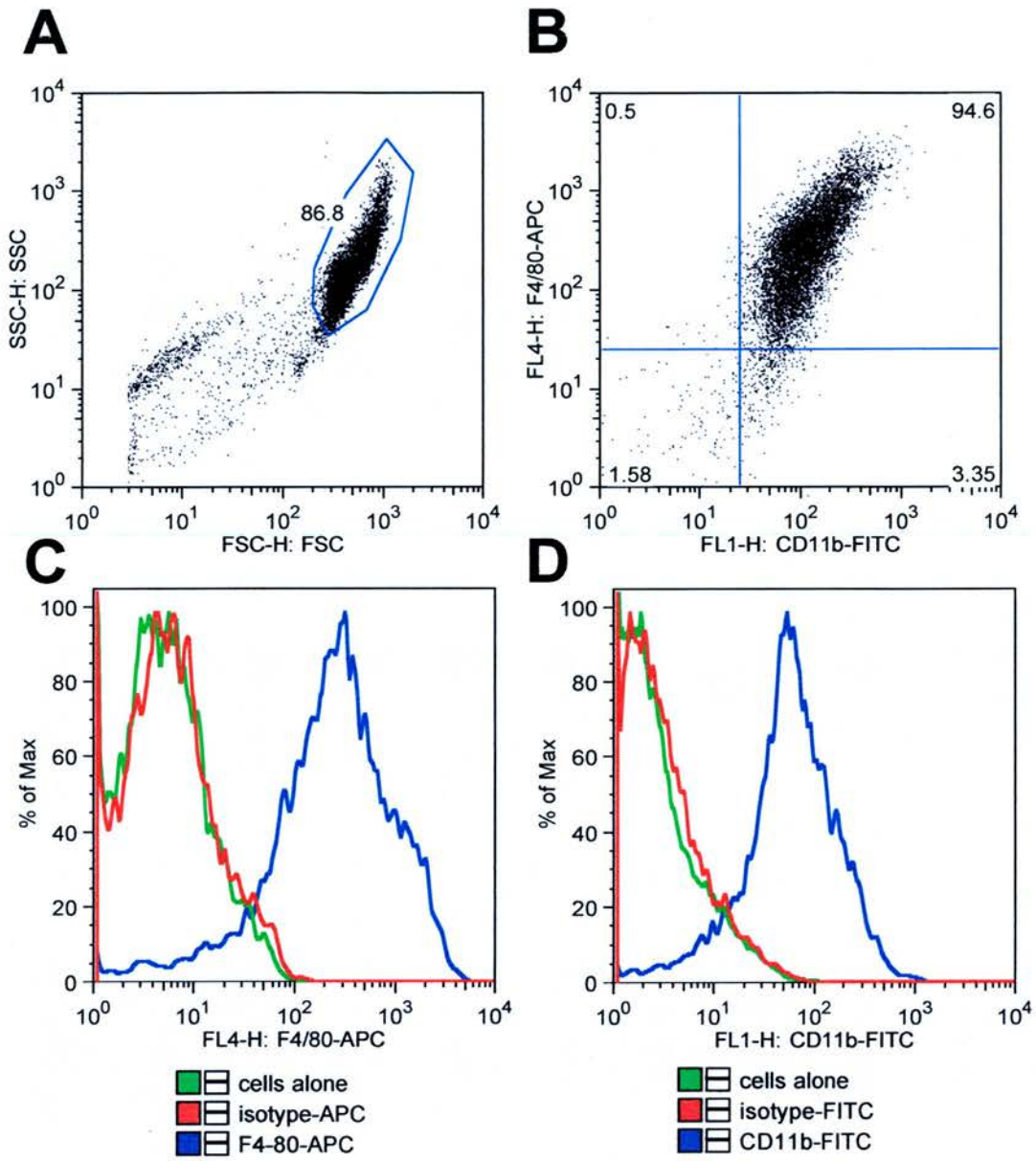

Figure 2- 4 Phenotyping day 7 BMDM by flow cytometric analysis for the expression of F4/80 and CD11b.

Maturation of day 7 BMDM was assessed by staining for the specific Mϕ marker F4/80 together with CD11b and the level of expression was analysed by flow cytometry. FACS dot blot showing the gating in forward scatter (FSC) and side scatter (SSC) (**A**). A pure Mϕ population (94.6%) expressing both F4/80 and CD11b is seen in the upper right quadrant of the FACS dot blot (**B**). Histograms for F4/80 staining (**C**) and CD11b staining (**D**). The cells were stained as described in Chapter 2.3.1.2.

2.4 CO-CULTURE EXPERIMENTS

The interaction BMDM with MDCK cells and PTE cells was studied by using a robust microscopically quantifiable co-culture assay which was previously developed by Jeremy Duffield in our Department (Duffield et al., 2000). A schematic diagram for the co-culture experiment is illustrated in Figure 2-5.

2.4.1 Direct co-culture of BMDM with tubular epithelial cells

MDCK or PTE cells were pre-labelled with fluorescent CellTracker Green whilst in some experiments mature BMDM (7-10 day) were pre-labelled with fluorescent CellTracker Orange (both CellTracker dyes obtained from Molecular Probes, USA). The CellTracker dyes are thiol-reactive fluorescent dyes that are retained by live cells following cell division and do not have any deleterious biological effects on the cells. The dyes are lipid soluble and interact with cellular and serum proteins. 70-80% confluent T25 or T75 flasks of tubular epithelial cells (MDCK or PTE cells) were washed twice with 5ml serum-free medium. This was aspirated and replaced with serum-free medium containing 5µl of CellTracker green stock solution (1mg/ml in DMSO) in 5ml for a T25 flask (10µl of CellTracker green in 10ml for a T75 flask). The cells were incubated for 1h at 37˚C. After this the medium was aspirated and replaced with 5-10ml of medium containing 10% FCS to remove any unbound CellTracker dye. The cells were further incubated for 15min to make sure that all free dye was removed.

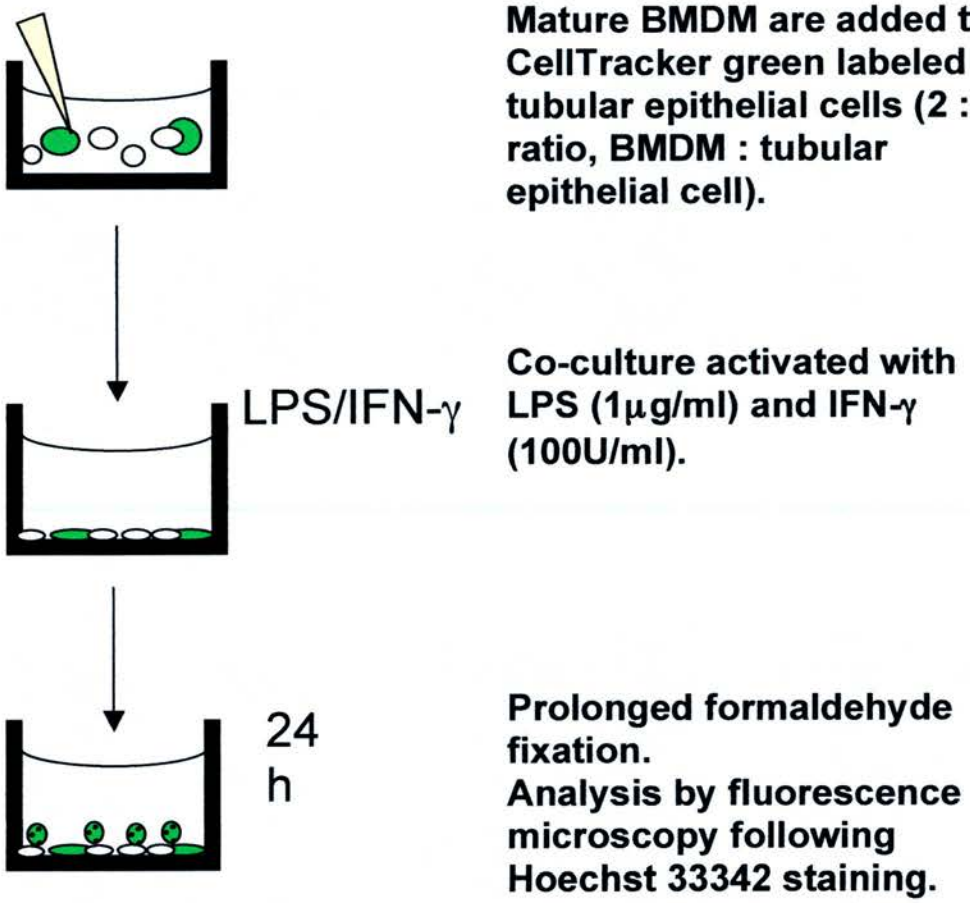

Figure 2- 5 Schematic diagram of the *in vitro* co-culture assay that was used to study the interaction between BMDM and tubular epithelial cells.

The tubular epithelial cells were then trypsinised and cell number was determined after counting with the haemocytometer. Tubular epithelial cells were seeded into the wells of Costar 48-well plates, to cover 60-70% of the well surface: this typically required $1x10^4$ MDCK cells/well and $1.5x10^4$ PTE cells/well. The outer wells of the 48-well plates were not used for experiments since they tended to dry out. To maintain moisture, the outer wells were overlaid with PBS. The MDCK cells were left to adhere for 4h whilst PTE cells were left to adhere overnight. After this the wells were washed twice with HBSS to remove non-adherent cells prior to addition of BMDM.

In some experiments the BMDM were pre-labelled with fluorescent CellTracker orange. BMDM were harvested from the Teflon pots and centrifuged at 300*g* for 5min at RT. The medium was carefully aspirated and the cells from one Teflon pot (i.e. derived from one femur) were resuspended in 5ml of serum-free medium and 5µl of CellTracker orange stock solution (1mg/ml in DMSO) was added. The cell suspension was transferred into a 15 ml Teflon pot and incubated for 30min at RT. After this 10ml of medium containing 10% FCS was added and incubated for further 15min in order to remove any free dye. The cells were then centrifuged at 300*g* for 5min and the medium was carefully aspirated.

For MDCK co-cultures the BMDM were resuspended in DMEM/F12 medium containing 10% FCS but for co-cultures involving PTE cells, the BMDM were washed twice with PTE medium prior to final resuspension in PTE medium containing 1% FCS. BMDM were added to epithelial cells at a ratio of 2 BMDM : 1 epithelial cell. Pilot experiments were undertaken, where the number of BMDM were titrated against a constant number of epithelial cells and various BMDM:

epithelial cell ratios were tested (10:1, 5:1, 4:1, 3:1, 2:1, 1:1 and 0.5:1). Higher BMDM:epithelial cell ratios (ratio 4:1 upwards) exhibited a reduction in total cell number, whilst the level of free apoptotic cells remained low. It was felt that this may reflect Mϕ phagocytosis of apoptotic cells. The highest level of epithelial cell apoptosis was observed at a ratio of 2 BMDM:1 epithelial cell and therefore this ratio was chosen for experiments. Control wells with tubular epithelial cells alone (without BMDM) and wells with BMDM alone were also prepared. MDCK experiments were conducted in DMEM/F12 medium containing 10% FCS and PTE cell experiments were conducted in PTE cell medium containing 1% FCS. In later MDCK co-culture experiments, the BMDM were plated prior to the MDCK cells but this had no effect on the results. However, the PTE cells were always plated prior to the BMDM since the PTE cells proliferated slowly. The BMDM were left to adhere for 3-4h, and non-adherent cells were removed by washing the wells twice with HBSS.

Selected co-cultures were then activated (in a total volume of 300μl/well) with 1μg/ml LPS and 100U/ml of IFN-γ, whilst non-activated co-cultures were exposed to medium alone. After 24h incubation, the undisturbed co-cultures underwent *in situ* fixation with formaldehyde (approximately 4% final concentration) by adding 33μl of 38% formaldehyde solution (BDH, UK) to each well in the fume hood. The plates were fixed for 48h at 4˚C to ensure firm retention of the apoptotic target cells before being processed for fluorescent microscopy analysis.

2.5 PREPARATION OF CONDITIONED SUPERNATANTS FROM BMDM

I undertook experiments involving the transfer of conditioned supernatants from LPS/IFN-γ activated BMDM, in order to determine whether soluble mediators present in the supernatants from activated BMDM could induce apoptosis of tubular epithelial cells. $2.5x10^5$ mature BMDM were cultured in 0.5ml of BMDM media (with 10% FCS for experiments involving MDCK cells) and in PTE media (with 1% FCS for experiments involving PTE cells), in the presence or absence of LPS (1μg/ml) and IFN-γ (100U/ml). After 24h incubation, the BMDM supernatants were harvested and clarified at RT by centrifugation at 300*g* x 5min, followed by centrifugation at 10,000*g* x 5min. Cell-free supernatants from either activated or non-activated BMDM or media with or without LPS/IFN-γ was then added directly to 24-well plates containing tubular epithelial cells ($1.25x10^5$ tubular epithelial cells/well; i.e. a ratio of BMDM conditioned supernatant : tubular epithelial cell ratio of 2:1) and incubated for 24h. The cultures were fixed with 4% formaldehyde and processed for fluorescent microscopy after 48h of pro-longed fixation.

2.5.1 CO-CULTURE USING TISSUE CULTURE INSERTS

In order to study whether direct cell-to-cell contact is important during the co-culture, I used tissue-culture inserts (TCI) to separate the target tubular epithelial cells from the BMDM. The TCI (BD Falcon, UK) have a 0.4μM semi-permeable membrane ($1.6x10^6$ pores/cm^2, effective growth area $0.3cm^2$), which allows the sharing of the same culture medium whilst preventing direct cell contact between cells above and below the insert.

Tubular epithelial cells were cultured on the tissue-culture membrane with BMDM being present in the bottom of 24-well tissue-culture insert companion plates (BD Falcon, UK). This arrangement represents the spatial relationship present *in vivo*. Confluent tubular epithelial cells grown on TCI become polarised with apical and basolateral domains. *In vivo* interstitial infiltrating Mϕ will be adjacent to the basal aspect of tubular epithelial cells. In order to reproduce this spatial arrangement *in vitro*, the Mϕ were placed in the bottom of the wells of the companion plates. Thus the basal aspect of the overlying tubular epithelial cells would be directly exposed to secreted products from the Mϕ. The distance from the cell culture membrane and the bottom of the companion plate well was 0.8mm.

0.9 ml of pre-warmed tubular epithelial cell medium was added to the wells of the companion plate and the tissue-culture insets were gently placed inside the wells. 0.3ml of tubular epithelial cell medium was then added to the insert compartment and the inserts were secured so that the 'flanges' were resting in the notches of each well. The tubular epithelial cells were trypsinised and $5x10^4$ cells/per insert were seeded and incubated until the cultures became confluent. Mature BMDM ($1.25x10^5$/well) were seeded to the bottom of the wells of a fresh companion plate and left to adhere for 3-4 hours. Non-adherent BMDM were removed after washing with HBSS. The confluent tubular epithelial cells growing on the TCI (inside a different companion plate) were also washed with HBSS. Co-culture was established by transferring the TCI to the companion plates containing the BMDM. Tubular cells cultured alone on the inserts (without BMDM) were also set up as controls. Both compartments shared the same medium and selected cultures were activated with 1μg/ml of LPS and 100U/ml of IFN-γ. After 24h incubation the

cultures were terminated by adding 4% formaldehyde solution (final concentration) to both compartments. The cultures were fixed for 48h at 4°C and processed for fluorescent microscopy. A schematic diagram for the steps involved in this experiment is shown in Figure 3-8 (Chapter 3).

2.6 ASSESMEMT OF TUBULAR EPITHELIAL CELL APOPTOSIS AND PROLIFERATION BY INVERTED FLUORESCENT MICROSCOPY

Bisbenzimide Hoechst 33342 is a dye that fluoresces blue at 365nm and this dye is a specific stain for AT-rich regions of double-stranded DNA. Hoechst 33342 labels both apoptotic and necrotic cells whilst live cells are able to 'pump it out'. Fixation with formaldehyde permeabilises all cells thereby allowing the entry of the dye into all cells. After fixation and Hoechst 33342 staining, apoptotic cells are easily discernible from healthy cells as they fluoresce extremely brightly. Identification of cells undergoing mitosis is also possible due to their characteristic chromatin pattern. This staining method of formaldehyde fixed co-cultures was chosen since it allowed the simultaneous detection of apoptotic and mitotic cells as well as the total number of target tubular epithelial cells.

2.6.1 Collection of 'floaters'

Prolonged formaldehyde fixation of the co-culture plates allowed firm fixation and retention of the apoptotic cells. However, there was a possibility that this fixation process could be incomplete and allow a partial loss in cell number since late apoptotic and necrotic cells tend to 'de-adhere' and float in the culture medium. Therefore, after 48h of fixation the formaldehyde solution (containing any

unattached cells termed 'floaters') was collected into FACS tubes. The monolayer was washed with PBS and the washing fraction was also collected to the same tube. To remove the formaldehyde, the FACS tubes were centrifuged at 300*g* x 5min at 4°C and the supernatant was carefully removed inside the fume hood. The floaters were finally resuspended in 200μl of PBS and analysed by flow cytometry. Flow check counting beads were also added to determine the total cell number. Results from FACS analysis showed that only a very minor proportion of the cells were lost. The floaters represented less than 1% of tubular epithelial cells and I decided not to collect the floaters routinely in experiments.

2.6.2 Hoechst 33342 staining of fixed co-cultures

After fixation with formaldehyde, the co-culture was stained with 1μg/ml of Hoechst 333342 and incubated for 15min at RT. The stain was removed and the fixed cells were overlaid with a fluorescent-quenching mounting medium containing 90% glycerol, 10% PBS pH 8.6 and 1-4-diazabicyclo-2-2-2-octane (DABCO) at 5mg/ml. Target tubular epithelial cell apoptosis and proliferation was then assessed by inverted fluorescent microscopy. The advantage of this method was that the co-culture plates could be stored and analysed later.

2.6.3 Inverted fluorescence microscopy

The co-culture plates were analysed by inverted fluorescent microscopy on a Zeiss Axiovert microscope equipped with FITC/GFP, DAPI and Rhodamine filters. (Carl Zeiss Ltd, UK). Target tubular epithelial cells undergoing apoptosis were

identified by their green condensed nuclei when viewed under the FITC filter and their bright pyknotic nuclei when viewed under the DAPI filter (Figure 2-6d). Healthy cells exhibit much larger nuclei which were not condensed and did not exhibit bright fluorescence (Figure 2-6b). Mitotic epithelial cells were discernible by their characteristic chromatin pattern (Figure 2-6e-j). Orange BMDM were visualised under the Rhodamine filter. BMDM phagocytosis of green apoptotic epithelial cells was also identified after inspection under all 3 filters (Figure 2-7).

The following routine was undertaken to ensure that each well was assessed in an unbiased way. After Hoechst 33342 staining, the experimental plates were coded and the lids were removed prior to analysis by fluorescent microscopy. Using inverted fluorescent microscopy (x32 objective), 5 to 8 non-overlapping high power fields (hpf) from each well were randomly and blindly chosen so that at least 200 epithelial cells were counted per well. For each hpf, the number of apoptotic, mitotic and total number of tubular epithelial cells was counted. The number of BMDM that had phagocytosed apoptotic tubular epithelial cells was also recorded. The records were maintained by the 'well code' stamped on the plate (B2, B3 etc) and once all the wells were counted, the lids were matched with the plates to reveal the experimental conditions.

The results were expressed as the number of apoptotic or mitotic tubular epithelial cells per hpf or as a percentage of the total number of epithelial cells (% apoptosis and % mitosis).

Each experimental condition was in triplicate wells and the experiments were performed on at least three separate occasions (unless otherwise stated).

BMDM and primary tubular epithelial cell cultures were derived from at least three different mice (unless otherwise stated).

Sometimes the fluorescent images were captured using a Coolsnap camera (24-bit colour, Princeton Instruments/Acton, UK) connected to the inverted fluorescent microscope. For each hpf, 3 photos were captured under each filter set (red, blue and green), using Open Lab version 3.0 software (Improvision, UK). The images were saved in a TIFF format (Tagged Image File Format) for later analysis with Adobe Photoshop (version 7.0, Adobe Systems, USA). A single image was created in Adobe Photoshop by merging the 3 separate images using automated 'plugins'. The merged images were then scored for apoptosis, mitosis, phagocytosis and total cell number. The advantage of performing image analysis on captured photos allowed the use of a tool called 'opacity'. This facilitated the graded transfer of one colour to another and this was very useful for the quantification of phagocytosis (Figure 2-7).

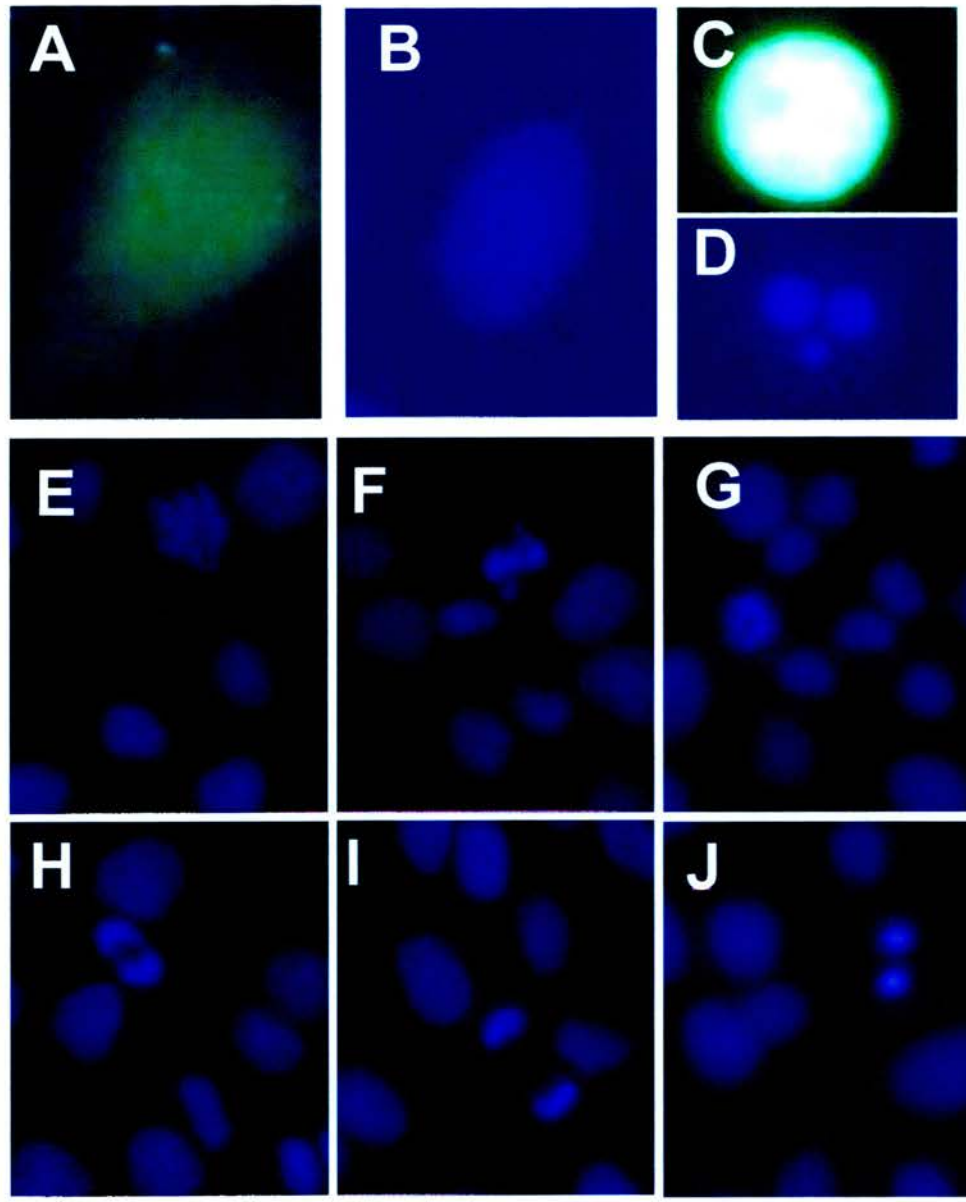

Figure 2- 6 Fluorescent micrographs of healthy, apoptotic and mitotic MDCK cells after Hoechst 33342 staining.
MDCK cell apoptosis and mitosis was analysed by fluorescent microscopy after counterstaining with Hoechst 33342. (**A**) Healthy CellTracker Green labeled MDCK cell. (**B**) Same cell after Hoechst 33342 staining (**C**) Apoptotic green MDCK cell, exhibiting cytoplasmic condensation. (**D**) Same cell after Hoechst 33342 staining. Note the nucleus of the apoptotic cells is much smaller than the healthy MDCK cell. (**E-K**) MDCK cells in different stages of mitosis. (x320 original magnification).

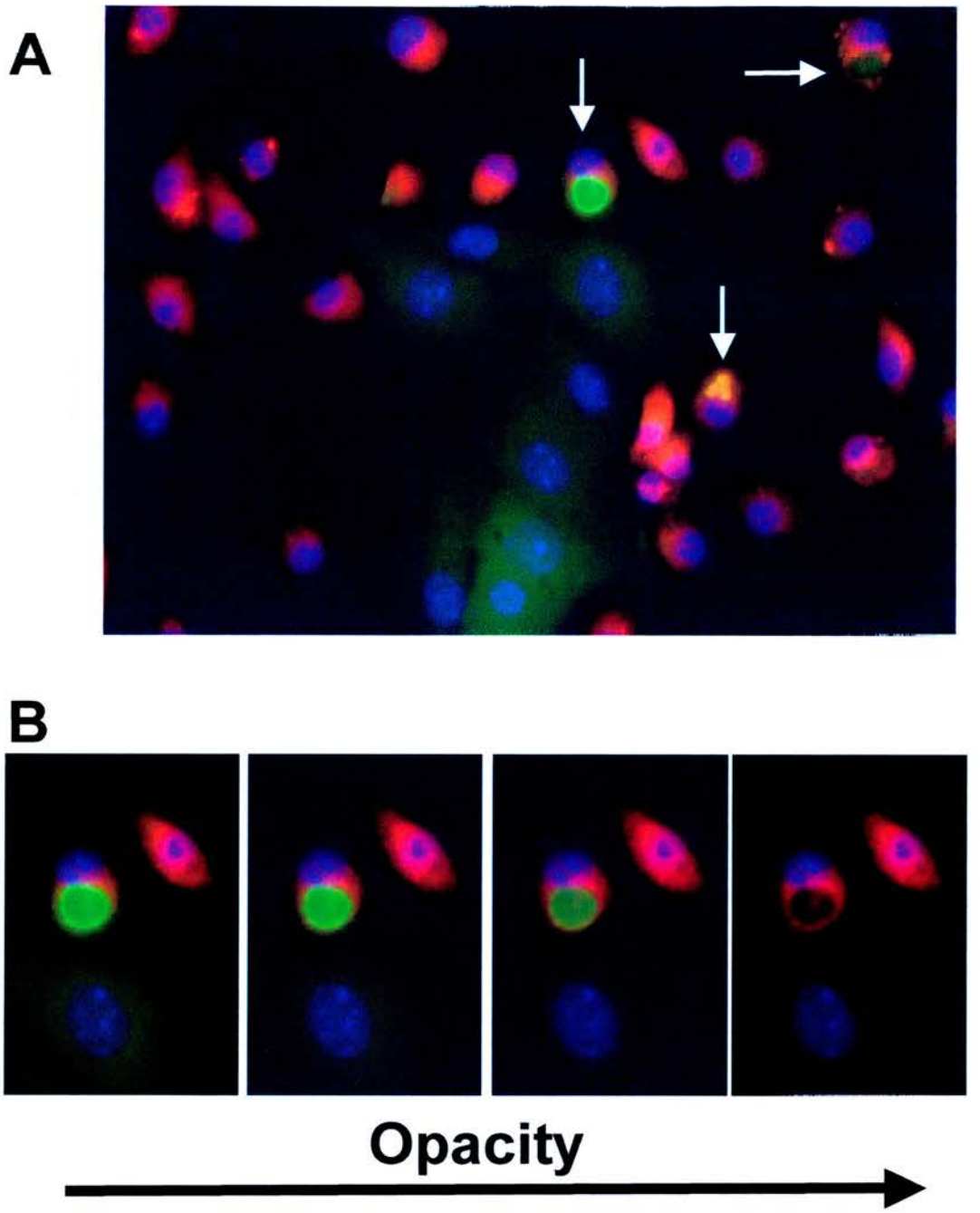

Figure 2- 7 Fluorescent micrographs of activated co-culture of PTE cells with BMDM at 24h.
CellTracker green labeled PTE cells were cultured in the presence of cytokine activated CellTracker orange labeled BMDM. The culture was fixed after 24h incubation followed by Hoechst 33342 staining. Photomicrograph indicating 3 phagocytosed apoptotic PTE cells (examples arrowed) (**A**). The use of the opacity tool is demonstrated (**B**). (x320 original magnification).

2.7 ASSESMEMT OF TUBULAR EPITHELIAL CELL APOPTOSIS BY FACS

The microscopical method for quantifying apoptosis was very time consuming and therefore it was decided to try to develop a rapid and sensitive flow cytometric based assay for quantifying tubular epithelial cell apoptosis after co-culture with BMDM. I decided to use the method of Annexin V staining. I first tested this method on PTE cells alone in the presence or absence of NO-donors before I went on to try to optimise a 4-colour FACS for the co-culture experiments.

2.7.1 Annexin V-PE/7AAD staining

In normal cells, PS residues are found in the inner leaflet of the cytoplasmic membrane. During the onset of apoptosis, PS residues flip to the outer leaflet of the membrane. Annexin V is a calcium dependent phospholipid-binding protein with a high affinity for PS. Translocation of PS is not unique to apoptosis but occurs also during cell necrosis. The difference between these two forms of cell death is that during the initial stages of apoptosis the cell membrane remains intact while the cell membrane of necrotic cells loses its integrity and becomes leaky. Therefore the measurement of Annexin V binding has to be performed in conjunction with a dye exclusion to test to establish the integrity of the cell membrane. The dye 7AAD can be used to indicate membrane disruption. Thus, apoptosis and necrosis can be determined by labelling cells with Annexin V conjugated phycoerythrin (PE) and 7AAD and then analysing by flow cytometry.

$2.5x10^5$ PTE cells were seeded in the wells of 24-well Costar plates containing 500µl of PTE cell medium and left to adhere over-night. The next day,

unbound cells were washed off with HBSS. The cells were then treated with the following NO donors SNP (3mM), DEA/NO (1.5mM) and Spermine-NO (0.1μM), (both NONOates were obtained from Axxora Ltd, UK) for 24h at 37°C. NO-induced apoptosis of PTE cells was assessed by flow cytometric analysis after staining with the Annexin V-PE and 7AAD apoptosis detection kit (Becton Dickinson, UK).

Cell supernatants containing any detached cells were harvested from the wells, placed in FACS tubes and stored on ice. The adherent PTE cells were trypsinised and combined with the detached cells. Cells were pelleted by centrifugation at 300*g* for 5min at 4°C and the cell pellet was washed twice with 1x Annexin V binding buffer (Becton Dickinson, UK), followed by centrifugation at 300*g* for 5min at 4°C. The supernatant was carefully aspirated and the cells were resuspended in 100μl of Annexin V binding buffer. Subsequently 2μl of Annexin V-PE and 2μl of 7ADD (Both from Becton Dickinson, UK) were added per tube and allowed to bind for 10min at RT in the dark. Detection of viable cells (Annexin V-PE negative 7-AAD negative), early apoptotic (Annexin V-PE positive, 7AAD negative), late apoptotic cells that had undergone secondary necrosis (Annexin V-PE positive, 7AAD positive) and necrotic cells (Annexin V-PE negative, 7AAD positive) was performed by flow cytometric analysis. The effect of the inclusion of 3mM of SNP upon PTE cell apoptosis is shown in Figure 2-8. Note that control PTE cells have a high level of cell death.

I also tried to optimise a four-colour FACS assay for assessing PTE cell apoptosis in co-culture experiments with BMDM with the following labelling combinations:

(1) CellTracker green labeled PTE cells (detected in the FL1 channel)

(2) BMDM labeled with F4/80-APC (detected in the FL4 channel)

(3) Annexin V-PE (detected in the FL2 channel)

(4) 7AAD (detected in the FL3 channel)

The 4-colour FACS experiments were problematic. Control non-apoptotic PTE cells bound Annexin V non-specifically and the level of apoptosis in these control cultures was high in comparison to the results obtained with microscopical assessment of apoptosis following Hoechst 33342 staining (data not shown). In addition control BMDM cultured alone also bound Annexin V non-specifically (data not shown) and not all the BMDM were released after the trypsinisation process. BMDM adhere avidly to tissue-culture plastics and I did not want to scrape off the cells as this might affect their membrane function and integrity. The Annexin V-PE/7AAD staining kit is usually employed for cells in suspension and not adherent cell cultures and there is a possibility that the trypsinisation process facilitates the non-specific binding of Annexin V.

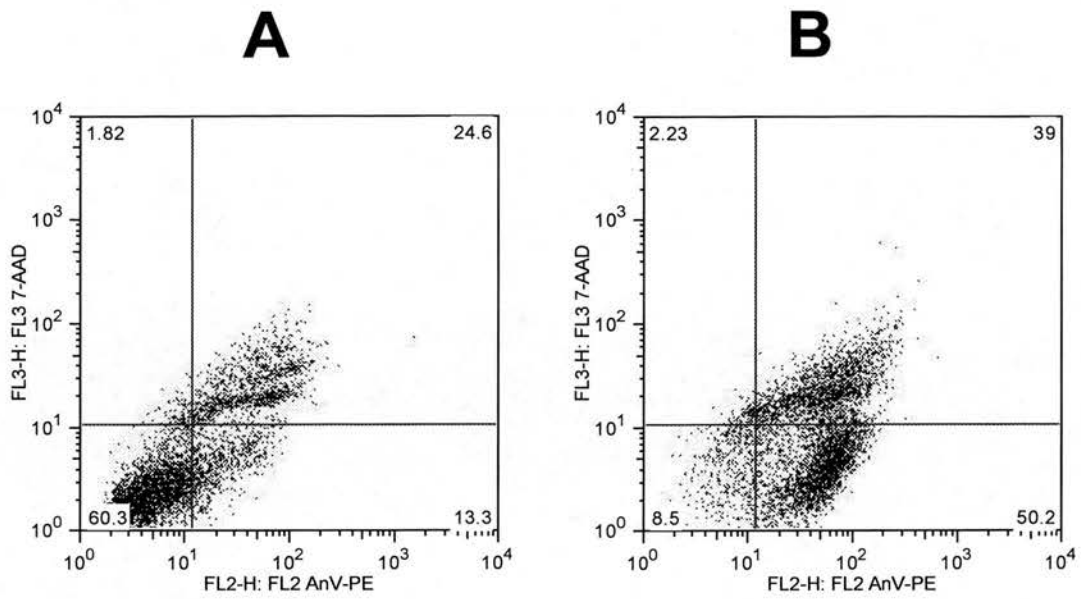

Figure 2- 8 FACS analysis of PTE cell apoptosis after treatment with 3mM SNP.

PTE cells were incubated with PTE medium (control), or in the presence of 3mM SNP for 24h and the percentages of Annexin V-positive (apoptotic) cells were analysed by flow cytometry after double staining with Annexin V-PE and 7AAD (Chapter 2.11). Cells were distinguished as being viable (Annexin V-PE^{neg}/7-AAD^{neg}) bottom left quadrant, early apoptotic (Annexin V-PE^{pos}/7-AAD^{neg}) bottom right quadrant, late apoptotic cells that had undergone secondary necrosis (Annexin V-PE^{pos}/7-AAD^{pos}), top right quadrant and necrotic cells (Annexin V-PE^{neg}/7-AAD^{pos}), top left quadrant. Note that the level of cell death was high (13% early apoptotic and 24% late apoptotic) in control PTE cells (**A**). Treatment with PTE cells with 3mM SNP induced 89% cell death (50% early apoptotic and 39% late apoptotic cells) (**B**).

2.8 EXPERIMENTAL ANIMALS

The following experimental animals were used:

(1) C57BL/6 mice were bred in-house at the University of Edinburgh.

(2) iNOS KO and WT control mice (on the 129/sv background) were obtained from B and K Universal, UK.

(3) Homozygous CD11b-DTR mice (on the FVB/N background) were bred at the University of Edinburgh.

(4) FVB/N mice were obtained from Harland, UK.

All experiments were performed in accordance with the UK Government Home Office regulations. The mice were housed in cages with free access to food and drinking water in a constant temperature room with a 12-hour dark/12-hour light cycle.

2.9 THE MODEL OF EXPERIMENTAL HYDRONEPHROSIS

Experimental hydronephrosis was induced by performing unilateral ligation of the left ureter to induce unilateral ureteric obstruction (UUO). The left ureter of mice was ligated at the ureteropelvic junction under inhalational anaesthesia. (All surgery was kindly performed by Dr. Jeremy Hughes and Experimental Surgeon Spike Clay).

2.9.1 Effect of genetic ablation of iNOS in UUO

The effect of genetic ablation of iNOS in the UUO model was studied by inducing UUO in iNOS KO mice and control iNOS WT mice. The mice underwent surgery at day 0 and were sacrificed on day 7 (n=7 per group) (Figure 2-9a).

2.9.2 Effect of pharmacological blockade of iNOS in UUO

In order to pharmacologically inhibit iNOS activity in the model of experimental hydronephrosis, the specific, irreversible iNOS inhibitor L-NIL was administered in the drinking water. FVB/N mice underwent surgery at day 0 and were treated with either L-NIL or the control inactive isomer D-N6-(1-iminoethyl)-lysine (D-NIL) (n=7-8 per group) in the drinking water (1mg/ml) for 48 hours prior to sacrifice at day 7 (Figure 2-9b). L-NIL and D-NIL were obtained from Fluorochem Ltd (Old Glossop, UK) and were made up fresh in nitrite free water. The dose used in this study has previously been reported to significantly inhibit iNOS activity in murine models of inflammation (Reilly et al., 2002; Westenfeld et al., 2002). Mice were examined daily and the volume of drinking water drinking consumed and body weight were monitored. The mean water consumption of mice from preliminary metabolic cage tests was 3ml/day.

2.9.3 Effect of conditional Mϕ ablation in UUO

UUO was induced in CD11b-DTR mice at day 0 and DT was administered on day 5 after induction of UUO when there is a prominent Mϕ infiltration. In the first Mϕ ablation experiment, DT was administered *i.p* on day 5 (20ng/gBW) and on

day 6 (10ng/g BW) whilst an equal volume of PBS was administered to control animals (n=5 per group, Figure 2-9c). The mice were culled at day 7. In the second Mϕ ablation experiment, DT (25ng/g BW) or an equal volume of PBS was administered *i.p.* on days 5, 6 and 7 (n=5-6 mice per group, Figure 2-9d).

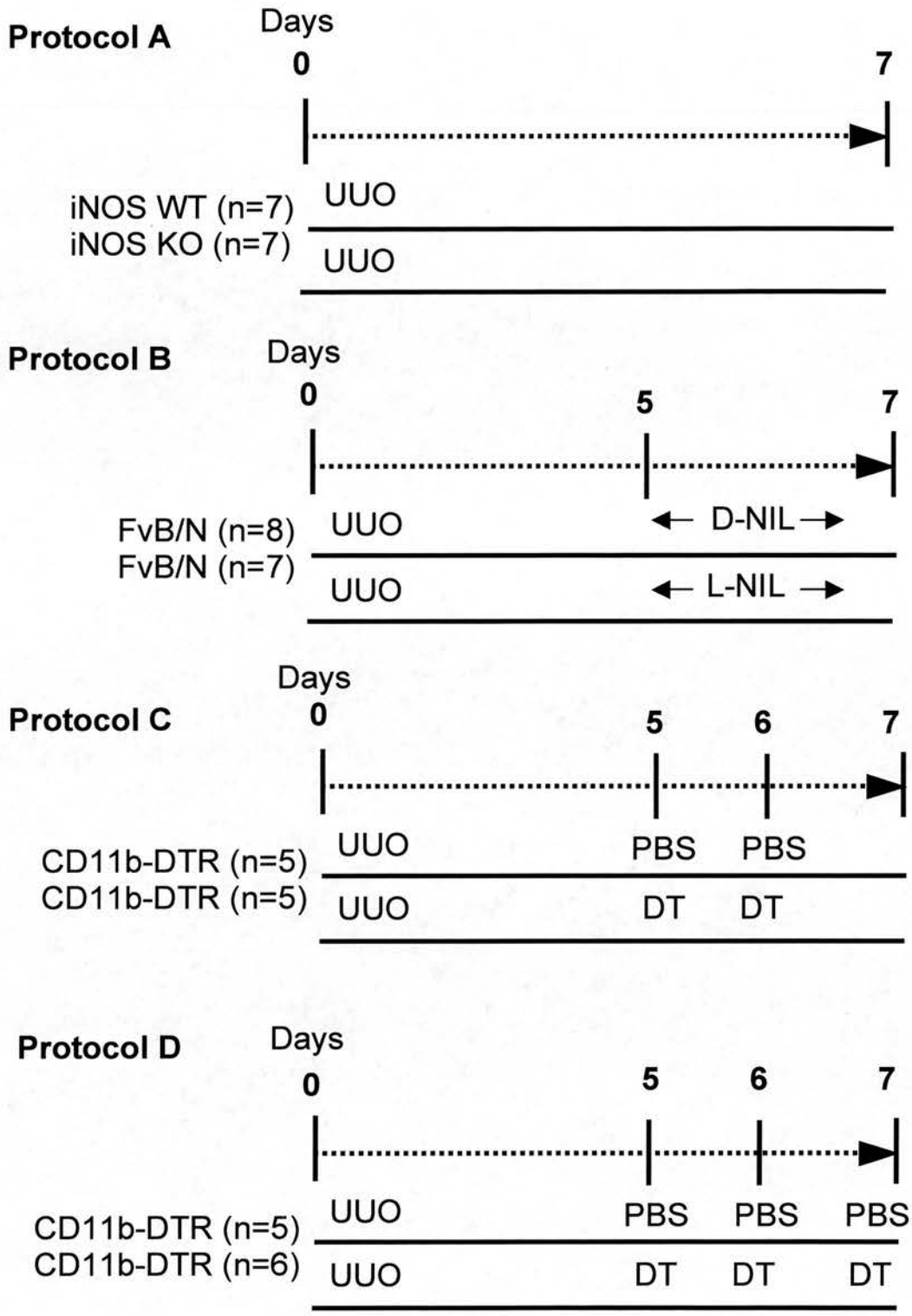

Figure 2- 9 Experimental designs for the UUO studies.

2.9.3.1 **Removal of tissue for histological analysis**

The obstructed hydronephrotic kidneys were removed at day 7 following ureteric ligation and normal non-obstructed kidneys were used as controls. The kidneys were decapsulated, divided sagitally sections and processed in the following order:

1/6 of the kidney was immediately removed for mRNA analysis and placed inside 500µl of RNAlater (Ambion, UK),

1/6 of the kidney was embedded in OCT compound (Bright Instrument Ltd, UK) and snap frozen in liquid nitrogen,

1/3 of the kidney was placed inside a clear glass bottle containing 3ml Methyl Carnoys solution (a fixative comprising MeOH:Chloroform:Glacial Acetic acid in the ratio 60:30:10),

1/3 of the kidney was placed in a plastic vial containing 3ml of 10% neutral buffered formalin solution (4% formaldehyde, 1.5% (MeOH), pH 7.0, Costar, Fischer Scientific, UK).

The RNAlater samples were incubated at 4˚C overnight and then transferred to -80˚C. The OCT snap frozen tissues were transferred to -80˚C. The formalin and Methyl Carnoys biopsies were fixed overnight at 4˚C and the fixative was carefully removed and discarded into special containers in the fume hood the next day. Methyl Carnoys was replaced with 3ml of 100% (MeOH) and the formalin was replaced with 3ml PBS. The biopsies were processed by the Department of Pathology (University of Edinburgh), embedded in paraffin and tissue sections cut as required.

2.10 IMMUNOHISTOCHEMISTRY

Methyl Carnoys fixed tissue was routinely used for the majority of immunostaining. Methyl Carnoys fixed kidney tissue sections of 4μm thickness were deparaffinised by dewaxing in Histoclear solution (Raymond A Lamb Ltd, UK) for 5x3min and rehydrated in decreasing grades of EtOH, 100% EtOH (3x3min), 95% EtOH (2x2min) and 70% EtOH (1x1min).

Endogenous peroxidase activity was blocked by incubating the slides in 3% hydrogen peroxide (H_2O_2) (20ml of H_2O_2 +180ml MeOH, freshly prepared) for 20min. The tissue sections were then washed in PBS (3x2.5min) and the tissue section carefully encircled with a Pap pen (Vector Laboratories, UK). To perform single immunoperoxidase staining, the tissue sections were incubated with the primary and secondary antibodies as indicated below. Antibody dilutions were made in 1% BSA or in ChemMate Antibody diluent (DakoCytomation, UK). The sections underwent three washes in PBS (3x2.5min) between the application of each antibody. Negative controls for immunostaining comprised the substitution of an irrelevant isotype control for the primary antibody. Positive control tissue included sections from diseased mice that were known to express the antigens. All antibodies were titrated so that optimal specific staining with minimal background staining was obtained. The following antibodies were used:

- Rat monoclonal antibody (IgG2b) directed against mouse F4/80, a murine Mϕ marker, (1/500 dilution; Caltag Laboratories, UK) was incubated at 4°C overnight, followed by a mouse-adsorbed biotinylated rabbit-anti-rat IgG (1/1000 dilution; Vector Laboratories, UK) at RT for 30min.

- A monoclonal mouse anti-human-α-SMA (clone 1A4, IgG2a) directed against α-SMA (1/1000 dilution) at 4°C overnight, followed by a biotinylated rat-anti-mouse IgG2a (Zymed Laboratories, USA) at RT for 30min.

- A goat-anti-human type I collagen antibody which also detects murine type I collagen (1/250 dilution; Cambridge BioScience Ltd,UK) at 4°C overnight, followed by a biotinylated rabbit-anti-goat IgG (1/100 dilution, Vector Laboratories) at RT for 30min.

- A goat-anti-human type III collagen antibody which also detects murine type III collagen (1/50 dilution; Cambridge BioScience Ltd, UK) at 4°C overnight, followed by a biotinylated rabbit-anti-goat IgG (1/100 dilution, Vector Laboratories) at RT for 30 min.

- A rabbit-anti-human iNOS antibody which also detects murine iNOS (1/150 dilution, Abcam, UK) at 4°C overnight, followed by a biotinylated goat-anti-rabbit (1/300 dilution, Dako Cytomation, UK) at RT for 30 min.

- A chicken polyclonal TGF-β antibody which also detects murine TGF-β (1/100 dilution, R&D, UK) at 4°C overnight, followed by a biotinylated hamster-anti-chicken IgG (1/300 dilution, Vector Laboratories, UK) at RT for 30 min.

Following washing in PBS (3x2.5min), tissue sections were incubated in horseradish peroxidase (HRP) conjugated avidin D (1/2000 dilution in distilled water; Vector Laboratories, UK) at RT for 20min. Sections were washed in PBS (3x2.5min) and then colour was developed using diaminobenzidine (DAB) without nickel as the chromogen. The developing reaction was terminated by placing the slides in distilled water for 5min and sections were then counterstained with methyl

green (Raymond A Lamb Ltd, UK) for 5min. Sometimes slides were counterstained with hematoxylin for 10s followed by a dip in Scott's tap water (0.1% sodium bicarbonate diluted in distilled water) and rinsing the slides in running tap water for 2-5 min (counterstaining appears blue). Tissue sections were then dehydrated in increasing grades of EtOH: two quick 'dips' in 95% EtOH (following counterstaining with Methyl green), 3x2min in 100% EtOH, followed by clearing in Histoclear 3x3min. The slides were then mounted by adding few drops of histomount (Raymond A Lamb Ltd, UK) and then coverslipped. Air bubbles were removed by gently pressing on the top of the glass cover slip with the wooden end of a cotton bud. The slides were left to dry before analysis.

2.10.1 Double immunofluorescent staining for iNOS and F4/80

Methyl carnoys fixed tissue sections were deparaffinised and rehydrated. All washing steps between antibody incubations consisted of 3x 5min rinses in Tris-buffered Saline (TBS) buffer pH 7.6, and the tissue-sections were protected from light. The sections were first stained with primary iNOS antibody as described for flow cytometric analysis of iNOS expression (Chapter 2.3.1.2) with the following modifications: the secondary Alexa Fluor®-488 conjugated goat-anti rabbit antibody, used to detect iNOS was diluted in TBS. Subsequent staining for F4/80 was carried out as described in Chapter 2.10, but instead of using HRP-conjugated strepavidin the sections were incubated with Alexa Fluor®-568-conjugated strepavidin (1/300 dilution in TBS, Molcecuar Probes, USA) for 30min at RT. Finally the sections were mounted with Vectashield Hard-set mounting medium (Vector Laboratories, UK)

and coverslipped. The sections were left to dry overnight in the dark before analysis by fluorescent microscopy.

2.10.2 Picrosirius red staining

Picrosirius red staining is commonly used for the assessment of tissue fibrosis as the Sirius Red stain is specific for polymeric and monomeric collagen matrix (Junqueira et al., 1979). Picrosirius red staining for collagen was kindly performed on 10μm formalin fixed tissue sections by Susan Harvey (Department of Pathology, University of Edinburgh). The tissue sections were deparaffinised, rehydrated and stained with 0.1% Sirius red F3B solution for 1h at RT. The sections were then washed twice (2x5min) with acidified water (0.5% acetic acid diluted in distilled water). Excess water from the slides was removed with a damp filter paper and the sections were then dehydrated, mounted and coverslipped.

2.11 DETECTION OF APOPTOSIS AND CELL PROLIFERATION

2.11.1 TUNEL staining

Apoptotic cells were detected by the terminal deoxynucleotidyl transferase (TdT)-mediated dUTP biotin nick end labeling (TUNEL) assay (Gavrieli et al., 1992). 4μm formalin fixed tissue sections were deparaffinised, rehydrated in EtOH and endogenous peroxidase activity was blocked as described previously. Antigen retrieval was performed by boiling the slides in sodium citrate (10mM, pH 6.0) for 3min in a 750W microwave. The slides were cooled for 15min in an ice-slurry and rinsed in 2 changes of PBS (2x3min). Excess fluid from the slides was removed by

wiping the periphery of the slide with absorbent paper and the tissue section was carefully encircled with a pap pen. Sections were then incubated with 6.2 μg/ml of proteinase K (2μl of Proteinase K stock [Roche Molecular Biochemicals, UK] in 6ml of sterile water) to strip nuclear protein for a maximum 20min followed by washing in PBS (2x3min). Slides were then pre-incubated in 1x One-Phor-All buffer (diluted with sterile water from the 10x stock, Amersham Pharmacia Biotech, UK) for 5min at RT. The buffer was removed and slides were incubated with TdT reaction mixture [300 enzyme units/ml TdT; (Amersham Pharmacia Biotech, UK) and 0.94mM Bio-14-dATP, Gibco BRL, Life Technologies, UK)] for 1h at RT. The TdT reaction was terminated by washing the slides in PBS (2x3min). The sections were then blocked in 2% BSA in water for 10min at RT followed by washes in PBS (2x3min). Biotinylated ATP was detected after incubating the slides with R.T.U Vectastain Elite ABC Reagent (Vector Laboratories, UK) for 30min at RT. Following washes in PBS (2x3min), the slides were incubated in Tris buffer (0.05M, pH 7.6) for 5min at RT. Colour was developed using DAB with nickel as the chromogen. The reaction was terminated by placing the slides in distilled water for 5min. The sections were counterstained by 'dipping' once in 25% eosin diluted in distilled water (Raymond A Lamb Ltd, UK) and were then dehydrated, mounted and coverslipped. The positive control tissue section was pre-treated with *DNase I* buffer (10mM Tris-HCl pH 7.4; 1mM $MgCl_2$ and 1mg/ml BSA) for 5min at RT. The buffer was removed and 20 Kunitz units/ml of *DNAse I* (Roche Molecular Biochemicals, UK, 1:100 dilution in *DNase I* buffer) was added and incubated for 10min at RT followed by two washes in distilled water (2x3min). The positive control slide was thereafter incubated with the TdT reaction mixture as described above but incubated separately since *DNase*

contamination may result in false positive staining. As a negative control the TdT was omitted. Kidney tissue sections from day 14 obstructed mice were used as positive tissue control since these kidneys showed increased number of apoptotic cells, whereas non-obstructed kidneys served as a negative tissue control as minimal number of apoptotic cells were present.

The TUNEL technique may result in 'false positive' staining if cells are necrotic or proliferating. I therefore regarded cells as 'apoptotic' if their nuclei were TUNEL positive and exhibited an apoptotic morphology characterised by typical nuclear pyknosis and chromatin condensation. The number of TUNEL positive cells in each biopsy was quantified in a blinded fashion by counting the number of TUNEL positive tubular in 20 sequentially selected non-overlapping fields of renal cortex at 100x magnification and expressed as the mean number per hpf.

2.11.2 PAS staining

PAS stained tissue sections were used to quantify proximal and distal tubular epithelial cell apoptosis and proliferation as proximal tubular cells exhibit a characteristic PAS-positive luminal brush border (Hughes et al., 1999). Tissue sections (4μm thickness) of Methyl Carnoys or formalin fixed tissue sections were deparaffinised and rehydrated to distilled water as described previously. Slides were then immersed in PAS solution for 5min at RT followed by three washes with distilled water (3x2min). Slides were then immersed in Schiff's solution for 10min at RT. The reaction was terminated by washing the slides in running tap water for 10min. Slides were counterstained with hematoxylin solution for 1min, rinsed under tap water, dehydrated, cleared and mounted.

Apoptotic proximal and distal tubular epithelial cells were characterised by their pyknotic condensed nuclei whilst mitotic cells were readily identifiable. Proximal and distal cell apoptosis and proliferation was calculated in a blinded fashion by counting the number of apoptotic or mitotic proximal and distal tubular epithelial cells in 20-30 sequentially selected non-overlapping fields of renal cortex at 400x magnification and expressed as the mean number per hpf.

2.12 MORPHOMETRIC ANALYSIS USING COMPUTER ASSISTED IMAGE ANALYSIS

Assessment of immunohistochemical staining can be performed using computerised image analysis (Hunter et al., 2005; Johansson et al., 2001). Computerised image analysis can calculate the number of 'immunostained objects' per section as well as the area of the immunostained objects expressed as a percentage of the total area examined. Interstitial Mϕ infiltration was quantified in a blinded fashion by analysing 10 sequentially selected non-overlapping fields of renal cortex of F4/80 stained tissue sections at 100x magnification using computer assisted image analysis (ImageJ 1.30h National Institutes of Health, USA, http://rsb.info.nih.gov/ij/Java1.3.1_03). Images were digitally captured using the Open Lab version 3.0 software (Improvision, UK). The original colour image was converted to a red, green and blue (RGB) stack and split into 3 separate grey-scale images, each representing red, green and blue, using the ImageJ software. The grey-scale has 256 shades of grey, where 0=is pure black and 255=pure white. The green-grey images were used for analysis. Lower and upper grey-scale thresholds were set to highlight the pixels specific for the detection of F4/80 positive stained area (Figure

2.10b) and for intratubular luminal space (tubular dilatation) (Figure 2.10c). Automated Plug-ins were recorded for the thresholds with the ImageJ software so that the number of thresholded pixels in each image was automatically measured. Mϕ infiltration is expressed as the percentage of tissue surface area positive for F4/80 immunostaining. Interstitial myofibroblast accumulation and interstitial fibrosis were quantified in a similar fashion using tissue sections immunostained for α-SMA and collagens type I, III and IV as well as picrosirius red staining. In addition, I quantified the degree of tubular dilatation (as a percentage of total cortical area) in order to exclude differences between groups as this would result in variation in the amount of interstitial tissue examined.

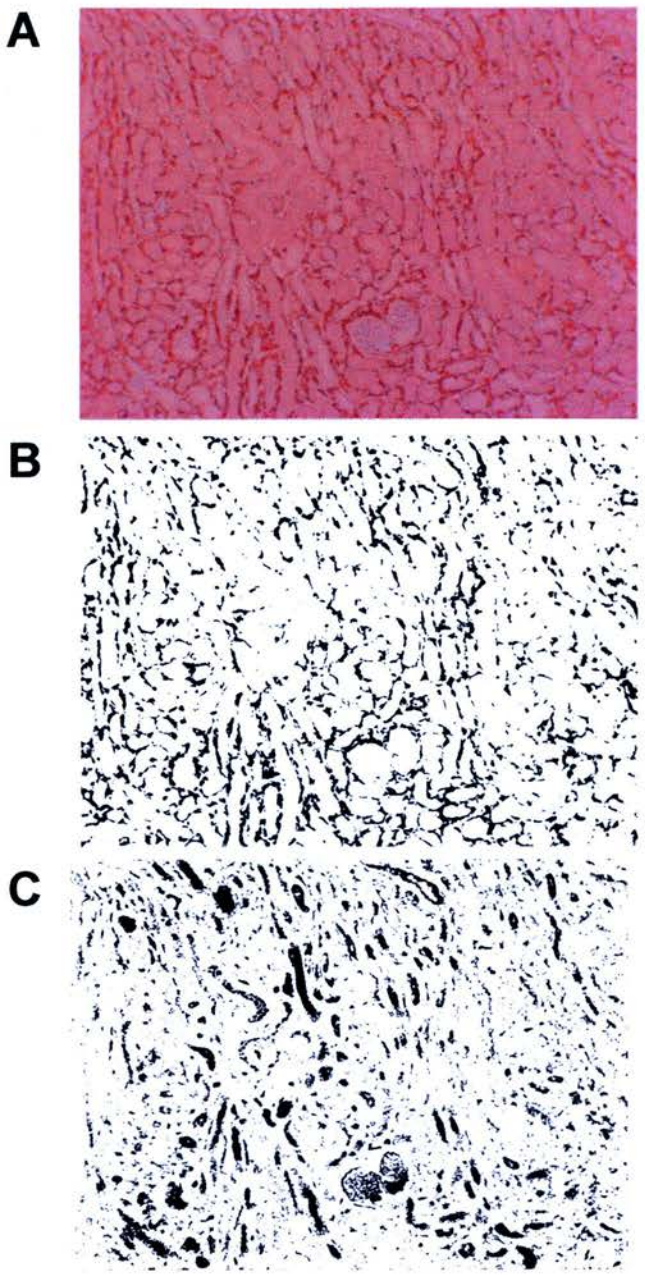

Figure 2- 10 Morphometric analysis of F4/80 stained sections.
The original light bright field image stained for F4/80 is shown in (**A**). F4/80 positive pixels are highlighted in (**B**) whilst pixels detecting tubular space are highlighted in (**C**) (x100 original magnification).

2.13 GRIESS ASSAY

NO is rapidly converted into the stable end products nitrite and nitrate and these may be used as indirect measures of the amount of NO produced. I used the Modified Griess reagent from Sigma to measure nitrite. This assay is based on the reaction between nitrites and the Griess reagent containing sulfanilic acid and N-(1-naphtyl) ethylendiamine, which produces a deep purple chromophoric azo-derivative molecule that absorbs light at 540 nm (Green et al., 1982). Nitrite accumulation in cell-free supernatants from non-activated or cytokine activated BMDM was analysed by the Griess assay. $2.5x10^5$ day 7 mature BMDM were plated in the wells of 24-well Costar tissue-culture plates and left to adhere overnight. The next day, unbound cells were washed off with PBS -/- and the BMDM were incubated in control medium alone or medium containing activating cytokines (LPS [1μg/ml] and IFN-γ [100U/ml] in a total volume of 500μl medium per well. After 24h incubation the supernatants were harvested and clarified by centrifugation. 100μl of cell-free BMDM supernatant was incubated with an equal volume of the Griess reagent in a 96-well flat-bottom Costar assay plate. After 15min incubation at RT, the absorbance (A) was read at 560nm in an automated plate reader. The nitrite concentrations were calculated from a standard curve using 9 standard samples of sodium nitrite (serial dilutions :75, 50, 25, 12.5, 6.25, 3.12, 1.56, 0.78, 0.39μM). The Griess reagent is a sensitive assay between concentrations of 0.5 μM to 65 μM nitrite. A representative nitrite standard curve is shown in figure 2-11.

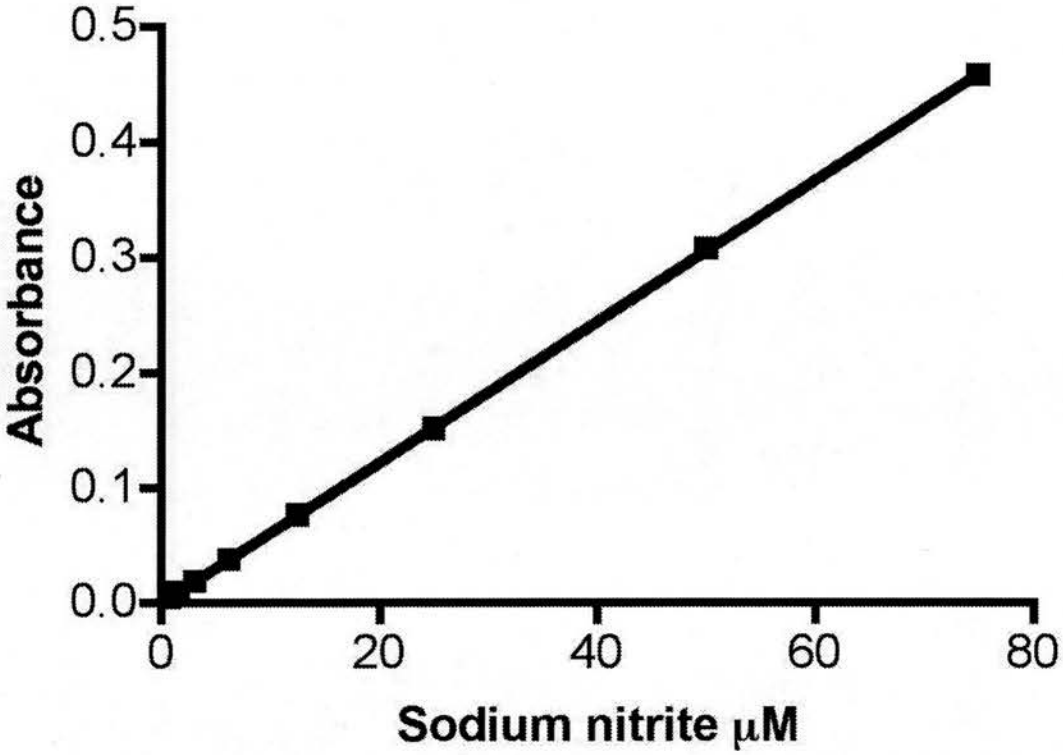

Figure 2- 11 Nitrite standard curve used in the Griess assay.
Standard curve of sodium nitrite against absorbance at 560nm.

2.14 GENOTYPING CD11b-DTR MICE

The genotype of CD11b-DTR mice was determined by PCR using genomic DNA derived from an ear punch. The genotyping primers amplify a 970bp fragment from the DTR-eGFP fusion protein sequence (1.4 Kb total).

2.14.1 Genomic DNA extraction

Ear samples were placed inside 1.5ml eppendorf tubes and incubated in 200µl of lysis buffer (0.2 % SDS, 0.1M Tris-buffer pH 8.5, 5 mM EDTA, 200 mM NaCl and 50µg/ml of proteinase K) overnight at 55°C in a 'shaking incubator'. The next day the samples were centrifuged at 13,000*g* for 10min at RT. The supernatant was thereafter gently transferred to a fresh 1.5ml eppendorf tube and an equal volume of 100% isopropanol was added. The solution was gently mixed by inversion (no vortex) and left undisturbed for 1h at RT in order to give clean DNA). Following centrifugation at 13,000*g* for 10min at RT, the supernatant was carefully removed and 200µl of ice-cold 70% EtOH was added. The samples were then centrifuged at 13,000*g* for 5min at RT and all of the supernatant was carefully removed and left to air-dry until no liquid could be visualised. The DNA was finally resuspended in 50µl of 10 mM TE (Tris-EDTA) buffer and incubated at 50°C for 20min.

The DNA was diluted 1/100 with milli-q-water and the yield and quality of DNA was determined by spectrophotometric analysis at A_{260} and A_{280}.

2.14.2 PCR

100ng of genomic DNA per PCR reaction was used to amplify the 970bp segment of with primers specific for the DTR-eGFP fusion protein and in a separate tube 100ng of DNA/PCR reaction was used to amplify the 450bp segment with primers specific for the human house keeping gene GAPDH which also detect murine GAPDH. All primers were obtained from TAGN (TAGN, UK) and the primer sequences are shown below:

Forward Primer (5'DTR): 5'-TTCCACTGGATCTACGGACC-3'

Reverse Primer (3'eGFP): 5'-TGTCGGCCATGATATAGACG-3'

Forward Primer (GAPDH) 5'-TGCCTCCTGCACCACCAACTGC-3'

Forward Primer (GAPDH) 5'-AATGCCAGCCCCAGCGTCAAAG -3'

The PCR reagents obtained from Qiagen (Qiagen, UK) and each PCR reaction consisted of: 40.2µl milli-q-water, 5µl of 10x PCR reaction buffer, 1µl $MgCl_2$ (2mM final concentration), 0.4µl dNTPs (0.2mM of each), 1µl forward primer (100pmoles), 1µl reverse primer (100pmoles), 1µl of genomic DNA (100ng/reacion) and 0.4µl of Taq polymerase (1Units/reaction). The PCR conditions were as follows: hot start at 110°, initial denaturation (96°C, 2min), 3 step cycling - denaturation (96°C, 30s), primer annealing 56°C and primer extension (72°C, 1.5min) repeated for 35 cycles. The last condition was for final extension at 72°C for 9min.

2.14.3 Preparation of agarose gels and DNA electrophoresis

1% agarose gel was prepared in 1x Tris-acetate-EDTA (TAE) and agarose was dissolved by boiling inside the mirowave. Inside a fume-hood cabinet, ethidium bromide (10μg/ml final concentration) was added once the agarose had cooled to a hand held temperature and then poured into gel electrophoresis plates. Finally a 'well-comb' was inserted and the gel was allowed to set.

10μl of final PCR reaction product was mixed with 5μl of loading buffer dye and in order to estimate the size of the DNA products, 5μl of 1kb ladder (Promega, UK) was diluted with 5ul loading buffer dye. The samples were then loaded into the wells of the 1% agarose gel, which had been placed inside a gel electrophoresis tank containing 1xTAE. Electrophoresis was carried out at 90 volts for 1h and the DNA bands were later visualised after inspection under UV-light. A typical result from PCR of ear genomic DNA from CD11b-DTR mice run on 1% agarose gel containing ethidium bromide is shown in figure 2-12.

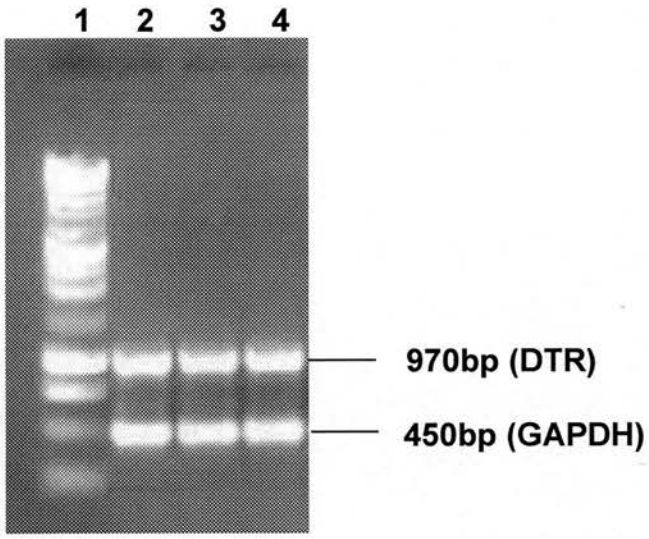

Figure 2- 12 Genotyping CD11b-DTR mice by PCR of genomic DNA run on 1% agarose gel containing ethidium bromide.
Lane 1 shows 1kB ladder and genomic ear DNA from CD11b-DTR mice (lanes 2-4). The expected PCR products are indicated: DTR (970bp) and GAPDH (450bp).

2.15 STATISTICAL ANALYSIS

Results are presented as mean ± standard error. Statistical analysis was based on a series of independent experiments, where each value contains a pooled/averaged intra-assay replicate data (applied to n=/>3 independent experiments. Statistical analysis was performed using GraphPad Prism 4.0 (GraphPad software, USA). The Student's t-test was employed for comparisons involving two groups and statistical differences among multiple groups of data were assessed by one-way ANOVA followed by Student Newman Keuls *post-hoc* test. Correlation between data sets was analysed with Pearsons correlation coefficient. All results are considered significant at $p<0.05$.

Chapter 3.

Inflammatory Macrophages Induce Tubular Epithelial Cell Apoptosis *in vitro*

3.1 INTRODUCTION

Although previous studies have shown that inflammatory Mϕ induce apoptosis of tubular epithelial cells *in vitro* (Lange-Sperandio et al., 2003; Tesch et al., 1999), there is no data regarding the pro-apoptotic mechanism employed by the Mϕ. Lange-Sperandio et al used a co-culture assay involving the murine J774 Mϕ cell line with murine PKSV-PR proximal tubular cells (an immortalised cell line) and although cytokine activated Mϕ induced tubular cell apoptosis *in vitro* the death effector mechanism remained unclear (Lange-Sperandio et al., 2003). This work, however, did not demonstrate any role for TNF-α, FasL, TRAIL or TGF-β. Tesch et al co-cultured murine primary tubular epithelial (PTE) cells with activated murine BMDM but was unable to define the mechanism although the pro-apoptotic mediator was soluble and was present in medium conditioned by activated BMDM (Tesch et al., 1999).

In the studies outlined in this chapter I used a well established microscopically quantifiable *in vitro* co-culture assay previously developed by Dr. Jeremy Duffield in our group to study the cytotoxic interaction between murine BMDM and both MDCK cells (a canine distal tubular cell line) and murine primary tubular epithelial (PTE) cells. In this chapter I will describe the results of these studies and the mechanism by which inflammatory Mϕ induce tubular cell death *in vitro*.

3.2 RESULTS

3.2.1 Cytokine activated Mϕ induce apoptosis of MDCK cells and inhibit MDCK cell proliferation

To determine whether Mϕ could induce apoptosis of MDCK cells, BMDM and MDCK cells were co-cultured for 24 hours. The MDCK cells were pre-labeled with fluorescent CellTracker Green whilst in some experiments mature (7-10 day) BMDM derived from FVB/N mice were pre-labeled with CellTracker Orange. Target MDCK cells were trypsinised and added to 48-well plates such that the adherent cells covered 60-70% of the well surface area. Wells were washed after 4 hours to remove any non-adherent MDCK cells. Mature BMDM were then added to wells containing MDCK cells at a ratio of 2 BMDM to 1 MDCK cell. Control cultures comprising MDCK cells cultured in the absence of BMDM were also prepared. Once the BMDM were adherent (3-4h), the wells were washed and DMEM/F12 medium containing 10% FCS was added. Some wells were activated with LPS (1μg/ml) and IFN-γ (100U/ml); a stimulus previously shown to be optimal for classical Mϕ activation (Duffield et al., 2000). After 24 hours incubation the undisturbed co-cultures underwent *in situ* fixation with formaldehyde for 48 hours in order to ensure retention of all cells including any 'free' apoptotic cells. Fixed co-cultures were then stained with the blue fluorescent DNA binding dye Hoechst 33342, thereby allowing the identification of healthy, apoptotic and mitotic MDCK cells. Using inverted fluorescent microscopy, the number of apoptotic or mitotic MDCK cells was counted and expressed as either the number of apoptotic or mitotic cells per high power field (hpf) or as a percentage of the total number of MDCK cells (% apoptosis and % mitosis respectively).

The first finding was that co-culture of MDCK cells with non-activated BMDM did not induce significant levels of MDCK cell apoptosis (Figure 3-1a) indicating that non-activated BMDM are not inherently cytotoxic. Also, the presence of non-activated BMDM did not significantly affect the level of MDCK cell proliferation (Figure 3-1b) although there was a trend to reduced levels of MDCK cell proliferation. In addition, MDCK cells cultured alone in the presence of the activating cytokines (LPS and IFN-γ) did not exhibit an increased level of apoptosis (Figure 3-1a) or a reduced level of proliferation (Figure 3-1b). However, when MDCK cells were co-cultured with cytokine activated BMDM, there was a significant increase in the level of MDCK cell apoptosis after 24 hours (Figure 3-1a). Apoptotic MDCK cells exhibited characteristic cytoplasmic condensation (Figure 3-2a and 3-2b) and nuclear pyknosis (Figure 3-2c). Cytokine activated BMDM also inhibited MDCK cell proliferation (Figure 3-1b) but there was no difference in target cell number (Table 3-1). The results of experiments depicted in Figure 3-1 are also presented in Table 3-1 but the levels of target MDCK cell apoptosis and mitosis have been expressed as a percentage of total cell number rather than the number of apoptotic cells or mitotic cells per hpf since this is how other investigators have presented their data (Bergin et al., 2000; Tanaka et al., 2005). It should be noted that the level of target cell death in my studies was comparable to previously published work examining Mϕ induction of mesangial and tubular cell death (Duffield et al., 2000; Lange-Sperandio et al., 2003). However, I have expressed the remaining results of the *in vitro* co-culture experiments described in this chapter as the 'number of apoptotic cells or mitotic cells per high power field'. This readout is more robust as it is not confounded by any effect of BMDM upon the total cell number: total cell

number would be reduced by inhibition of cell proliferation and/or the induction of apoptosis. Such an effect on total cell number would change the denominator of the calculation for '% apoptosis'.

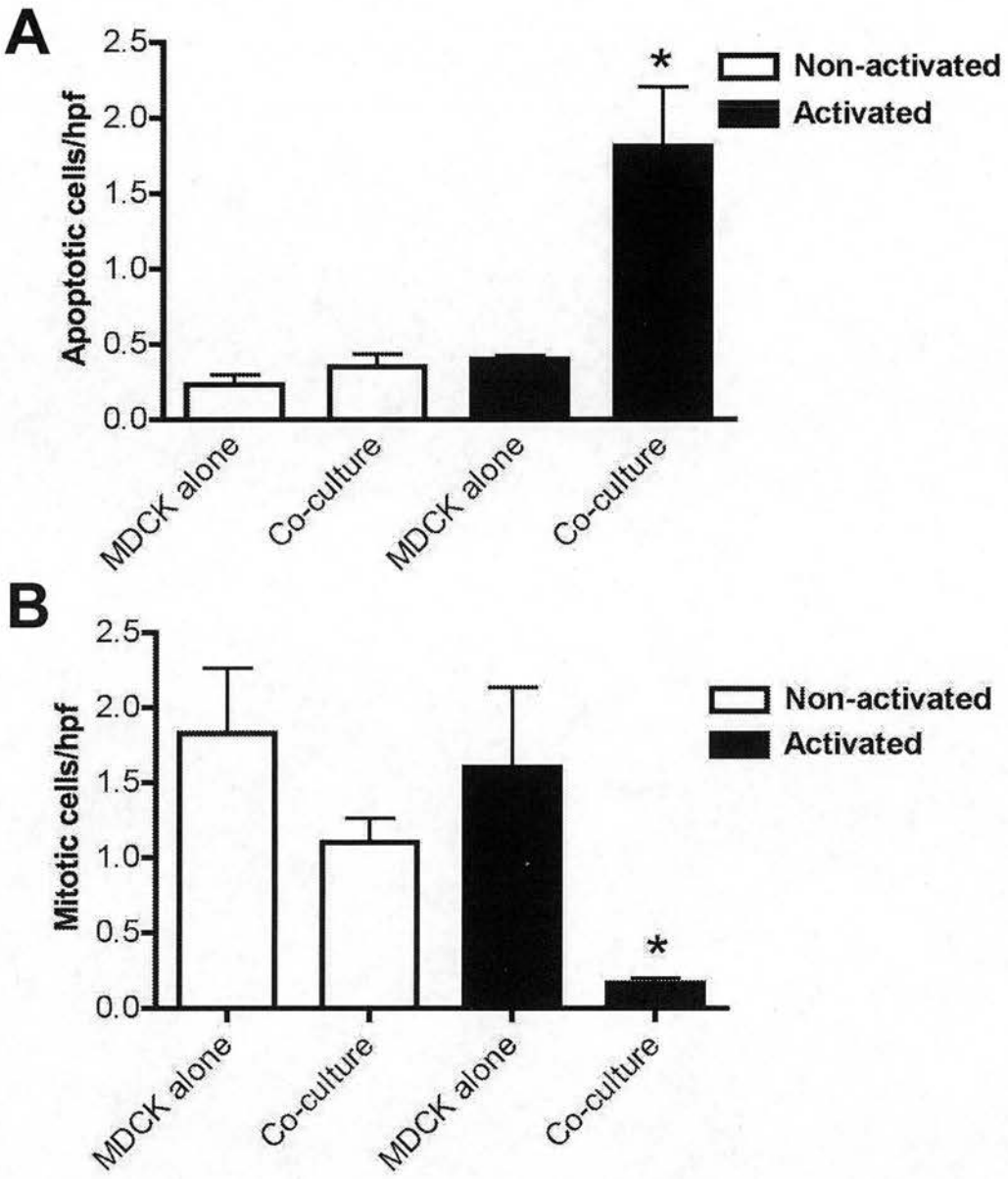

Figure 3- 1 Cytokine activated BMDM induce MDCK cell apoptosis and inhibit MDCK cell proliferation.

MDCK cells were cultured alone or in the presence of mature BMDM from FVB/N mice (BMDM : MDCK cell ratio= 2 : 1) in the presence or absence of LPS (1µg/ml) and IFN-γ (100U/ml). After 24h of incubation the co-culture was fixed with formaldehyde solution. Following counterstaining with Hoechst 33342, the level of MDCK cell apoptosis and mitosis was scored by fluorescence microscopy. Cytokine activated BMDM induce significant MDCK cell death (**A**) and inhibit MDCK cell proliferation (**B**) *$p<0.05$ vs non-activated co-culture, (n=4).

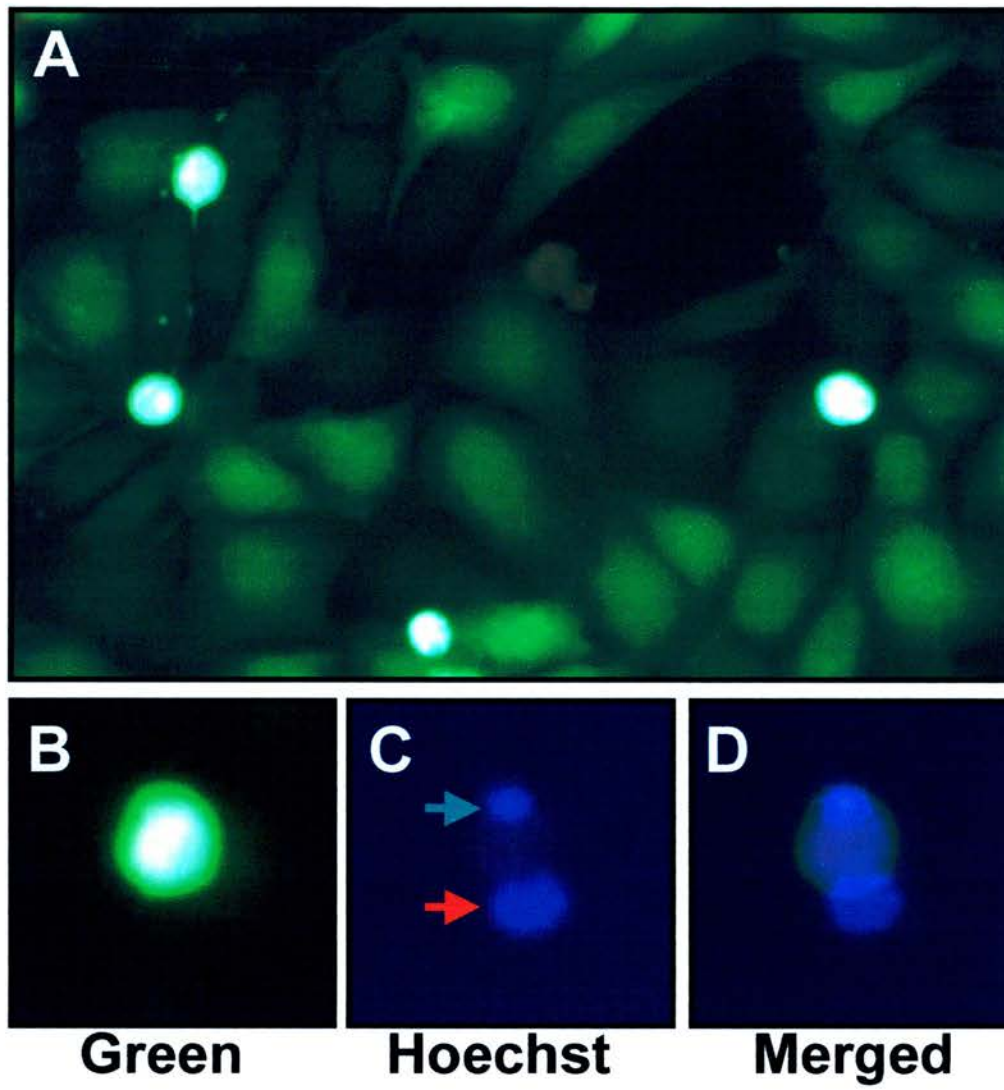

Figure 3- 2 Fluorescent photomicrographs of activated co-culture of BMDM and MDCK cells.
CellTracker green labeled MDCK cells were cultured in the presence of cytokine activated mature unlabeled BMDM from FVB/N mice. After 24h incubation the co-culture was fixed with formaldehyde solution and counterstained with Hoechst 33342. (**A**) Low power view (x100 magnification) of bright green apoptotic MDCK cells exhibiting cytoplasmic condensation. (**B**) High power view (x320 magnification) of one green apoptotic MDCK cell. (**C**) The nucleus of a rounded apoptotic MDCK cell is pyknotic (green arrow). The nucleus of an adjacent unlabelled BMDM is also evident (red arrow). (**D**) The merged image demonstrates the close proximity of the BMDM to the MDCK cell.

Table 3- 1 The effect of cytokine-activated BMDM upon MDCK cell apoptosis, proliferation and cell number at 24h.

	Non-activated	Activated
% Apoptosis		
MDCK cells alone	0.96 ± 0.3%	1.4 ± 0.3%
Co-culture	1.5 ± 0.3%	12.3 ± 4.1%*
% Mitosis		
MDCK cells alone	7.2 ± 3.0%	4.6 ± 1.1%
Co-culture	4.5 ± 0.6%	0.90 ± 0.5%*
Cell number per 5 hpf		
MDCK cells alone	148 ± 44	168 ± 50
Co-culture	113 ± 19	94 ± 26

*$p<0.05$ vs non-activated co-culture (n=4)

3.2.2 BMDM-derived NO is an important mediator of MDCK cell apoptosis, but does not modulate MDCK cell proliferation

Previous work in the Centre for Inflammation Research indicated the involvement of NO in the induction of mesangial cell apoptosis (Duffield et al., 2000). I employed two approaches to determine whether Mϕ-derived NO also induced apoptosis of MDCK cells. First, I used potent pharmacological inhibitors of NO production in co-culture experiments with MDCK cells. In addition, I determined the cytotoxic effect of BMDM derived from either iNOS KO mice or iNOS WT mice in co-culture experiments with MDCK cells.

3.2.2.1 Cytokine-activated BMDM produce NO

I initially determined the level of NO production from cytokine stimulated BMDM derived from different strains of mice. BMDM from FVB/N, C57BL/6, iNOS WT and iNOS KO mice were plated onto 24 well-plates ($2.5x10^5$ mature BMDM/well) and left to adhere overnight. The cells were washed and cultured in 0.5ml of DMEM/F12 media containing 10% FCS and some wells were activated with LPS (1μg/ml) and IFN-γ (100U/ml). After 24h incubation, the BMDM supernatants were harvested and clarified by centrifugation. The generation of NO was determined by the Griess assay which measures nitrite; a stable product of NO release. Non-activated BMDM do not produce significant amounts of NO. In contrast, cytokine-activated BMDM of all strains of mice with the predictable exception of iNOS KO mice produced significant amounts of NO (Table 3-2). It is of interest, however, that activated iNOS KO Mϕ did produce NO (Table 3-2). The reasons underlying this are unclear but there is a possibility that other NOS isoforms

such as eNOS could be upregulated, which generate NO less efficiently (Wei et al., 1995). It should be noted that previous work by Jeremy Duffield also demonstrated that cytokine activated BMDM from commercially obtained iNOS KO mice (also from B and K Universal, Hull) generate NO. Indeed, cytokine activated iNOS KO BMDM exhibited a 13-fold increase in the level of NO production compared to non-activated control iNOS KO Mϕ (Duffield et al., 2000).

I also cultured cytokine activated FVB/N BMDM in the presence or absence of the non-competitive NOS inhibitor Nitro-L-arginine methyl ester hydrochloride (L-NAME), (concentration range 100μM-2mM). Nitrite generation by activated FVB/N BMDM was significantly reduced by the inclusion of the non-competitive NOS inhibitor L-NAME (Table 3-3).

Table 3- 2 Nitrite produced by BMDM after 24h.

	Non-activated	Activated (LPS+IFN-γ)
FVB/N BMDM	54.5 ± 5	2038 ± 130*
C57BL/6 BMDM	61 ± 12	1811 ± 42*
iNOS WT (129/sv) BMDM	50 ± 10	2093 ± 99*
iNOS KO BMDM	29 ± 8	588 ± 115*

Nitrite accumulation μM/10^6 cells *p<0.05 (n=5) vs non-activated.

Table 3- 3 The effect of L-NAME on nitrite production by activated FVB/N BMDM at 24h.

	μM nitrite/10^6 cells
Non-activated	41 ± 9*
Activated (LPS+IFN-γ)	1672 ± 113
2 mM L-NAME	356 ± 17*
1 mM L-NAME	607 ± 19*
0.5 mM L-NAME	656 ± 17*
0.2 mM L-NAME	774 ± 18*
0.1 mM L-NAME	1036 ± 19*

*p<0.05 (n=3) vs activated.

Since the Griess analysis demonstrated that cytokine activated iNOS KO BMDM were able to produce nitrite, I assessed the level of iNOS expression by flow cytometry and immunofluorescence. Flow cytometric analysis for iNOS expression demonstrated that non-activated iNOS WT BMDM (Figure 3-3a) and iNOS KO BMDM (Figure 3-3c) did not express iNOS. However, following cytokine activation (LPS+IFN-γ) for 24h, the level of iNOS expression was markedly increased in activated iNOS WT BMDM (Figure 3-3b). Cytokine activated iNOS KO BMDM also expressed iNOS (Figure 3-3d) although the flow cytometric profile suggested that the expression of iNOS was limited to a sub-set of BMDM derived from iNOS KO mice. Furthermore, immunofluorescent staining for iNOS indicated that the level of iNOS expression in activated iNOS KO BMDM was significantly less (Figure 3-4d) than that evident in activated iNOS WT BMDM (Figure 3-4b).

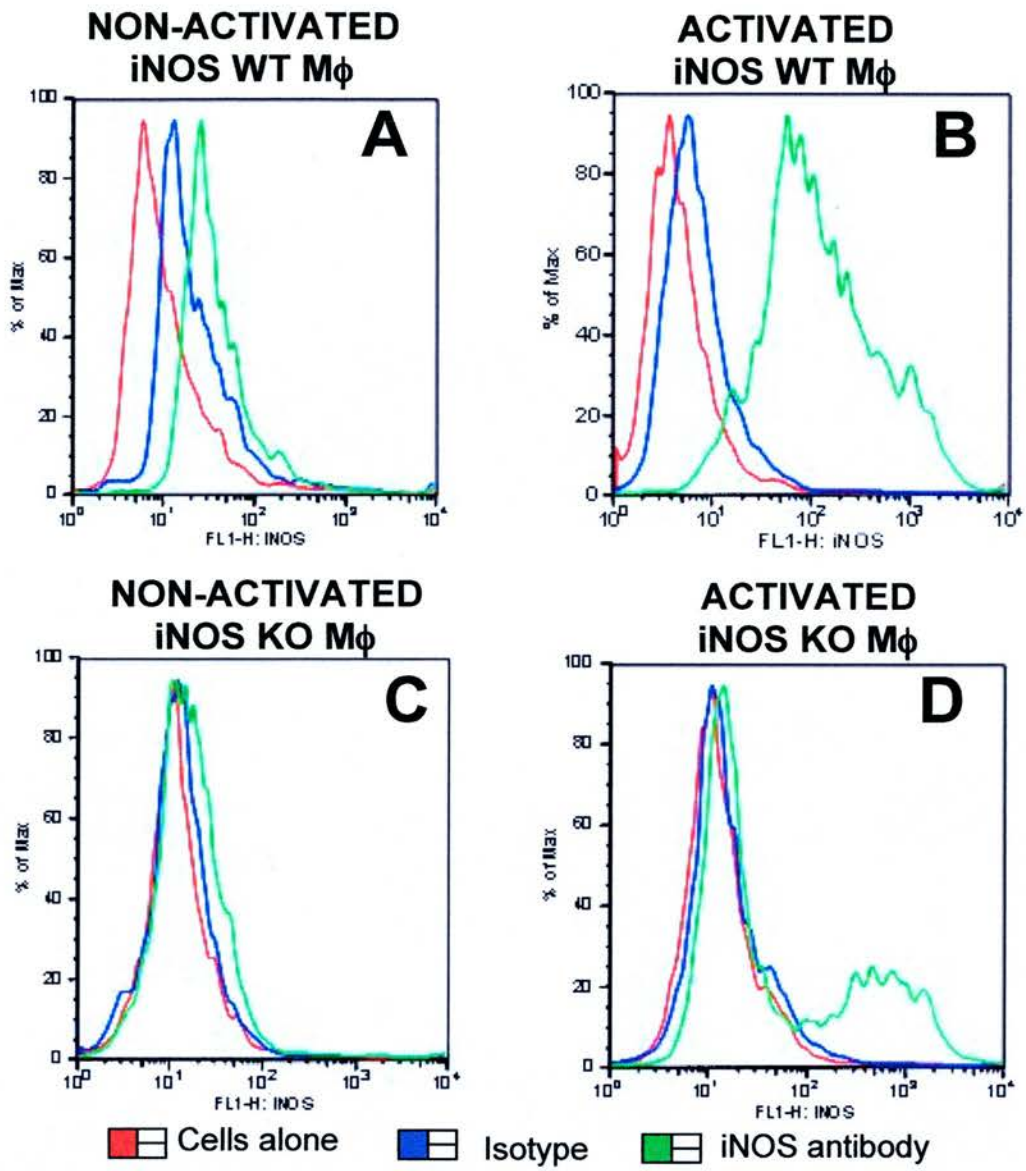

Figure 3- 3 Phenotyping iNOS WT BMDM and iNOS KO BMDM by flow cytometric analysis of iNOS expression.

Mature BMDM from iNOS WT and iNOS KO mice were cultured for 24 h in the presence or absence of LPS+IFN-γ. The BMDM were stained with rabbit-anti-human iNOS antibody or an isotype control, followed by an Alexa-488 conjugated secondary antibody. Flow cytometric analysis of iNOS expression showed that non-activated iNOS WT BMDM (**A**) and iNOS KO BMDM (**C**) do not express iNOS. There was a marked increase in the level of iNOS expression in activated iNOS WT BMDM (**B**). Note that activated iNOS KO BMDM also expressed iNOS although the level of expression was significantly less than iNOS WT BMDM (**D**).

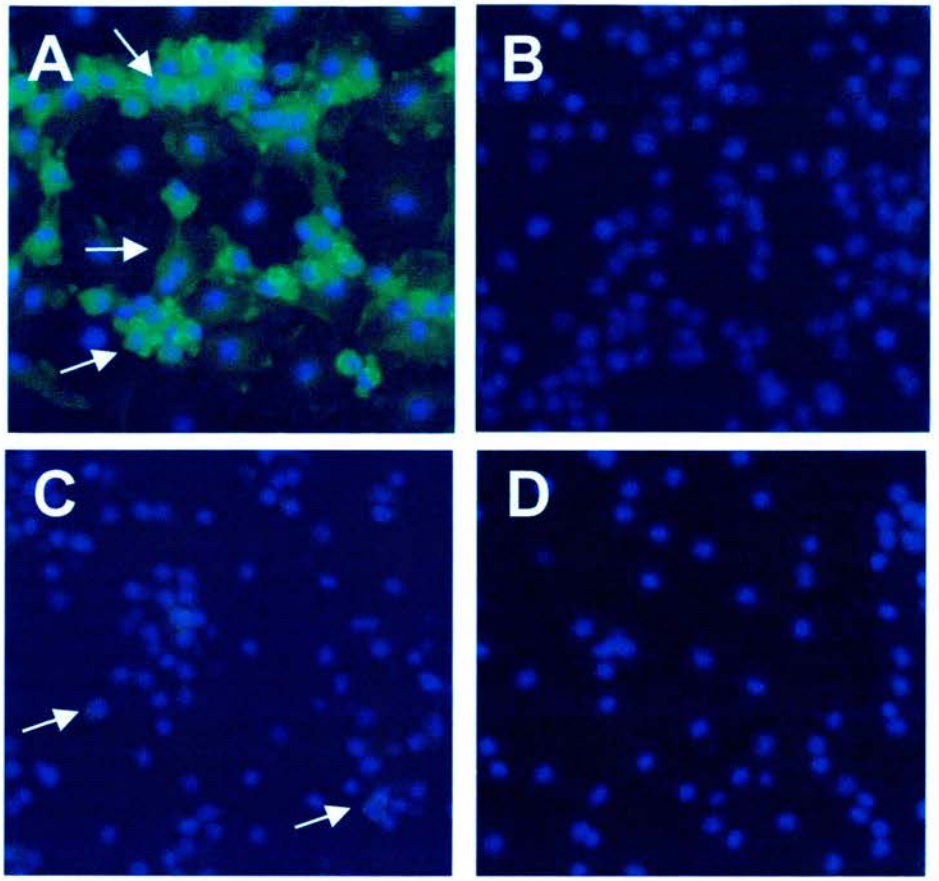

Figure 3- 4 Phenotyping iNOS WT BMDM and iNOS KO BMDM by immunofluorescence staining for iNOS.
Mature BMDM from iNOS WT and iNOS KO mice were cultured for 24h in the presence of LPS+IFN-γ. The BMDM were stained with rabbit-anti-human iNOS antibody (**A**) and (**C**) or an isotype control (**B**) and (**D**), followed by an Alexa-488 conjugated secondary antibody. The level of iNOS expression was evaluated by immunofluorescence microscopy after counterstaining with Hoechst 33342. Cytokine activated iNOS WT BMDM strongly express iNOS (examples arrowed) (**A**), compared to isotype control antibody (**B**). Occasional expression of iNOS is evident in some cytokine activated iNOS KO BMDM (examples arrowed) (**C**), whereas no immunofluorescent staining is evident in iNOS WT or iNOS KO BMDM stained with an isotype control antibody (**B**, **D**). (x320 original magnification).

These experiments establish that cytokine (LPS+IFN-γ) activated BMDM produce significant levels of NO and that activated iNOS KO BMDM produce significantly less NO. My data does, however, indicate that a sub-set of activated iNOS KO BMDM can express iNOS protein and generate NO in response to stimulation with LPS and IFN-γ. I then wished to determine whether BMDM-derived NO was involved in the induction of MDCK cell apoptosis. I therefore performed co-culture experiments with MDCK cells and BMDM derived from either iNOS KO mice or control iNOS WT mice. In addition, pharmacological inhibition of NO was achieved by the addition of the non-competitive NOS inhibitor L-NAME to the culture medium. The co-cultures were established as previously described.

Co-cultures of activated iNOS WT BMDM and MDCK cells exhibited a 3.5 fold higher level of MDCK cell apoptosis compared to co-cultures of MDCK cells with activated iNOS KO BMDM (Figure 3-5). In addition, cytokine activated iNOS KO BMDM did not induce apoptosis above the background level evident in cytokine treated MDCK cells alone, thereby suggesting a key role for BMDM-derived NO in the induction of MDCK death (Figure 3-5). Furthermore, the cytotoxic effect of activated iNOS WT BMDM was completely abrogated by the inclusion of the non-competitive NOS inhibitor L-NAME (final concentration 200μM), thereby reinforcing the importance of NO as a death effector in these cytokine activated co-cultures (Figure 3-5). Importantly, inclusion of the control isomer D-NAME (final concentration 200μM) did not prevent the cytotoxic action of cytokine activated iNOS WT BMDM (Figure 3-5).

MDCK cell proliferation was significantly inhibited by co-culture with BMDM with the anti-proliferative effect being independent of cytokine activation of BMDM with LPS/IFN-γ (Figure 3-6). Furthermore, this anti-proliferative effect was unaffected by the inclusion of the NOS inhibitor L-NAME in the co-culture or the use of iNOS WT or KO BMDM (Figure 3-6). This indicates, in contrast to previous work examining the effect of cytokine activated BMDM upon mesangial cells (Duffield et al., 2000) that NO was not involved in the modulation of MDCK cell proliferation. It is interesting, however, that my previous experiments demonstrated no significant reduction in MDCK cell mitosis in non-activated co-cultures (Figure 3-1b). It should be noted that these experiments still demonstrated a trend towards a reduced level of MDCK cell mitosis in non-activated co-cultures. Previous work suggest that MDCK cell proliferation may be modulated by TGF-β (Nicolas et al., 2003; Yang et al., 1998) and it is possible that non-activated iNOS WT and KO BMDM secrete more TGF-β than non-activated BMDM derived from FVB/N mice. I did not pursue this observation as the main focus of these studies was the investigation of BMDM-mediated tubular cell apoptosis. Lastly, no difference was evident in total cell number in these experiments (Table 3-4).

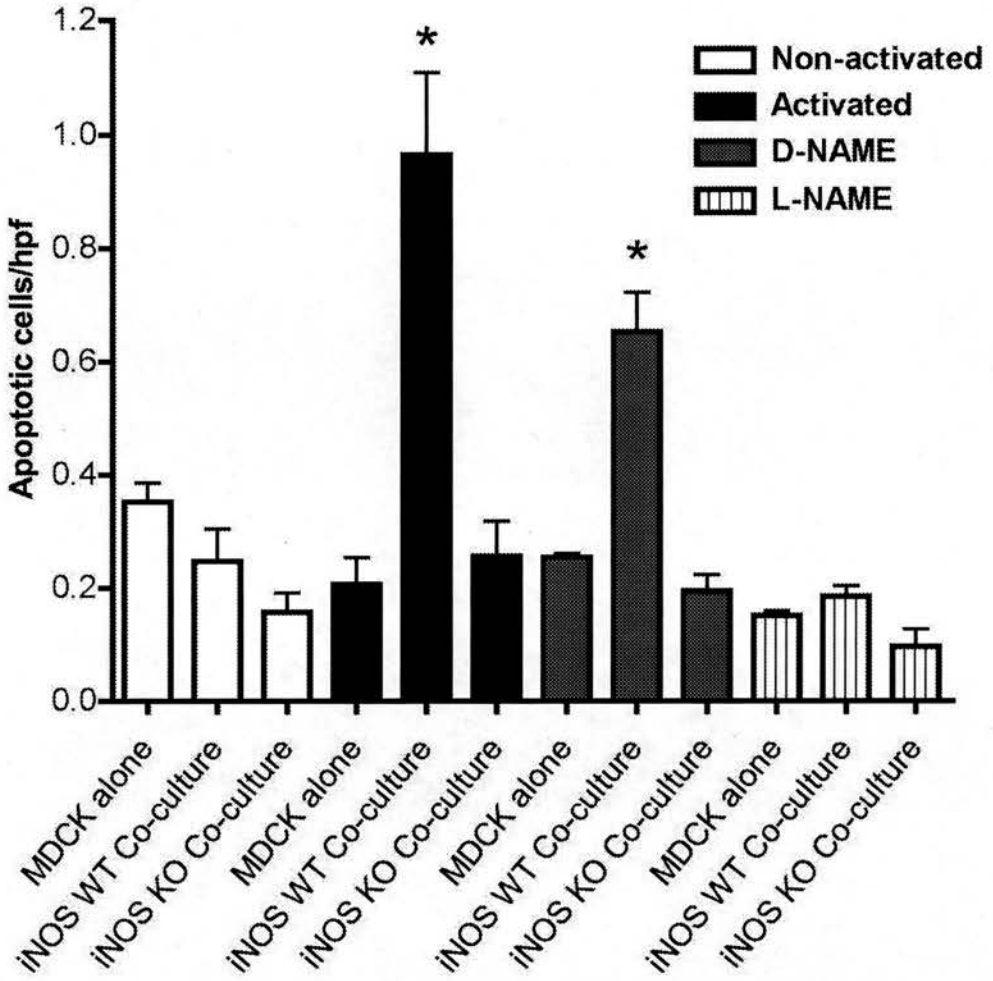

Figure 3- 5 BMDM-derived NO is an important mediator of MDCK cell apoptosis.

CellTracker-green labeled MDCK cells were cultured alone or in the presence of CellTracker-orange labeled BMDM derived from either iNOS WT or iNOS KO mice. Co-culture was established (BMDM : MDCK cell ratio of 2 : 1). Cultures were activated with LPS (1μg/ml) and IFN-γ (100U/ml) in the presence or absence of the NOS inhibitor L-NAME or control D-NAME (final concentration 200μM for both reagents). iNOS KO BMDM are not cytotoxic under any conditions, whilst the cytotoxicity of iNOS WT BMDM is abrogated by pharmacological inhibition of NO production,*$p<0.05$ vs non-activated iNOS WT BMDM co-cultures (n=3).

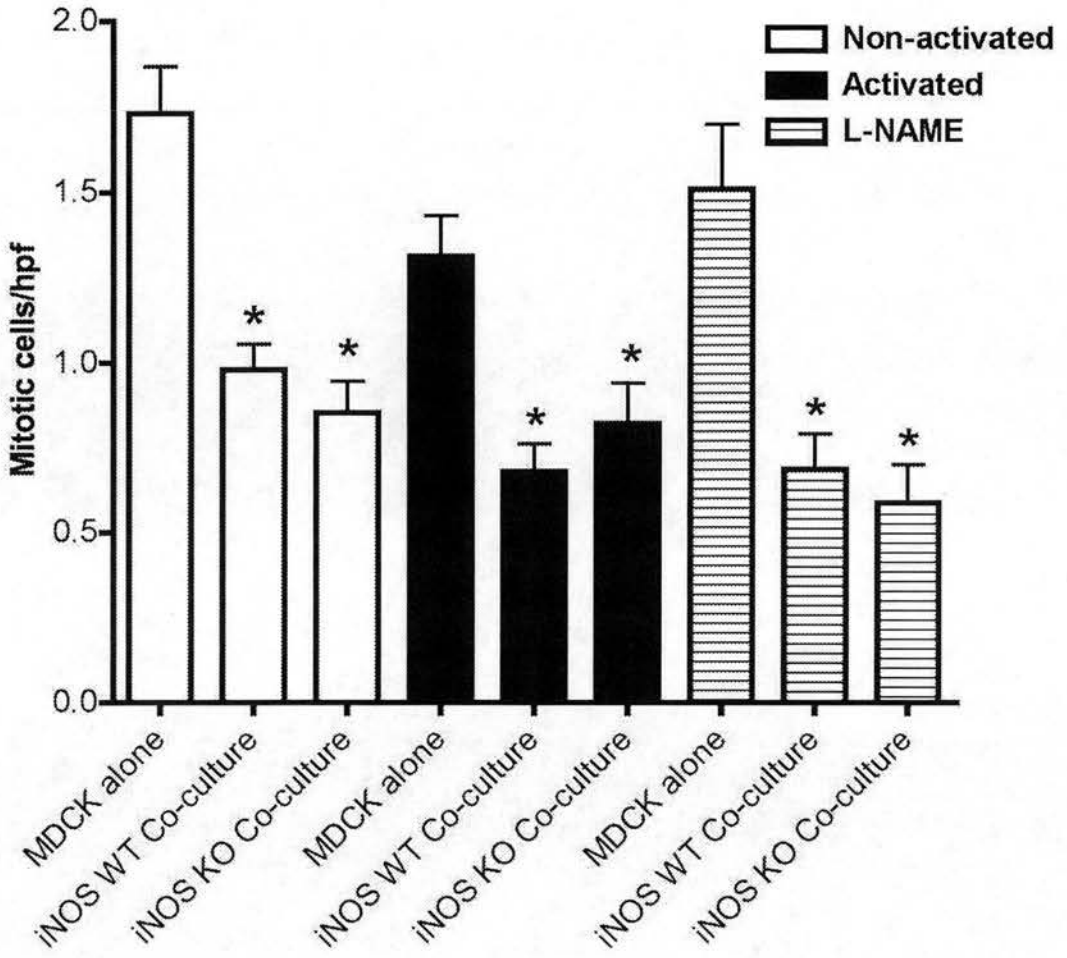

Figure 3- 6 BMDM-derived NO does not modulate MDCK cell proliferation.

CellTracker-green labeled MDCK cells were cultured alone or in the presence of CellTracker-orange labeled BMDM derived from either iNOS WT or iNOS KO mice. Co-culture was established (BMDM : MDCK cell ratio of 2 : 1). Cultures were activated with LPS (1µg/ml) and IFN-γ (100U/ml) in the presence of the NOS inhibitor L-NAME (final concentration 200µM). BMDM inhibition of MDCK cell proliferation is independent of cytokine activation, BMDM genotype or pharmacological inhibition of NO production * $p<0.05$ vs MDCK cells alone (n=3).

Table 3- 4 The effect of cytokine-activated BMDM from iNOS WT or iNOS KO mice in the presence or absence of L-NAME or D-NAME, upon MDCK cell number at 24h.

	Non-activated	Activated (LPS+IFN-γ)	L-NAME (200μM)
MDCK cells alone	309 ± 82	254 ± 61	257 ± 67
iNOS WT BMDM	231 ± 37	215 ± 31	193 ± 45
iNOS KO BMDM	211 ± 58	216 ± 27	184 ± 25

(n=3) Cell number per 8 hpf.

3.2.3 Conditioned supernatant transfer from activated BMDM does not induce apoptosis of MDCK cells

Previous work by Tesch et al (Tesch et al., 1999) suggested that activated BMDM generated soluble mediators that played a role in the induction of tubular cell apoptosis. In order to determine whether soluble mediators, present in the supernatants from activated BMDM could induce apoptosis of MDCK cells, I undertook experiments involving the transfer of conditioned supernatants from LPS/IFN-γ activated BMDM to MDCK cells. $2.5x10^5$ mature BMDM were cultured in 0.5ml of BMDM media with 10% FCS in the presence or absence of LPS (1μg/ml) and IFN-γ (100U/ml). After 24h incubation, the BMDM supernatants were harvested and clarified by centrifugation. Cell-free supernatants from either activated or non-activated BMDM or media with or without LPS/IFN-γ was then added directly to 24-well plates containing MDCK cells ($1.25x10^5$ MDCK cells/well; i.e. a ratio of BMDM conditioned supernatant : MDCK cell ratio of 2:1). The MDCK cells were fixed after 24 hours of incubation and the level of apoptosis and mitosis was analysed by fluorescent microscopy following Hoechst 33342 staining.

Conditioned supernatants from cytokine-activated BMDM failed to induce MDCK cell apoptosis (Figure 3-7a). This suggested that the death effector of cytokine-activated BMDM could be a short-lived molecule that was rapidly degraded or inactivated during the conditioned supernatant transfer process or it might be bound to the cell surface. Neither MDCK cell proliferation nor total cell number was affected by incubation with conditioned supernatants from non-activated or activated BMDM (Figure 3-7b, c). These experiments were performed with BMDM derived from two separate mice. Statistical analysis was not performed since n is <2 for

independent experimental data. It should be noted that this was the result of time constraints and work was prioritised. However, I would have liked further time to ensure that these data were not statistically significant even after 3 or 4 independent experiments.

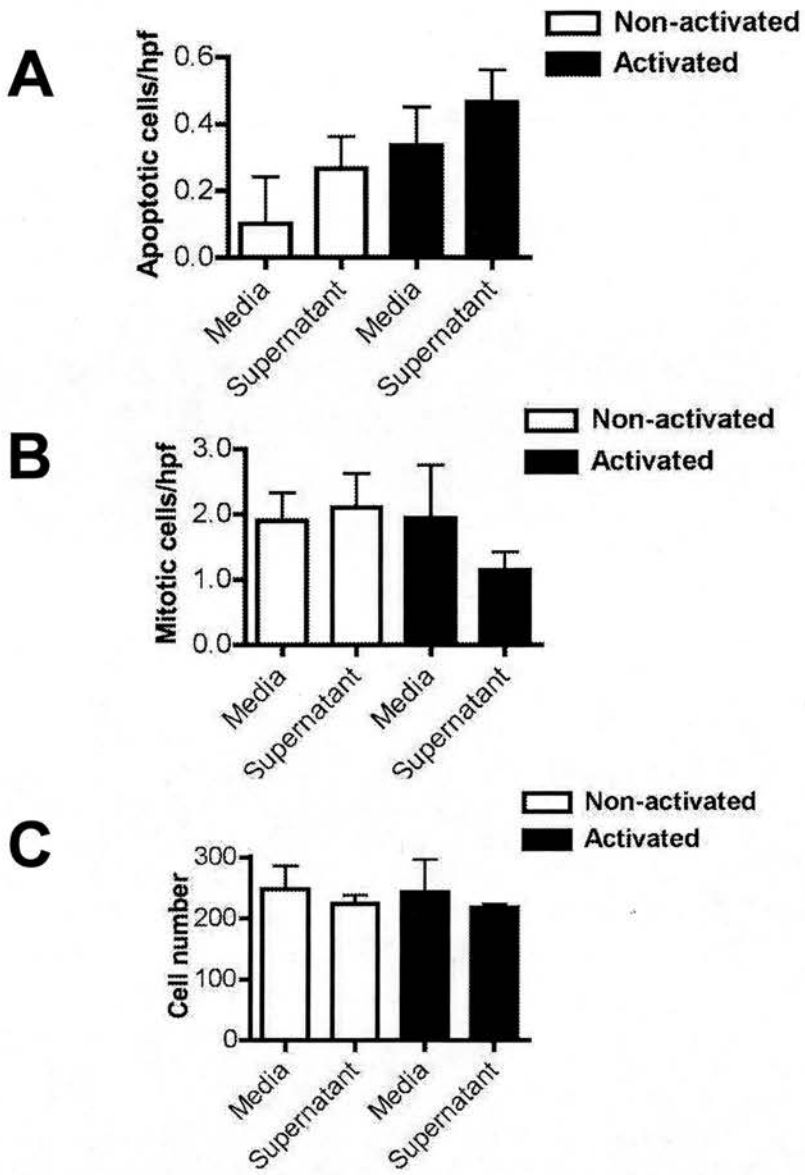

Figure 3- 7 Conditioned supernatants from activated BMDM fail to induce MDCK cell apoptosis.

Mature BMDM ($2.5x10^5$/well) were cultured in the presence or absence of LPS (1μg/ml) and IFN-γ (100U/ml). After 24h incubation, the conditioned BMDM supernatants were harvested, clarified by centrifugation and added to MDCK cells ($1.25x10^5$/well). Cells were cultured with either BMDM conditioned supernatants, media alone or media supplemented with cytokines. After 24h wells were fixed with formaldehyde and counterstained with Hoechst 33342. The level of MDCK cell apoptosis and proliferation was scored by fluorescent microscopy. Conditioned supernatants from activated BMDM failed to induce MDCK cell apoptosis (**A**) and had no effect upon MDCK proliferation (**B**) or total cell number (**C**) (n=2, error bars are standard deviations of the mean).

3.2.4 Direct cell contact or 'close proximity' may be required for the induction of MDCK cell apoptosis by activated BMDM

Since the transfer of conditioned supernatant from activated BMDM failed to induce MDCK cell apoptosis, I wanted to determine whether direct cell contact between BMDM and the target cell was required. Co-cultures were set up as previously described but the target MDCK cells were separated from the BMDM by a tissue culture insert (TCI). A schematic diagram for this experiment is illustrated in Figure 3-8. The inserts have a semi-permeable membrane with a pore size of 0.4μM and the distance between the insert and the well inside TCI companion plate is 8mm. This allows the sharing of the same culture medium, but prevents the cells from being in direct contact with each other. MDCK cells were trypsinised and $5x10^4$ MDCK cells were plated onto each TCI. The cells were left to grow until confluent. Meanwhile, mature BMDM ($1.25x10^5$/well) were plated to the bottom of the wells of a TCI companion plate. The inserts containing the MDCK cells were then placed above the Mϕ. This arrangement represents the spatial relationship present *in vivo*. Confluent tubular epithelial cells grown on TCI become polarised with apical and basolateral domains. *In vivo* interstitial infiltrating Mϕ will be adjacent to the basal aspect of tubular epithelial cells. In order to reproduce this spatial arrangement *in vitro*, the Mϕ were placed in the bottom of the wells of the companion plates. Thus the basal aspect of the overlying tubular epithelial cells would be directly exposed to secreted products from the Mϕ. Control wells had MDCK cells on the inserts but no BMDM in the bottom of the wells. The cultures were then activated with 1μg/ml of LPS and 100U/ml of IFN-γ. The medium was placed in both the upper and lower compartments. After 24h incubation the cultures were fixed with formaldehyde and

target cell apoptosis and mitosis was analysed by fluorescence microscopy following Hoechst 33342 staining.

Cytokine activated BMDM failed to induce MDCK cell apoptosis when the MDCK cells were separated from the BMDM by tissue-culture inserts (Figure 3-9a), thereby indicating that cell-to-cell contact or 'close proximity' between BMDM and the target cell was likely to be important. This experiments was performed with 3 replicates but the BMDM were derived from the same mouse. Statistical analysis was not performed since n is <2 for independent experimental data. It should be noted that this was the result of time constraints and work was prioritised. However, I would have liked further time to ensure that these data were not statistically significant even after 3 or 4 independent experiments.

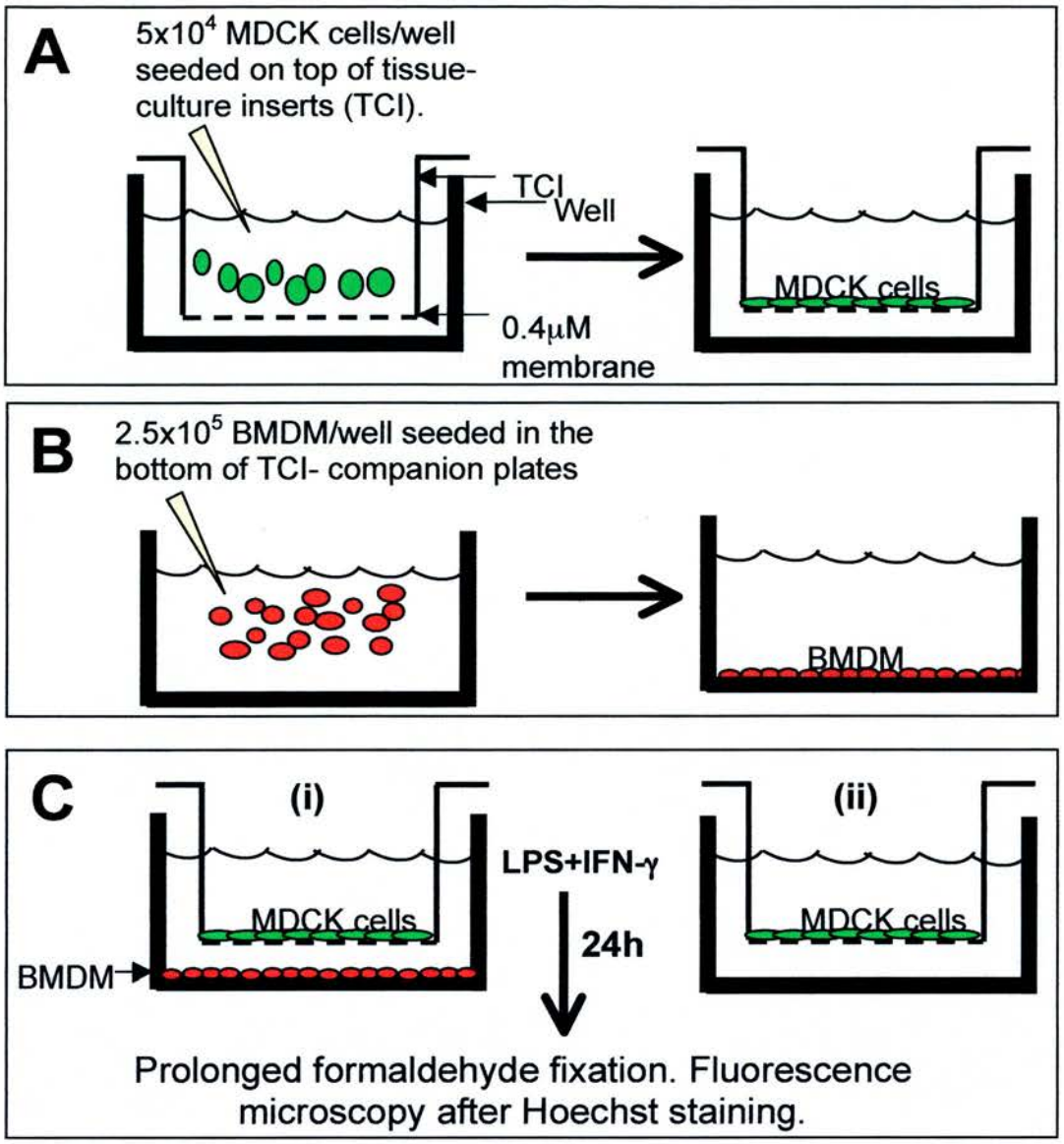

Figure 3- 8 A schematic diagram illustrating the steps involved in co-culture experiments using tissue culture inserts.
$5x10^4$ MDCK are seeded onto each tissue-culture insert (TCI) and left to grow until confluent (**A**). Meanwhile BMDM are seeded into the bottom of TCI companion plates (**B**). Co-culture without contact is facilitated by transferring the TCI containing the MDCK cells above the BMDM ($2.5x10^5$/well) inside the TCI companion plate (**C,i**). Control MDCK cells on TCI (**C,ii**) do not have BMDM in the bottom of the companion plate. The cultures were activated with cytokines and incubated for 24h. The cultures were fixed with formaldehyde solution and analysed by florescence microscopy after Hoechst 33342 staining.

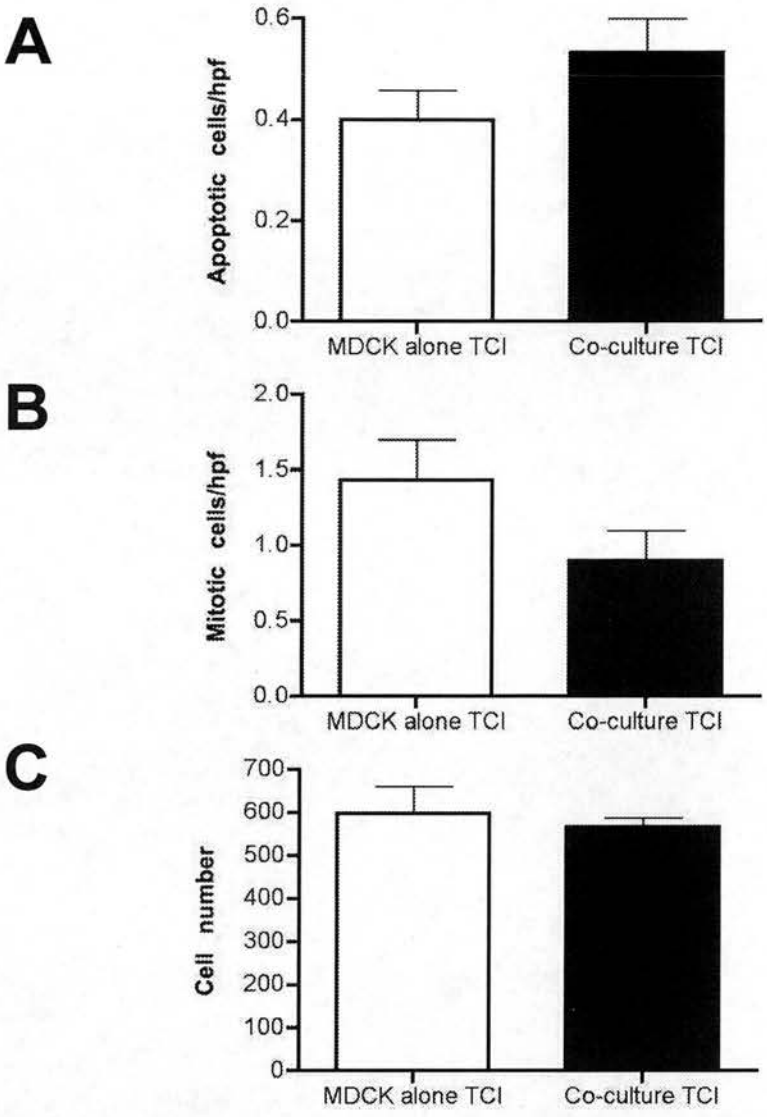

Figure 3- 9 Cell contact or 'close proximity' is required for BMDM to induce MDCK cell apoptosis

$5x10^4$ CellTracker green labeled MDCK cells were plated onto the semi-permeable membranes of TCI and left to grow until confluent. $1.25x10^5$ mature BMDM were plated in the wells of the TCI companion plates. Some inserts containing the MDCK cells were then placed above the BMDM. LPS (1μg/ml) and IFN-γ (100U/ml) was added to all cultures and incubated for 24h. The wells were fixed with formaldehyde and counterstained with Hoechst 33342. The level of MDCK cell apoptosis and proliferation was analysed by fluorescent microscopy. Activated BMDM separated from target MDCK cells failed to induce MDCK cell apoptosis, **(A)**. No effect was evident upon MDCK proliferation (**B**) or total cell number (cells/insert) (**C**). (n=1, error bars are standard deviations of the mean).

3.2.5 Cytokine activated BMDM induce apoptosis of murine primary tubular epithelial (PTE) cells but do not modulate PTE cell proliferation

The data presented so far indicates that cytokine-activated murine BMDM are capable of inducing significant apoptosis of MDCK cells and that BMDM-derived NO is an important key mediator of this cytotoxic effect. Even though the MDCK cells are a well-established tubular cell line, they are of canine origin and may therefore not be susceptible to other putative murine BMDM-derived death effectors such as FasL and TNF-α. I therefore undertook a similar series of experiments using murine primary tubular epithelial (PTE) cells.

The PTE cells were cultured and characterised as described previously (Harrison et al., 2006). Since PTE cells were of primary origin, the handling of these cells differed from that of MDCK cells. PTE cells had to be grown in specified media supplemented with EGF, dexamethasone etc, and the PTE could only be passaged once as they lost their characteristic epithelial cell phenotype on subsequent culture/passage.

The co-cultures were set up in a similar manner as for MDCK cells, but the CellTracker green labeled PTE cells were left to adhere overnight before co-cultures with CellTracker orange labeled mature murine BMDM were established (Chapter 2-4.1). A ratio of 2 Mϕ : 1 PTE cell was used in experiments. Control cultures were also established comprising of PTE cells alone. Some wells were activated with 1μg/ml of LPS and 100U/ml of IFN-γ and following 24 hours incubation the co-cultures were fixed with formaldehyde. Apoptotic and mitotic PTE cells were

quantified by inverted fluorescence microscopy after staining with Hoechst 33342. Although I made several attempts to assess the level of PTE cell apoptosis by flow cytometric based assays of apoptosis, they were not successful (data not shown).

Non-activated BMDM did not induce significant PTE cell apoptosis in co-culture studies, thereby indicating that BMDM are not inherently cytotoxic (Figure 3-10a). In addition, treatment of PTE cells alone with LPS and IFN-γ had no significant effect upon the level of PTE cell apoptosis (Figure 3-10a). However, co-cultures with cytokine activated BMDM induced a significant 3-fold increase in PTE cell apoptosis compared to non-activated co-cultures (Figure 3-10a) and apoptotic PTE cells exhibited characteristic cytoplasmic condensation (Figure 3-11). Furthermore, inclusion of the NOS inhibitor L-NAME reduced PTE cell death to baseline levels (Figure 3-10a). In contrast to MDCK cells, incubation of PTE cells with non-activated BMDM or activated BMDM had no effect upon the level of PTE cell proliferation (Figure 3-10b). It should, however, be noted that PTE cells were of primary origin and therefore exhibited a much lower level of proliferation compared to MDCK cells. No difference was evident in total cell number in these experiments (Table 3-5).

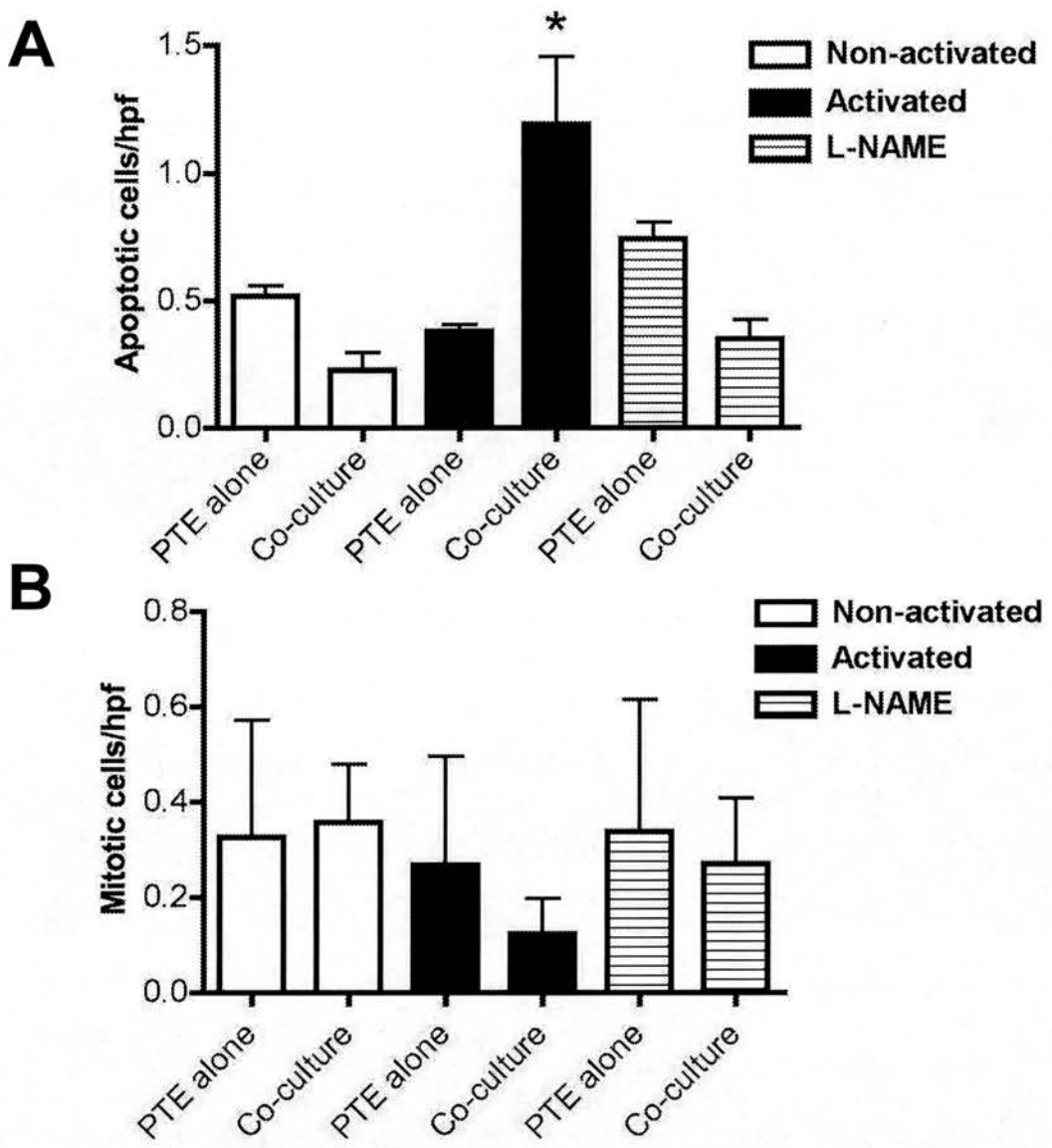

Figure 3- 10 Cytokine activated BMDM induce apoptosis of murine PTE cells but do not affect PTE cell proliferation.

CellTracker green labeled PTE cells were cultured alone or in the presence of mature Cell-Tracker orange labeled BMDM derived from FVB/N mice. Co-culture was established (BMDM : PTE cell ratio = 2 : 1). Selected cultures were activated with LPS/IFN-γ in the presence or absence of L-NAME (final concentration 200μM). After 24h, the co-culture was fixed with formaldehyde, counterstained with Hoechst 33342 and PTE cell apoptosis and mitosis was scored by fluorescence microscopy. Co-culture with activated BMDM induce significant levels of PTE cell apoptosis (**A**). *$p<0.05$ vs activated co-cultures in the presence or absence of L-NAME. No significant difference in the level of PTE cell proliferation was seen (**B**). (n=3).

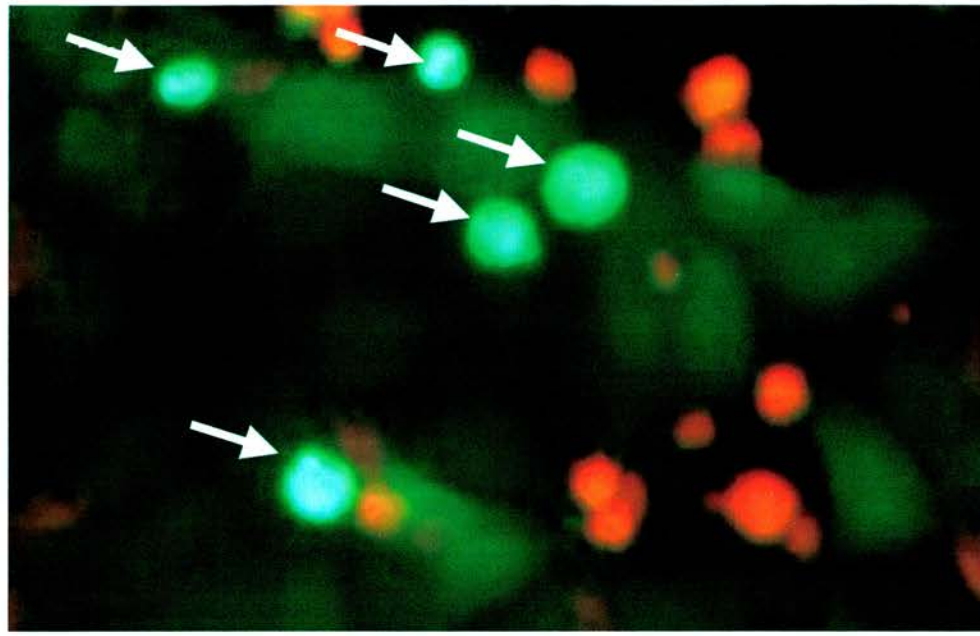

Figure 3- 11 Fluorescent photomicrograph of cytokine activated co-culture of BMDM and murine PTE cells.
CellTracker green labeled PTE cells were cultured in the presence of cytokine activated mature Cell-Tracker orange labeled BMDM from FVB/N mice. Co-culture was established (BMDM : PTE cell ratio = 2 : 1). After 24h incubation the co-culture was fixed with formaldehyde solution and counterstained with Hoechst 33342. Fluorescent photomicrograph showing apoptotic green PTE cells exhibiting cytoplasmic condensation (examples arrowed). (x320 original magnification).

Table 3- 5 The effect of cytokine-activated BMDM in the presence or absence of L-NAME upon PTE cell number at 24h.

	Non-activated	Activated (LPS+IFN-γ)	L-NAME (200μM)
PTE cells alone	199 ± 57	206 ± 50	224 ± 27
FVB/N BMDM	177 ± 45	187 ± 34	219 ± 39

(n=3), PTE cell number per 8 hpf.

3.2.6 iNOS KO BMDM fail to induce apoptosis of murine PTE cells

Next, I went on to determine whether BMDM-derived NO was the key mediator for BMDM-directed apoptosis of murine PTE cells by performing co-cultures of PTE cells with BMDM derived from either iNOS KO mice or iNOS WT mice.

The results from these experiments demonstrated that co-cultures with non-activated BMDM did not induce significant levels of PTE cell apoptosis (Figure 3-12). However activated iNOS WT BMDM, induced significant levels of PTE cell apoptosis (Figure 3-12), whilst co-cultures involving activated iNOS KO BMDM did not exhibit significant PTE cell apoptosis compared to control non-activated iNOS KO BMDM co-cultures (Figure 3-12).

In contrast to co-cultures of BMDM with MDCK cells, I noted phagocytosis of apoptotic PTE cells by BMDM in this primary cell co-culture system (Figure 13-a and b). The effect of phagocytosis and subsequent rapid degradation of the ingested cell would be predicted to reduce the level of 'free' apoptotic cells evident and this may explain why a lower number of apoptotic PTE cells were detected in these experiments compared to experiments using MDCK cells. Interestingly, in accordance with the increased level of PTE cell apoptosis in activated co-cultures of iNOS WT BMDM compared to iNOS KO BMDM, an increased number of Mϕ containing phagocytosed apoptotic PTE cells was also seen (Figure 3-13b) although this did not reach statistical significance.

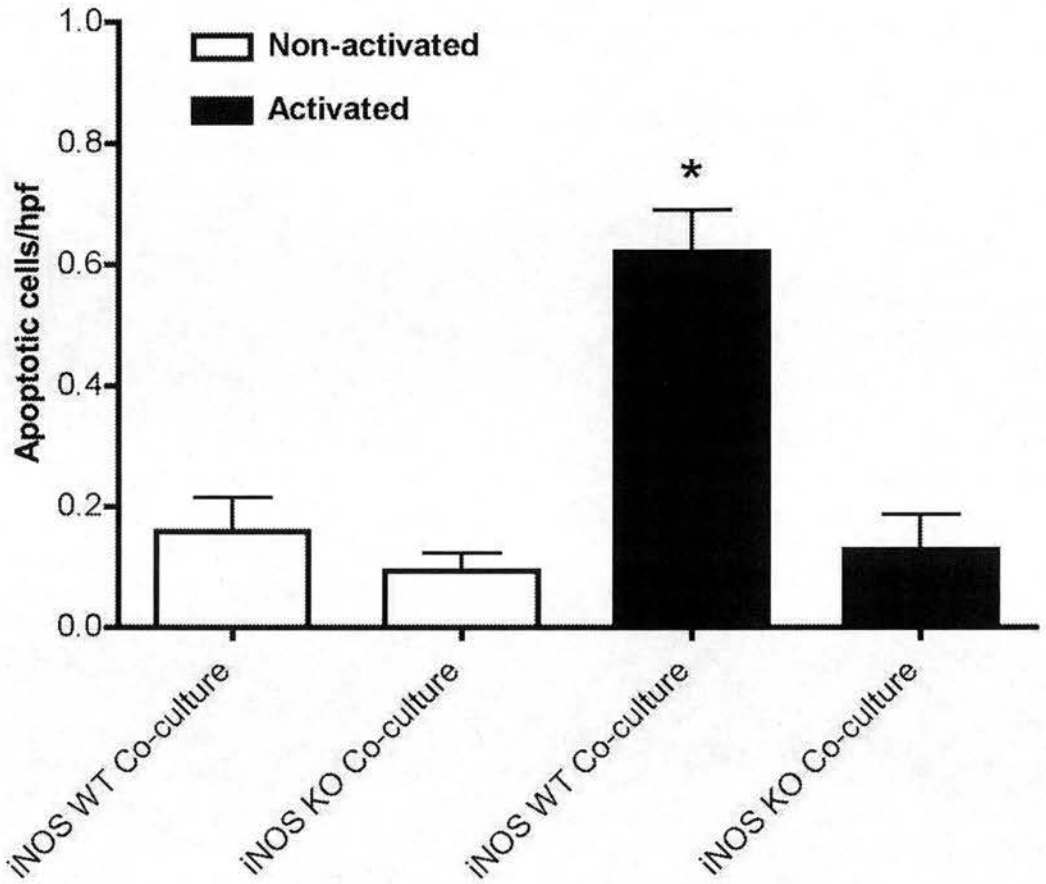

Figure 3- 12 BMDM-derived NO is an important mediator of murine PTE cell apoptosis.

CellTracker green labeled PTE cells were cultured in the presence of Cell-Tracker orange labeled mature BMDM derived from either iNOS WT or iNOS KO mice. Co-culture was established (BMDM : PTE cell ratio = 2 : 1) and selected cultures were activated with LPS (1μg/ml) and IFN-γ (100U/ml). After 24h incubation the co-culture was fixed with formaldehyde solution and counterstained with Hoechst 33342. The level of PTE cell apoptosis was scored by fluorescence microscopy. Cytokine activation of iNOS WT BMDM induced significant PTE cell apoptosis whilst activated iNOS KO BMDM were not cytotoxic. *$p<0.05$ vs non-activated co-culture (n=5).

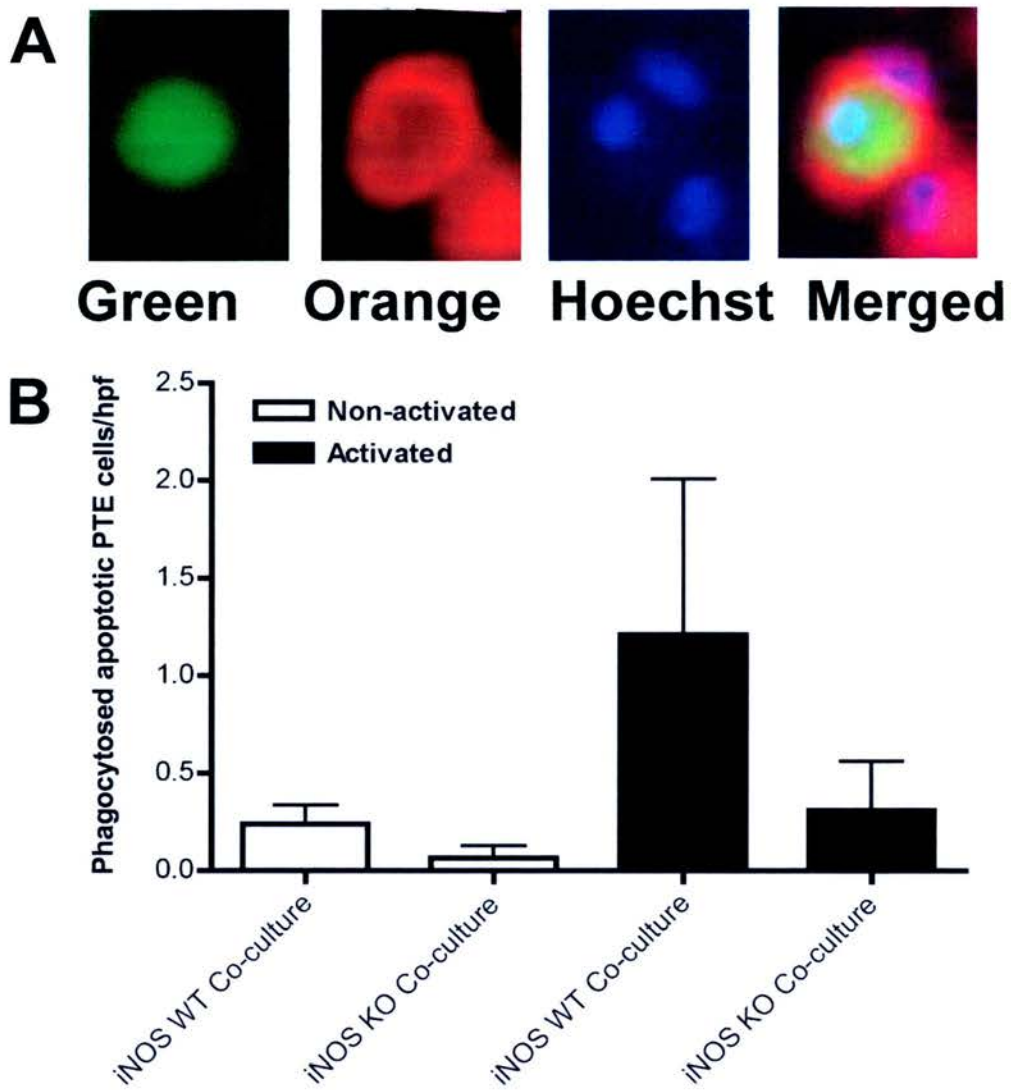

Figure 3- 13 Activated co-cultures of BMDM and murine PTE cells exhibit phagocytosis of apoptotic PTE cells.

CellTracker green labeled PTE cells were cultured in the presence of Cell-Tracker orange labeled mature BMDM derived from either iNOS WT or iNOS KO mice. Co-culture was established (BMDM : PTE cell ratio = 2 : 1) and selected cultures were activated with LPS (1μg/ml) and IFN-γ (100U/ml). After 24h, the co-culture was fixed with formaldehyde, counterstained with Hoechst 33342 and phagocytosis of apoptotic PTE cells was scored by fluorescence microscopy. (**A**) Photomicrographs from an activated co-culture demonstrating evidence of BMDM recognition and phagocytosis of apoptotic tubular cells. The merged image demonstrates a condensed apoptotic CellTracker green labeled PTE cell with a pyknotic nucleus that has been ingested by a CellTracker orange labeled BMDM. (x320 original magnification). (**B**) A trend towards increased phagocytosis of apoptotic PTE cells by activated iNOS WT Mϕ was observed. (n=5).

I also attempted to perform some co-culture experiments with PTE cells derived from either iNOS WT and iNOS KO mice but unfortunately these experiments were unsuccessful as the PTE cells did not adhere well in the 48-well plates and the level of basal apoptosis was high in the non-activated control wells. This may have been secondary to the age of the mice, which were 9 months old.

In addition, I also performed experiments involving the addition of NO donors to iNOS WT and iNOS KO PTE cells to determine whether the presence or absence of iNOS might modulate the level of apoptosis in response to NO. Unfortunately I used a flow cytometry based assay (Chapter 2.7) and high levels of apoptosis were evident in control non-treated (medium alone) PTE cells. However, the level of apoptosis between the iNOS WT and KO PTE cells after treatment with NO donors was comparable (Table 3-6). These experiments were performed with PTE cells derived from two separate mice. Statistical analysis was not performed since n is <2 for independent experimental data. It should be noted that this was the result of time constraints and work was prioritised. However, I would have liked further time to ensure that these data were not statistically significant even after 3 or 4 independent experiments.

Table 3- 6 The effect of NO donors upon tubular epithelial cell apoptosis on PTE cells derived from either iNOS WT or iNOS KO mice.

	iNOS WT PTE cells % Apoptosis*	iNOS KO PTE cells % Apoptosis*
Medium alone	15.8 ± 4.2	18.4 ± 4.5
0.1 µM Spermine/NO	31.5 ± 10.7	26.6 ± 1.4
1.5mM DEA/NO	25.9 ± 1.8	26.0 ± 8.3

Tubular epithelial cell apoptosis was analysed by flow cytometry after double staining with Annexin V and 7AAD. *(Annexin $V^{positive}$ and $7AAD^{negative}$)

n=2 mice and standard deviations of the mean.

3.2.7 Activated BMDM from syngeneic and allogeneic BMDM induce similar levels of murine PTE cell apoptosis

The PTE cells used in these experiments were always derived from C57BL/6 mice since these mice were readily available. The data from the PTE cell co-culture experiments presented thus far has involved the use of allogeneic BMDM derived from FVB/N mice. In order to rule out the confounding issue of MHC mismatch between the target cell and the BMDM, co-culture of C57BL/6 PTE cells was performed with either allogeneic FVB/N BMDM or syngeneic C57BL/6 BMDM. In these experiments there was no significant difference in the level of C57BL/6 PTE cell apoptosis between activated co-cultures comprising either allogeneic FVB/N BMDM or syngeneic C57BL/6 BMDM (0.58±0.1 versus (vs) 0.42±0.06 apoptotic cells per hpf; FVB/N derived BMDM vs C57BL/6 derived BMDM, $p>0.05$).

3.2.8 Direct cell contact or 'close proximity' is required for BMDM induction of murine PTE cell apoptosis

The effect of BMDM conditioned supernatant transfer was tested as described previously for MDCK cells. Conditioned supernatants from cytokine-activated BMDM failed to induce significant PTE cell apoptosis (Figure 3-14a). The level of apoptosis in PTE cells cultured alone under control conditions with non-activated media was higher than that evident in cytokine activated PTE cells alone (Compare to Figure 3-10a). Incubation of PTE cells with conditioned supernatant from non-activated or cytokine activated BMDM did not affect PTE cell proliferation or cell number (Figure 3-14b and c). These experiments were performed

with BMDM derived from two separate mice. Statistical analysis was not performed since n is <2 for independent experimental data. It should be noted that this was the result of time constraints and work was prioritised. However, I would have liked further time to ensure that these data were not statistically significant even after 3 or 4 independent experiments. This finding, is in contrast to previous published work demonstrating that supernatants from cytokine activated Mϕ can indeed induce apoptosis of primary murine tubular epithelial cells (Tesch et al., 1999). However, my results are in accordance with previous work from our group as activated BMDM conditioned supernatants did not induce apoptosis of mesangial cells *in vitro* (Duffield et al., 2000).

Since the transfer of conditioned supernatant from activated BMDM failed to induce PTE cell apoptosis, I investigated whether direct cell contact between BMDM and the target cell was required. This was tested as previously described for the MDCK cells. $5x10^4$ PTE cells were plated onto tissue-culture inserts (TCI) and left to grow until confluent. The inserts were then placed on top of the TCI companion plates containing $1.25x10^5$ BMDM per well. Control wells comprised of only the PTE cells on the inserts with no BMDM in the bottom of the wells. The experimental set up was similar to that of MDCK cells (Figure 3-8), except that PTE medium with 1% FCS was used. This medium was placed in both the upper and lower compartment and the cultures were then incubated in the presence of 1μg/ml of LPS and 100U/ml of IFN-γ. After 24h of incubation the cultures were fixed with formaldehyde and target cell apoptosis and mitosis was analysed by fluorescence microscopy following Hoechst 33342 staining.

There was a trend for higher PTE cell apoptosis when the PTE cells on the inserts were cultured with cytokine activated BMDM (Figure 3-15a) but this did not reach statistical significance ($p=0.38$, activated PTE alone TCI vs activated Co-culture TCI). These data indicates that direct cell-to-cell contact or 'close proximity' may be important in the induction of PTE cell apoptosis by cytokine activated BMDM. There was also a non-significant trend for lower PTE cell proliferation, when PTE cells on TCI were cultured in the presence of cytokine activated BMDM ($p=0.40$, activated PTE alone TCI vs activated Co-culture TCI).

This finding differed from the work of Lange-Sperandio et al work since they demonstrated comparable levels of tubular cell apoptosis regardless of whether activated Mϕ and tubular cells were separated from each other by an insert or in direct contact thereby suggesting that direct cell contact was not a critical factor (Lange-Sperandio et al., 2003). It must, however, be noted that in their study they plated the Mϕ onto the inserts and the tubular cells were placed in the bottom of the wells. Thus, the cells had a different spatial orientation to each other compared to my experiments. The experimental protocol adopted in my experiments is more likely to reflect the spatial orientation found *in vivo.*

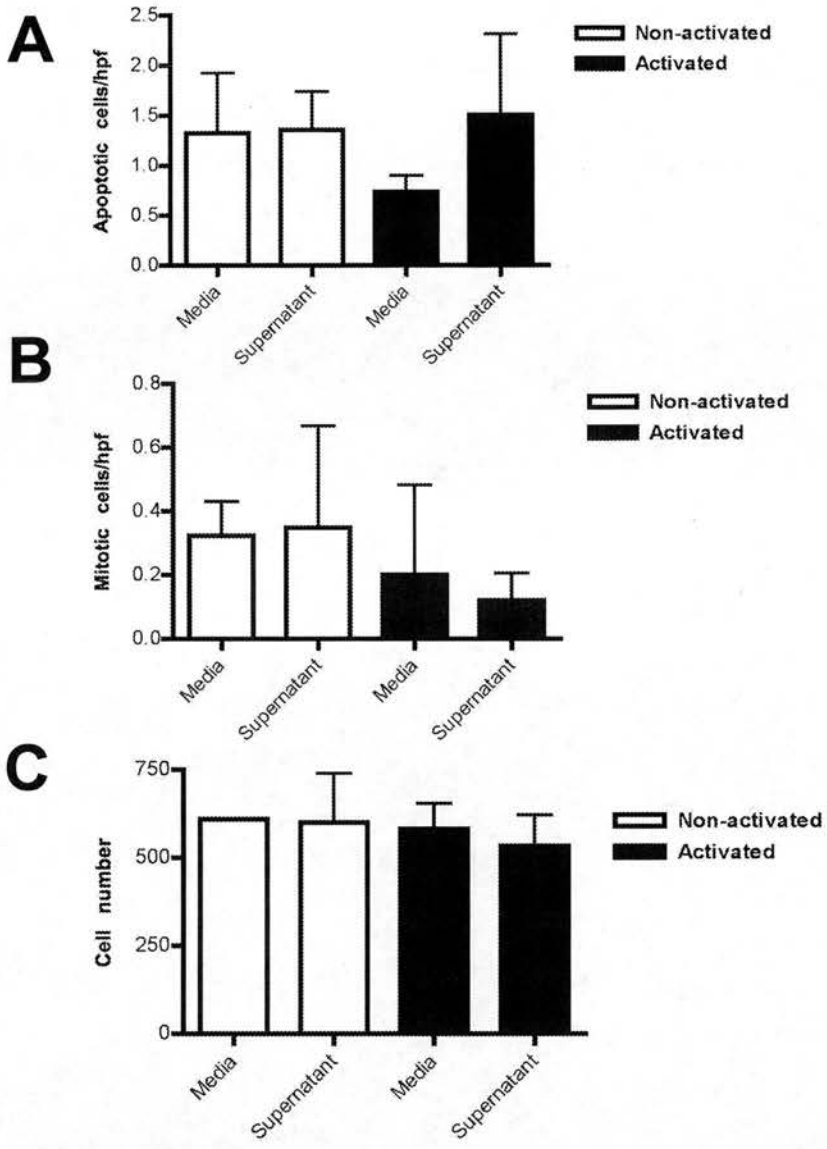

Figure 3- 14 Conditioned supernatant from activated BMDM fail to induce murine PTE cell apoptosis

Mature BMDM ($2.5x10^5$ mature BMDM/well) were cultured in the presence or absence of LPS (1μg/ml) and IFN-γ (100U/ml). After 24h incubation, the conditioned BMDM supernatants were harvested, clarified by centrifugation and added to PTE cells ($1.25x10^5$/well). The wells were fixed with formaldehyde and counterstained with Hoechst 33342 after 24h incubation with BMDM supernatants, media alone or media supplemented with LPS and IFN-γ. The level of PTE cell apoptosis and proliferation was scored by fluorescent microscopy. Conditioned supernatants from activated BMDM did not induce significant PTE cell apoptosis (**A**). Also, no effect on PTE cell proliferation (**B**) or total cell number (**C**) was evident, (n=2, error bars are standard deviations).

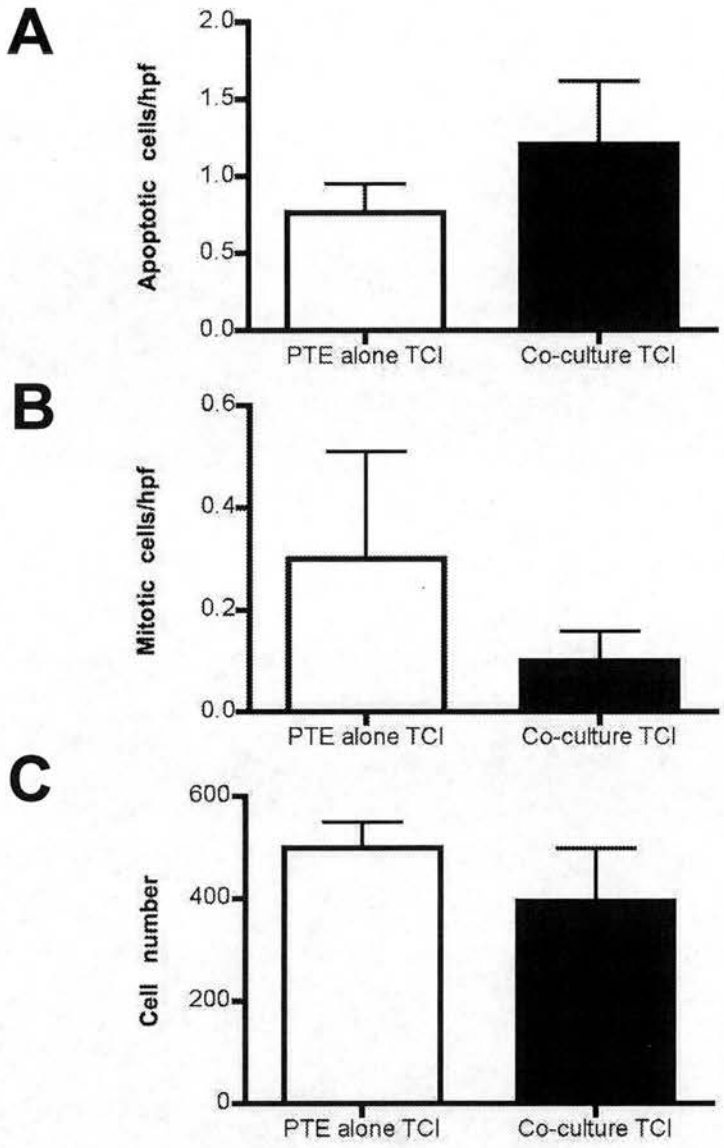

Figure 3- 15 Cell contact or 'close proximity' is important for activated BMDM induction of PTE cell apoptosis.

$5x10^4$ CellTracker green labeled PTE cells were plated onto the semi-permeable membranes of TCI and left to grow until confluent. $1.25x10^5$ mature BMDM were plated in the wells of the TCI companion plates. Some inserts containing the PTE cells were then placed above the BMDM. Cells were incubated the presence of LPS (1μg/ml) and IFN-γ (100U/ml). Following 24h, the wells were fixed with formaldehyde and counterstained with Hoechst 33342. The level of PTE cell apoptosis and proliferation was analysed by fluorescent microscopy. Activated BMDM do not induce significant PTE cell apoptosis when physically separated from the target PTE cells (**A**). No effect upon PTE proliferation (**B**) or total cell number (**C**) was evident (n=3).

3.3 SUMMARY

The experiments described in this chapter shed light upon the interaction of Mϕ with renal tubular epithelial cells *in vitro*. I investigated the effect of activated BMDM upon both MDCK cells and murine primary tubular epithelial cells and some findings were common to both cell types. For example, although non-activated BMDM were not cytotoxic to MDCK or PTE cells, co-culture with cytokine activated BMDM induced significant levels of apoptosis. Higher levels of apoptosis was evident in experiments involving MDCK cells but this may well reflect the increased proliferation seen with cell lines compared to primary cells, since proliferating cells may be more vulnerable to undergoing apoptosis.

Studies with pharmacological inhibitors of NO synthase as well as the use of BMDM derived from iNOS KO or WT mice indicated that BMDM cytotoxicity is dependent upon iNOS-derived NO. Indeed, cytokine activated iNOS KO BMDM were not cytotoxic and were comparable to control non-activated BMDM. It is pertinent that the pharmacological inhibition of iNOS with L-NIL does not affect the release of TNF-α or the expression of FasL by cytokine activated BMDM (Anya Adair, personal communication). This suggests that NO is the prime mechanism involved in the induction of tubular cell death by cytokine activated BMDM under these *in vitro* conditions.

Differences were observed in the effect of BMDM upon MDCK and PTE cell proliferation. MDCK cell proliferation was significantly suppressed by both non-activated and activated BMDM from iNOS WT and iNOS KO mice (with a trend

evident when BMDM derived from FVB/N mice were utilised). This effect was independent of pharmacological inhibition of NO production. In contrast, no effect upon PTE cell proliferation was evident in these studies.

I observed that activated BMDM ingested apoptotic PTE cells but this was not observed with apoptotic MDCK cells. The reasons for this are unclear but it may reflect the difference in cell size between MDCK and PTE cells. Lastly, experiments involving the use of conditioned supernatant transfer or tissue culture inserts suggest that direct cell-to-cell contact or 'close proximity' between the target tubular epithelial cell and BMDM is an important requirement for BMDM induction of tubular cell death; a finding at odds with previous reports in the literature (Lange-Sperandio et al., 2003; Tesch et al., 1999).

Chapter 4.

iNOS-derived Nitric Oxide and Tubular Epithelial Cell Apoptosis *in vivo*

4.1 INTRODUCTION

Mϕ play a critical role during the initiation, progression and resolution of renal inflammation (Kluth et al., 2004). An accumulating body of data indicates that Mϕ play an active role in inducing tubular epithelial cell apoptosis *in vivo* (Duffield et al., 2005a; Lange-Sperandio et al., 2002; Lenda et al., 2003; Tesch et al., 1999). However, despite the documented association between the severity of the Mϕ infiltrate and the level of tubular epithelial cell apoptosis, there is currently no data regarding the mechanism employed by Mϕ to induce tubular cell apoptosis *in vivo*.

The results from the *in vitro* co-culture experiments in the previous chapter indicated a key role for Mϕ-derived NO in inducing tubular cell death *in vitro*. Therefore the next pertinent step was to seek a role for Mϕ-derived NO in inducing tubular cell apoptosis during tubulointerstitial inflammation *in vivo*. In this section of work, I employed the model of experimental hydronephrosis induced by unilateral ureteric obstruction (UUO). UUO is an excellent neutrophil and lymphocyte independent *in vivo* model of renal inflammation (Shappell et al., 1998) and is characterised by marked Mϕ infiltration and significant levels of tubular epithelial cell apoptosis (Diamond, 1995; Hughes and Johnson, 1999).

In this chapter I will describe the results obtained after inducing UUO in iNOS WT and iNOS KO mice. I will also present the results obtained after pharmacologically inhibiting the activity of the NO-generating enzyme iNOS during experimental hydronephrosis.

4.2 RESULTS

4.2.1 Obstructed kidneys exhibit prominent infiltration of tubulointerstitial Mϕ at day 7 following UUO

UUO was induced by ligation of the left ureter under general anaesthesia and the kidneys were removed at day 7. Normal non-manipulated kidneys served as controls. Tubulointerstitial Mϕ infiltration was detected by staining kidney sections for the specific murine Mϕ marker F4/80. Normal non-obstructed kidneys exhibited occasional scattered F4/80 positive resident Mϕ, whilst obstructed kidneys developed a prominent Mϕ infiltrate in the tubulointerstitium (Figure 4-1). The degree of tubulointerstitial Mϕ infiltration was quantified by careful computer-assisted image analysis (Figure 4-2).

4.2.2 iNOS positive Mϕ are present within the tubulointerstitium in obstructed kidneys

The obstructed kidneys were stained for iNOS and infiltrating iNOS positive cells were present in the interstitium of the obstructed kidney at day 7 (Figure 4-3). In order to determine whether interstitial infiltrating Mϕ expressed iNOS, I performed double immunofluorescent staining for iNOS and F4/80. This demonstrated the presence of infiltrating Mϕ expressing iNOS within the tubulointerstitium of obstructed kidneys at day 7 (Figure 4-4).

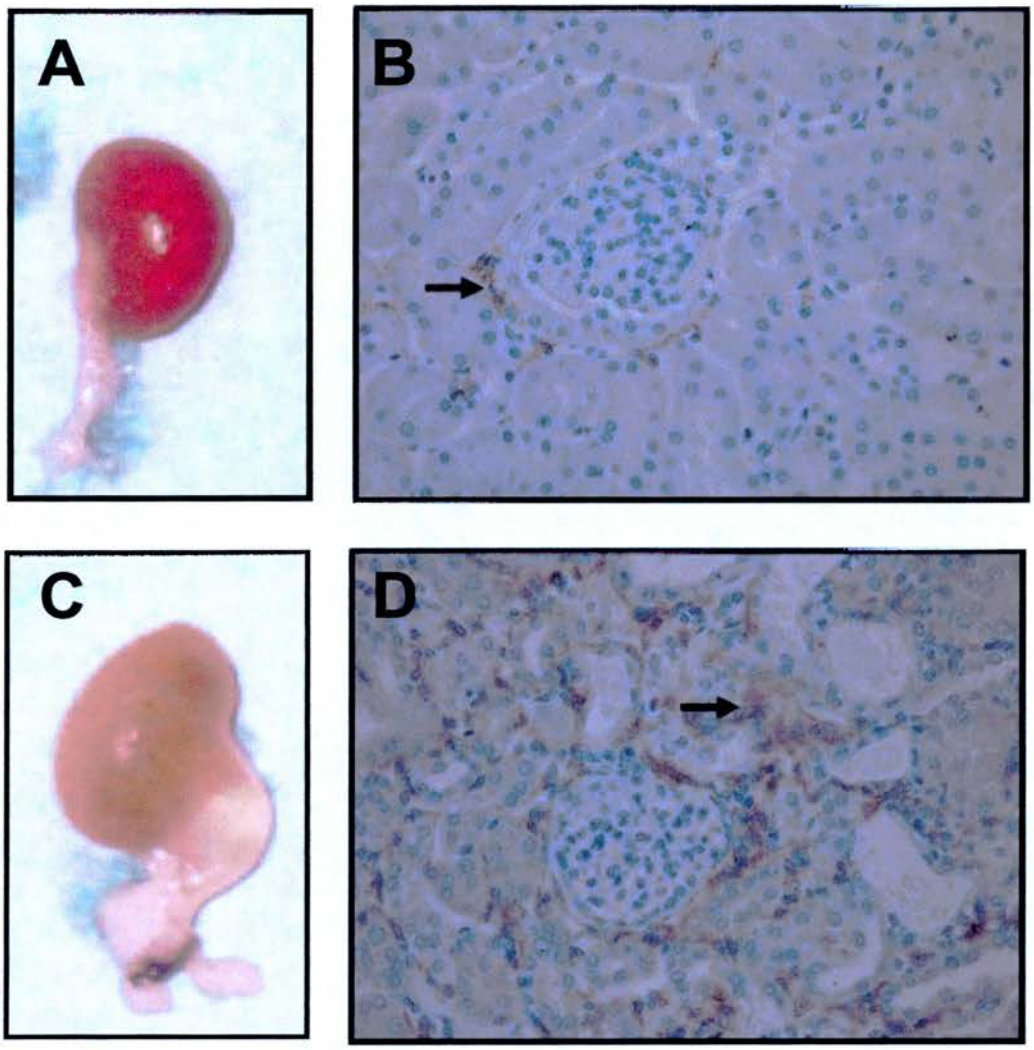

Figure 4- 1 Photomicrographs of non-obstructed and hydronephrotic kidney (day 7) after immunostaining for the Mϕ marker F4/80.
Digital camera photographs of a non-obstructed kidney (**A**) and a hydronephrotic kidney after 7 days of UUO (**C**). The kidneys were fixed in Methyl-carnoys solution and underwent processing for histology. Tissue sections were immunostained for the Mϕ marker F4/80. Normal non-obstructed kidneys exhibited occasional F4/80 positive resident Mϕ (example arrowed) (**B**). In contrast, a prominent population of infiltrating F4/80 positive Mϕ (example arrowed) was evident in the interstitium of obstructed kidneys (**D**). (x100 original magnification)

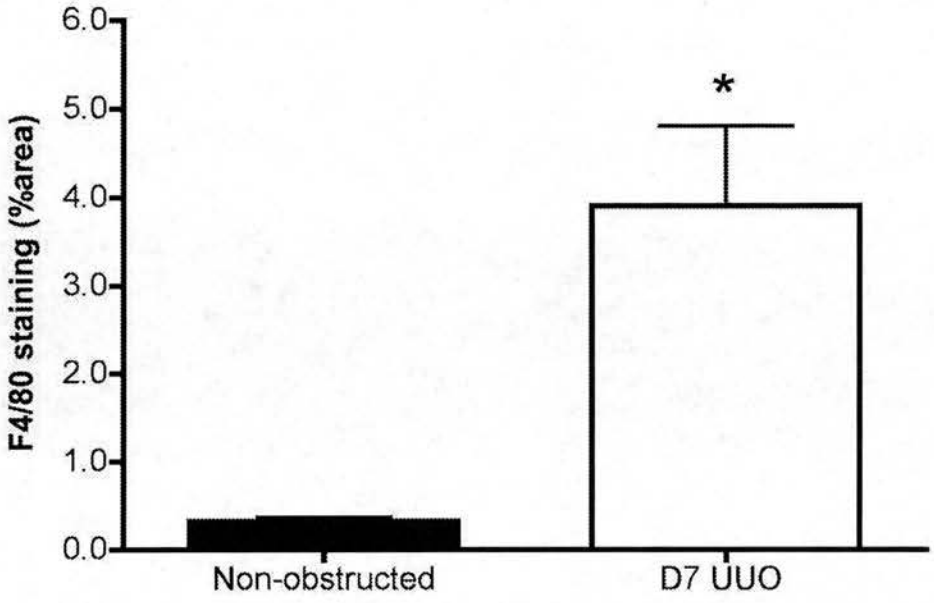

Figure 4- 2 Quantitative analysis of tubulointerstitial Mϕ infiltration in non-obstructed and hydronephrotic kidneys (day 7 post UUO).
Immunostaining was performed for the Mϕ marker F4/80 and the level of Mϕ infiltration was quantified by computer assisted image analysis. Hydronephrotic kidneys removed 7 days following UUO exhibited a significant increase in tubulointerstitial Mϕ infiltration (*$p<0.001$ vs non-obstructed control kidneys).

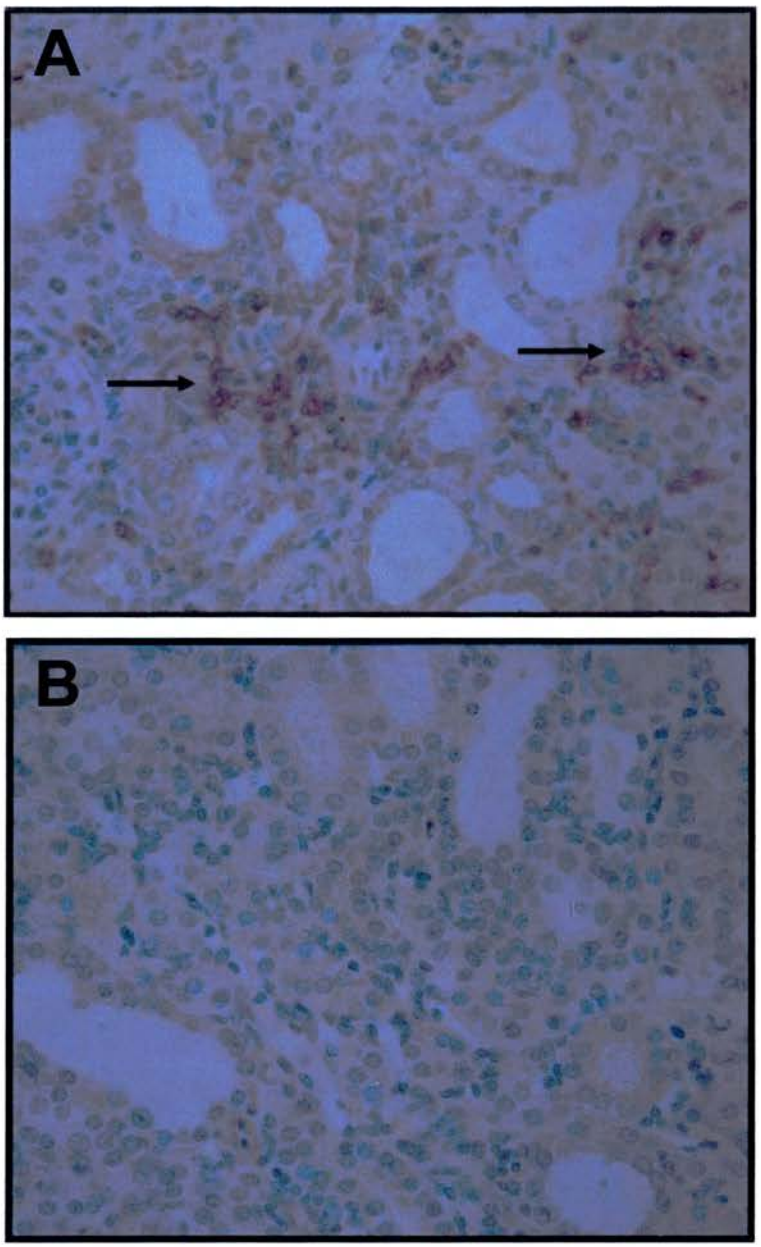

Figure 4- 3 Obstructed kidneys exhibit tubulointerstitial infiltration with iNOS positive cells.

Obstructed kidneys were removed at day 7 following UUO and the tissue sections were immunostained for iNOS. Obstructed kidneys exhibit a population of iNOS positive interstitial cells (example arrowed) (**A**). The specificity of iNOS immunostaining is indicated by incubation of day 7 UUO tissue sections with an irrelevant isotype antibody (negative control) since no significant interstitial immunostaining is evident (**B**). (x100 original magnification).

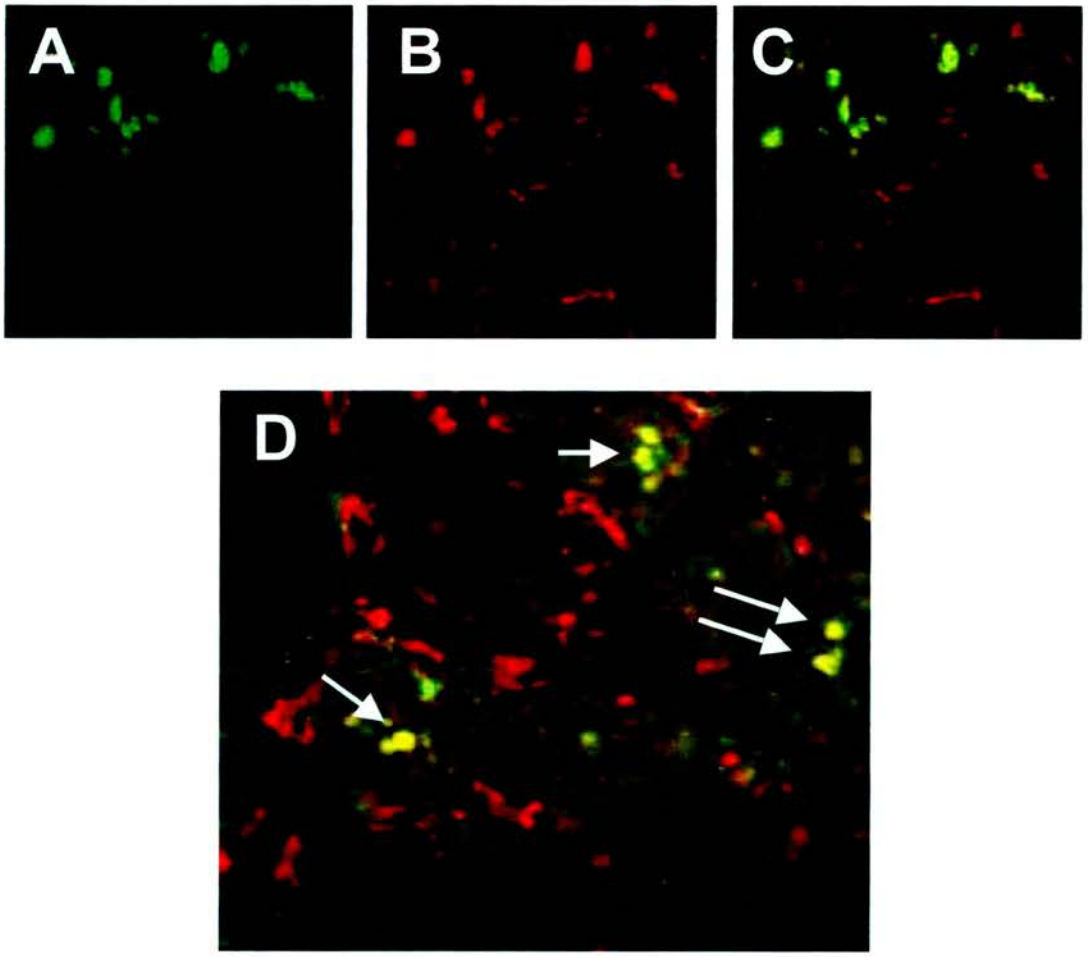

Figure 4- 4 Fluorescent photomicrographs showing iNOS positive Mϕ within the tubulointerstitium of obstructed kidneys (day 7 post UUO). Obstructed kidneys were removed at day 7 and tissue sections underwent double immunofluorescent staining for iNOS and F4/80. Fluorescent photomicrographs showing iNOS positive cells stained green (**A**) and F4/80 positive interstitial Mϕ stained red (**B**). The merged image demonstrates colocalisation (yellow) of iNOS and F4/80 indicating the presence of infiltrating Mϕ expressing iNOS (**C**). An additional merged image demonstrating multiple iNOS positive infiltrating Mϕ (examples arrowed) (**D**). (x1000 original magnification).

4.2.3 iNOS KO mice exhibit increased Mϕ infiltration in experimental hydronephrosis

iNOS WT and iNOS KO mice underwent UUO under general anaesthesia. The kidneys were removed at day 7, fixed in 10% formalin and Methyl carnoys and embedded in paraffin (n=5 per group). Tissue sections were immunostained for the specific Mϕ marker F4/80. The degree of tubulointerstitial Mϕ infiltration (expressed as F4/80 positive surface area) was quantitated by computer-assisted image analysis. The obstructed kidneys of iNOS KO mice exhibited a significantly increased Mϕ infiltrate (Figure 4-5c). Morphometric measurement of tubular luminal space was also performed. Importantly, no difference in the percentage tubular luminal space occupying the cortical area was observed between experimental groups, thereby excluding this potential confounding factor (Figure 4-5d).

4.2.4 iNOS KO mice exhibit a trend toward lower levels of tubular epithelial apoptosis at day 7 of UUO

Tubular epithelial cell apoptosis was evaluated in day 7 obstructed kidneys of iNOS WT and iNOS KO mice by analysis of PAS stained tissue sections. This method was able to discriminate between proximal (Figure 4-6a) and distal (Figure 4-6b) tubular epithelial cell apoptosis and enables the quantification of tubular cell death in these different tubular compartments. Interestingly, iNOS KO mice exhibited a slightly reduced level of both proximal and distal tubular cell apoptosis despite the significantly increased tubulointerstitial Mϕ infiltrate. The reduction in tubular cell apoptosis did not, however, reach statistical significance (Figure 4-6c).

To further investigate the interesting observation that the obstructed kidneys of iNOS KO mice exhibited a trend towards lower levels of both proximal and distal tubular epithelial cell apoptosis I increased the number of animals in each group to 7 per group. I also used the TUNEL assay to determine the level of tubular epithelial cell death (Figure 4-7a) in the obstructed kidneys of iNOS WT and iNOS KO mice at day 7 following UUO. The iNOS KO mice still exhibited again a trend toward a lower level of tubular epithelial cell apoptosis in obstructed kidneys although this did not reach statistical significance despite increasing the number of animals studied (Figure 4-7b).

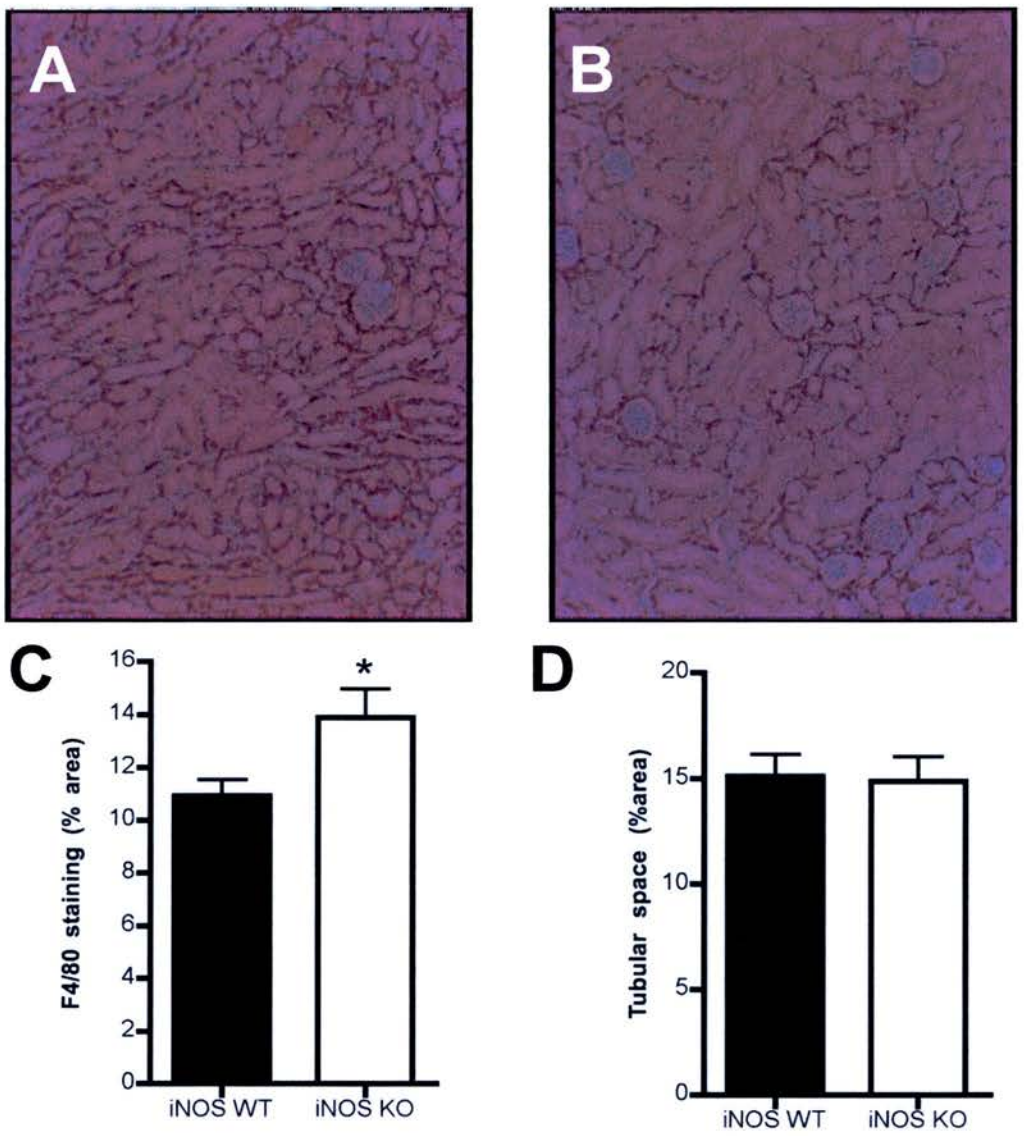

Figure 4- 5 Quantitative analysis of tubulointerstitial Mϕ infiltration and tubular dilatation in the cortex of iNOS WT and iNOS KO mice at day 7 following UUO.

Immunostaining was performed for the Mϕ marker F4/80. iNOS KO mice displayed marked interstitial Mϕ infiltration (x100 magnification) (**A**) that was greater than that evident in iNOS WT mice (**B**). Quantification of Mϕ infiltration by computer assisted image analysis demonstrated that iNOS KO mice exhibited a significant increase in tubulointerstitial Mϕ infiltration (*$p<0.05$ vs iNOS WT mice). (**C**). The area occupied by the tubular lumina was quantified by computer-assisted image analysis. The tubular luminal space is expressed as a percentage of total cortical area. No significant difference in the degree of tubular luminal space was evident between groups (**D**), (n=5 mice per group).

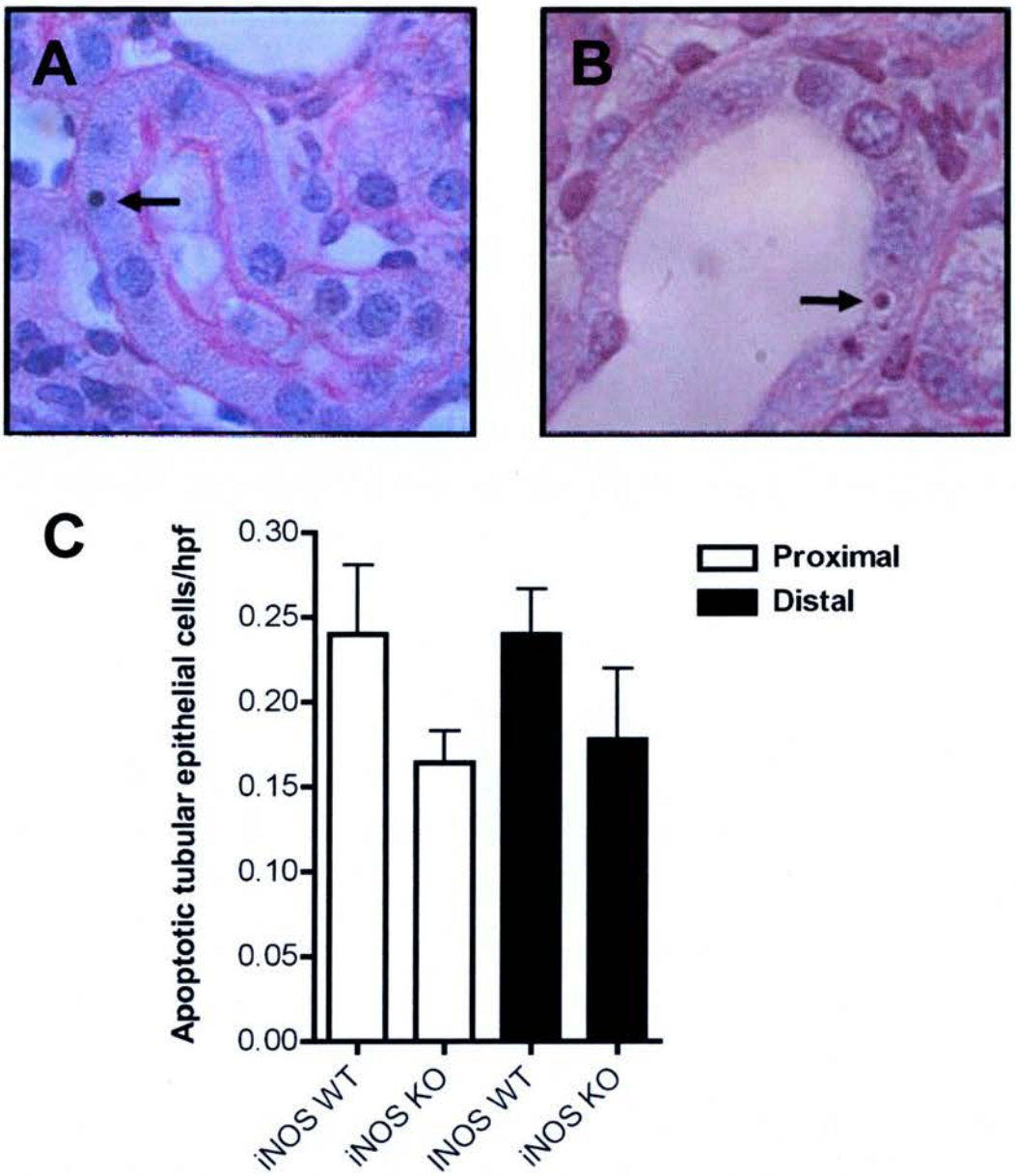

Figure 4- 6 Detection and quantitation of apoptotic proximal and distal tubular epithelial cells in the obstructed kidneys of iNOS WT and iNOS KO mice at day 7 following UUO

PAS staining was used to identify apoptotic proximal (**A**) and distal (**B**) tubular epithelial cells (x1000 magnification). iNOS KO mice exhibit a trend towards lower levels of both proximal and distal tubular epithelial cell apoptosis, though this was not statistically significant (p=0.14 proximal and p=0.23 distal apoptosis, vs iNOS WT mice) (**C**), (n=5 mice per group).

4.2.5 iNOS WT mice but not iNOS KO mice, exhibit a significant correlation between interstitial Mϕ infiltration and tubular epithelial cell apoptosis at day 7 following UUO

Previous work has demonstrated a highly significant correlation between the level of Mϕ infiltration and the degree of tubular cell apoptosis in experimental hydronephrosis as well as the immunological model of nephrotoxic nephritis (Lange-Sperandio et al., 2002; Tesch et al., 1999). I therefore analysed the correlation between the degree of Mϕ infiltration (F4/80 positive area) and the levels of tubular epithelial cell apoptosis evident in each genotype. iNOS WT mice exhibited a significant positive correlation between Mϕ infiltration and the level of tubular epithelial cell death (R^2 = 0.61, $p<0.04$, Figure 4-8a), thereby indicating a clear relationship between these parameters. In contrast, there was no correlation between Mϕ infiltration and the level of tubular epithelial cell death in iNOS KO mice (R^2 = 0.017, $p=0.78$, Figure 4-8b).

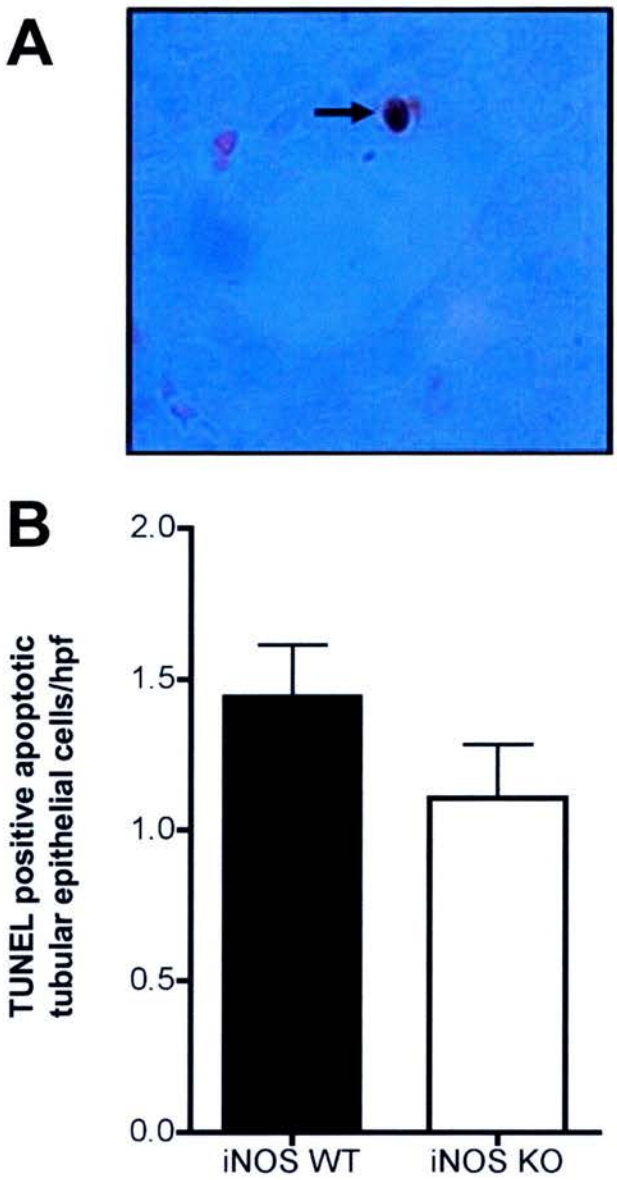

Figure 4- 7 Detection and quantitation of TUNEL positive apoptotic tubular epithelial cells in the obstructed kidneys of iNOS WT and iNOS KO mice at day 7 following UUO.

Tubular epithelial cell apoptosis was detected by TUNEL staining (**A**). (x1000 magnification). iNOS KO mice exhibit a trend towards a lower level of tubular epithelial cell apoptosis, though this was not statistically significant (p=0.19, vs iNOS WT mice) (**B**), (n=7 mice per group).

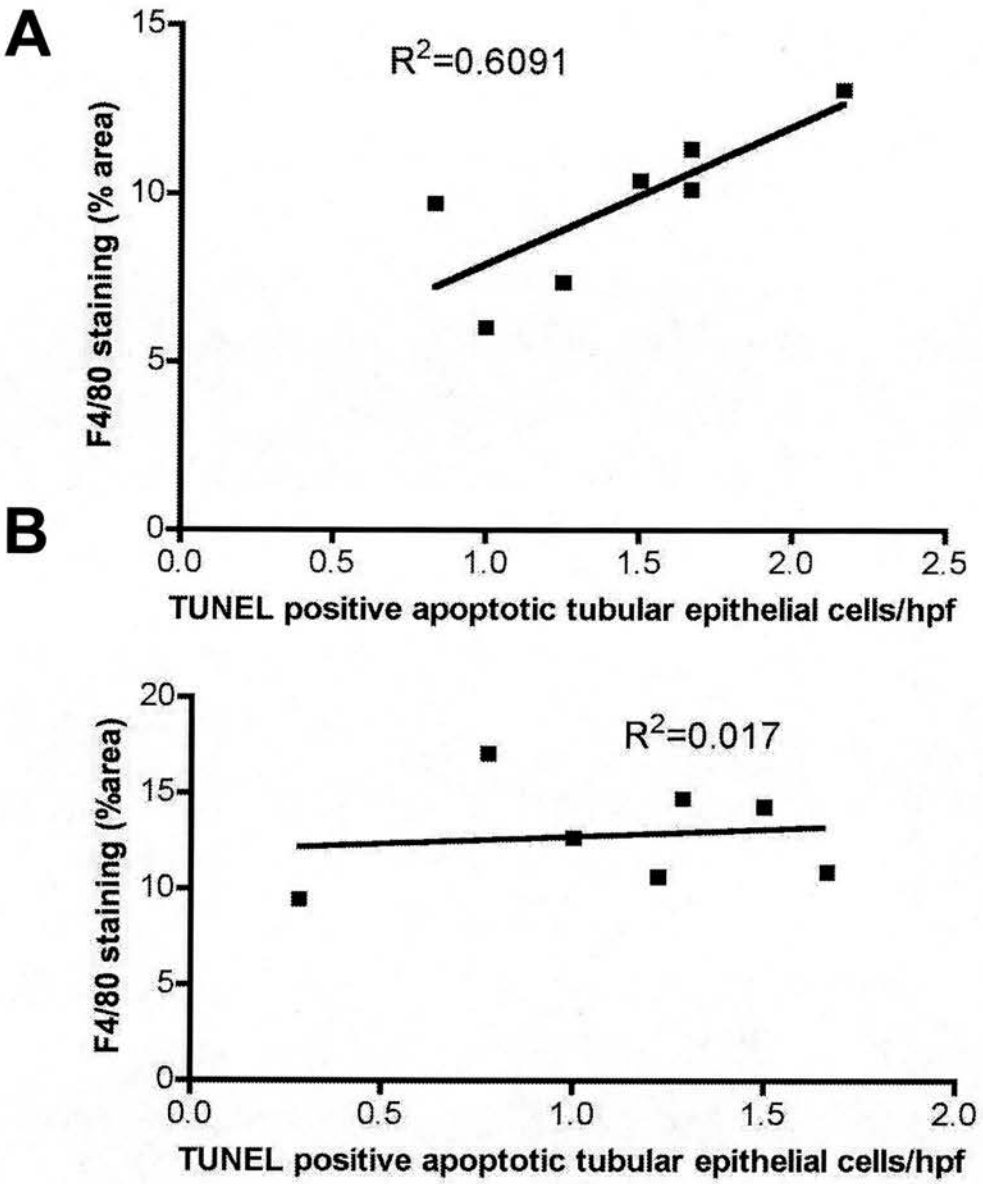

Figure 4- 8 Mϕ infiltration in iNOS WT mice but not iNOS KO mice significantly correlates with tubular epithelial cell apoptosis.
Tubular epithelial cell apoptosis was detected by TUNEL staining and Mϕ infiltration was determined by F4/80 immunostaining. (**A**) Mϕ infiltration is significantly correlated with the level of tubular cell apoptosis in iNOS WT mice (R^2= 0.61, $p<0.04$). (**B**) In contrast, no significant correlation was evident in iNOS KO mice (R^2= 0.017, $p=0.78$). Correlation was analysed with Pearsons correlation coefficient (n=7 mice per group).

4.2.6 Experimental hydronephrosis does not affect the level of tubular epithelial cell proliferation in iNOS WT and iNOS KO mice

Tubular epithelial cell proliferation in the obstructed kidney of iNOS WT and iNOS KO mice at day 7 following UUO was determined by analysis of PAS stained tissue sections as mitotic figures were readily identifiable (see Figure 4.10a and b). This method allowed the specific quantification of proximal and distal tubular cell mitosis. There was no significant difference in the levels of proximal or distal tubular cell mitosis between iNOS WT and iNOS KO mice (Table 4-1).

Table 4- 1 Quantification of proximal and distal tubular epithelial cell proliferation in iNOS WT and iNOS KO mice at day 7 following UUO.

	iNOS WT mice	iNOS KO mice
Mitotic cells/hpf		
Proximal	0.13 ± 0.03	0.18 ± 0.06
Distal	0.22 ± 0.06	0.19 ± 0.09

(n=7 mice per group)

4.2.7 Pharmacological blockade of iNOS by administration of L-NIL in the drinking water during experimental hydronephrosis

Since the obstructed kidneys of iNOS KO mice exhibited an increased level of tubulointerstitial Mϕ infiltration, I decided to circumvent this confounding effect by using a pharmacological approach. L-NIL, a specific irreversible iNOS inhibitor, was administered in the drinking water of mice in order to pharmacologically inhibit the enzyme iNOS during the model of experimental hydronephrosis. UUO was performed in FVB/N mice and L-NIL (1mg/ml) was administered in the drinking water between day 5 and day 7. I chose to commence L-NIL administration for a 48 hour period commencing at day 5 in order to minimise any potential impact upon Mϕ infiltration. This dose and route of administration of L-NIL was chosen since it had previously been demonstrated to effectively inhibit iNOS *in vivo* (Reilly et al., 2002; Westenfeld et al., 2002). In order to prove that this dose was effective in blocking iNOS in the study presented in this thesis, I would have liked to perform an enzymatic assay of iNOS activity from L-NIL treated day 7 obstructed kidney tissue homogenates. NOS activity in kidney homogenates can be measured using a radiolabeled citrulline assay that monitors the conversion of tritiated [^{3}H]-arginine to [^{3}H]-citrulline. The contribution of iNOS activity to total NOS activity can be measured by the inclusion of a calcium chelator in the above reaction since iNOS activity is Ca^{2+} independent (Miyajima et al., 2001). However, time constraints during this thesis, prohibited the development of such an assay which utilised radiolabeled substrate (tritiated arginine) for the measurement of iNOS activity. Urinary nitrate levels were not measured from the obstructed kidneys, since iNOS

blockade was undertaken for only 48 hours and hence the urinary nitrate levels would not be meaningful as the urine had accumulated over the preceding 7 days.

The obstructed kidneys were removed for histological analysis at day 7 following 48 hrs of iNOS blockade. Administration of the inactive isomer D-NIL (1mg/ml) served as control.

4.2.8 Pharmacological blockade of iNOS by L-NIL does not affect the degree of tubulointerstitial Mϕ infiltration in experimental hydronephrosis

The level of Mϕ infiltration (F4/80 positive surface area) was analysed by computer assisted image analysis. This analysis indicated that pharmacological inhibition of iNOS between day 5 and day 7 did not have any significant effect upon the level of Mϕ infiltration at day 7 (3.2±0.7 vs 3.9±0.9 % F4/80 positive surface area; L-NIL vs control; $p>0.05$).

4.2.9 Pharmacological blockade of iNOS by L-NIL reduces tubular epithelial cell apoptosis but does not affect the level of tubular epithelial cell proliferation in experimental hydronephrosis

Tubular epithelial cell apoptosis was determined by TUNEL staining (Figure 4-9a). Administration of L-NIL significantly reduced the level of tubular cell apoptosis compared to control D-NIL (Figure 4-9b). The level of tubular epithelial cell proliferation was determined by counting the number of tubular cell undergoing mitoses using PAS stained tissue sections with both proximal (Figure 4-10a) and distal (Figure 4-10b) tubular cell proliferation being quantified. In contrast to the

effect upon tubular cell apoptosis, L-NIL administration did not affect the level of tubular cell proliferation (Figure 4-10c).

4.2.10 Administration of L-NIL reduces interstitial cell apoptosis but does not affect interstitial cell proliferation in experimental hydronephrosis

Interstitial cell apoptosis and proliferation was similarly determined by TUNEL (Figure 4-11a) and PAS staining respectively (Figure 4-12a). Pharmacological blockade of iNOS by L-NIL also resulted in a significant reduction in the level of interstitial cell apoptosis (Figure 4-11b) with no effect upon interstitial cell proliferation being evident (Figure 4-12b).

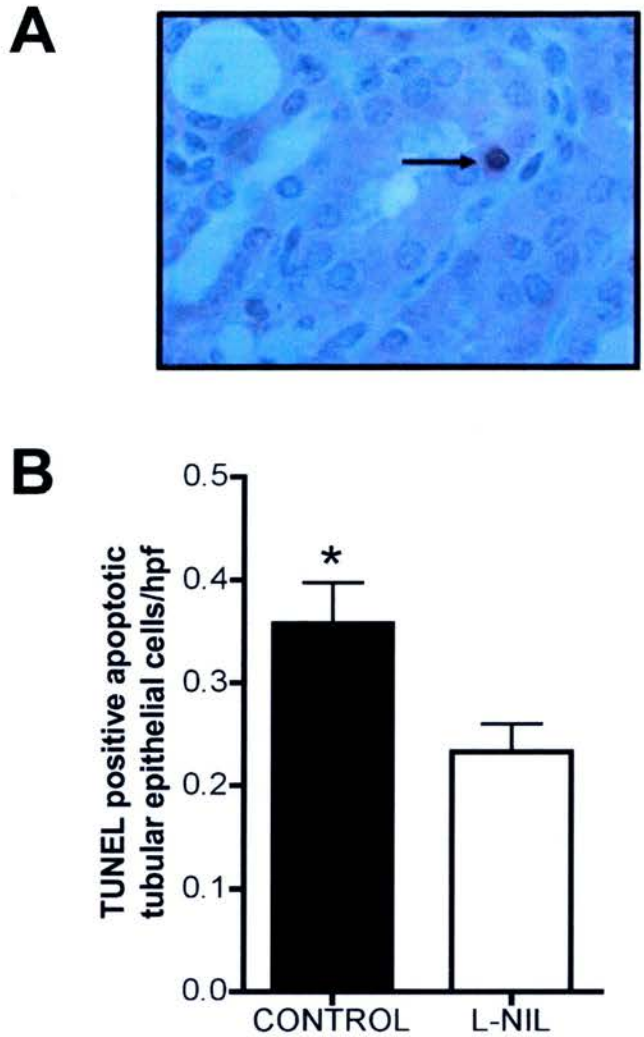

Figure 4- 9 Pharmacological blockade of iNOS reduces tubular epithelial cell apoptosis at day 7 following UUO.
Mice were administered L-NIL (1mg/ml), an irreversible pharmacological inhibitor of the enzyme iNOS, or the isomeric control D-NIL (1mg/ml) in the drinking water from day 5 after UUO. The obstructed kidneys were removed at day 7 and tissue sections underwent TUNEL staining to detect apoptotic cells. High power view (x1000 magnification) of a TUNEL positive apoptotic tubular cell (**A**). The level of tubular cell apoptosis in obstructed kidneys is significantly reduced following the administration of L-NIL (**B**) *$p<0.05$ vs control (n=7-8 mice per group).

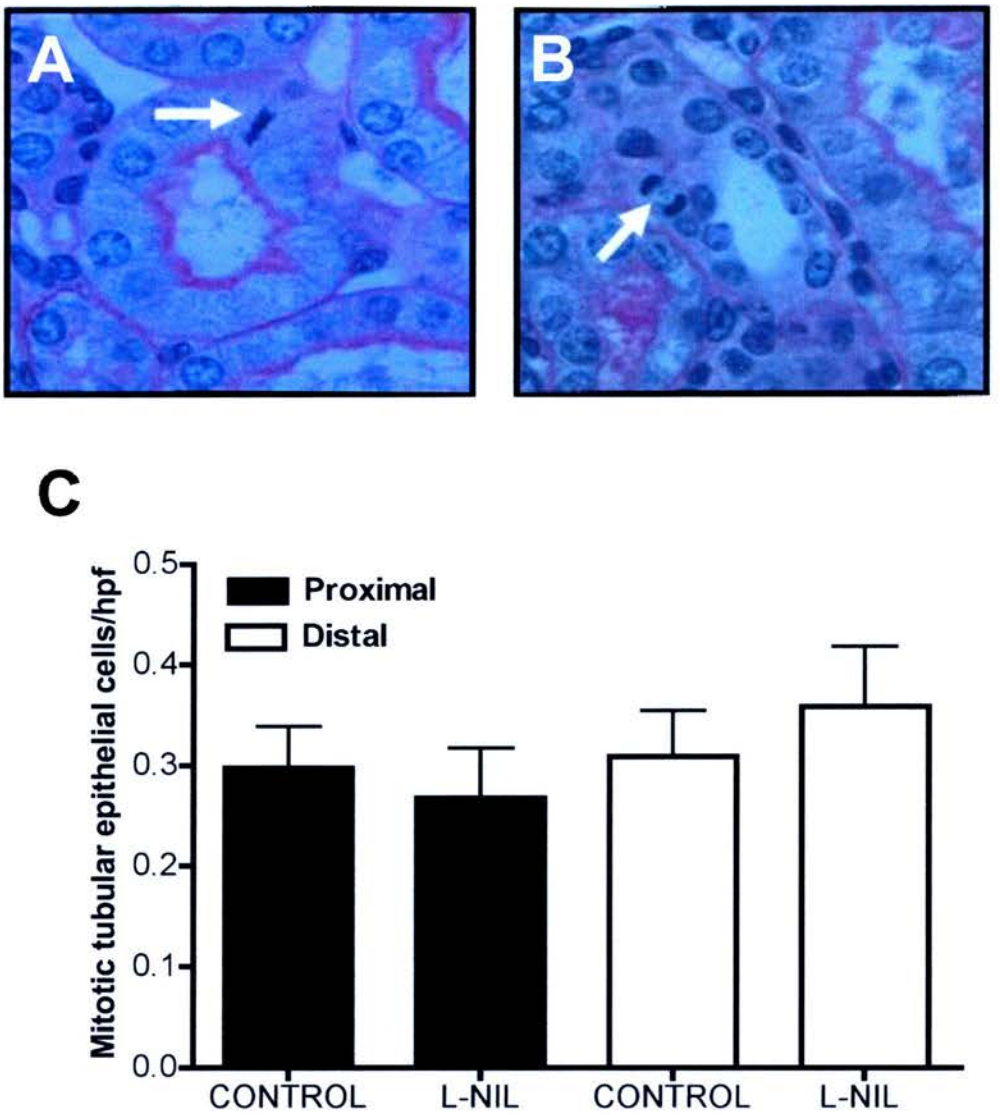

Figure 4- 10 Pharmacological blockade of iNOS does not affect proximal or distal tubular epithelial cell proliferation at day 7 following UUO.

Mice were administered L-NIL (1mg/ml), an irreversible pharmacological inhibitor of the enzyme iNOS, or the isomeric control D-NIL (1mg/ml) in the drinking water from day 5 after UUO. The obstructed kidneys were removed at day 7 and tissue sections underwent PAS staining to detect mitotic cells. High power view (x1000magnification) of a mitotic proximal tubular cell (**A**) and a mitotic distal tubular cell (**B**). The level of tubular cell proliferation in obstructed kidneys is unaffected following the administration of L-NIL (**C**) (n=7- 8 mice per group).

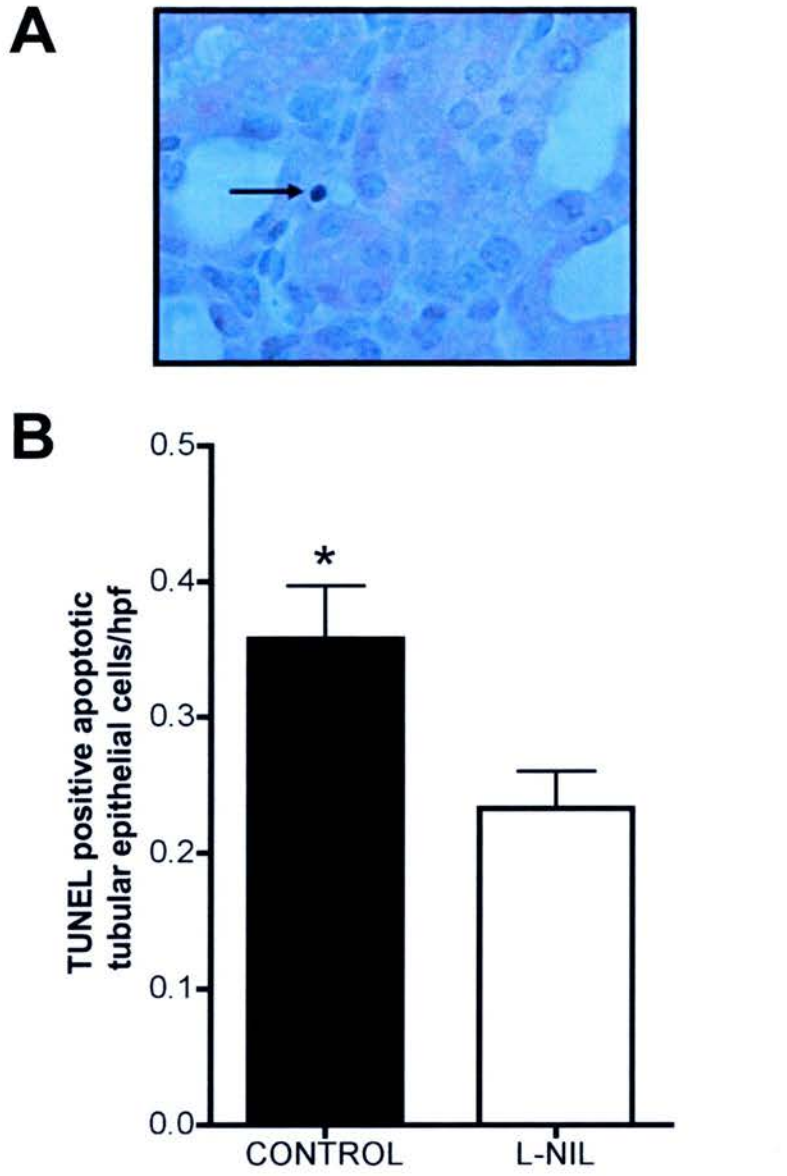

Figure 4- 11 Pharmacological blockade of iNOS reduces interstitial cell apoptosis at day 7 following UUO.
Mice were administered L-NIL (1mg/ml), an irreversible pharmacological inhibitor of the enzyme iNOS, or the isomeric control D-NIL (1mg/ml) in the drinking water from day 5 after UUO. The obstructed kidneys were removed at day 7 and tissue sections underwent TUNEL staining to detect apoptotic cells. High power view (x1000 magnification) of a TUNEL positive apoptotic interstitial cell (**A**). The level of interstitial cell apoptosis in obstructed kidneys is significantly reduced following the administration of L-NIL (**B**) *$p<0.05$ vs control (n=7-8 mice per group).

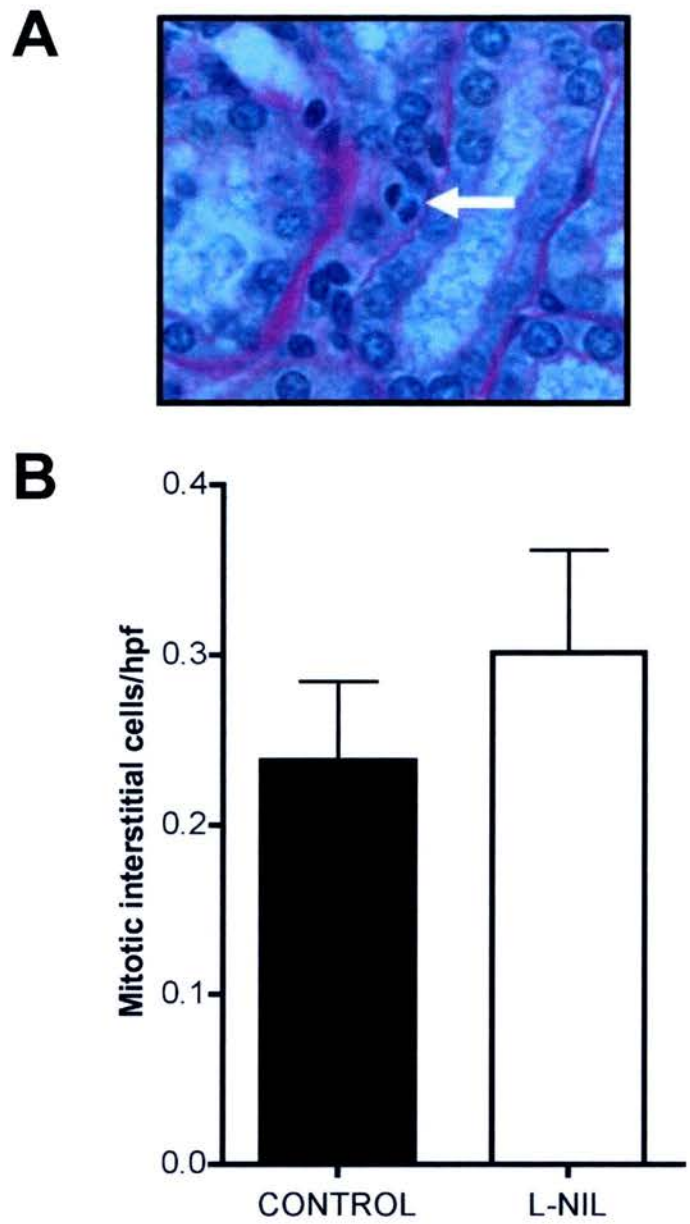

Figure 4- 12 Pharmacological blockade of iNOS does not affect interstitial cell proliferation at day 7 following UUO

Mice were administered L-NIL (1mg/ml), an irreversible pharmacological inhibitor of the enzyme iNOS, or the isomeric control D-NIL (1mg/ml) in the drinking water from day 5 after UUO. The obstructed kidneys were removed at day 7 and tissue sections underwent PAS staining to detect mitotic cells. High power view (x1000 magnification) of a mitotic interstitial cell (**A**). The level of interstitial cell proliferation in obstructed kidneys is unaffected following the administration of L-NIL (**B**) (n=7-8 mice per group).

4.2.11 Pharmacological blockade of iNOS by L-NIL increases tubulointerstitial fibrosis in experimental hydronephrosis

Tubulointerstitial fibrosis was assessed by immunohistochemical staining for collagen III, which is deposited by fibroblasts and myofibroblasts and is a representative collagen of the scarred and injured tubulointerstitium (Mazzali et al., 2003). Careful morphometric analysis of collagen III immunostaining indicated that pharmacological blockade of the enzyme iNOS resulted in increased collagen III deposition (Figure 4-12).

4.2.12 Pharmacological blockade of iNOS by L-NIL does not effect the myofibroblast accumulation in experimental hydronephrosis

Kidney tissue sections were stained for α-SMA, which is expressed by tubulointerstitial myofibroblasts (Hughes et al., 1999). Interstitial myofibroblasts play an important role in the pathogenesis of tissue fibrosis and scarring since they actively produce extracellular matrix molecules such as collagens types I, III and IV. The area of the renal tubulointerstitium occupied by α-SMA staining was assessed morphometrically as an indirect measure of the tubulointerstitial myofibroblast population. Interestingly, despite the increased level of interstitial collagen III deposition, this analysis indicated no significant difference in α-smooth muscle actin staining following short-term blockade of iNOS (Figure 4-14).

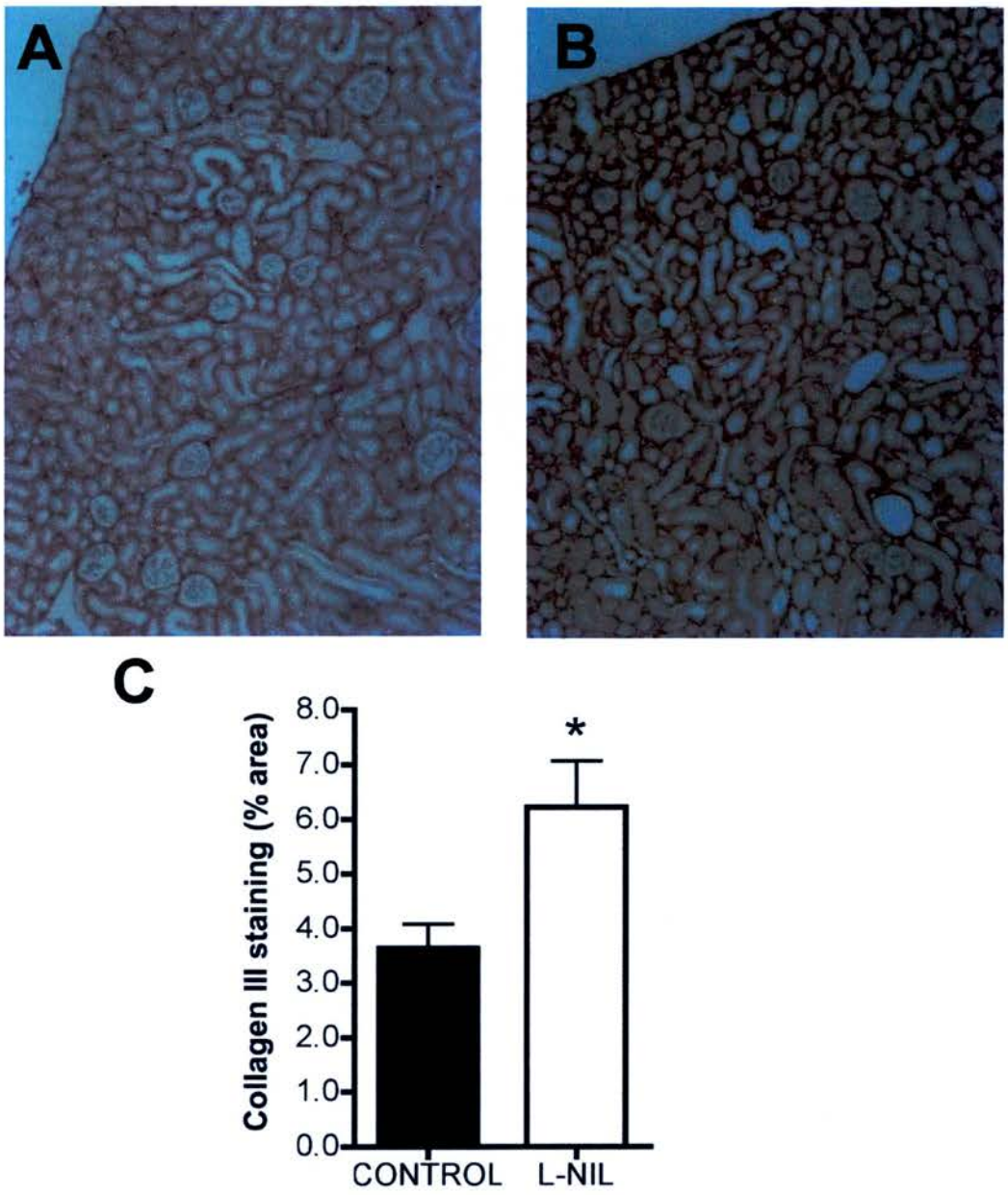

Figure 4-13 Pharmacological blockade of iNOS increases tubulointerstitial deposition of collagen III at day 7 following UUO.
Mice were administered L-NIL (1mg/ml), an irreversible pharmacological inhibitor of the enzyme iNOS, or the isomeric control D-NIL (1mg/ml) in the drinking water from day 5 after UUO. The obstructed kidneys were removed at day 7. Photomicrographs of collagen III immunostaining at day 7 in control mice (**A**) and mice treated with L-NIL (**B**). (x100 magnification). The administration of L-NIL increases the tubulointerstitial deposition of collagen III assessed by computer image analysis (**C**) * $p<0.05$ vs control (n=7- 8 mice per group).

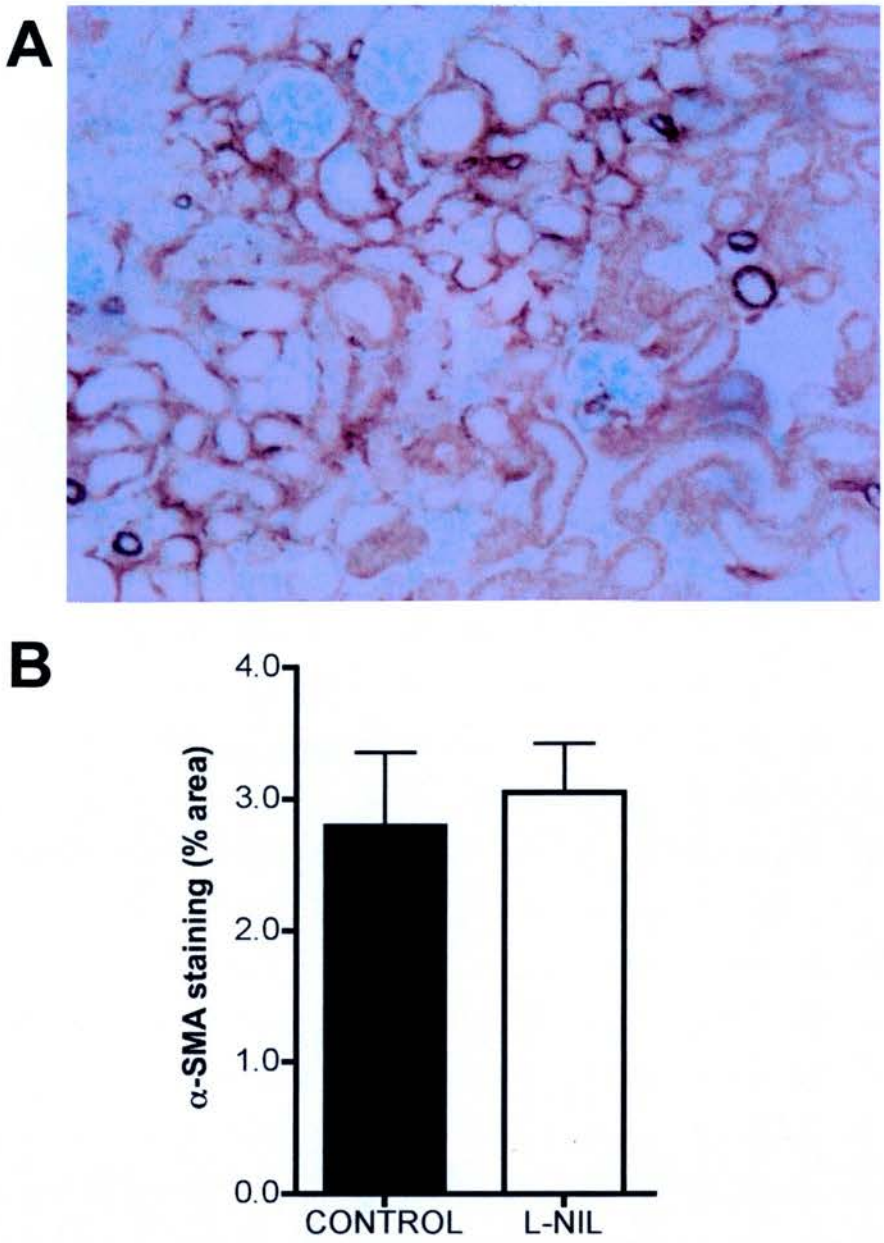

Figure 4- 14 Pharmacological blockade of iNOS does not affect the accumulation of interstitial myofibroblasts at day 7 following UUO.
Mice were administered L-NIL (1mg/ml), an irreversible pharmacological inhibitor of the enzyme iNOS, or the isomeric control D-NIL (1mg/ml) in the drinking water from day 5 after UUO. The obstructed kidneys were removed at day 7 and tissue sections were stained for α-SMA which is a marker for myofibroblasts. Photomicrographs of α-SMA immunostaining at day 7 in control mice (**A**) (x100 original magnification). The administration of L-NIL does not affect the interstitial myofibroblast population (**B**) (n =7- 8 mice per group).

4.3 SUMMARY

The experiments described in this chapter shed light upon the interaction of Mϕ and renal tubular epithelial cells *in vivo*. I employed the model of experimental hydronephrosis induced by UUO to seek a role for iNOS-derived NO in inducing tubular cell apoptosis during tubulointerstitial inflammation *in vivo*.

Following seven days of UUO, there was a marked increase in the level of F4/80 positive Mϕ within the tubulointerstitium. Further characterisation of these interstitial Mϕ showed that many Mϕ stained positive for iNOS. UUO was induced in iNOS WT and iNOS KO mice. The obstructed kidneys of iNOS KO mice exhibited significantly higher Mϕ infiltration than iNOS WT mice. I therefore analysed if there was a correlation between the level of Mϕ infiltration and the degree of tubular cell apoptosis in each genotype. Mϕ infiltration in iNOS WT mice but not iNOS KO mice, exhibited a positive correlation with TEC apoptosis; a finding found in other studies (Lange-Sperandio et al., 2002; Tesch et al., 1999).

In view of the confounding effect upon Mϕ infiltration seen in the iNOS KO mice, I adopted a pharmacological approach of inhibiting the activity of the NO-generating enzyme iNOS during experimental hydronephrosis. L-NIL was administered in the drinking water between day 5 and day 7 following UUO. In order to minimise any potential impact upon Mϕ infiltration, I chose to commence L-NIL administration for a 48 hour period commencing at day 5. I observed that this drug treatment did not affect the level of tubulointerstitial Mϕ infiltration. Pharmacological blockade of iNOS by L-NIL reduced the levels of TEC and

interstitial cell apoptosis but did not affect their proliferation. Interestingly, tubulointerstitial fibrosis was significantly increased after L-NIL administration, although there was no difference in α-SMA staining.

Chapter 5.

Macrophage Depletion Ameliorates Tubulointerstitial Fibrosis In Experimental Hydronephrosis

5.1 INTRODUCTION

The results from the *in vivo* experiments in the previous chapter indicated a key role for the enzyme iNOS in the induction of tubular epithelial cell and interstitial cell death *in vivo* in the model of experimental hydronephrosis. In contrast, iNOS did not play a role in modulating the level of tubular epithelial cell and interstitial cell proliferation, although interstitial fibrosis was increased by inhibition of iNOS. Since my studies demonstrated infiltrating iNOS positive Mϕ in the interstitium of obstructed kidneys, I went on to investigate the effect of Mϕ ablation in this model.

I used a model of conditional Mϕ ablation strategy (Cailhier et al., 2005) to investigate the effect of Mϕ depletion upon tubular cell death *in vivo* in the model of experimental hydronephrosis. In this chapter I will describe the results obtained after ablating interstitial inflammatory Mϕ during the course of UUO.

5.2 RESULTS

5.2.1 Administration of Diphtheria toxin (DT) reduces tubulointerstitial Mϕ infiltration in experimental hydronephrosis

CD11b-DTR mice on the FVB/N background underwent UUO at day 0 and diphtheria toxin (DT) was administered intraperitoneally on day 5 (20ng/g BW) and day 6 (10ng/gBW) following UUO. Control mice were injected with an equal volume of vehicle (PBS) with 5 mice per group. The kidneys were removed at day 7 and underwent histological processing. Tubulointerstitial Mϕ infiltration was detected by staining the kidney sections for the specific Mϕ marker F4/80. The degree of Mϕ infiltration was quantified by careful computer-assisted image analysis. DT treatment induced a significant 2-fold reduction in tubulointerstitial Mϕ accumulation in obstructed kidneys at day 7 (Figure 5-1c).

I then determined whether increased Mϕ ablation could be achieved by increasing the dose of DT. CD11b-DTR mice underwent UUO at day 0 and DT (25ng/g BW) or an equal volume of PBS was injected intraperitoneally on days 5, 6 and 7 following UUO. Morphometric analysis of F4/80 positive tubulointerstitial Mϕ indicated that 3 doses of DT resulted in a 3-fold reduction of tubulointerstitial Mϕ (Figure 5-1d) although there was a slightly higher level of Mϕ infiltration in the mice receiving PBS compared to the control group for the study involving the administration of 2 doses of DT (compare Figure 5-1c and d).

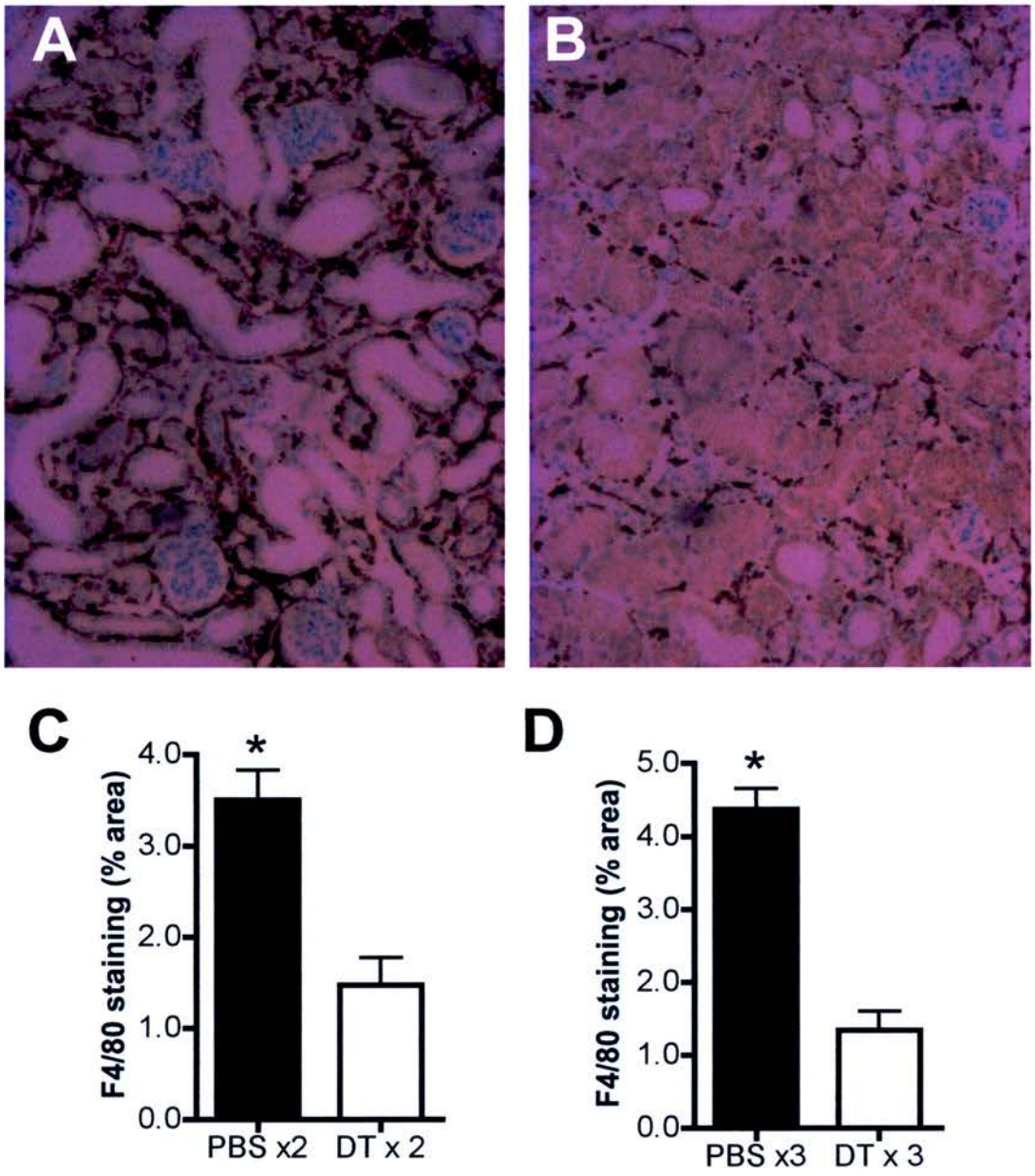

Figure 5- 1 Tubulointerstitial Mϕ accumulation is reduced after DT treatment during experimental hydronephrosis.
F4/80 immunostaining of day 7 UUO kidneys after 3 doses of PBS (**A**) and after 3 doses of DT (**B**). Quantification of Mϕ infiltration by computer assisted image analysis demonstrated a 2-fold reduction of interstitial Mϕ infiltration after 2 doses of DT (**C**) and a 3-fold reduction after 3 doses of DT (**D**) (*$p<0.01$ vs PBS treated mice, (n=5-6 mice per group).

5.2.2 Mϕ depletion does not ameliorate tubular cell apoptosis nor affect the level of tubular cell proliferation in experimental hydronephrosis.

The effect of Mϕ depletion after 2 and 3 doses of DT upon tubular cell and interstitial cell apoptosis was evaluated by TUNEL staining or PAS staining (to distinguish between proximal and distal apoptosis) of tissue sections at day 7 following UUO. Mϕ depletion had no effect upon the level of tubular cell or interstitial cell apoptosis in mice receiving 2 doses of DT (Figure 5-2). In addition apoptosis of proximal and distal tubular cells or interstitial cells was not reduced in mice treated with 3 doses of DT (Figure 5-3a).

PAS staining was used to quantify tubular cell and interstitial cell proliferation. Mϕ ablation following 2 doses of DT did not have any effect upon tubular or interstitial cell apoptosis (Figure 5-2b) and there was no effect upon the numbers of tubular cells undergoing mitosis in mice treated with 3 doses of DT (Figure 5-3b). In the light of data previously presented in thesis, it was surprising that a 3-fold reduction of infiltrating Mϕ did not exert any significant effect upon tubular cell apoptosis.

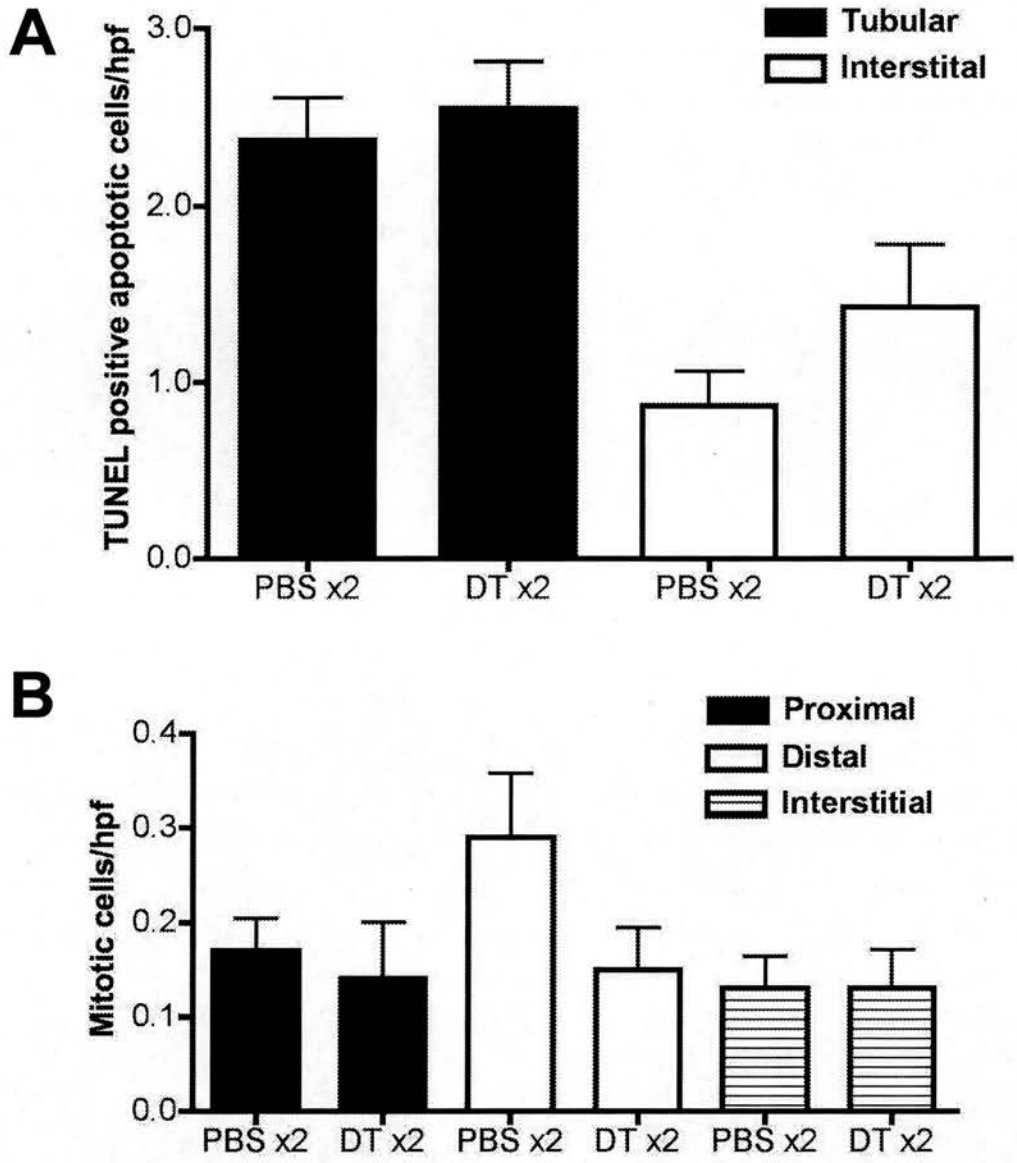

Figure 5- 2 2-fold Mϕ depletion does not affect tubular cell nor interstitial cell apoptosis or proliferation at day 7 following UUO.
CD11b-DTR mice were administered two doses of DT *i.p* at day 5 (20ng/g BW) and day 6 (10 ng/g BW) and control mice received an equal volume of PBS. The obstructed kidneys were removed at day 7 and tissue sections underwent TUNEL staining to detect apoptotic cells and PAS staining to detect mitotic cells. DT treatment did not reduce the level of TEC or interstitial cell apoptosis (**A**) and the level of proliferation was unaffected following DT administration (**B**), n=5 mice per group).

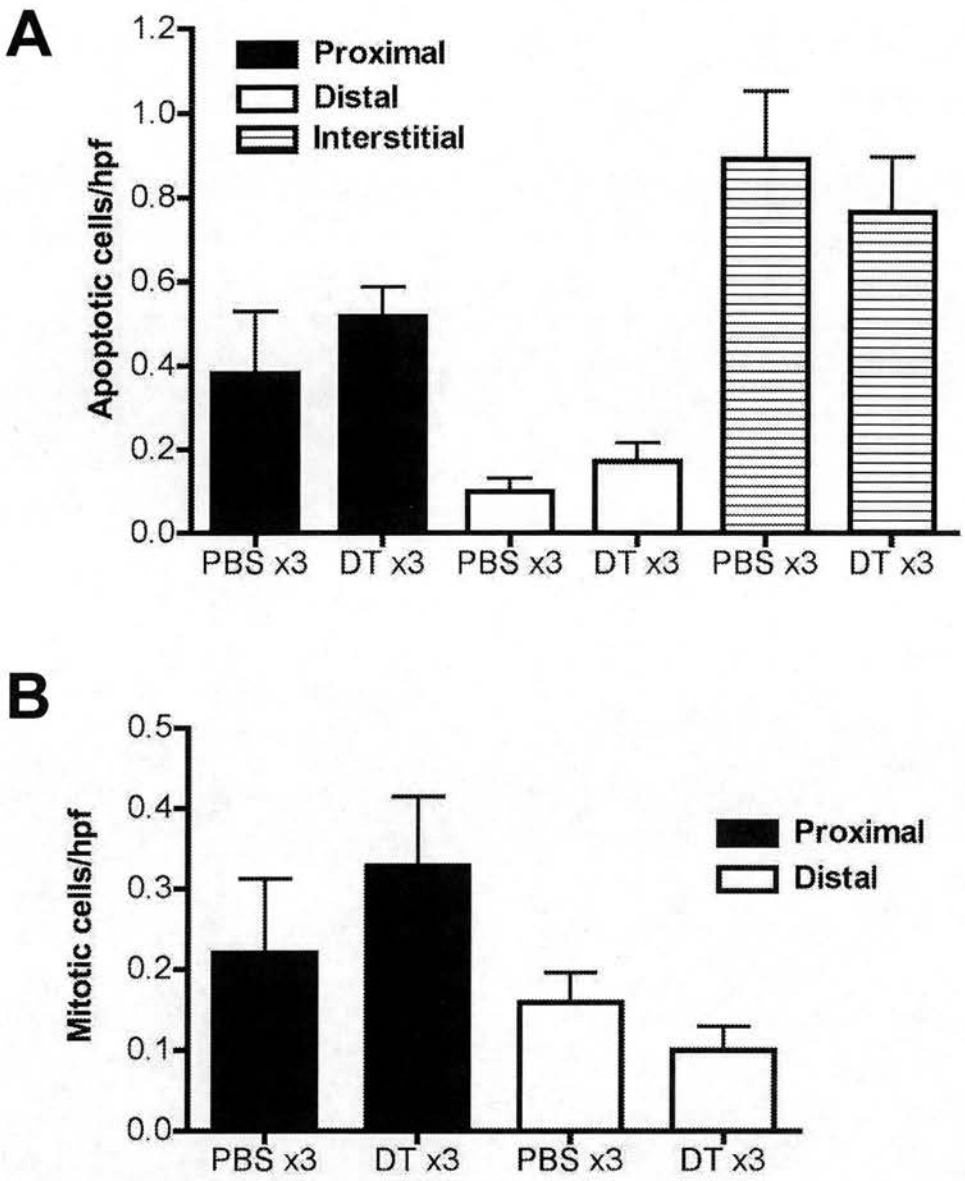

Figure 5- 3 3-fold Mϕ depletion does not affect tubular cell or interstitial cell apoptosis or proliferation at day 7 following UUO.
CD11b-DTR mice underwent UUO at day 0 and DT (25ng/g BW) or and equal volume of PBS was injected *i.p* on days 5, 6 and 7. The obstructed kidneys were removed at day 7 and tissue sections underwent PAS staining. DT treatment did not reduce the level of tubular cell or interstitial cell apoptosis (**A**) and the level of tubular cell proliferation was unaffected following DT administration (**B**), (n=5-6 mice per group).

5.2.3 Mϕ depletion reduces tubulointerstitial fibrosis in experimental hydronephrosis

Tubulointerstitial fibrosis of kidney sections at day 7 following UUO was assessed by immunostaining for collagens I and III and by picrosirius red staining for fibrillary collagen. The percentage area for each stain was quantified by computer assisted image analysis. Deposition of collagen I was diminished in mice treated with 2 doses of DT (Figure 5-4a) and also in mice treated with 3 doses of DT (Figure 5-5c). Pro-collagen I gene expression was quantified by real-time RT-PCR (kindly performed by Sarah Farnworth and Dr. Alison MacKinnon, MRC Centre for Inflammation Research, University of Edinburgh) and analysis indicated that there was a trend towards reduced pro-collagen I gene expression in mice treated with 3 doses of DT but this was not statistically significant (2.9±0.6 vs 24.3±14.4, DT vs PBS, p=0.13) The expression of pro-collagen I was corrected for the house keeping gene ribosomal RNA 18S. These data indicated that Mϕ depletion induced by DT treatment had an anti-fibrotic effect.

Collagen III deposition was also reduced in the obstructed kidneys of mice treated with 3 doses of DT (Figure 5-6c). There was a trend for reduced levels of collagen III deposition in the obstructed kidneys of mice treated with 2 doses of DT (Figure 5-4b). Lastly, although picrosirius red staining showed a trend towards reduced levels of fibrillary collagen deposition, this was not statistically significant (Figure 5-4c).

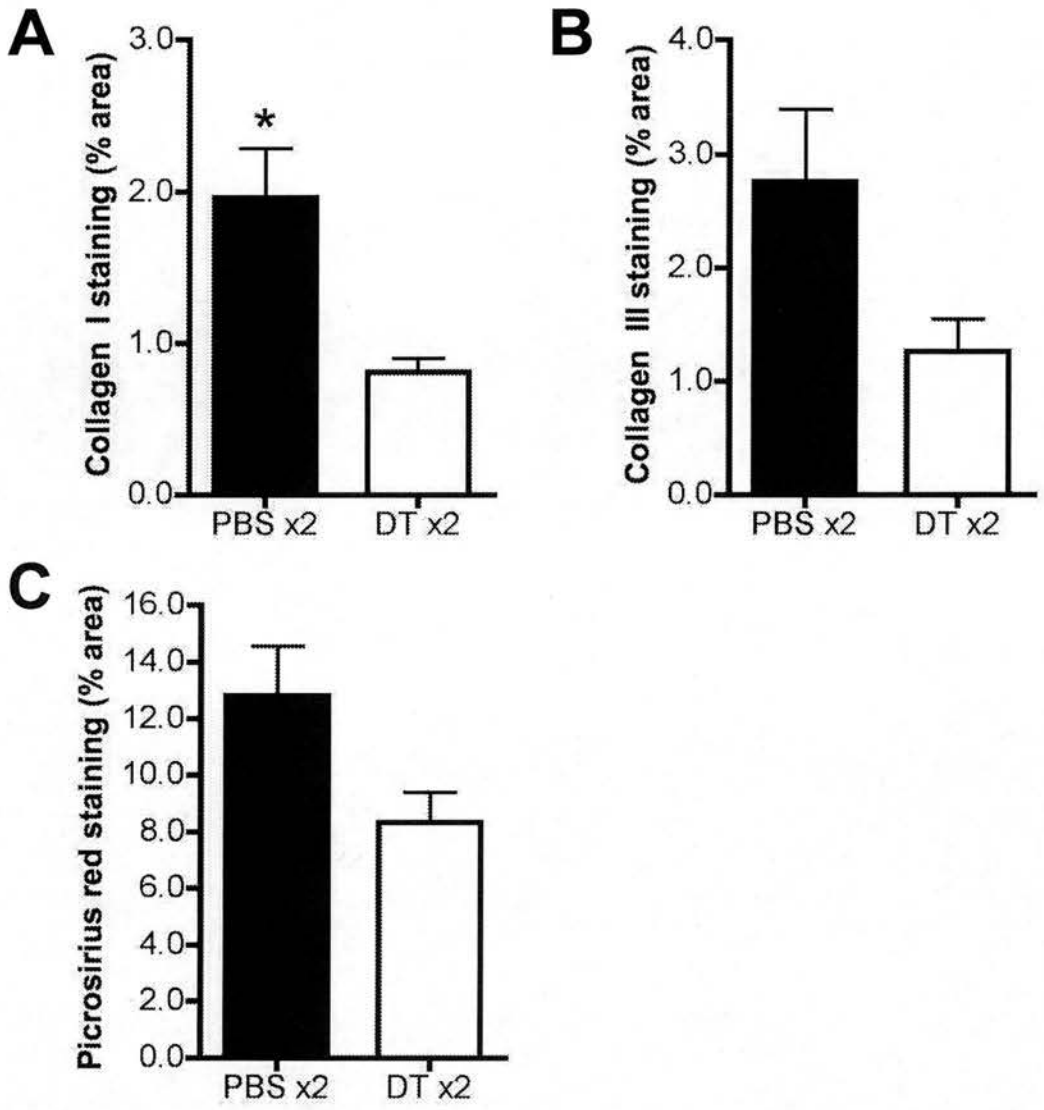

Figure 5- 4 The effect of 2 doses of DT (inducing a 2-fold Mϕ depletion) upon collagen deposition at day 7 following UUO.

Quantitation of tubulointerstitial fibrosis of kidneys at day 7 following UUO was assessed by computer assisted image analysis after staining for collagen I (**A**). DT treatment and the resultant 2-fold Mϕ depletion resulted in a significant reduction in collagen I deposition (*$p<0.01$ vs PBS x2 treated mice). There was a trend for reduced levels of collagen III deposition ($p=0.055$ vs PBS x2) (**B**) and fibrillary collagen deposition (latter assessed by picrosirius red staining, $p=0.057$) (**C**), n=5 mice per group).

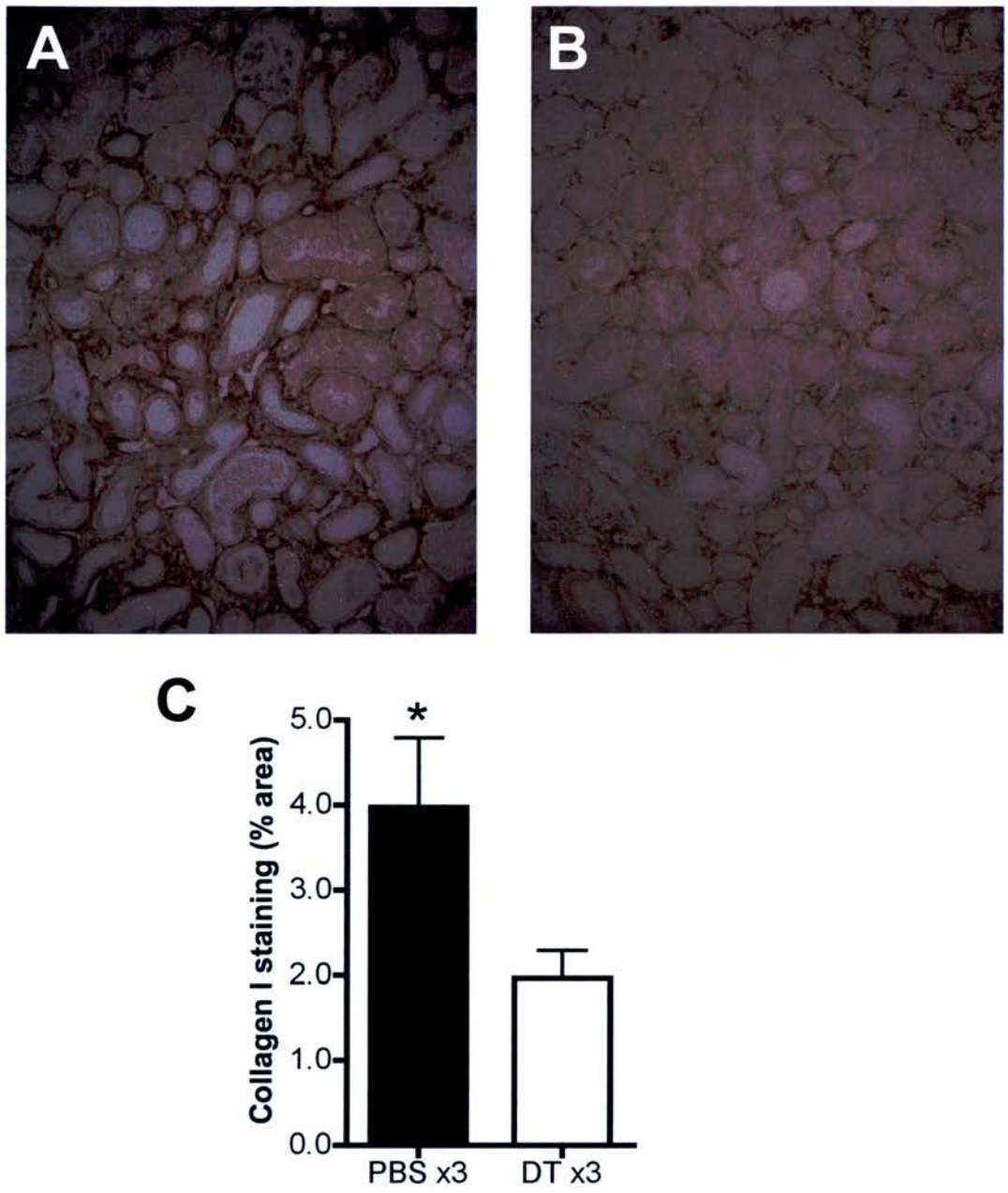

Figure 5- 5 3-fold Mϕ depletion reduces collagen I deposition at day 7 following UUO.

Collagen I immunostaining of day 7 UUO kidneys after 3 doses of PBS (**A**) and after 3 doses of DT (**B**). Collagen I deposition was quantified by computer assisted image analysis and this was significantly reduced in mice treated with 3 doses of DT (**C**). (*$p<0.05$ vs PBS x3 treated mice) (n=5- 6 mice per group).

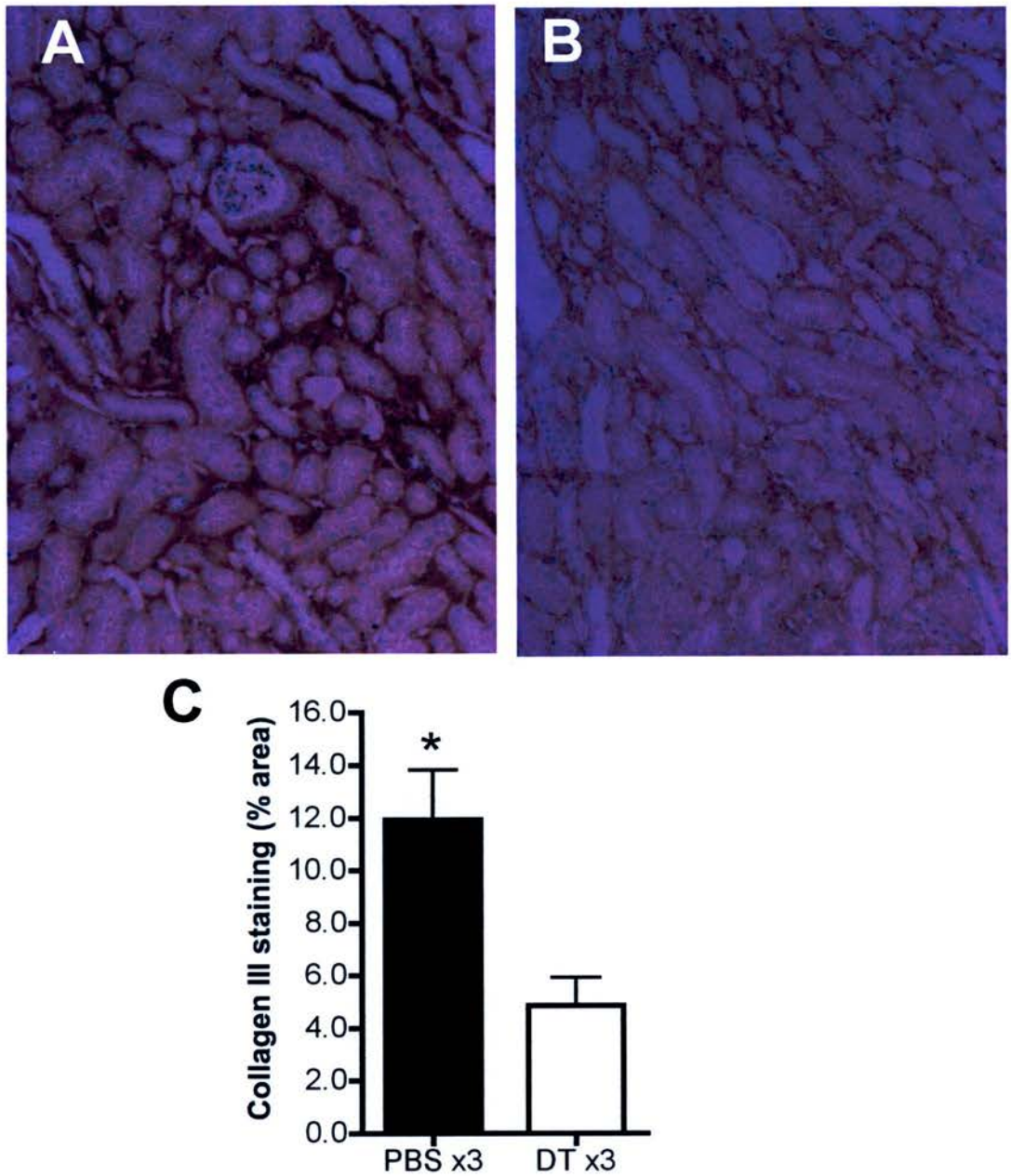

Figure 5- 6 3-fold Mϕ depletion reduces collagen III deposition at day 7 following UUO.

Collagen III immunostaining of day 7 UUO kidneys after 3 doses of PBS (**A**) and after 3 doses of DT (**B**). Collagen III deposition was quantified by computer assisted image analysis and this was significantly reduced in mice treated with 3 doses of DT(**C**). (*$p<0.01$ vs PBS x3 treated mice) (n=5- 6 mice per group).

5.2.4 Mϕ depletion in experimental hydronephrosis results in a trend towards lower levels of myofibroblast accumulation

The accumulation of myofibroblasts was assessed by computer assisted image analysis after staining day 7 UUO kidneys with α-SMA. Mice treated with 2 does of DT displayed a trend towards lower levels of myofibroblast accumulation but this was statistically not significant (Figure 5-7c). Similar results were found in mice treated with 3 doses of DT (Figure 5-7d). α-SMA gene expression was quantified by RT-PCR (kindly performed by Sarah Farnworth and Dr. Alison MacKinnon (Centre for Inflammation Research, University of Edinburgh) and analysis indicated that α-SMA gene expression was significantly reduced in mice treated with 3 doses of DT (0.00049±0.00032 vs 0.0051±0.0015, DT vs PBS, $P<0.01$) The expression of α-SMA was corrected for the house keeping gene ribosomal RNA 18S.

5.2.5 iNOS positive Mϕ are present in the kidneys of Mϕ depleted mice

Since Mϕ depletion did not affect the level of tubular cell apoptosis, I went on to investigate potential explanations. Mice treated with 3 doses of DT still had infiltrating Mϕ present within the tubulointerstitium since DT treatment induced a 3-fold reduction and did not completely deplete all infiltrating Mϕ. The work so far has indicated the Mϕ-derived NO is a key mediator for TEC apoptosis *in vitro* with iNOS-derived NO being key in UUO *in vivo*. I therefore double stained the kidney sections of Mϕ depleted mice for F4/80 and iNOS. Interestingly the presence of Mϕ expressing iNOS was still observed in kidney sections which had received 3-doses of DT (Figure 5-8).

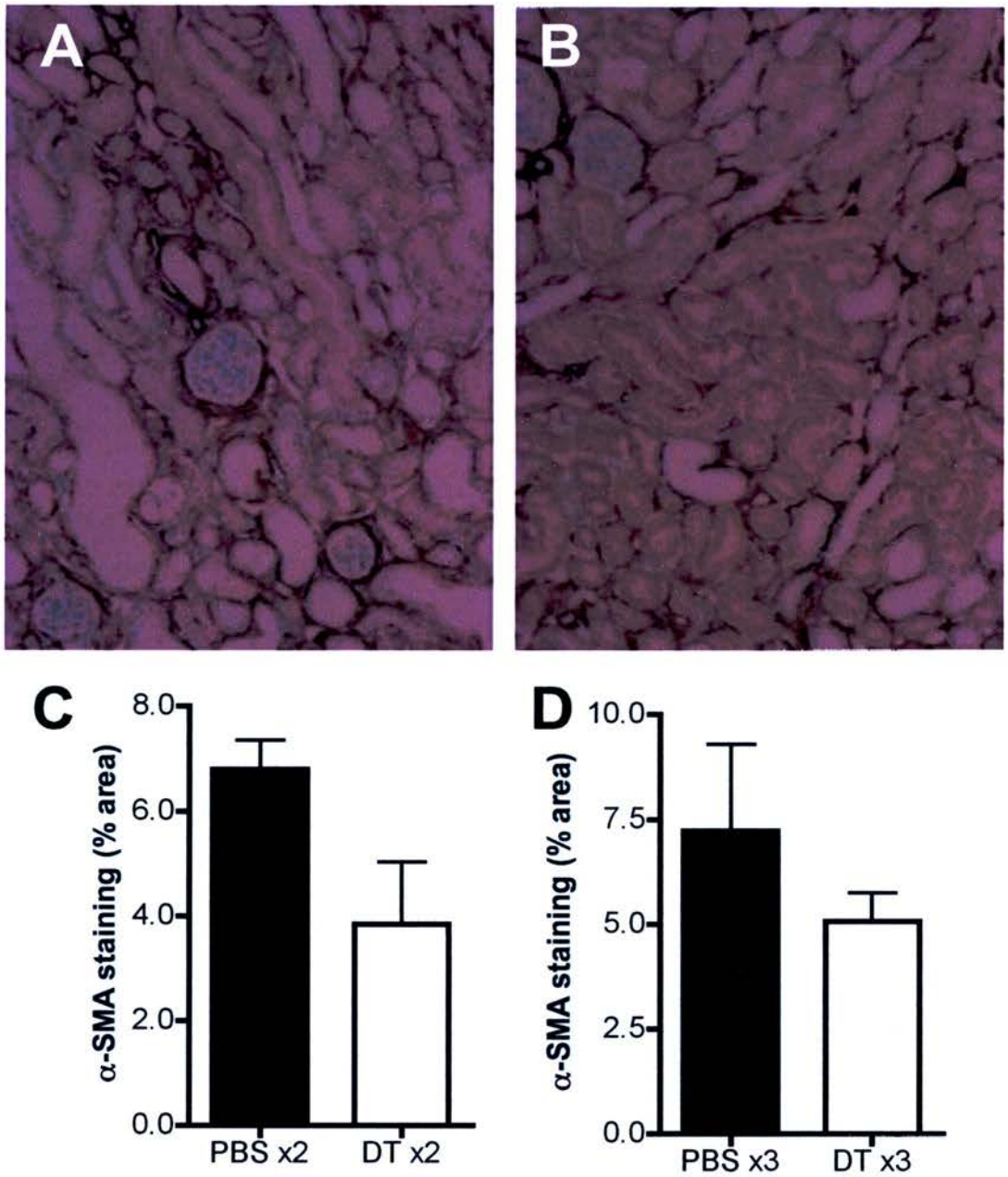

Figure 5- 7 A trend towards lower levels of myofibroblast accumulation following Mϕ ablation.

Photomicrographs of α-SMA immunostaining (x100) at day 7 following UUO in PBS treated control mice (**A**) and mice treated with DT (**B**). Quantification of percentage area of α-SMA staining by computer assisted image analysis (**C**) and (**D**). There was a non-significant trend towards lower levels of myofibroblast accumulation in mice receiving either 2 doses (p=0.051) or 3 doses (p=0.3) of DT.(n=5-6 mice per group).

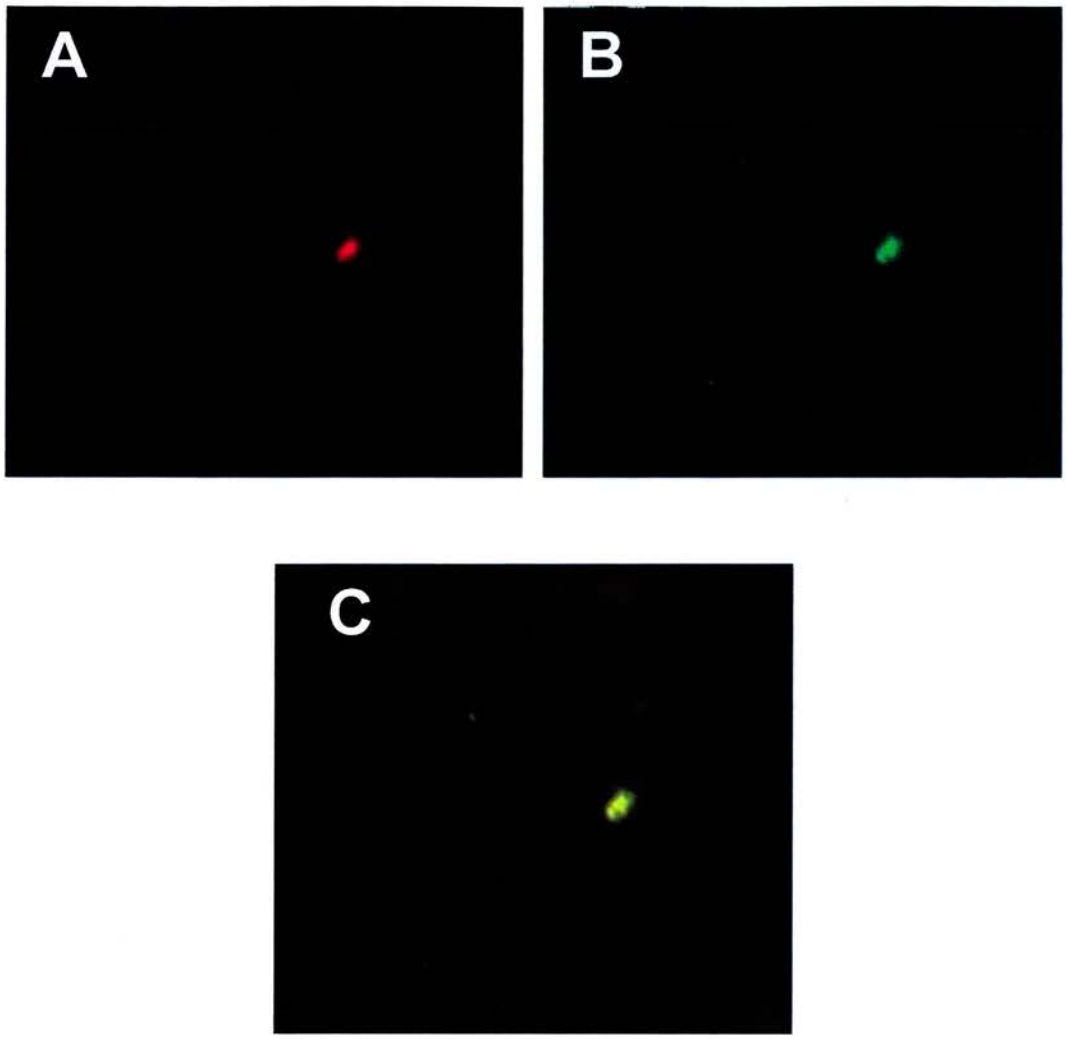

Figure 5- 8 Fluorescent photomicrographs showing the presence of iNOS positive Mϕ in obstructed kidneys receiving 3-doses of DT.
CD11b-DTR mice underwent UUO at day 0 and DT (25ng/gBW) *i.p* on days 5, 6 and 7. The obstructed kidneys were removed at day 7 and tissue sections underwent double immunofluorescent staining for F4/80 and iNOS. Fluorescent photomicrographs showing F4/80 positive Mϕ stained red **(A)** and iNOS positive cell stained green (**B**). The merged image demonstrates colocalisation (yellow) of iNOS and F4/80 indicating the presence of infiltrating Mϕ expressing iNOS in the mice treated with D (**C**).

5.3 TGF-β expression following Mϕ ablation

Since Mϕ depletion ameliorated tubulointerstitial fibrosis, I investigated if TGF-β expression was altered in mice receiving DT since numerous studies have demonstrated a critical role for TGF-β during kidney fibrosis (Choi et al., 2005; Kelly et al., 2004; Sato et al., 2003).

TGF-β expression was detected by staining the kidney sections with a chicken polyclonal anti-TGF-β antibody, which recognises murine TGF-β. Specificity of staining was determined by staining tissue sections with the isotype control antibody (chicken IgG). Although I have not formally quantified the level of TGF-β expression the preliminary results suggest that a 3-fold Mϕ depletion did not markedly affect the level of TGF-β expression (Figure 5-9a) as the level of TGF-β expression was similar in control mice receiving PBS (Figure 5-9b). I did not, however, analyse the expression of factors that can activate TGF-β such as thrombospondin as altered expression of such factors would affect the level of active TGF-β in the kidney (Daniel et al., 2003). TGF-β gene expression was quantified by RT-PCR (kindly performed by Sarah Farnworth and Dr. Alison MacKinnon in the MRC Centre for Inflammation Research, University of Edinburgh) and analysis indicated that a 3-fold Mϕ depletion did not affect the level of TGF-β gene expression (26.6±2.7 vs 20.7±6.3, DT vs PBS). The expression of TGF-β was corrected for the house keeping gene β-actin.

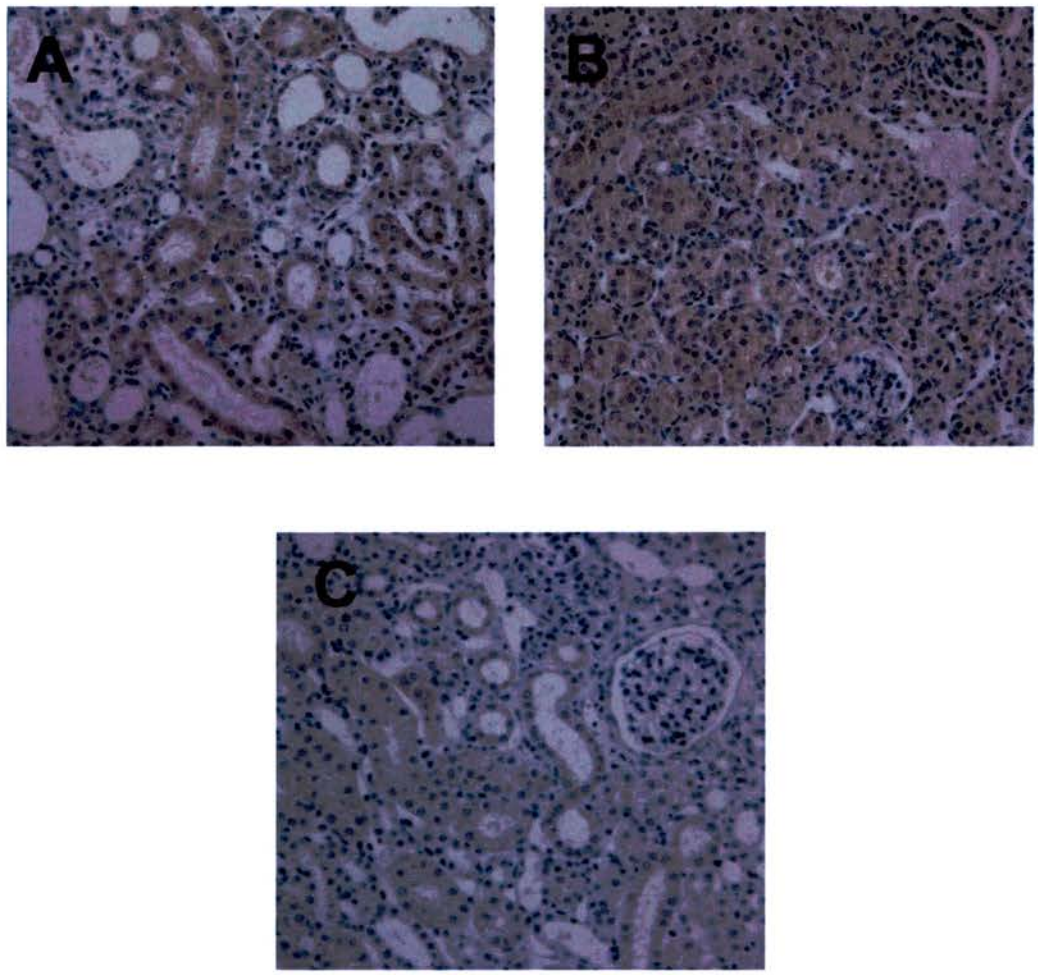

Figure 5- 9 Photomicrographs of TGF-β immunostaining of day 7 obstructed kidneys after 3 doses of PBS or 3 doses of DT.
CD11b-DTR mice underwent UUO at day 0 and DT (25ng/gBW) or and equal volume of PBS was injected *i.p* on days 5, 6 and 7. The obstructed kidneys were removed at day 7 and tissue sections were immunostained for TGF-β. Photomicrographs (x100 magnification), showing TGF-β staining after 3 doses of PBS (**A**) and after 3 doses of DT (**B**). The specificity of TGF-β staining is indicated by incubation of tissue sections with an irrelevant isotype antibody (negative control) since no significant immunostaining is evident (**C**).

5.4 SUMMARY

In the experiments described in this chapter, a conditional Mϕ ablation strategy was used to investigate the effect of Mϕ depletion upon tubular cell death *in vivo* in the model of experimental hydronephrosis. Mice underwent UUO and were either treated with 2 doses of DT or 3 doses of DT, while control mice received equal volumes of vehicle. Administration of 2 or 3 doses of DT resulted in a 2-fold or 3-fold reduction of tubulointerstitial Mϕ infiltration respectively. DT administration did not reduce the level of tubular epithelial cell or interstitial cell apoptosis or affect their level of proliferation. Interestingly, phenotyping of the interstitial Mϕ still present in the DT treated obstructed kidneys, demonstrated the presence of iNOS positive Mϕ within the tubulointerstitium

Interestingly tubulointerstitial fibrosis was ameliorated after Mϕ depletion and α-SMA gene expression was reduced, although no effect was seen upon of interstitial myofibroblast accumulation.

Lastly preliminary staining for TGF-β expression and RT-PCR quantitation of TGF-β gene expression indicated that Mϕ depletion did not affect this.

Chapter 6.

Discussion

6.1 DISCUSSION

In this thesis I examined the cytotoxic mechanism underlying Mϕ-mediated tubular epithelial cell death *in vitro* and *in vivo*. I used the well established microscopically quantifiable co-culture assay (Duffield et al., 2000), the model of experimental hydronephrosis (Diamond, 1995; Lange-Sperandio et al., 2002; Lenda et al., 2003) and a conditional Mϕ ablation strategy in these studies. This area of renal cell biology has been studied previously (Lange-Sperandio et al., 2003; Tesch et al., 1999) but - these reports did not determine the mechanisms underlying Mϕ-mediated apoptosis of tubular cells.

The experiments described in Chapter 3 shed light upon the interaction of murine BMDM with renal tubular epithelial cells *in vitro*. The first major finding of my *in vitro* co-culture studies was that, although non-activated BMDM were not cytotoxic to MDCK cells or PTE cells, cytokine-activated BMDM induced significant levels of tubular cell apoptosis. The level of PTE cell apoptosis evident was less than the level of MDCK cell apoptosis. This may reflect various factors including the different species of origin of the tubular cells and their proliferative status. In addition, the data suggested that murine Mϕ were able to phagocytose apoptotic PTE cells but not MDCK cells and this may be at least partly responsible for the differing level of 'free' apoptotic cells evident in the assays as apoptotic cells may be rapidly recognised, ingested and degraded (Barres et al., 1992).

The *in vitro* studies also demonstrated that the induction of tubular cell apoptosis by cytokine activated BMDM was significantly reduced by inhibitors of

NO synthase. Furthermore, experiments using cytokine activated BMDM derived from either iNOS KO or WT mice indicated that BMDM cytotoxicity was dependent upon iNOS-derived NO.

These data are in accordance with previous reports indicating that NO is an important mediator of Mϕ cytotoxicity towards various target cells (Cui et al., 1994; Duffield et al., 2000). Despite the fact that previous work has indicated the involvement of NO in Mϕ induction of apoptosis in various cells including mesangial cells (Duffield et al., 2000) and vascular smooth muscle cells (Boyle et al., 2002), other death effectors such as TNF-α (Boyle et al., 2003; Duffield et al., 2001) and FasL (Boyle et al., 2001; Boyle et al., 2002) have also been implicated. In addition, Meldrum et al used a pegylated form of soluble TNFR1 to inhibit the action of TNF-α in a rat model of UUO (Meldrum et al., 2006). This study demonstrated a reduced level of renal tubular cell apoptosis and the authors suggest that TNF-α is a key mediator of tubular cell death in this model. The authors did not, however, determine whether the inhibition of TNF-α affected Mϕ infiltration, iNOS expression or NO production by Mϕ. Also Guo et al performed UUO in mice deficient in either the TNFR1 or TNFR2 receptors and demonstrated that TNF-α contributed to the interstitial pathology (Guo et al., 1999) but tubular cell apoptosis was not examined in this study. Work in our laboratory has investigated the effect of pharmacological inhibition of iNOS upon the production of other potential death effectors and demonstrated that L-NIL treatment of cytokine stimulated BMDM does not affect TNF-α release or FasL expression *in vitro* (Anya Adair, personal communication). This suggests that NO is the prime mechanism involved in the

induction of tubular cell death by cytokine activated BMDM under the *in vitro* conditions employed in these studies.

The effect of BMDM upon the level of target cell proliferation varied according to the nature of the target cell. The proliferation of MDCK cells was reduced by incubation with both non-activated and activated BMDM from iNOS WT and iNOS KO mice (with a trend evident when BMDM derived from FVB/N mice were utilised). This effect was independent of pharmacological inhibition of NO production. BMDM secrete significant levels of TGF-β and this cytokine has been documented to inhibit MDCK cell proliferation (Nicolas et al., 2003; Yang et al., 1998) and therefore it is possible that non-activated iNOS WT and KO BMDM secrete more TGF-β than non-activated BMDM derived from FVB/N mice. In contrast, Mϕ exerted no significant effects upon PTE cell proliferation in this study and this may reflect the significantly lower level of proliferation of these primary cells.

I undertook studies involving the transfer of conditioned supernatants from cytokine activated or control BMDM to cultures of tubular epithelial cells and these conditioned supernatants failed to induce tubular cell death. This finding was in contrast to previous published work demonstrating that supernatants from cytokine activated Mϕ induced apoptosis of immortalised or primary murine tubular epithelial cells (Lange-Sperandio et al., 2003; Tesch et al., 1999). Also, previous work by Lenda et al (Lenda et al., 2003) has demonstrated that the ability of conditioned Mϕ medium to induce apoptosis could be modulated since blockade of the CSF-1 receptor reduced Mϕ activation (determined by expression of activation markers and

reactive oxygen species generation) and the ability of Mϕ conditioned supernatant to induce tubular cell apoptosis. However, my results are in accordance with previous work from our group as activated BMDM conditioned supernatants did not induce apoptosis of mesangial cells *in vitro* (Duffield et al., 2000). The differing results found by various investigators may reflect differences in the experimental methods and cells used in the studies.

Lastly, the experiments involving the use of tissue culture inserts suggested that either direct cell-to-cell contact or 'close proximity' between the target tubular epithelial cell and BMDM was an important requirement for BMDM induction of tubular cell death. It is important to note that my experimental protocol involved the tubular epithelial cells being plated on the inserts with the Mϕ being located in the bottom of the wells as this arrangement reflects the spatial orientation that is likely to be present *in vivo*. However, the work of Lange-Sperandio et al (Lange-Sperandio et al., 2003), suggested that cell contact was not a critical factor since they demonstrated comparable levels of tubular cell apoptosis regardless of whether activated Mϕ and tubular cells were separated from each other by an insert or in direct contact. My results also raise the possibility that a short acting cytotoxic mediator may be involved and this may be degraded or neutralised if it is unable to act rapidly upon a target cell. It should be noted, however, that the spatial orientation found *in vivo* was not present in the co-culture studies but this is also the case for other investigators.

The *in vitro* data indicated a prominent role for Mϕ-derived NO in inducing tubular epithelial cell apoptosis and therefore I employed the experimental model of hydronephrosis induced by UUO, to test the *in vivo* relevance of the findings. The neutrophil and lymphocyte independent model of UUO was chosen for several reasons. First, UUO is characterised by a prominent Mϕ infiltrate and significant levels of tubular cell apoptosis (Diamond, 1995; Hughes et al., 1999). Indeed, the tubular cell apoptosis present in this model is believed to underlie the development of severe renal tubular atrophy (Gobe and Axelsen, 1987). In addition it is characterised by interstitial fibrosis which represent an additional important experimental read-out.

There was a marked increase in the level of F4/80 positive Mϕ within the tubulointerstitium at the day 7 time-point of UUO in FVB/N mice. Double immunolabeling revealed F4/80 positive Mϕ that were strongly iNOS positive within the tubulointerstitium of obstructed kidneys indicating that infiltrating Mϕ may express iNOS *in vivo*. In order to determine the role of iNOS-derived NO, UUO was induced in iNOS WT and KO mice. Unexpectedly, the obstructed kidneys of iNOS KO mice displayed a significantly increased tubulointerstitial Mϕ infiltrate compared to iNOS WT mice. The reasons for this are unclear as the kinetics of Mϕ trafficking through the tubulointerstitium in the model is unknown at present. However, it is possible that the increased Mϕ infiltrate in the iNOS KO mice may result from a reduced level of Mϕ death, since Mϕ may undergo apoptosis during renal inflammation (Lan et al., 1997) and such death may involve Mϕ expression of iNOS (Albina et al., 1993). The increased Mϕ infiltrate may also be a consequence of

increased recruitment to the inflamed tubulointerstitium as iNOS deficient Mϕ secreted increased levels of the CC chemokine MCP-1 (Speyer et al., 2003) and this chemokine is involved in Mϕ recruitment to the inflamed tubulointerstitium (Tesch et al., 1999).

Despite the confounding increased Mϕ infiltrate, the obstructed kidneys of iNOS KO mice, exhibited a trend towards less tubular cell apoptosis compared to iNOS WT mice although this never reached statistical significance. I performed additional analysis of the correlation between the degree of Mϕ infiltration and the levels of tubular cell apoptosis evident in each genotype since a positive correlation has been previously demonstrated in the experimental models of UUO and NTN (Lange-Sperandio et al., 2002; Tesch et al., 1999). Correlation analysis demonstrated that iNOS WT mice exhibited a significant positive correlation between the degree of Mϕ infiltration and the level of tubular cell death whilst this relationship was absent in iNOS KO mice. These experiments raise several issues. They suggest that there is a significant level of Mϕ independent tubular cell death in the UUO model. In addition, in view of the lack of any correlation between iNOS KO Mϕ infiltration and tubular apoptosis, iNOS KO Mϕ do not appear to upregulate additional death effector mechanisms in this model. It is also possible that the tubular cells within the obstructed kidneys of iNOS KO mice may be more vulnerable to apoptosis as iNOS expression by mesangial cells can protect the cells from undergoing apoptosis (Nitsch et al., 1997). Additional studies examining the level of tubular cell death in iNOS WT mice that have received either an iNOS WT or KO bone marrow

transplant would be informative as this would predominantly restrict the iNOS deficiency to infiltrating Mϕ.

In order to circumvent the confounding effect of increased Mϕ infiltration seen in iNOS KO mice and UUO, I chose a pharmacological approach to inhibit iNOS during UUO. L-NIL, a specific irreversible iNOS inhibitor, was administered in the drinking water of mice between day 5 and day 7 in order to minimise any potential impact upon Mϕ infiltration. L-NIL treatment did not affect the level of interstitial Mϕ infiltration but significantly reduced the level of tubular cell apoptosis compared to the control group. L-NIL had no effect upon tubular cell proliferation. However, since L-NIL administration resulted in a partial inhibition of tubular cell apoptosis, it may be the case that additional pro-apoptotic mediators are utilised by the infiltrating inflammatory Mϕ to induce tubular cell apoptosis *in vivo* (Nikolic-Paterson, 2003). For example, Mϕ production of MMPs may result in degradation of TBM and resultant tubular cell apoptosis by anoikis in the murine model of Alports syndrome (Frisch and Francis, 1994; Rodgers et al., 2003). A role for TNF-α in the induction of tubular cell death in the rat UUO model has also been proposed since obstructed rat kidneys up-regulated both TNF-α and FasL (Misseri et al., 2005) and blockade of the actions of TNF-α by systemic administration of a pegylated form of soluble TNF receptor type 1 is protective (Meldrum et al., 2006). However, the level of Mϕ infiltration was not quantified in this study and it is likely that TNF-α inhibition may have reduced Mϕ infiltration.

Pharmacological blockade of iNOS also reduced the level of interstitial cell apoptosis. These apoptotic interstitial cells might have been dying myofibroblasts but this is difficult to determine unequivocally even with double staining for α-SMA and TUNEL since the majority of apoptotic renal cells are located within the phagolysosomes of neighbouring non-apoptotic cells (Coles et al., 1993). Despite the reduction of interstitial cell apoptosis, I found that L-NIL treatment did not affect the level of myofibroblast accumulation. This might have been due to the fact that the period of pharmacological blockade of iNOS was relatively short (48hrs).

L-NIL treatment significantly increased the tubulointerstitial deposition of collagen III that is characteristically found in tubulointerstitial scarring suggesting that iNOS-derived NO may be anti-fibrotic. Interestingly Hochberg et al demonstrated that iNOS KO mice developed increased levels of fibrosis following UUO (Hochberg et al., 2000). Primary murine renal fibroblasts are also susceptible to NO-mediated apoptosis *in vitro* (Claire Taylor, personal communication) and it is possible that the increased fibrosis may reflect diminished induction of interstitial fibroblast apoptosis by Mϕ.

The interpretation of the data from the obstructed kidneys of iNOS KO mice was complicated by the increased Mϕ infiltration evident in the iNOS KO mice. However, pharmacological blockade of the generation of pro-apoptotic NO by iNOS reduced tubular cell apoptosis without affecting Mϕ infiltration and this reinforces the importance of Mϕ phenotype as well as Mϕ numbers during renal inflammation. This paradigm has been supported by the work of Anders et al (Anders et al., 2003)

as inhibition of the CC chemokine ligand 5/RANTES in a model of immune complex glomerulonephritis resulted in diminished glomerular Mϕ number but increased glomerular Mϕ expression of iNOS and an associated increase in glomerular injury.

My data indicating that pharmacological blockade of iNOS-derived NO ameliorated the level of tubular cell apoptosis is not in accordance with previous work by Miyajima et al (Miyajima et al., 2001). They obstructed the kidneys of iNOS KO and iNOS WT mice and demonstrated increased levels of tubular epithelial cell apoptosis in iNOS KO mice. In contrast, I found a trend for reduced levels of tubular epithelial cell apoptosis in the iNOS KO mice (despite increased Mϕ infiltration) and, unlike the iNOS WT mice, no correlation between the level of Mϕ infiltration and tubular epithelial cell apoptosis. In addition, Miyajima et al subjected rat renal tubular epithelial cells to mechanical stretch *in vitro* and demonstrated that stretch-induced apoptosis was increased when a NOS inhibitor was added to the cells thereby implicating NO as a protective factor in stretch induced tubular cell apoptosis *in vitro* and UUO *in vivo* (Miyajima et al., 2001). The reasons for the apparent discrepancies between this study and my results are unclear. Although previous work has suggested that strain differences as they may affect the amount of NO generated by Mϕ (Mills et al., 2000).

Lastly, it should be noted that a significant level of Mϕ independent tubular cell death occurs in the UUO model and it is undoubtedly the case that additional pro-apoptotic stimuli including mechanical stretch, hypoxia, ischemia etc are likely

to play a role in the apoptosis of tubular epithelial cells *in vivo* (Cachat et al., 2003; Fine et al., 1998; Kiley et al., 2005).

The results presented in Chapter 3 and 4 indicated that inflammatory Mϕ play an important role in inducing tubular epithelial cell apoptosis *in vitro* and are likely to be involved *in vivo.* In Chapter 5 I described my experiments involving conditional Mϕ ablation in UUO. The administration of DT to CD11b-DTR transgenic mice results in the rapid ablation of resident/infiltrating Mϕ and circulating monocytes (Cailhier et al., 2005; Cailhier et al., 2006; Duffield et al., 2005a). Work from our group has demonstrated that a single dose of DT (25ng/g body weight) *i.p* induces circulating monocyte depletion for 24-48 hrs and peritoneal Mϕ for 72hrs (Cailhier et al., 2005). This dose of DT resulted in the ablation of resident Mϕ in normal kidneys of CD11b-DTR mice at 24 hours (Cailhier et al., 2005). In my initial studies, CD11b-DTR mice underwent UUO and mice were administered two doses of DT *i.p* at day 5 (20ng/g BW) and day 6 (10ng/gBW). This treatment resulted in a 2-fold reduction in the level of interstitial Mϕ infiltration compared to control mice receiving PBS. I then determined whether increased Mϕ ablation was possible by increasing the dose of DT. CD11b-DTR mice underwent UUO and mice were administered three doses of DT *i.p* on days 5, 6 and 7 (25ng/g BW) while control animals received an equal volume of PBS. 3 doses of DT resulted in a 3-fold reduction of interstitial Mϕ infiltration but despite the increased dose of DT this did result in the complete ablation of all interstitial Mϕ in the obstructed kidneys.

Surprisingly, my studies demonstrated that mice treated with either 2 or 3 doses of DT did not exhibit any reduction in the level of tubular or interstitial cell apoptosis. In addition DT treatment did not have any effect upon the level of proliferation of tubular nor interstitial cells. These findings are in contrast with many other studies where Mϕ have been implicated in the deleterious induction of tubular cell apoptosis *in vivo* (Lange-Sperandio et al., 2002; Lenda et al., 2003; Tesch et al., 1999). In addition, Mϕ depletion in the immunological murine model of progressive NTN does result in reduced levels of tubular cell apoptosis and proliferation (Duffield et al., 2005a).

What may account for these findings? First, it is undoubtedly true that Mϕ are professional phagocytes and play a critical role in the recognition and clearance of apoptotic cells. Therefore, it is possible that Mϕ depletion resulted in a simultaneous reduction in both the level of tubular cell apoptosis and the phagocytic clearance of apoptotic tubular cells (i.e. a phagocytosis defect). However, apoptotic tubular cells may also by cleared by desquamation into the tubular lumen (although I saw little evidence of this in my studies) or ingestion by neighbouring epithelial cells in addition to interstitial infiltrating Mϕ. These data also suggest that the phenotype (i.e. activation status) of the infiltrating Mϕ, rather than Mϕ numbers *per se* is likely to be important as shown previously in a murine model of experimental glomerulonephritis (Anders et al., 2003). For example, it is possible that the remaining interstitial Mϕ present in the DT treated mice could still produce sufficient pro-inflammatory mediators capable of inducing tubular cell death. I performed immunofluorescent double staining for iNOS and F4/80 and iNOS positive

interstitial Mϕ are present in the obstructed kidneys of DT treated mice. The failure of Mϕ ablation to reduce tubular cell apoptosis may thus result from the persistent presence of a population of iNOS positive interstitial Mϕ.

Mϕ depletion did, however, ameliorate tubulointerstitial fibrosis as assessed by staining for interstitial collagens suggesting that Mϕ play an important role in modulating interstitial fibrosis. The potential mechanisms by which Mϕ promote interstitial matrix deposition include the direct release of cytokines such as TGF-β by Mϕ or Mϕ stimulation of other renal cells to release pro-fibrotic factors. In addition, Mϕ generate factors such as thrombospondin that can activate latent TGF-β to the active form (Daniel et al., 2003; Daniel et al., 2004).

I undertook somewhat preliminary studies of TGF-β expression in the Mϕ and this suggests that the level of TGF-β detectable by immunostaining was not obviously affected by DT treatment. It is important to note, however, that this may not indicate the level of bioactive TGF-β and it is therefore possible that the level of active TGF-β may have differed between groups. Interestingly, real-time PCR analysis demonstrated that TGF-β gene expression was not affected by DT treatment.

Mϕ ablation did not affect the level of myofibroblast accumulation identified after staining for α-SMA despite the reduced deposition of extracellular matrix. Interestingly, Mϕ ablation reduced the level of α-SMA gene expression assessed by real-time PCR. My findings are partially compatible with the reduced fibrosis noted following Mϕ ablation during murine NTN although this study did show reduced myofibroblast accumulation (Duffield et al., 2005a).

A summary diagram of NO release and the resulting biological cascade that may ultimately lead to tubular epithelial cell apoptosis is illustrated in Figure 6.1 and a simplified schema for the role of NO and inflammatory Mϕ in the events leading to end-stage renal failure is shown in Figure 6.2.

The work described in this thesis will hopefully contribute to a better understanding of the roles of inflammatory Mϕ in tubulointerstitial inflammation of the kidney. Further characterisation of the role of Mϕ and Mϕ-derived mediators are needed to understand the role of Mϕ in inflammatory processes in other organs.

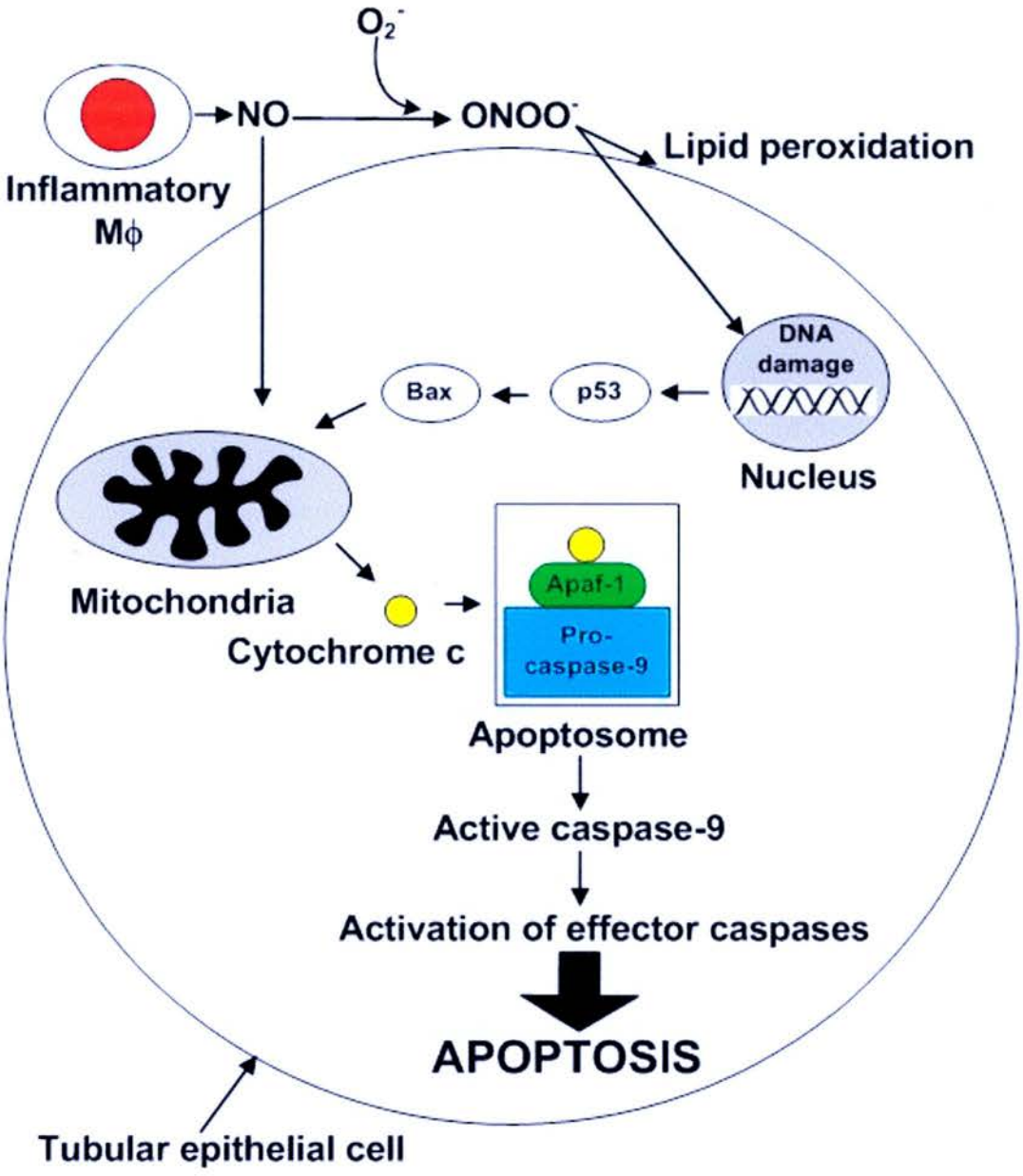

Figure 6- 1 Summary diagram depicting the potential mechanisms underlying NO induced tubular epithelial cell apoptosis.

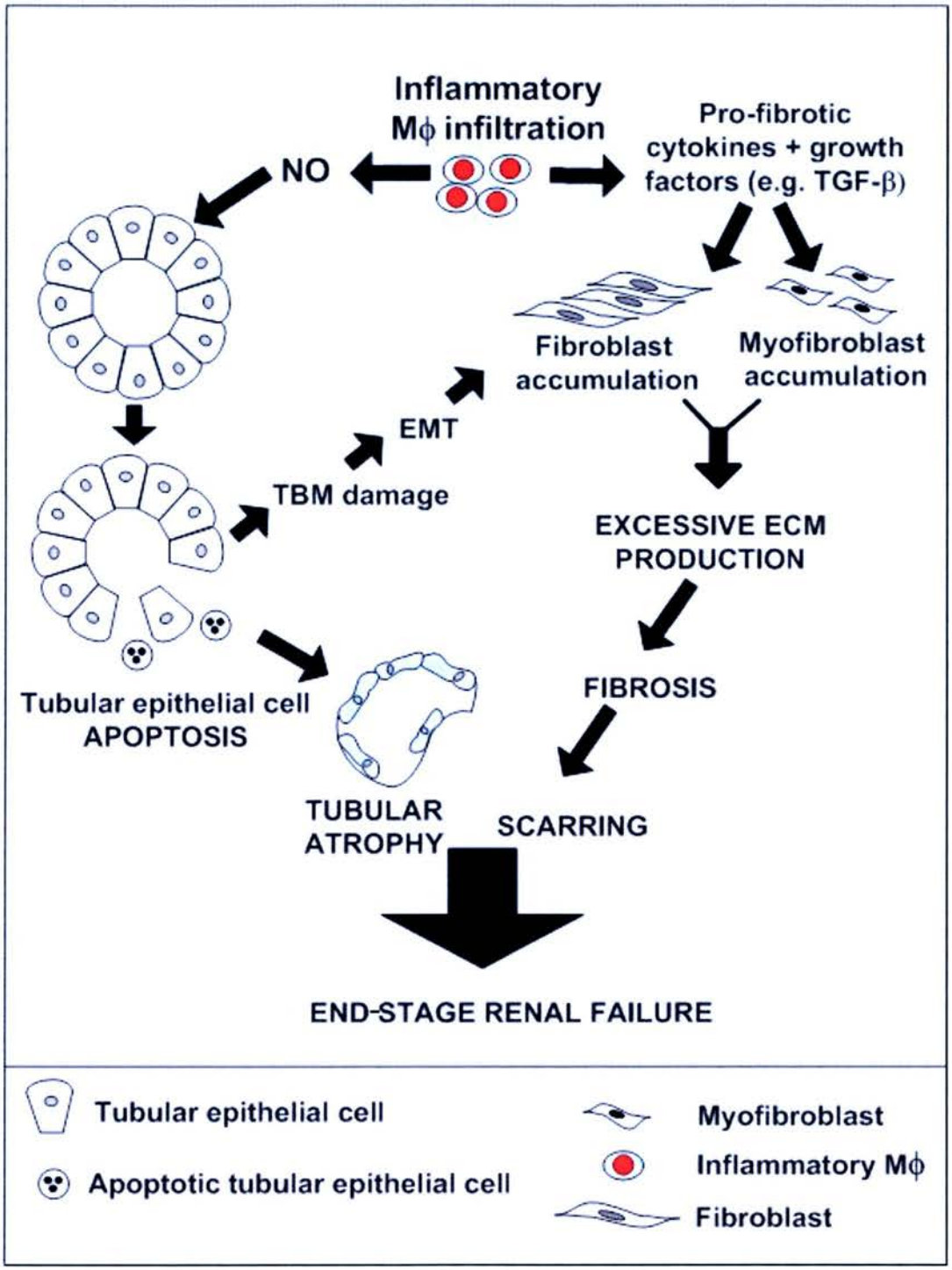

Figure 6- 2 Summary diagram depicting the role of NO, inflammatory Mϕ and possible pathways leading to end-stage renal failure.

6.2 FUTURE WORK

This work raises several questions that could be pursued by additional studies.

(1) The *in vitro* work could be extended to include cytokine priming of the tubular cells with pro-inflammatory cytokines as this may upregulate receptors such as Fas etc that may increased the susceptibility of tubular cells to death effectors other than NO. Also, my primary tubular cell cultures comprised a mixed population of tubular cells and it would be of interest to undertake co-culture studies of purified proximal and distal tubular cells. Most experimental studies have been performed in rodents and the rodent Mϕ may use iNOS to a greater extent than human Mϕ. However, iNOS positive Mϕ are present in renal biopsies from renal transplant recipients with chronic allograft nephropathy (Anya Adair, personal communication). It would therefore be informative to undertake studies using human monocyte-derived Mϕ and either human tubular cell lines or primary human tubular cells. In this work, I have focused upon iNOS-derived NO but NO may react with reactive oxygen species (ROS) to form the cytotoxic mediator peroxynitrite. It would thus be interesting to undertake studies employing inhibitors of ROS generation including studies employing both iNOS and ROS inhibitors seeking synergy.

(2) In this work I studied a single time point in the UUO model and it would be informative to undertake more extended *in vivo* studies examining both earlier and later time points in order to examine the kinetics of various processes such as Mϕ infiltration, tubular cell apoptosis and interstitial fibrosis. Also, an extended period of

L-NIL treatment in the UUO model would be interesting as this may result in reduced accumulation of interstitial myofibroblasts.

(3) It would be interesting to perform UUO in irradiated iNOS WT mice reconstituted with bone marrow derived from iNOS KO mice or control iNOS WT mice, as this would localise the defective expression of iNOS to the infiltrating leukocyte population. This experiment would give information regarding Mϕ-derived NO in the induction of tubular cell apoptosis *in vivo* and the increased levels of tubulointerstitial fibrosis evident in the obstructed kidneys of iNOS KO mice.

(4) L-NIL treatment resulted in comparable levels of Mϕ infiltration and α-SMA immunostaining but increased interstitial fibrosis. It would be interesting to quantify the expression of TGF-β as well as the expression of activators of TGF-β such as thrombospondin in obstructed kidneys from both the L-NIL treatment and DT treatment experiments. Study of the renal expression of MMPs and TIMPs would also be informative. In addition, further work carefully investigating and quantifying the phenotype of the infiltrating Mϕ would be of interest. This could be performed by single or double immunostaining but methods are now available in the lab for enzymatic dissociation of renal tissue and analysis of infiltrating leukocyte populations by flow cytometry. Mϕ expression of TNF-α and FasL in DT treated mice as well as alternative Mϕ activation markers such as YM1 and FIZZ would be of interest.

REFERENCES

Abe, R., Donnelly, S. C., Peng, T., Bucala, R., and Metz, C. N. (2001). Peripheral blood fibrocytes: differentiation pathway and migration to wound sites. J Immunol *166*, 7556-7562.

Acehan, D., Jiang, X., Morgan, D. G., Heuser, J. E., Wang, X., and Akey, C. W. (2002). Three-dimensional structure of the apoptosome: implications for assembly, procaspase-9 binding, and activation. Mol Cell *9*, 423-432.

Albina, J. E., Cui, S., Mateo, R. B., and Reichner, J. S. (1993). Nitric oxide-mediated apoptosis in murine peritoneal macrophages. J Immunol *150*, 5080-5085.

Anders, H. J., Frink, M., Linde, Y., Banas, B., Wornle, M., Cohen, C. D., Vielhauer, V., Nelson, P. J., Grone, H. J., and Schlondorff, D. (2003). CC chemokine ligand 5/RANTES chemokine antagonists aggravate glomerulonephritis despite reduction of glomerular leukocyte infiltration. J Immunol *170*, 5658-5666.

Anders, H. J., Vielhauer, V., Frink, M., Linde, Y., Cohen, C. D., Blattner, S. M., Kretzler, M., Strutz, F., Mack, M., Grone, H. J., *et al.* (2002). A chemokine receptor CCR-1 antagonist reduces renal fibrosis after unilateral ureter ligation. J Clin Invest *109*, 251-259.

Anderson, C. F., and Mosser, D. M. (2002). A novel phenotype for an activated macrophage: the type 2 activated macrophage. J Leukoc Biol *72*, 101-106.

Antonsson, B. (2004). Mitochondria and the Bcl-2 family proteins in apoptosis signaling pathways. Mol Cell Biochem *256-257*, 141-155.

Aurrand-Lions, M., Johnson-Leger, C., and Imhof, B. A. (2002). The last molecular fortress in leukocyte trans-endothelial migration. Nat Immunol *3*, 116-118.

Badid, C., Vincent, M., Fouque, D., Laville, M., and Desmouliere, A. (2001). Myofibroblast: a prognostic marker and target cell in progressive renal disease. Ren Fail *23*, 543-549.

Baer, P. C., Bereiter-Hahn, J., Schubert, R., and Geiger, H. (2006). Differentiation status of human renal proximal and distal tubular epithelial cells in vitro: Differential expression of characteristic markers. Cells Tissues Organs *184*, 16-22.

Baer, P. C., Nockher, W. A., Haase, W., and Scherberich, J. E. (1997). Isolation of proximal and distal tubule cells from human kidney by immunomagnetic separation. Technical note. Kidney Int *52*, 1321-1331.

Bagchus, W. M., Jeunink, M. F., and Elema, J. D. (1990). The mesangium in anti-Thy-1 nephritis. Influx of macrophages, mesangial cell hypercellularity, and macromolecular accumulation. Am J Pathol *137*, 215-223.

Baker, A. J., Mooney, A., Hughes, J., Lombardi, D., Johnson, R. J., and Savill, J. (1994). Mesangial cell apoptosis: the major mechanism for resolution of glomerular hypercellularity in experimental mesangial proliferative nephritis. J Clin Invest *94*, 2105-2116.

Barres, B., Hart, I. K., Coles, H. S. R., Burne, J. F., Voyvodic, J. T., Richardson, W. D., and Raff, M. C. (1992). Cell death and control of cell survival in the oligodendrocyte lineage. Cell *70*, 31-46.

Bascands, J. L., and Schanstra, J. P. (2005). Obstructive nephropathy: insights from genetically engineered animals. Kidney Int *68*, 925-937.

Bautista-Garcia, P., Sanchez-Lozada, L. G., Cristobal-Garcia, M., Tapia, E., Soto, V., Avila-Casado, M. C., Marquez-Velasco, R., Bojalil, R., Franco, M., and Herrera-Acosta, J. (2006). Chronic inhibition of NOS-2 ameliorates renal injury, as well as COX-2 and TGF-beta 1 overexpression in 5/6 nephrectomized rats. Nephrol Dial Transplant *21*, 3074-3081.

Bedford, J. J., Leader, J. P., and Walker, R. J. (2003). Aquaporin expression in normal human kidney and in renal disease. J Am Soc Nephrol *14*, 2581-2587.

Bennett, M., Macdonald, K., Chan, S. W., Luzio, J. P., Simari, R., and Weissberg, P. (1998). Cell surface trafficking of Fas: a rapid mechanism of p53-mediated apoptosis. Science *282*, 290-293.

Bergin, E., Levine, J. S., Koh, J. S., and Lieberthal, W. (2000). Mouse proximal tubular cell-cell adhesion inhibits apoptosis by a cadherin-dependent mechanism. Am J Physiol Renal Physiol *278*, F758-768.

Bird, J. E., Giancarli, M. R., Kurihara, T., Kowala, M. C., Valentine, M. T., Gitlitz, P. H., Pandya, D. G., French, M. H., and Durham, S. K. (2000). Increased severity of glomerulonephritis in C-C chemokine receptor 2 knockout mice. Kidney Int *57*, 129-136.

Bohle, A., Muller, G. A., Wehrmann, M., Mackensen-Haen, S., and Xiao, J. C. (1996). Pathogenesis of chronic renal failure in the primary glomerulopathies, renal vasculopathies, and chronic interstitial nephritides. Kidney Int Suppl *54*, S2-9.

Bohle, A., Wehrmann, M., Bogenschutz, O., Batz, C., Vogl, W., Schmitt, H., Muller, C. A., and Muller, G. A. (1992). The long-term prognosis of the primary glomerulonephritides. A morphological and clinical analysis of 1747 cases. Pathol Res Pract *188*, 908-924.

Bohle, A., Wehrmann, M., Mackensen-Haen, S., Gise, H., Mickeler, E., Xiao, T. C., Muller, C., and Muller, G. A. (1994). Pathogenesis of chronic renal failure in primary glomerulopathies. Nephrol Dial Transplant *9 Suppl 3*, 4-12.

Bosca, L., and Hortelano, S. (1999). Mechanisms of nitric oxide-dependent apoptosis: involvement of mitochondrial mediators. Cell Signal *11*, 239-244.

Bottinger, E. P., and Bitzer, M. (2002). TGF-beta signaling in renal disease. J Am Soc Nephrol *13*, 2600-2610.

Boyle, J. J., Bowyer, D. E., Weissberg, P. L., and Bennett, M. R. (2001). Human blood-derived macrophages induce apoptosis in human plaque-derived vascular smooth muscle cells by Fas-ligand/Fas interactions. Arterioscler Thromb Vasc Biol *21*, 1402-1407.

Boyle, J. J., Weissberg, P. L., and Bennett, M. R. (2002). Human macrophage-induced vascular smooth muscle cell apoptosis requires NO enhancement of Fas/Fas-L interactions. Arterioscler Thromb Vasc Biol *22*, 1624-1630.

Boyle, J. J., Weissberg, P. L., and Bennett, M. R. (2003). Tumor necrosis factor-alpha promotes macrophage-induced vascular smooth muscle cell apoptosis by direct and autocrine mechanisms. Arterioscler Thromb Vasc Biol *23*, 1553-1558.

Briere, N., Martel, M., Plante, G., and Petitclerc, C. (1985). Identification of proximal tubule segments in the mouse nephron by simultaneous visualization of alkaline phosphatase and gamma-glutamyl transpeptidase. Acta Histochem *77*, 37-45.

Brown, G. C. (1999). Nitric oxide and mitochondrial respiration. Biochim Biophys Acta *1411*, 351-369.

Brown, G. C., and Borutaite, V. (2006). Interactions between nitric oxide, oxygen, reactive oxygen species and reactive nitrogen species. Biochem Soc Trans *34*, 953-956.

Brown, S. B., and Savill, J. (1999). Phagocytosis triggers macrophage release of Fas ligand and induces apoptosis of bystander leukocytes. J Immunol *162*, 480-485.

Brugarolas, J., Chandrasekaran, C., Gordon, J. I., Beach, D., Jacks, T., and Hannon, G. J. (1995). Radiation-induced cell cycle arrest compromised by p21 deficiency. Nature *377*, 552-557.

Brune, B. (2003). Nitric oxide: NO apoptosis or turning it ON? Cell Death Differ *10*, 864-869.

Busiek, D. F., Baragi, V., Nehring, L. C., Parks, W. C., and Welgus, H. G. (1995). Matrilysin expression by human mononuclear phagocytes and its regulation by cytokines and hormones. J Immunol *154*, 6484-6491.

Butler, A. R., and Megson, I. L. (2002). Non-heme iron nitrosyls in biology. Chem Rev *102*, 1155-1166.

Cachat, F., Lange-Sperandio, B., Chang, A. Y., Kiley, S. C., Thornhill, B. A., Forbes, M. S., and Chevalier, R. L. (2003). Ureteral obstruction in neonatal mice elicits segment-specific tubular cell responses leading to nephron loss. Kidney Int *63*, 564-575. .

Cailhier, J. F., Partolina, M., Vuthoori, S., Wu, S., Ko, K., Watson, S., Savill, J., Hughes, J., and Lang, R. A. (2005). Conditional macrophage ablation demonstrates that resident macrophages initiate acute peritoneal inflammation. J Immunol *174*, 2336-2342.

Cailhier, J. F., Sawatzky, D. A., Kipari, T., Houlberg, K., Walbaum, D., Watson, S., Lang, R. A., Clay, S., Kluth, D., Savill, J., and Hughes, J. (2006). Resident pleural macrophages are key orchestrators of neutrophil recruitment in pleural inflammation. Am J Respir Crit Care Med *173*, 540-547.

Casciola-Rosen, L. A., Anhalt, G., and Rosen, A. (1994). Autoantigens targeted in systemic lupus erythematosus are clustered in two populations of surface structures on apoptotic keratinocytes. J Exp Med *179*, 1317-1330.

Catania, J. M., Chen, G., and Parrish, A. R. (2007). Role of matrix metalloproteinases in renal pathophysiologies. Am J Physiol Renal Physiol *292*, F905-911.

Cattell, V. (2002). Nitric oxide and glomerulonephritis. Kidney Int *61*, 816-821.

Chatterjee, P. K., Patel, N. S., Kvale, E. O., Cuzzocrea, S., Brown, P. A., Stewart, K. N., Mota-Filipe, H., and Thiemermann, C. (2002). Inhibition of inducible nitric oxide synthase reduces renal ischemia/reperfusion injury. Kidney Int *61*, 862-871.

Chatterjee, P. K., Patel, N. S., Sivarajah, A., Kvale, E. O., Dugo, L., Cuzzocrea, S., Brown, P. A., Stewart, K. N., Mota-Filipe, H., Britti, D., *et al.* (2003). GW274150, a potent and highly selective inhibitor of iNOS, reduces experimental renal ischemia/reperfusion injury. Kidney Int *63*, 853-865.

Cheng, Q. L., Chen, X. M., Li, F., Lin, H. L., Ye, Y. Z., and Fu, B. (2000). Effects of ICAM-1 antisense oligonucleotide on the tubulointerstitium in mice with unilateral ureteral obstruction. Kidney Int *57*, 183-190.

Cheng, S., Pollock, A. S., Mahimkar, R., Olson, J. L., and Lovett, D. H. (2006). Matrix metalloproteinase 2 and basement membrane integrity: a unifying mechanism for progressive renal injury. Faseb J *20*, 1898-1900.

Chinnaiyan, A. M., O'Rourke, K., Tewari, M., and Dixit, V. M. (1995). FADD, a novel death domain-containing protein, interacts with the death domain of Fas and initiates apoptosis. Cell *81*, 505-512.

Choi, B. M., Pae, H. O., Jang, S. I., Kim, Y. M., and Chung, H. T. (2002). Nitric oxide as a pro-apoptotic as well as anti-apoptotic modulator. J Biochem Mol Biol *35*, 116-126.

Choi, Y. J., Mendoza, L., Rha, S. J., Sheikh-Hamad, D., Baranowska-Daca, E., Nguyen, V., Smith, C. W., Nassar, G., Suki, W. N., and Truong, L. D. (2001). Role of p53-dependent activation of caspases in chronic obstructive uropathy: evidence from p53 null mutant mice. J Am Soc Nephrol *12*, 983-992.

Choi, Y. K., Moon, I. J., Jung, H. K., Jang, B. C., Seo, S. I., and Park, J. G. (2005). Prevention of tissue injury by ribbon antisense to TGF-beta1 in the kidney. Int J Mol Med *15*, 391-399.

Chung, H. T., Pae, H. O., Choi, B. M., Billiar, T. R., and Kim, Y. M. (2001). Nitric oxide as a bioregulator of apoptosis. Biochem Biophys Res Commun *282*, 1075-1079.

Chung, S. D., Alavi, N., Livingston, D., Hiller, S., and Taub, M. (1982). Characterization of primary rabbit kidney cultures that express proximal tubule functions in a hormonally defined medium. J Cell Biol *95*, 118-126.

Clancy, R. M., Amin, A. R., and Abramson, S. B. (1998). The role of nitric oxide in inflammation and immunity. Arthritis Rheum *41*, 1141-1151.

Coles, H. S., Burne, J. F., and Raff, M. C. (1993). Large-scale normal cell death in the developing rat kidney and its reduction by epidermal growth factor. Development *118*, 777-784.

Cui, S., Reichner, J. S., Mateo, R. B., and Albina, J. E. (1994). Activated murine macrophages induce apoptosis in tumor cells through nitric oxide-dependent or -independent mechanisms. Cancer Res *54*, 2462-2467.

Cuzzocrea, S., Chatterjee, P. K., Mazzon, E., McDonald, M. C., Dugo, L., Di Paola, R., Serraino, I., Britti, D., Caputi, A. P., and Thiemermann, C. (2002). Beneficial effects of GW274150, a novel, potent and selective inhibitor of iNOS activity, in a rodent model of collagen-induced arthritis. Eur J Pharmacol *453*, 119-129.

Daniel, C., Takabatake, Y., Mizui, M., Isaka, Y., Kawashi, H., Rupprecht, H., Imai, E., and Hugo, C. (2003). Antisense oligonucleotides against thrombospondin-1 inhibit activation of tgf-beta in fibrotic renal disease in the rat in vivo. Am J Pathol *163*, 1185-1192.

Daniel, C., Wiede, J., Krutzsch, H. C., Ribeiro, S. M., Roberts, D. D., Murphy-Ullrich, J. E., and Hugo, C. (2004). Thrombospondin-1 is a major activator of TGF-beta in fibrotic renal disease in the rat in vivo. Kidney Int *65*, 459-468.

Detrisac, C. J., Sens, M. A., Garvin, A. J., Spicer, S. S., and Sens, D. A. (1984). Tissue culture of human kidney epithelial cells of proximal tubule origin. Kidney Int *25*, 383-390.

Diamond, J. R. (1995). Macrophages and progressive renal disease in experimental hydronephrosis. Am J Kidney Dis *26*, 133-140.

Diamond, J. R., Ricardo, S. D., and Klahr, S. (1998). Mechanisms of interstitial fibrosis in obstructive nephropathy. Semin Nephrol *18*, 594-602.

Diamond, J. R., van Goor, H., Ding, G., and Engelmyer, E. (1995). Myofibroblasts in experimental hydronephrosis. Am J Pathol *146*, 121-129.

Diez-Roux, G., Argilla, M., Makarenkova, H., Ko, K., and Lang, R. A. (1999). Macrophages kill capillary cells in G1 phase of the cell cycle during programmed vascular regression. Development *126*, 2141-2147.

Dimmeler, S., and Zeiher, A. M. (1997). Nitric oxide and apoptosis: another paradigm for the double-edged role of nitric oxide. Nitric Oxide *1*, 275-281.

Downer, G., Phan, S. H., and Wiggins, R. C. (1988). Analysis of renal fibrosis in a rabbit model of crescentic nephritis. J Clin Invest *82*, 998-1006.

Du, C., Jiang, J., Guan, Q., Yin, Z., Masterson, M., Parbtani, A., Zhong, R., and Jevnikar, A. M. (2004). Renal tubular epithelial cell self-injury through Fas/Fas ligand interaction promotes renal allograft injury. Am J Transplant *4*, 1583-1594.

Duffield, J. S., Erwig, L.-P., Wei, X.-q., Liew, F. Y., Rees, A. J., and Savill, J. S. (2000). Activated Macrophages Direct Apoptosis and Suppress Mitosis of Mesangial Cells. J Immunol *164*, 2110-2119.

Duffield, J. S., Tipping, P. G., Kipari, T., Cailhier, J. F., Clay, S., Lang, R., Bonventre, J. V., and Hughes, J. (2005a). Conditional ablation of macrophages halts progression of crescentic glomerulonephritis. Am J Pathol *167*, 1207-1219.

Duffield, J. S., Forbes, S. J., Constandinou, C. M., Clay, S., Partolina, M., Vuthoori, S., Wu, S., Lang, R., and Iredale, J. P. (2005b). Selective depletion of macrophages reveals distinct, opposing roles during liver injury and repair. J Clin Invest *115*, 56-65.

Duffield, J. S., Ware, C. F., Ryffel, B., and Savill, J. (2001). Suppression by Apoptotic Cells Defines Tumor Necrosis Factor-Mediated Induction of Glomerular Mesangial Cell Apoptosis by Activated Macrophages. Am J Pathol *159*, 1397-1404.

Duymelinck, C., Dauwe, S. E., De Greef, K. E., Ysebaert, D. K., Verpooten, G. A., and De Broe, M. E. (2000). TIMP-1 gene expression and PAI-1 antigen after unilateral ureteral obstruction in the adult male rat. Kidney Int *58*, 1186-1201.

Eddy, A. A. (2000). Molecular basis of renal fibrosis. Pediatr Nephrol *15*, 290-301.

Eddy, A. A., Kim, H., Lopez-Guisa, J., Oda, T., and Soloway, P. D. (2000). Interstitial fibrosis in mice with overload proteinuria: deficiency of TIMP-1 is not protective. Kidney Int *58*, 618-628.

Edgtton, K. L., Gow, R. M., Kelly, D. J., Carmeliet, P., and Kitching, A. R. (2004). Plasmin is not protective in experimental renal interstitial fibrosis. Kidney Int *66*, 68-76.

Edwards, J. P., Zhang, X., Frauwirth, K. A., and Mosser, D. M. (2006). Biochemical and functional characterization of three activated macrophage populations. J Leukoc Biol.

Eis, V., Luckow, B., Vielhauer, V., Siveke, J. T., Linde, Y., Segerer, S., De Lema, G. P., Cohen, C. D., Kretzler, M., Mack, M., *et al.* (2004). Chemokine receptor CCR1 but not CCR5 mediates leukocyte recruitment and subsequent renal fibrosis after unilateral ureteral obstruction. J Am Soc Nephrol *15*, 337-347.

Elliget, K. A., and Trump, B. F. (1991). Primary cultures of normal rat kidney proximal tubule epithelial cells for studies of renal cell injury. In Vitro Cell Dev Biol *27A*, 739-748.

Erwig, L. P., Kluth, D. C., Walsh, G. M., and Rees, A. J. (1998). Initial cytokine exposure determines function of macrophages and renders them unresponsive to other cytokines. J Immunol *161*, 1983-1988.

Fadok, V. A., Bratton, D. L., Konowal, A., Freed, P. W., Westcott, J. Y., and Henson, P. M. (1998). Macrophages that have ingested apoptotic cells in vitro inhibit proinflammatory cytokine production through autocrine/paracrine mechanisms involving TGF-beta, PGE2, and PAF. J Clin Invest *101*, 890-898.

Fadok, V. A., Savill, J. S., Haslett, C., Bratton, D. L., Doherty, D. E., Campbell, P. A., and Henson, P. M. (1992a). Different populations of macrophages use either the vitronectin receptor or the phosphatidylserine receptor to recognize and remove apoptotic cells. J Immunol *149*, 4029-4035.

Fadok, V. A., Voelker, D. R., Campbell, P. A., Cohen, J. J., Bratton, D. L., and Henson, P. M. (1992b). Exposure of phosphatidylserine on the surface of apoptotic lymphocytes triggers specific recognition and removal by macrophages. J Immunol *148*, 2207-2216.

Feldenberg, L. R., Thevananther, S., del Rio, M., de Leon, M., and Devarajan, P. (1999). Partial ATP depletion induces Fas- and caspase-mediated apoptosis in MDCK cells. Am J Physiol *276*, F837-846.

Feldmann, M., Brennan, F. M., and Maini, R. N. (1996). Role of cytokines in rheumatoid arthritis. Annu Rev Immunol *14*, 397-440.

Fine, L. G., Orphanides, C., and Norman, J. T. (1998). Progressive renal disease: the chronic hypoxia hypothesis. Kidney Int Suppl *65*, S74-78.

Fogg, D. K., Sibon, C., Miled, C., Jung, S., Aucouturier, P., Littman, D. R., Cumano, A., and Geissmann, F. (2006). A clonogenic bone marrow progenitor specific for macrophages and dendritic cells. Science *311*, 83-87.

Forino, M., Torregrossa, R., Ceol, M., Murer, L., Vella, M. D., Prete, D. D., D'Angelo, A., and Anglani, F. (2006). TGFbeta1 induces epithelial-mesenchymal transition, but not myofibroblast transdifferentiation of human kidney tubular epithelial cells in primary culture. Int J Exp Pathol *87*, 197-208.

Frisch, S. M., and Francis, H. (1994). Disruption of epithelial cell-matrix interactions induces apoptosis. J Cell Biol *124*, 619-626.

Fujihara, C. K., De Nucci, G., and Zatz, R. (1995). Chronic nitric oxide synthase inhibition aggravates glomerular injury in rats with subtotal nephrectomy. J Am Soc Nephrol *5*, 1498-1507.

Fukuda, K., Yoshitomi, K., Yanagida, T., Tokumoto, M., and Hirakata, H. (2001). Quantification of TGF-beta1 mRNA along rat nephron in obstructive nephropathy. Am J Physiol Renal Physiol *281*, F513-521.

Furchgott, R. F., and Zawadzki, J. V. (1980). The obligatory role of endothelial cells in the relaxation of arterial smooth muscle by acetylcholine. Nature *288*, 373-376.

Gao, X., Mae, H., Ayabe, N., Takai, T., Oshima, K., Hattori, M., Ueki, T., Fujimoto, J., and Tanizawa, T. (2002). Hepatocyte growth factor gene therapy retards the progression of chronic obstructive nephropathy. Kidney Int *62*, 1238-1248.

Garrido, C., Galluzzi, L., Brunet, M., Puig, P. E., Didelot, C., and Kroemer, G. (2006). Mechanisms of cytochrome c release from mitochondria. Cell Death Differ *13*, 1423-1433.

Gavrieli, Y., Sherman, Y., and Ben-Sasson, S. A. (1992). Identification of programmed cell death in situ via specific labeling of nuclear DNA fragmentation. J Cell Biol *119*, 493-501.

Geissmann, F., Jung, S., and Littman, D. R. (2003). Blood monocytes consist of two principal subsets with distinct migratory properties. Immunity *19*, 71-82.

Genovese, T., Cuzzocrea, S., Di Paola, R., Failla, M., Mazzon, E., Sortino, M. A., Frasca, G., Gili, E., Crimi, N., Caputi, A. P., and Vancheri, C. (2005). Inhibition or knock out of inducible nitric oxide synthase result in resistance to bleomycin-induced lung injury. Respir Res *6*, 58.

Gesek, F. A., Wolff, D. W., and Strandhoy, J. W. (1987). Improved separation method for rat proximal and distal renal tubules. Am J Physiol *253*, F358-365.

Gibbs, D. F., Warner, R. L., Weiss, S. J., Johnson, K. J., and Varani, J. (1999). Characterization of matrix metalloproteinases produced by rat alveolar macrophages. Am J Respir Cell Mol Biol *20*, 1136-1144.

Gobe, G. C., and Axelsen, R. A. (1987). Genesis of renal tubular atrophy in experimental hydronephrosis in the rat. Role of apoptosis. Lab Invest *56*, 273-281.

Gonzalez-Cuadrado, S., Lorz, C., Garcia del Moral, R., O'Valle, F., Alonso, C., Ramiro, F., Ortiz-Gonzalez, A., Egido, J., and Ortiz, A. (1997). Agonistic anti-Fas antibodies induce glomerular cell apoptosis in mice in vivo. Kidney Int *51*, 1739-1746.

Gordon, S. (2003). Alternative activation of macrophages. Nat Rev Immunol *3*, 23-35.

Gordon, S., and Taylor, P. R. (2005). Monocyte and macrophage heterogeneity. Nat Rev Immunol *5*, 953-964.

Gouwy, M., Struyf, S., Proost, P., and Van Damme, J. (2005). Synergy in cytokine and chemokine networks amplifies the inflammatory response. Cytokine Growth Factor Rev *16*, 561-580.

Green, D. R., and Kroemer, G. (2004). The pathophysiology of mitochondrial cell death. Science *305*, 626-629.

Green, D. R., and Reed, J. C. (1998). Mitochondria and apoptosis. Science *281*, 1309-1312.

Green, L. C., Wagner, D. A., Glogowski, J., Skipper, P. L., Wishnok, J. S., and Tannenbaum, S. R. (1982). Analysis of nitrate, nitrite, and [15N]nitrate in biological fluids. Anal Biochem *126*, 131-138.

Griffin, S. V., Pichler, R., Dittrich, M., Durvasula, R., and Shankland, S. J. (2003a). Cell cycle control in glomerular disease. Springer Semin Immunopathol *24*, 441-457.

Griffin, S. V., Pichler, R., Wada, T., Vaughan, M., Durvasula, R., and Shankland, S. J. (2003b). The role of cell cycle proteins in Glomerular disease. Semin Nephrol *23*, 569-582.

Grupp, C., and Muller, G. A. (1999). Renal fibroblast culture. Exp Nephrol *7*, 377-385.

Guo, G., Morrissey, J., McCracken, R., Tolley, T., and Klahr, S. (1999). Role of TNFR1 and TNFR2 receptors in tubulointerstitial fibrosis of obstructive nephropathy. Am J Physiol *277*, F766-772.

Hall, S. E., Savill, J. S., Henson, P. M., and Haslett, C. (1994). Apoptotic neutrophils are phagocytosed by fibroblasts with participation of the fibroblast vitronectin receptor and involvement of a mannose/fucose-specific lectin. J Immunol *153*, 3218-3227.

Harrison, E. M., McNally, S. J., Devey, L., Garden, O. J., Ross, J. A., and Wigmore, S. J. (2006). Insulin induces heme oxygenase-1 through the phosphatidylinositol 3-kinase/Akt pathway and the Nrf2 transcription factor in renal cells. Febs J *273*, 2345-2356.

Hattori, T., Shindo, S., and Kawamura, H. (1998). Apoptosis and expression of Bax protein and Fas antigen in glomeruli of a remnant-kidney model. Nephron *79*, 186-191.

Haverty, T. P., Kelly, C. J., Hines, W. H., Amenta, P. S., Watanabe, M., Harper, R. A., Kefalides, N. A., and Neilson, E. G. (1988). Characterization of a renal tubular epithelial cell line which secretes the autologous target antigen of autoimmune experimental interstitial nephritis. J Cell Biol *107*, 1359-1368.

Helbert, M. J., Dauwe, S. E., and De Broe, M. E. (2001). Flow cytometric immunodissection of the human distal tubule and cortical collecting duct system. Kidney Int *59*, 554-564.

Hengartner, M. O. (2000). The biochemistry of apoptosis. Nature *407*, 770-776.

Henson, P. M. (2005). Dampening inflammation. Nat Immunol *6*, 1179-1181.

Hochberg, D., Johnson, C. W., Chen, J., Cohen, D., Stern, J., Vaughan, E. D., Jr., Poppas, D., and Felsen, D. (2000). Interstitial fibrosis of unilateral ureteral obstruction is exacerbated in kidneys of mice lacking the gene for inducible nitric oxide synthase. Lab Invest *80*, 1721-1728.

Huang, X. R., Tipping, P. G., Apostolopoulos, J., Oettinger, C., D'Souza, M., Milton, G., and Holdsworth, S. R. (1997). Mechanisms of T cell-induced glomerular injury in anti-glomerular basement membrane (GBM) glomerulonephritis in rats. Clin Exp Immunol *109*, 134-142.

Hughes, J. (2006). Leukocytes in tubulointerstitial inflammation. Kidney Int *69*, 8-10.

Hughes, J., Brown, P., and Shankland, S. J. (1999). Cyclin kinase inhibitor p21CIP1/WAF1 limits interstitial cell proliferation following ureteric obstruction. Am J Physiol *277*, F948-956.

Hughes, J., and Johnson, R. J. (1999). Role of Fas (CD95) in tubulointerstitial disease induced by unilateral ureteric obstruction. Am J Physiol *277*, F26-32.

Hughes, J., Liu, Y., Van Damme, J., and Savill, J. (1997). Human glomerular mesangial cell phagocytosis of apoptotic neutrophils: mediation by a novel CD36-independent vitronectin receptor/thrombospondin recognition mechanism that is uncoupled from chemokine secretion. J Immunol *158*, 4389-4397.

Hughes, J., and Shankland, S. J. (1999). Cyclin Kinase Inhibitor p21CIP1/WAF1 Limits Interstitial Cell Proliferation Following Ureteric Obstruction. Am J Physiol *277*, F948-F956.

Hull, R. N., Cherry, W. R., and Weaver, G. W. (1976). The origin and characteristics of a pig kidney cell strain, LLC-PK. In Vitro *12*, 670-677.

Hunter, M. G., Hurwitz, S., Bellamy, C. O., and Duffield, J. S. (2005). Quantitative morphometry of lupus nephritis: The significance of collagen, tubular space, and inflammatory infiltrate. Kidney Int *67*, 94-102.

Hwang, M., Kim, H. J., Noh, H. J., Chang, Y. C., Chae, Y. M., Kim, K. H., Jeon, J. P., Lee, T. S., Oh, H. K., Lee, Y. S., and Park, K. K. (2006). TGF-beta1 siRNA suppresses the tubulointerstitial fibrosis in the kidney of ureteral obstruction. Exp Mol Pathol *81*, 48-54.

Irmler, M., Thome, M., Hahne, M., Schneider, P., Hofmann, K., Steiner, V., Bodmer, J. L., Schroter, M., Burns, K., Mattmann, C., *et al.* (1997). Inhibition of death receptor signals by cellular FLIP. Nature *388*, 190-195.

Isaka, Y., Tsujie, M., Ando, Y., Nakamura, H., Kaneda, Y., Imai, E., and Hori, M. (2000). Transforming growth factor-beta 1 antisense oligodeoxynucleotides block interstitial fibrosis in unilateral ureteral obstruction. Kidney Int *58*, 1885-1892.

Iwano, M., and Neilson, E. G. (2004). Mechanisms of tubulointerstitial fibrosis. Curr Opin Nephrol Hypertens *13*, 279-284.

Iwano, M., Plieth, D., Danoff, T. M., Xue, C., Okada, H., and Neilson, E. G. (2002). Evidence that fibroblasts derive from epithelium during tissue fibrosis. J Clin Invest *110*, 341-350.

Jefferson, J. A., and Johnson, R. J. (1999). Experimental mesangial proliferative glomerulonephritis (the anti-Thy-1.1 model). J Nephrol *12*, 297-307.

Jin, Z., and El-Deiry, W. S. (2005). Overview of cell death signaling pathways. Cancer Biol Ther *4*, 139-163.

Johansson, A. C., Visse, E., Widegren, B., Sjogren, H. O., and Siesjo, P. (2001). Computerized image analysis as a tool to quantify infiltrating leukocytes: a comparison between high- and low-magnification images. J Histochem Cytochem *49*, 1073-1079.

Johnson, D. W., Saunders, H. J., Baxter, R. C., Field, M. J., and Pollock, C. A. (1998). Paracrine stimulation of human renal fibroblasts by proximal tubule cells. Kidney Int *54*, 747-757.

Jung, S., Unutmaz, D., Wong, P., Sano, G., De los Santos, K., Sparwasser, T., Wu, S., Vuthoori, S., Ko, K., Zavala, F., *et al.* (2002). In vivo depletion of CD11c(+) dendritic cells abrogates priming of CD8(+) T cells by exogenous cell-associated antigens. Immunity *17*, 211-220.

Junqueira, L. C., Bignolas, G., and Brentani, R. R. (1979). Picrosirius staining plus polarization microscopy, a specific method for collagen detection in tissue sections. Histochem J *11*, 447-455.

Kalluri, R., and Neilson, E. G. (2003). Epithelial-mesenchymal transition and its implications for fibrosis. J Clin Invest *112*, 1776-1784.

Kanduc, D., Mittelman, A., Serpico, R., Sinigaglia, E., Sinha, A. A., Natale, C., Santacroce, R., Di Corcia, M. G., Lucchese, A., Dini, L., *et al.* (2002). Cell death: apoptosis versus necrosis (review). Int J Oncol *21*, 165-170.

Kelly, D. J., Zhang, Y., Gow, R., and Gilbert, R. E. (2004). Tranilast attenuates structural and functional aspects of renal injury in the remnant kidney model. J Am Soc Nephrol *15*, 2619-2629.

Kerr, J. F., Wyllie, A. H., and Currie, A. R. (1972). Apoptosis: a basic biological phenomenon with wide-ranging implications in tissue kinetics. Br J Cancer *26*, 239-257.

Kiley, S. C., Thornhill, B. A., Belyea, B. C., Neale, K., Forbes, M. S., Luetteke, N. C., Lee, D. C., and Chevalier, R. L. (2005). Epidermal growth factor potentiates renal cell death in hydronephrotic neonatal mice, but cell survival in rats. Kidney Int *68*, 504-514. .

Kim, H., Oda, T., Lopez-Guisa, J., Wing, D., Edwards, D. R., Soloway, P. D., and Eddy, A. A. (2001a). TIMP-1 deficiency does not attenuate interstitial fibrosis in obstructive nephropathy. J Am Soc Nephrol *12*, 736-748.

Kim, P. K., Zamora, R., Petrosko, P., and Billiar, T. R. (2001b). The regulatory role of nitric oxide in apoptosis. Int Immunopharmacol *1*, 1421-1441.

Kitagawa, K., Wada, T., Furuichi, K., Hashimoto, H., Ishiwata, Y., Asano, M., Takeya, M., Kuziel, W. A., Matsushima, K., Mukaida, N., and Yokoyama, H. (2004). Blockade of CCR2 ameliorates progressive fibrosis in kidney. Am J Pathol *165*, 237-246.

Klahr, S. (1991). New insights into the consequences and mechanisms of renal impairment in obstructive nephropathy. Am J Kidney Dis *18*, 689-699.

Klahr, S. (1998). Obstructive nephropathy. Kidney Int *54*, 286-300.

Kluth, D. C., Erwig, L.-P., and Rees, A. J. (2004). Multiple facets of macrophages in renal injury. Kidney Int *66*, 542-557.

Koopman, G., Reutelingsperger, C. P., Kuijten, G. A., Keehnen, R. M., Pals, S. T., and van Oers, M. H. (1994). Annexin V for flow cytometric detection of phosphatidylserine expression on B cells undergoing apoptosis. Blood *84*, 1415-1420.

Kopp, J. B., Factor, V. M., Mozes, M., Nagy, P., Sanderson, N., Bottinger, E. P., Klotman, P. E., and Thorgeirsson, S. S. (1996). Transgenic mice with increased plasma levels of TGF-beta 1 develop progressive renal disease. Lab Invest *74*, 991-1003.

Krammer, P. H. (2000). CD95's deadly mission in the immune system. Nature *407*, 789-795.

Lacave, R., Bens, M., Cartier, N., Vallet, V., Robine, S., Pringault, E., Kahn, A., and Vandewalle, A. (1993). Functional properties of proximal tubule cell lines derived from transgenic mice harboring L-pyruvate kinase-SV40 (T) antigen hybrid gene. J Cell Sci *104 (Pt 3)*, 705-712.

Lan, H. Y., Mitsuhashi, H., Ng, Y. Y., Nikolic-Paterson, D. J., Yang, N., Mu, W., and Atkins, R. C. (1997). Macrophage apoptosis in rat crescentic glomerulonephritis. Am J Pathol *151*, 531-538.

Lan, H. Y., Mu, W., Tomita, N., Huang, X. R., Li, J. H., Zhu, H. J., Morishita, R., and Johnson, R. J. (2003). Inhibition of renal fibrosis by gene transfer of inducible Smad7 using ultrasound-microbubble system in rat UUO model. J Am Soc Nephrol *14*, 1535-1548.

Lang, R., Lustig, M., Francois, F., Sellinger, M., and Plesken, H. (1994). Apoptosis during macrophage-dependent ocular tissue remodelling. Development *120*, 3395-3403.

Lang, R. A., and Bishop, J. M. (1993). Macrophages are required for cell death and tissue remodeling in the developing mouse eye. Cell *74*, 453-462.

Lange-Sperandio, B., Cachat, F., Thornhill, B. A., and Chevalier, R. L. (2002). Selectins mediate macrophage infiltration in obstructive nephropathy in newborn mice. Kidney Int *61*, 516-524.

Lange-Sperandio, B., Fulda, S., Vandewalle, A., and Chevalier, R. L. (2003). Macrophages induce apoptosis in proximal tubule cells. Pediatr Nephrol *18*, 335-341.

Lange-Sperandio, B., Schimpgen, K., Rodenbeck, B., Chavakis, T., Bierhaus, A., Nawroth, P., Thornhill, B., Schaefer, F., and Chevalier, R. L. (2006). Distinct roles of Mac-1 and its counter-receptors in neonatal obstructive nephropathy. Kidney Int *69*, 81-88.

Le Meur, Y., Tesch, G. H., Hill, P. A., Mu, W., Foti, R., Nikolic-Paterson, D. J., and Atkins, R. C. (2002). Macrophage accumulation at a site of renal inflammation is dependent on the M-CSF/c-fms pathway. J Leukoc Biol *72*, 530-537.

Lee, J. M., Dedhar, S., Kalluri, R., and Thompson, E. W. (2006). The epithelial-mesenchymal transition: new insights in signaling, development, and disease. J Cell Biol *172*, 973-981.

Lenda, D. M., Kikawada, E., Stanley, E. R., and Kelley, V. R. (2003). Reduced macrophage recruitment, proliferation, and activation in colony-stimulating factor-1-deficient mice results in decreased tubular apoptosis during renal inflammation. J Immunol *170*, 3254-3262.

Liles, W. C., Kiener, P. A., Ledbetter, J. A., Aruffo, A., and Klebanoff, S. J. (1996). Differential expression of Fas (CD95) and Fas ligand on normal human phagocytes: implications for the regulation of apoptosis in neutrophils. J Exp Med *184*, 429-440.

Liu, L., and Stamler, J. S. (1999). NO: an inhibitor of cell death. Cell Death Differ *6*, 937-942.

Liu, Y. (2004). Epithelial to mesenchymal transition in renal fibrogenesis: pathologic significance, molecular mechanism, and therapeutic intervention. J Am Soc Nephrol *15*, 1-12.

Liu, Y. (2006). Renal fibrosis: new insights into the pathogenesis and therapeutics. Kidney Int *69*, 213-217.

Lloyd, C. M., Minto, A. W., Dorf, M. E., Proudfoot, A., Wells, T. N., Salant, D. J., and Gutierrez-Ramos, J. C. (1997). RANTES and monocyte chemoattractant protein-1 (MCP-1) play an important role in the inflammatory phase of crescentic nephritis, but only MCP-1 is involved in crescent formation and interstitial fibrosis. J Exp Med *185*, 1371-1380.

Lorz, C., Ortiz, A., Justo, P., Gonzalez-Cuadrado, S., Duque, N., Gomez-Guerrero, C., and Egido, J. (2000). Proapoptotic Fas ligand is expressed by normal kidney tubular epithelium and injured glomeruli. J Am Soc Nephrol *11*, 1266-1277.

Lucas, M., Stuart, L. M., Savill, J., and Lacy-Hulbert, A. (2003). Apoptotic cells and innate immune stimuli combine to regulate macrophage cytokine secretion. J Immunol *171*, 2610-2615.

Luo, X., Budihardjo, I., Zou, H., Slaughter, C., and Wang, X. (1998). Bid, a Bcl2 interacting protein, mediates cytochrome c release from mitochondria in response to activation of cell surface death receptors. Cell *94*, 481-490.

Luo, Y., Hurwitz, J., and Massague, J. (1995). Cell-cycle inhibition by independent CDK and PCNA binding domains in p21Cip1. Nature *375*, 159-161.

Luster, A. D. (1998). Chemokines--chemotactic cytokines that mediate inflammation. N Engl J Med *338*, 436-445.

Luster, A. D., Alon, R., and von Andrian, U. H. (2005). Immune cell migration in inflammation: present and future therapeutic targets. Nat Immunol *6*, 1182-1190.

Mackay, C. R. (2001). Chemokines: immunology's high impact factors. Nat Immunol *2*, 95-101.

Maragos, C. M., Morley, D., Wink, D. A., Dunams, T. M., Saavedra, J. E., Hoffman, A., Bove, A. A., Isaac, L., Hrabie, J. A., and Keefer, L. K. (1991). Complexes of .NO with nucleophiles as agents for the controlled biological release of nitric oxide. Vasorelaxant effects. J Med Chem *34*, 3242-3247.

Mark, L. A., Robinson, A. V., and Schulak, J. A. (2005). Inhibition of nitric oxide synthase reduces renal ischemia/reperfusion injury. J Surg Res *129*, 236-241.

Marshall, C. B., and Shankland, S. J. (2006). Cell cycle and glomerular disease: a minireview. Nephron Exp Nephrol *102*, e39-48.

Martinon, F., and Tschopp, J. (2004). Inflammatory caspases: linking an intracellular innate immune system to autoinflammatory diseases. Cell *117*, 561-574.

Matsuo, S., Lopez-Guisa, J. M., Cai, X., Okamura, D. M., Alpers, C. E., Bumgarner, R. E., Peters, M. A., Zhang, G., and Eddy, A. A. (2005). Multifunctionality of PAI-1

in fibrogenesis: evidence from obstructive nephropathy in PAI-1-overexpressing mice. Kidney Int *67*, 2221-2238.

Mazzali, M., Jefferson, J. A., Ni, Z., Vaziri, N. D., and Johnson, R. J. (2003). Microvascular and tubulointerstitial injury associated with chronic hypoxia-induced hypertension. Kidney Int *63*, 2088-2093.

McKnight, A. J., Macfarlane, A. J., Dri, P., Turley, L., Willis, A. C., and Gordon, S. (1996). Molecular cloning of F4/80, a murine macrophage-restricted cell surface glycoprotein with homology to the G-protein-linked transmembrane 7 hormone receptor family. J Biol Chem *271*, 486-489.

Meister, A., and Anderson, M. E. (1983). Glutathione. Annu Rev Biochem *52*, 711-760.

Meldrum, K. K., Metcalfe, P., Leslie, J. A., Misseri, R., Hile, K. L., and Meldrum, D. R. (2006). TNF-alpha neutralization decreases nuclear factor-kappaB activation and apoptosis during renal obstruction. J Surg Res *131*, 182-188.

Mentzel, S., Dijkman, H. B., Van Son, J. P., Koene, R. A., and Assmann, K. J. (1996). Organ distribution of aminopeptidase A and dipeptidyl peptidase IV in normal mice. J Histochem Cytochem *44*, 445-461.

Messmer, U. K., Ankarcrona, M., Nicotera, P., and Brune, B. (1994). p53 expression in nitric oxide-induced apoptosis. FEBS Lett *355*, 23-26.

Mills, C. D., Kincaid, K., Alt, J. M., Heilman, M. J., and Hill, A. M. (2000). M-1/M-2 macrophages and the Th1/Th2 paradigm. J Immunol *164*, 6166-6173.

Misseri, R., Meldrum, D. R., Dinarello, C. A., Dagher, P., Hile, K. L., Rink, R. C., and Meldrum, K. K. (2005). TNF-alpha mediates obstruction-induced renal tubular cell apoptosis and proapoptotic signaling. Am J Physiol Renal Physiol *288*, F406-411.

Miyajima, A., Chen, J., Lawrence, C., Ledbetter, S., Soslow, R. A., Stern, J., Jha, S., Pigato, J., Lemer, M. L., Poppas, D. P., *et al.* (2000). Antibody to transforming growth factor-beta ameliorates tubular apoptosis in unilateral ureteral obstruction. Kidney Int *58*, 2301-2313.

Miyajima, A., Chen, J., Poppas, D. P., Vaughan, E. D., Jr., and Felsen, D. (2001). Role of nitric oxide in renal tubular apoptosis of unilateral ureteral obstruction. Kidney Int *59*, 1290-1303.

Mizuno, S., Matsumoto, K., and Nakamura, T. (2001). Hepatocyte growth factor suppresses interstitial fibrosis in a mouse model of obstructive nephropathy. Kidney Int *59*, 1304-1314.

Moncada, S., and Higgs, E. A. (2006). The discovery of nitric oxide and its role in vascular biology. Br J Pharmacol *147 Suppl 1*, S193-201.

Moncada, S., Palmer, R. M., and Higgs, E. A. (1989). Biosynthesis of nitric oxide from L-arginine. A pathway for the regulation of cell function and communication. Biochem Pharmacol *38*, 1709-1715.

Moon, J. A., Kim, H. T., Cho, I. S., Sheen, Y. Y., and Kim, D. K. (2006). IN-1130, a novel transforming growth factor-beta type I receptor kinase (ALK5) inhibitor, suppresses renal fibrosis in obstructive nephropathy. Kidney Int.

Mooney, A., Jackson, K., Bacon, R., Streuli, C., Edwards, G., Bassuk, J., and Savill, J. (1999). Type IV collagen and laminin regulate glomerular mesangial cell susceptibility to apoptosis via beta(1) integrin-mediated survival signals. Am J Pathol *155*, 599-606.

Morel, F. (1981). Sites of hormone action in the mammalian nephron. Am J Physiol *240*, F159-164.

Morrissey, J., Hruska, K., Guo, G., Wang, S., Chen, Q., and Klahr, S. (2002). Bone morphogenetic protein-7 improves renal fibrosis and accelerates the return of renal function. J Am Soc Nephrol *13 Suppl 1*, S14-21.

Morrissey, J. J., Ishidoya, S., McCracken, R., and Klahr, S. (1996). Control of p53 and p21 (WAF1) expression during unilateral ureteral obstruction. Kidney Int Suppl *57*, S84-92.

Moser, B., Wolf, M., Walz, A., and Loetscher, P. (2004). Chemokines: multiple levels of leukocyte migration control. Trends Immunol *25*, 75-84.

Mosmann, T. R., Cherwinski, H., Bond, M. W., Giedlin, M. A., and Coffman, R. L. (1986). Two types of murine helper T cell clone. I. Definition according to profiles of lymphokine activities and secreted proteins. J Immunol *136*, 2348-2357.

Mosser, D. M. (2003). The many faces of macrophage activation. J Leukoc Biol *73*, 209-212.

Muller, W. A., and Randolph, G. J. (1999). Migration of leukocytes across endothelium and beyond: molecules involved in the transmigration and fate of monocytes. J Leukoc Biol *66*, 698-704.

Murphy, P. M., Baggiolini, M., Charo, I. F., Hebert, C. A., Horuk, R., Matsushima, K., Miller, L. H., Oppenheim, J. J., and Power, C. A. (2000). International union of pharmacology. XXII. Nomenclature for chemokine receptors. Pharmacol Rev *52*, 145-176.

Nagase, H., Visse, R., and Murphy, G. (2006). Structure and function of matrix metalloproteinases and TIMPs. Cardiovasc Res *69*, 562-573.

Nagase, H., and Woessner, J. F., Jr. (1999). Matrix metalloproteinases. J Biol Chem *274*, 21491-21494.

Naglich, J. G., Metherall, J. E., Russell, D. W., and Eidels, L. (1992). Expression cloning of a diphtheria toxin receptor: identity with a heparin-binding EGF-like growth factor precursor. Cell *69*, 1051-1061.

Narita, I., Border, W. A., Ketteler, M., and Noble, N. A. (1995). Nitric oxide mediates immunologic injury to kidney mesangium in experimental glomerulonephritis. Lab Invest *72*, 17-24.

Nicolas, F. J., Lehmann, K., Warne, P. H., Hill, C. S., and Downward, J. (2003). Epithelial to Mesenchymal Transition in Madin-Darby Canine Kidney Cells Is Accompanied by Down-regulation of Smad3 Expression, Leading to Resistance to Transforming Growth Factor-beta -induced Growth Arrest. J Biol Chem *278*, 3251-3256.

Nikolic-Paterson, D. J. (2003). A role for macrophages in mediating tubular cell apoptosis? Kidney Int *63*, 1582-1583.

Nitsch, D. D., Ghilardi, N., Muhl, H., Nitsch, C., Brune, B., and Pfeilschifter, J. (1997). Apoptosis and expression of inducible nitric oxide synthase are mutually exclusive in renal mesangial cells. Am J Pathol *150*, 889-900.

Nogae, S., Miyazaki, M., Kobayashi, N., Saito, T., Abe, K., Saito, H., Nakane, P. K., Nakanishi, Y., and Koji, T. (1998). Induction of apoptosis in ischemia-reperfusion model of mouse kidney: possible involvement of Fas. J Am Soc Nephrol *9*, 620-631.

Nouwen, E. J., Dauwe, S., van der Biest, I., and De Broe, M. E. (1993). Stage- and segment-specific expression of cell-adhesion molecules N-CAM, A-CAM, and L-CAM in the kidney. Kidney Int *44*, 147-158.

Oda, T., Jung, Y. O., Kim, H. S., Cai, X., Lopez-Guisa, J. M., Ikeda, Y., and Eddy, A. A. (2001). PAI-1 deficiency attenuates the fibrogenic response to ureteral obstruction. Kidney Int *60*, 587-596.

Ogawa, D., Shikata, K., Matsuda, M., Okada, S., Usui, H., Wada, J., Taniguchi, N., and Makino, H. (2002). Protective effect of a novel and selective inhibitor of inducible nitric oxide synthase on experimental crescentic glomerulonephritis in WKY rats. Nephrol Dial Transplant *17*, 2117-2121.

Okada, H., and Kalluri, R. (2005). Cellular and molecular pathways that lead to progression and regression of renal fibrogenesis. Curr Mol Med *5*, 467-474.

Ophascharoensuk, V., Fero, M. L., Hughes, J., Roberts, J. M., and Shankland, S. J. (1998). The cyclin-dependent kinase inhibitor p27Kip1 safeguards against inflammatory injury. Nat Med *4*, 575-580.

Ortiz, A., Lorz, C., Gonzalez-Cuadrado, S., Garcia del Moral, R., O'Valle, F., and Egido, J. (1997). Cytokines and Fas regulate apoptosis in murine renal interstitial fibroblasts. J Am Soc Nephrol *8*, 1845-1854.

Ortiz-Arduan, A., Danoff, T. M., Kalluri, R., Gonzalez-Cuadrado, S., Karp, S. L., Elkon, K., Egido, J., and Neilson, E. G. (1996). Regulation of Fas and Fas ligand expression in cultured murine renal cells and in the kidney during endotoxemia. Am J Physiol *271*, F1193-1201.

Ozen, S., Usta, Y., Sahin-Erdemli, I., Orhan, D., Gumusel, B., Yang, B., Gursoy, Y., Tulunay, O., Dalkara, T., Bakkaloglu, A., and El-Nahas, M. (2001). Association of nitric oxide production and apoptosis in a model of experimental nephropathy. Nephrol Dial Transplant *16*, 32-38.

Pacher, P., Beckman, J. S., and Liaudet, L. (2007). Nitric oxide and peroxynitrite in health and disease. Physiol Rev *87*, 315-424.

Palmer, R. M., Ashton, D. S., and Moncada, S. (1988). Vascular endothelial cells synthesize nitric oxide from L-arginine. Nature *333*, 664-666.

Panzer, U., Schneider, A., Wilken, J., Thompson, D. A., Kent, S. B., and Stahl, R. A. (1999). The chemokine receptor antagonist AOP-RANTES reduces monocyte infiltration in experimental glomerulonephritis. Kidney Int *56*, 2107-2115.

Parnaik, R., Raff, M. C., and Scholes, J. (2000). Differences between the clearance of apoptotic cells by professional and non-professional phagocytes. Curr Biol *10*, 857-860.

Peter, M. E., and Krammer, P. H. (2003). The CD95(APO-1/Fas) DISC and beyond. Cell Death Differ *10*, 26-35.

Quinn, A. C., Petros, A. J., and Vallance, P. (1995). Nitric oxide: an endogenous gas. Br J Anaesth *74*, 443-451.

Rastaldi, M. P., Ferrario, F., Giardino, L., Dell'Antonio, G., Grillo, C., Grillo, P., Strutz, F., Muller, G. A., Colasanti, G., and D'Amico, G. (2002). Epithelial-mesenchymal transition of tubular epithelial cells in human renal biopsies. Kidney Int *62*, 137-146.

Reilly, C. M., Farrelly, L. W., Viti, D., Redmond, S. T., Hutchison, F., Ruiz, P., Manning, P., Connor, J., and Gilkeson, G. S. (2002). Modulation of renal disease in MRL/lpr mice by pharmacologic inhibition of inducible nitric oxide synthase. Kidney Int *61*, 839-846.

Ren, Y., and Savill, J. (1998). Apoptosis: the importance of being eaten. Cell Death Differ *5*, 563-568.

Risdon, R. A., Sloper, J. C., and De Wardener, H. E. (1968). Relationship between renal function and histological changes found in renal-biopsy specimens from patients with persistent glomerular nephritis. Lancet *2*, 363-366.

Roberts, I. S., Burrows, C., Shanks, J. H., Venning, M., and McWilliam, L. J. (1997). Interstitial myofibroblasts: predictors of progression in membranous nephropathy. J Clin Pathol *50*, 123-127.

Rodgers, K. D., Rao, V., Meehan, D. T., Fager, N., Gotwals, P., Ryan, S. T., Koteliansky, V., Nemori, R., and Cosgrove, D. (2003). Monocytes may promote myofibroblast accumulation and apoptosis in Alport renal fibrosis. Kidney Int *63*, 1338-1355.

Rossi, D., and Zlotnik, A. (2000). The biology of chemokines and their receptors. Annu Rev Immunol *18*, 217-242.

Ryan, M. J., Johnson, G., Kirk, J., Fuerstenberg, S. M., Zager, R. A., and Torok-Storb, B. (1994). HK-2: an immortalized proximal tubule epithelial cell line from normal adult human kidney. Kidney Int *45*, 48-57.

Saikumar, P., Dong, Z., Patel, Y., Hall, K., Hopfer, U., Weinberg, J. M., and Venkatachalam, M. A. (1998). Role of hypoxia-induced Bax translocation and cytochrome c release in reoxygenation injury. Oncogene *17*, 3401-3415.

Saito, M., Iwawaki, T., Taya, C., Yonekawa, H., Noda, M., Inui, Y., Mekada, E., Kimata, Y., Tsuru, A., and Kohno, K. (2001). Diphtheria toxin receptor-mediated conditional and targeted cell ablation in transgenic mice. Nat Biotechnol *19*, 746-750.

Salvesen, G. S., and Duckett, C. S. (2002). IAP proteins: blocking the road to death's door. Nat Rev Mol Cell Biol *3*, 401-410.

Sato, M., Muragaki, Y., Saika, S., Roberts, A. B., and Ooshima, A. (2003). Targeted disruption of TGF-beta1/Smad3 signaling protects against renal tubulointerstitial fibrosis induced by unilateral ureteral obstruction. J Clin Invest *112*, 1486-1494.

Satriano, J., Lortie, M. J., Ishizuka, S., Valdivielso, J. M., Friedman, B., and Munger, K. A. (2005). Inhibition of Inducible Nitric Oxide Synthase Alters Thy-1 Glomeruonephritis in Rats. Nephron Physiol *102*, p17-p26.

Savill, J. (1994). Apoptosis and the kidney. J Am Soc Nephrol *5*, 12-21.

Savill, J. (1997). Recognition and phagocytosis of cells undergoing apoptosis. Br Med Bull *53*, 491-508.

Savill, J., Dransfield, I., Gregory, C., and Haslett, C. (2002). A blast from the past: clearance of apoptotic cells regulates immune responses. Nat Rev Immunol *2*, 965-975.

Savill, J., and Fadok, V. (2000). Corpse clearance defines the meaning of cell death. Nature *407*, 784-788.

Savill, J., Smith, J., Sarraf, C., Ren, Y., Abbott, F., and Rees, A. (1992). Glomerular mesangial cells and inflammatory macrophages ingest neutrophils undergoing apoptosis. Kidney Int *42*, 924-936.

Savill, J. S., Wyllie, A. H., Henson, J. E., Walport, M. J., Henson, P. M., and Haslett, C. (1989). Macrophage phagocytosis of aging neutrophils in inflammation.

Programmed cell death in the neutrophil leads to its recognition by macrophages. J Clin Invest *83*, 865-875.

Schreiner, G. F. (1991). The role of the macrophage in glomerular injury. Semin Nephrol *11*, 268-275.

Schreiner, G. F., Cotran, R. S., Pardo, V., and Unanue, E. R. (1978). A mononuclear cell component in experimental immunological glomerulonephritis. J Exp Med *147*, 369-384.

Sean Eardley, K., and Cockwell, P. (2005). Macrophages and progressive tubulointerstitial disease. Kidney Int *68*, 437-455.

Segal, A. W. (2005). How neutrophils kill microbes. Annu Rev Immunol *23*, 197-223.

Segerer, S. (2003). The role of chemokines and chemokine receptors in progressive renal diseases. Am J Kidney Dis *41*, S15-18.

Serhan, C. N., and Savill, J. (2005). Resolution of inflammation: the beginning programs the end. Nat Immunol *6*, 1191-1197.

Shankland, S. J., and Wolf, G. (2000). Cell cycle regulatory proteins in renal disease: role in hypertrophy, proliferation, and apoptosis. Am J Physiol Renal Physiol *278*, F515-529.

Shappell, S. B., Gurpinar, T., Lechago, J., Suki, W. N., and Truong, L. D. (1998). Chronic obstructive uropathy in severe combined immunodeficient (SCID) mice: lymphocyte infiltration is not required for progressive tubulointerstitial injury. J Am Soc Nephrol *9*, 1008-1017.

Sharma, V. K., Bologa, R. M., Li, B., Xu, G. P., Lagman, M., Hiscock, W., Mouradian, J., Wang, J., Serur, D., Rao, V. K., and Suthanthiran, M. (1996). Molecular executors of cell death--differential intrarenal expression of Fas ligand, Fas, granzyme B, and perforin during acute and/or chronic rejection of human renal allografts. Transplantation *62*, 1860-1866.

Sherr, C. J., and Roberts, J. M. (1999). CDK inhibitors: positive and negative regulators of G1-phase progression. Genes Dev *13*, 1501-1512.

Shi, H. P., Most, D., Efron, D. T., Tantry, U., Fischel, M. H., and Barbul, A. (2001). The role of iNOS in wound healing. Surgery *130*, 225-229.

Shipley, J. M., Wesselschmidt, R. L., Kobayashi, D. K., Ley, T. J., and Shapiro, S. D. (1996). Metalloelastase is required for macrophage-mediated proteolysis and matrix invasion in mice. Proc Natl Acad Sci U S A *93*, 3942-3946.

Siegel, R. M. (2006). Caspases at the crossroads of immune-cell life and death. Nat Rev Immunol *6*, 308-317.

Song, E., Ouyang, N., Horbelt, M., Antus, B., Wang, M., and Exton, M. S. (2000). Influence of alternatively and classically activated macrophages on fibrogenic activities of human fibroblasts. Cell Immunol *204*, 19-28.

Speyer, C. L., Neff, T. A., Warner, R. L., Guo, R. F., Sarma, J. V., Riedemann, N. C., Murphy, M. E., Murphy, H. S., and Ward, P. A. (2003). Regulatory effects of iNOS on acute lung inflammatory responses in mice. Am J Pathol *163*, 2319-2328.

Springer, T. A. (1994). Traffic signals for lymphocyte recirculation and leukocyte emigration: the multistep paradigm. Cell *76*, 301-314.

Strutz, F., Okada, H., Lo, C. W., Danoff, T., Carone, R. L., Tomaszewski, J. E., and Neilson, E. G. (1995). Identification and characterization of a fibroblast marker: FSP1. J Cell Biol *130*, 393-405.

Strutz, F., Zeisberg, M., Renziehausen, A., Raschke, B., Becker, V., van Kooten, C., and Muller, G. (2001). TGF-beta 1 induces proliferation in human renal fibroblasts via induction of basic fibroblast growth factor (FGF-2). Kidney Int *59*, 579-592.

Strutz, F., Zeisberg, M., Ziyadeh, F. N., Yang, C. Q., Kalluri, R., Muller, G. A., and Neilson, E. G. (2002). Role of basic fibroblast growth factor-2 in epithelial-mesenchymal transformation. Kidney Int *61*, 1714-1728.

Suda, T., Okazaki, T., Naito, Y., Yokota, T., Arai, N., Ozaki, S., Nakao, K., and Nagata, S. (1995). Expression of the Fas ligand in cells of T cell lineage. J Immunol *154*, 3806-3813.

Takemura, T., Murakami, K., Miyazato, H., Yagi, K., and Yoshioka, K. (1995). Expression of Fas antigen and Bcl-2 in human glomerulonephritis. Kidney Int *48*, 1886-1892.

Tan, K. H., and Hunziker, W. (2003). Compartmentalization of Fas and Fas ligand may prevent auto- or paracrine apoptosis in epithelial cells. Exp Cell Res *284*, 283-290.

Tanaka, T., Kojima, I., Ohse, T., Inagi, R., Miyata, T., Ingelfinger, J. R., Fujita, T., and Nangaku, M. (2005). Hypoxia-inducible factor modulates tubular cell survival in cisplatin nephrotoxicity. Am J Physiol Renal Physiol *289*, F1123-1133.

Taub, M., and Sato, G. (1980). Growth of functional primary cultures of kidney epithelial cells in defined medium. J Cell Physiol *105*, 369-378.

Taylor, P. R., and Gordon, S. (2003). Monocyte heterogeneity and innate immunity. Immunity *19*, 2-4.

Tesch, G. H., Schwarting, A., Kinoshita, K., Lan, H. Y., Rollins, B. J., and Kelley, V. R. (1999). Monocyte chemoattractant protein-1 promotes macrophage-mediated tubular injury, but not glomerular injury, in nephrotoxic serum nephritis. J Clin Invest *103*, 73-80.

Topham, P. S., Csizmadia, V., Soler, D., Hines, D., Gerard, C. J., Salant, D. J., and Hancock, W. W. (1999). Lack of chemokine receptor CCR1 enhances Th1 responses and glomerular injury during nephrotoxic nephritis. J Clin Invest *104*, 1549-1557.

Toutain, H., Vauclin-Jacques, N., Fillastre, J. P., and Morin, J. P. (1991). Biochemical, functional, and morphological characterization of a primary culture of rabbit proximal tubule cells. Exp Cell Res *194*, 9-18.

Trachtman, H. (2004). Nitric oxide and glomerulonephritis. Semin Nephrol *24*, 324-332.

Truong, L. D., Sheikh-Hamad, D., Chakraborty, S., and Suki, W. N. (1998). Cell apoptosis and proliferation in obstructive uropathy. Semin Nephrol *18*, 641-651.

Tschopp, J., Irmler, M., and Thome, M. (1998). Inhibition of fas death signals by FLIPs. Curr Opin Immunol *10*, 552-558.

Van Goor, H., Ding, G., Kees-Folts, D., Grond, J., Schreiner, G. F., and Diamond, J. R. (1994). Macrophages and renal disease. Lab Invest *71*, 456-464.

van Loo, G., Saelens, X., van Gurp, M., MacFarlane, M., Martin, S. J., and Vandenabeele, P. (2002). The role of mitochondrial factors in apoptosis: a Russian roulette with more than one bullet. Cell Death Differ *9*, 1031-1042.

Voll, R. E., Herrmann, M., Roth, E. A., Stach, C., Kalden, J. R., and Girkontaite, I. (1997). Immunosuppressive effects of apoptotic cells [letter]. Nature *390*, 350-351.

Vongwiwatana, A., Tasanarong, A., Rayner, D. C., Melk, A., and Halloran, P. F. (2005). Epithelial to mesenchymal transition during late deterioration of human kidney transplants: the role of tubular cells in fibrogenesis. Am J Transplant *5*, 1367-1374.

Vos, I. H., Joles, J. A., Schurink, M., Weckbecker, G., Stojanovic, T., Rabelink, T. J., and Grone, H. J. (2000). Inhibition of inducible nitric oxide synthase improves graft function and reduces tubulointerstitial injury in renal allograft rejection. Eur J Pharmacol *391*, 31-38.

Wada, T., Furuichi, K., Sakai, N., Iwata, Y., Kitagawa, K., Ishida, Y., Kondo, T., Hashimoto, H., Ishiwata, Y., Mukaida, N., *et al.* (2004). Gene therapy via blockade of monocyte chemoattractant protein-1 for renal fibrosis. J Am Soc Nephrol *15*, 940-948.

Walczak, H., and Krammer, P. H. (2000). The CD95 (APO-1/Fas) and the TRAIL (APO-2L) apoptosis systems. Exp Cell Res *256*, 58-66.

Wallach, D., Varfolomeev, E. E., Malinin, N. L., Goltsev, Y. V., Kovalenko, A. V., and Boldin, M. P. (1999). Tumor necrosis factor receptor and Fas signaling mechanisms. Annu Rev Immunol *17*, 331-367.

Wang, W., Koka, V., and Lan, H. Y. (2005). Transforming growth factor-beta and Smad signalling in kidney diseases. Nephrology (Carlton) *10*, 48-56.

Wei, X. Q., Charles, I. G., Smith, A., Ure, J., Feng, G. J., Huang, F. P., Xu, D., Muller, W., Moncada, S., and Liew, F. Y. (1995). Altered immune responses in mice lacking inducible nitric oxide synthase. Nature *375*, 408-411.

Weinberg, J. B., Granger, D. L., Pisetsky, D. S., Seldin, M. F., Misukonis, M. A., Mason, S. N., Pippen, A. M., Ruiz, P., Wood, E. R., and Gilkeson, G. S. (1994). The role of nitric oxide in the pathogenesis of spontaneous murine autoimmune disease: increased nitric oxide production and nitric oxide synthase expression in MRL-lpr/lpr mice, and reduction of spontaneous glomerulonephritis and arthritis by orally administered NG-monomethyl-L-arginine. J Exp Med *179*, 651-660.

Westenfeld, R., Gawlik, A., de Heer, E., Kitahara, M., Abou-Rebyeh, F., Floege, J., and Ketteler, M. (2002). Selective inhibition of inducible nitric oxide synthase enhances intraglomerular coagulation in chronic anti-Thy 1 nephritis. Kidney Int *61*, 834-838.

Westerhuis, R., van Straaten, S. C., van Dixhoorn, M. G., van Rooijen, N., Verhagen, N. A., Dijkstra, C. D., de Heer, E., and Daha, M. R. (2000). Distinctive roles of neutrophils and monocytes in anti-thy-1 nephritis. Am J Pathol *156*, 303-310.

Wink, D. A., Grisham, M. B., Mitchell, J. B., and Ford, P. C. (1996). Direct and indirect effects of nitric oxide in chemical reactions relevant to biology. Methods Enzymol *268*, 12-31.

Wright, E. J., McCaffrey, T. A., Robertson, A. P., Vaughan, E. D., Jr., and Felsen, D. (1996). Chronic unilateral ureteral obstruction is associated with interstitial fibrosis and tubular expression of transforming growth factor-beta. Lab Invest *74*, 528-537.

Wyllie, A. H. (1980). Glucocorticoid-induced thymocyte apoptosis is associated with endogenous endonuclease activation. Nature *284*, 555-556.

Wyllie, A. H., Kerr, J. F., and Currie, A. R. (1980). Cell death: the significance of apoptosis. Int Rev Cytol *68*, 251-306.

Yamasaki, K., Edington, H. D., McClosky, C., Tzeng, E., Lizonova, A., Kovesdi, I., Steed, D. L., and Billiar, T. R. (1998). Reversal of impaired wound repair in iNOS-deficient mice by topical adenoviral-mediated iNOS gene transfer. J Clin Invest *101*, 967-971.

Yang, J., Dai, C., and Liu, Y. (2005). A novel mechanism by which hepatocyte growth factor blocks tubular epithelial to mesenchymal transition. J Am Soc Nephrol *16*, 68-78.

Yang, J., and Liu, Y. (2001). Dissection of key events in tubular epithelial to myofibroblast transition and its implications in renal interstitial fibrosis. Am J Pathol *159*, 1465-1475.

Yang, J., and Liu, Y. (2003). Delayed administration of hepatocyte growth factor reduces renal fibrosis in obstructive nephropathy. Am J Physiol Renal Physiol *284*, F349-357.

Yang, J., Shultz, R. W., Mars, W. M., Wegner, R. E., Li, Y., Dai, C., Nejak, K., and Liu, Y. (2002). Disruption of tissue-type plasminogen activator gene in mice reduces renal interstitial fibrosis in obstructive nephropathy. J Clin Invest *110*, 1525-1538.

Yang, Y. L., Guh, J. Y., Yang, M. L., Lai, Y. H., Tsai, J. H., Hung, W. C., Chang, C. C., and Chuang, L. Y. (1998). Interaction between high glucose and TGF-beta in cell cycle protein regulations in MDCK cells. J Am Soc Nephrol *9*, 182-193.

Zeisberg, M., Hanai, J., Sugimoto, H., Mammoto, T., Charytan, D., Strutz, F., and Kalluri, R. (2003). BMP-7 counteracts TGF-beta1-induced epithelial-to-mesenchymal transition and reverses chronic renal injury. Nat Med *9*, 964-968.

Zeisberg, M., Shah, A. A., and Kalluri, R. (2005). Bone morphogenic protein-7 induces mesenchymal to epithelial transition in adult renal fibroblasts and facilitates regeneration of injured kidney. J Biol Chem *280*, 8094-8100.

Zeisberg, M., Strutz, F., and Muller, G. A. (2001). Renal fibrosis: an update. Curr Opin Nephrol Hypertens *10*, 315-320.

Zhang, G., Kim, H., Cai, X., Lopez-Guisa, J. M., Alpers, C. E., Liu, Y., Carmeliet, P., and Eddy, A. A. (2003). Urokinase receptor deficiency accelerates renal fibrosis in obstructive nephropathy. J Am Soc Nephrol *14*, 1254-1271.

Zlotnik, A., and Yoshie, O. (2000). Chemokines: a new classification system and their role in immunity. Immunity *12*, 121-127.

Appendix I: Published Paper resulting from work from this thesis

Nitric oxide is an important mediator of renal tubular epithelial cell death *in vitro* and in murine experimental hydronephrosis

Tiina Kipari, Jean-Francois Cailhier, David Ferenbach, Simon Watson, Kris Houlberg, David Walbaum, Spike Clay, John Savill and Jeremy Hughes.

American Journal of Pathology, 2006, 169, 388-399.

URL: http://ajp.amjpathol.org/cgi/reprint/169/2/388

This manuscript is included at the end of this thesis.

The American Journal of Pathology, Vol. 169, No. 2, August 2006

DOI: 10.2353/ajpath.2006.050964

Cell Injury, Repair, Aging and Apoptosis

Nitric Oxide Is an Important Mediator of Renal Tubular Epithelial Cell Death *in Vitro* and in Murine Experimental Hydronephrosis

Tiina Kipari, Jean-Francois Cailhier, David Ferenbach, Simon Watson, Kris Houlberg, David Walbaum, Spike Clay, John Savill, and Jeremy Hughes

From the Phagocyte Laboratory, Medical Research Council Centre for Inflammation Research, The Queen's Medical Research Institute, Edinburgh, Scotland

Macrophages play a pivotal role in tissue injury and fibrosis during renal inflammation. Although macrophages may induce apoptosis of renal tubular epithelial cells, the mechanisms involved are unclear. We used a microscopically quantifiable co-culture assay to dissect the cytotoxic interaction between murine bone marrow-derived macrophages and Madin-Darby canine kidney cells and primary murine renal tubular epithelial cells. The induction of tubular cell apoptosis by cytokine-activated macrophages was reduced by inhibitors of nitric oxide synthase whereas tubular cell proliferation was unaffected. Furthermore, cytokine-activated macrophages derived from mice targeted for the deletion of inducible nitric oxide synthase were noncytotoxic. We then examined the role of nitric oxide *in vivo* by inhibiting inducible nitric oxide synthase in the model of murine experimental hydronephrosis. L-N^6-(1-iminoethyl)-lysine was administered in the drinking water between days 5 and 7 after ureteric obstruction. Macrophage infiltration was comparable between groups, but treatment significantly inhibited tubular cell apoptosis at day 7. Tubular cell proliferation was unaffected. Inducible nitric oxide synthase blockade also reduced interstitial cell apoptosis and increased collagen III deposition. These data indicate that nitric oxide is a key mediator of macrophage-directed tubular cell apoptosis *in vitro* and *in vivo* and also modulates tubulointerstitial fibrosis. *(Am J Pathol 2006, 169:388–399; DOI: 10.2353/ajpath.2006.050964)*

Macrophages are remarkably versatile cells that play a major role in many key biological processes including host defense, wound healing, development, tissue remodeling, acute inflammation, and the clearance of apoptotic cells.[1–5] Macrophages may induce apoptosis of host cells and this is beneficial in the context of developmental sculpting of tissues[4,6,7] but is usually deleterious during renal inflammation.[8–10] Recent work indicates that macrophages may induce tubular epithelial cell apoptosis in both immunological and nonimmunological tubulointerstitial inflammation.[11–14] Tesch and colleagues[11] induced nephrotoxic glomerulonephritis in mice targeted for the deletion of monocyte chemoattractant protein-1 (MCP-1). The resultant diminished tubulointerstitial macrophage infiltrate was associated with a reduction in tubular epithelial cell apoptosis. This finding was reinforced by our recent work that used conditional macrophage ablation in progressive nephrotoxic glomerulonephritis because macrophage ablation significantly reduced the level of tubular epithelial cell apoptosis.[14] The role of macrophages in the nonimmunological model of experimental hydronephrosis induced by unilateral ureteric obstruction has also been studied.[12,13] Lenda and colleagues[12] obstructed the kidneys of colony-stimulating-factor-1 (CSF-1)-deficient mice and demonstrated a reduced interstitial macrophage infiltrate associated with a reduced level of tubular epithelial cell death. Lange-Sperandio and colleagues[13] obstructed the kidneys of triple E-, P-, and L-selectin knockout mice or wild-type control mice within the first 48 hours after birth. Triple selectin knockout mice exhibited diminished tubulointerstitial macrophage infiltration and reduced levels of tubular epithelial cell death compared to control mice.

Supported by the Wellcome Trust (Senior Research Fellowship in Clinical Science grant 061139 to J.H. and program grant 064487 to J.S.); the Canadian Institutes of Health Research (to J.-F.C.); the UK Medical Research Council (to S.W.); the National Kidney Research Fund, UK (to D.W. and D.F.); and the Emerald Foundation.

Accepted for publication April 13, 2006.

Address reprint requests to Jeremy Hughes, Room C2.05, MRC Centre for Inflammation Research, The Queen's Medical Research Institute, 47 Little France Crescent, Edinburgh, EH16 4TJ, UK. E-mail: jeremy.hughes@ed.ac.uk.

Although tubular cell apoptosis is invariably present during renal injury, excessive levels of tubular cell death are highly undesirable and result in renal tubular atrophy, hypocellular scarring and eventual organ failure.[15] Indeed, the tubulointerstitium of the kidney plays an important role in all renal diseases irrespective of the nature of the original injury[16] because there is a striking correlation between the severity of the tubulointerstitial changes in human biopsies and the subsequent development and progression of chronic renal failure to end-stage renal failure requiring dialysis.[17]

Currently, despite the documented correlation between the severity of macrophage infiltration and the level of tubular epithelial cell apoptosis,[12–14] there is scant data regarding the mechanisms involved in macrophage-mediated tubular cell apoptosis. Inflammatory macrophages produce myriad proapoptotic mediators that may kill neighboring cells, including nitric oxide (NO), tumor necrosis factor-α (TNF-α), as well as Fas ligand (FasL).[18–20] Previous *in vitro* studies addressing this issue used both macrophage and murine tubular cell lines[21] with cytokine-activated J774 macrophages inducing apoptosis of murine PKSV-PR proximal tubular cells. This study and previous work by Tesch and colleagues,[11] however, did not determine the nature of the macrophage death effector although no role for TNF-α, FasL, or transforming growth factor-β was demonstrable.[21]

In this study we have used a well-established microscopically quantifiable co-culture assay[18] and the model of experimental hydronephrosis[12,13,22] to examine the cytotoxic mechanism underlying macrophage-mediated tubular epithelial cell death *in vitro* and *in vivo*. We demonstrate an important role for macrophage-derived NO in the induction of tubular cell apoptosis *in vitro* and during tubulointerstitial inflammation *in vivo*. In addition, our data reinforces a role for NO in modulating tubulointerstitial fibrosis and scarring.

Materials and Methods

Materials

Tissue culture reagents were purchased from Life Technologies (Paisley, UK). Tissue culture plastics were obtained from Costar (Loughborough, Leicestershire, UK) and Falcon (Runcorn, Cheshire, UK). Cytokines were purchased from R&D Systems (Abingdon, Oxon, UK) and Peprotech EC Ltd. (London, UK). L-N^6-(1-iminoethyl)-lysine (L-NIL) and the control inactive isomer D-N^6-(1-iminoethyl)-lysine (D-NIL) were purchased from Fluorochem Ltd. (Old Glossop, Derbyshire, UK). All other reagents were from Sigma-Aldrich Co. Ltd. (Poole, UK) unless otherwise stated.

Experimental Animals

Inducible nitric oxide synthase (iNOS) knockout[23] and wild-type control mice were obtained from B and K Universal (Hull, UK). iNOS knockout and wild-type mice were on the 129/sv background. CB7BL/6 and FVB/N mice were bred at the University of Edinburgh.

Preparation of Bone Marrow-Derived Macrophages

Bone marrow-derived macrophages were used in these studies and were prepared from FVB/N mice, C57BL/6, or iNOS knockout and wild-type mice as described previously.[18] Briefly, bone marrow was isolated from femurs by standard sterile techniques and matured for 7 days in sterile Teflon wells in Dulbecco's modified Eagle's medium (DMEM)/F12 medium with 10% heat inactivated fetal calf serum (FCS), penicillin (100 U/ml), streptomycin (100 μg/ml), and 10% L929 cell-conditioned medium as a source of M-CSF. Macrophages were greater than 98% positive for the macrophage marker F4/80 by flow cytometry.

Renal Tubular Epithelial Cell Culture

Madin-Darby canine kidney (MDCK) cells (a gift from Dr. J. Davie, University of Edinburgh) were cultured as described previously.[24] Briefly, cells were grown as a monolayer culture in 75-cm^2 culture flasks and maintained with Eagle's minimum essential medium containing 1% nonessential amino acids, 100 U/ml penicillin, 100 μg/ml streptomycin, and 10% heat-inactivated FCS in a humidified atmosphere of 5% CO_2 at 37°C. Murine primary tubular epithelial (PTE) cells were derived from the kidneys of C57BL/6 mice after microdissection and brief collagenase digestion.[25] PTE cells were grown as a monolayer culture in 25-cm^2 culture flasks and maintained with DMEM/F12 medium containing insulin (10 μg/ml), transferrin (5.5 μg/ml), selenium (5 ng/ml), epidermal growth factor (25 ng/ml), and dexamethasone (36 ng/ml). PTE cells were cytokeratin-positive and vimentin-negative by immunochemistry.

Co-Culture Studies

MDCK or PTE cells were prelabeled with fluorescent CellTracker Green whereas in some experiments mature macrophages (7 to 10 days) were prelabeled with fluorescent CellTracker Orange (both CellTracker dyes obtained from Molecular Probes, Eugene, OR). Cells were washed with serum-free medium and incubated for 30 minutes (macrophage) or 1 hour (epithelial cells) in serum-free medium containing the respective CellTracker dye at a concentration of 5 ng/ml. Cells were washed in medium containing 10% FCS to remove unbound CellTracker dye. Epithelial cells were then trypsinized and added to 48-well plates at a density to cover 60 to 70% of the well surface: 1×10^4 MDCK cells/well and 1.5×10^4 PTE cells/well. Wells were washed after 2 to 4 hours to remove nonadherent cells. Macrophages were added to epithelial cells at a ratio of two macrophages to one epithelial cell. MDCK experiments were conducted in DMEM/F12 medium containing 10% FCS, and PTE cell

experiments were conducted in PTE cell medium containing 0.1% FCS.

Selected co-cultures were activated with lipopolysaccharide (LPS) (1 μg/ml) and murine interferon-γ (IFN-γ) (100 U/ml), with nonactivated co-cultures being exposed to medium alone. After 24 hours of incubation, the undisturbed co-cultures underwent *in situ* fixation with formaldehyde (4% final concentration) to ensure retention of apoptotic cells.[18] Fixed co-cultures were then stained with Hoechst 33342 at 1 μg/ml in phosphate-buffered saline (PBS) for 15 minutes. Using inverted fluorescent microscopy, nonoverlapping fields from each well were randomly and blindly chosen so that at least 200 epithelial cells were counted per well. Apoptotic epithelial cells were identified by their green condensed cytoplasm and pyknotic nuclei. Mitotic epithelial cells were discernible by their characteristic chromatin pattern. The number of apoptotic or mitotic epithelial cells was counted and expressed as apoptotic or mitotic cells per high-power field or as a percentage of the total number of epithelial cells (percent apoptosis). All experimental conditions were performed in triplicate and experiments performed on at least three separate occasions. Macrophage and primary PTE cell cultures were derived from at least three different animals.

The Model of Experimental Hydronephrosis

Experimental hydronephrosis was induced by performing unilateral ureteric obstruction.[26] The left ureter of age-matched male FVB/N mice was ligated under inhalational anesthesia. Mice were administered either L-NIL or the control inactive isomer D-NIL in the drinking water (1 mg/ml) for 48 hours before sacrifice at day 7 (n = seven to eight per group).[27,28] The removed kidneys were cut longitudinally and fixed in either 10% buffered formalin or methyl Carnoy's solution (60% methanol, 30% chloroform, and 10% acetic acid) and embedded in paraffin. All experiments were performed in accordance with the UK Government Home Office regulations.

Renal Morphology and Immunohistochemistry

To examine renal histology, 4-μm sections were stained with periodic acid-Schiff (PAS) reagent and counterstained with hematoxylin. Tubulointerstitial macrophage infiltration was quantified after immunostaining for the murine macrophage marker F4/80. Briefly, methyl Carnoy's fixed tissue sections were deparaffinized, rehydrated in ethanol, and incubated in 3% H_2O_2 in methanol to block endogenous peroxidase activity. Tissue sections were then incubated with rat monoclonal antibody (IgG2b) directed against mouse F4/80 (1/1000 dilution; Caltag Laboratories, Northampton, UK) at 4°C overnight, followed by a mouse-adsorbed biotinylated rabbit anti-rat IgG (1/1000 dilution; Vector Laboratories, Peterborough, UK) at room temperature for 30 minutes. For iNOS immunostaining, tissue sections were incubated with a polyclonal rabbit antibody (1/50 dilution; Abcam Laboratories, Cambridge, UK) at 4°C overnight, followed by a biotinylated goat anti-rabbit IgG (1/300 dilution; DakoCytomation, Glostrup, Denmark) at room temperature for 30 minutes. The tubulointerstitial myofibroblast population was quantified after immunostaining for the myofibroblast marker α-smooth muscle actin. Tissue sections were incubated with monoclonal mouse anti-human α-smooth muscle actin that cross-reacts with murine α-smooth muscle actin [clone 1A4 (IgG2a), 1/1000 dilution; Sigma-Aldrich Co. Ltd., Poole, UK] at 4°C overnight, followed by a biotinylated rat-anti-mouse IgG2a (1/100 dilution; Zymed Laboratories, San Francisco, CA) at room temperature for 30 minutes. Tubulointerstitial fibrosis was quantified after immunostaining for collagen III. Tissue sections were incubated with goat-anti-human type III collagen antibody, which also detects murine type III collagen (1/50 dilution; Cambridge BioScience Ltd., Cambridge, UK) at 4°C overnight, followed by a biotinylated rabbit-anti-goat IgG (1/100 dilution; Vector Laboratories) at room temperature for 30 minutes.

After washing in PBS, sections were incubated in horseradish peroxidase-conjugated avidin D (1/2000 dilution; Vector Laboratories) at room temperature for 20 minutes. Color was developed using diaminobenzidine as the chromogen and counterstained with methyl green or hematoxylin. An irrelevant isotype control primary antibody served as negative control. Positive control tissue included sections from diseased mice that were known to express F4/80-positive macrophages or exhibit significant renal scarring. Interstitial macrophage infiltration was quantified in a blinded manner by analyzing 10 sequentially selected nonoverlapping fields of renal cortex of F4/80-stained sections at ×100 magnification using computer-assisted image analysis (ImageJ 1.30h; National Institutes of Health, Bethesda, MD; *http://rsb.info.nih.gov/ij/Java1.3.1_03*).[14,29,30] Macrophage infiltration was expressed as the percentage of tissue surface area positive for F4/80 staining.[14,31] Tubulointerstitial collagen III deposition was quantified in a similar manner while myofibroblast accumulation was expressed as the percentage of tissue surface area positive for α-smooth muscle actin staining excluding blood vessels.

Double-Immunofluorescence Staining for iNOS and F4/80

Methyl Carnoy's fixed tissue sections were deparaffinized, rehydrated, and incubated in 3% H_2O_2 in methanol to block endogenous peroxidase activity. Nonspecific binding was blocked by incubation in 2% goat serum, 1% bovine serum albumin, 0.1% Triton X-100, and 0.05% Tween 20 for 30 minutes at room temperature. Tissue sections were then sequentially incubated in the following antibodies: 1) polyclonal rabbit anti-iNOS (1/50 dilution; BD Biosciences Pharmingen, Oxford, UK); 2) AlexaFluor-488-conjugated goat anti-rabbit IgG (1/300 dilution; Molecular Probes); 3) rat anti-mouse F4/80 (IgG2b, 1/1000 dilution; Caltag Laboratories, Northampton, UK); 4) mouse-adsorbed biotinylated rabbit anti-rat IgG (1/1000 dilution, Vector Laboratories); and 5) Alexa Fluor-568-conjugated streptavidin (1/300 dilution, Molec-

ular Probes). Primary antibodies were incubated overnight at 4°C, with remaining incubations being performed at room temperature for 30 minutes. After each incubation step tissue sections were washed three times in Tris-buffered saline (pH 7.6) for 5 minutes. To assess the specificity of the immunostaining, tissue sections were incubated with nonimmune rabbit or rat IgG in place of the primary anti-iNOS or anti-F4/80 antibodies and then processed under identical conditions. Tissue sections were mounted with anti-fade mounting medium (Vector Laboratories), and double-immunofluorescent staining was analyzed by inverted fluorescent microscopy.

Detection of Apoptosis and Proliferation

Apoptotic cells were detected by the terminal dUTP nick-end labeling (TUNEL) assay as previously described.[32] Briefly, 4-μm formalin-fixed tissue sections were deparaffinized and rehydrated in ethanol followed by an antigen retrieval step comprising of boiling in 0.01 mol/L sodium citrate buffer for 2 minutes. Sections were then incubated with proteinase K (6.2 μg/ml), followed by TdT (300 enzyme U/ml; Amersham Pharmacia Biotech) and Bio-14-dATP (0.94 nmol/L; Gibco BRL, Life Technologies, Paisley, Scotland). Biotinylated ATP was detected using the RTU Vectastain Elite ABC Reagent (Vector Laboratories) and slides were counterstained with methyl green and eosin. As a positive control, slides were pretreated with DNase I (20 Kunitz U/ml; Roche Molecular Biochemicals, Lewes, UK). Cells were regarded as TUNEL-positive if they exhibited stained nuclei with an apoptotic morphology. Tubular and interstitial cell apoptosis was quantified in a blinded manner by counting the number of TUNEL-positive tubular and interstitial cells in 20 to 25 sequentially selected nonoverlapping fields of renal cortex at ×400 magnification. Data were expressed as the mean number ± SEM per high-power field.

PAS-stained tissue sections were used to quantify proximal and distal tubular cell proliferation because proximal tubular cells exhibit a characteristic PAS-positive luminal brush border.[33] Mitotic cells were readily identifiable, and proximal and distal cell proliferation were calculated in a blinded manner by counting the number of mitotic proximal and distal tubular epithelial cells in 20 to 25 sequentially selected nonoverlapping fields of renal cortex at ×400 magnification and expressed as the mean number ± SEM per high-power field.

Statistical Analysis

All results are presented as mean ± SEM. Statistical analysis was performed using GraphPad Prism 3.02/Instat 1.1 (GraphPad Software, San Diego, CA). The Student's *t*-test was used for comparisons involving two groups, and statistical differences among multiple groups of data were assessed by one-way analysis of variance followed by a Newman-Keuls post hoc test. Results are considered significant at $P < 0.05$.

Results

Cytokine-Activated Macrophages Induce MDCK Cell Apoptosis

Nonactivated macrophages did not induce significant MDCK cell apoptosis in co-culture studies, thereby indicating that macrophages are not inherently cytotoxic (Figure 1A; 1.49 ± 0.3% versus 0.96 ± 0.3% apoptosis, nonactivated co-cultures versus control MDCK cells; $P > 0.05$). In addition, treatment of MDCK cells with LPS and IFN-γ had no effect on the level of MDCK cell apoptosis (1.42 ± 0.3% versus 0.96 ± 0.3% apoptosis, cytokine-activated MDCK cells versus nonactivated MDCK cells; $P > 0.05$). However, MDCK cells in co-cultures activated with LPS and IFN-γ exhibited significantly increased levels of apoptosis after 24 hours (Figure 1A; 12.3 ± 4.1% versus 1.49 ± 0.3% apoptosis; cytokine-activated co-cultures versus nonactivated co-cultures; $P < 0.01$). Apoptotic MDCK cells exhibited characteristic cytoplasmic condensation (Figure 1B) and nuclear pyknosis (Figure 1C).

Macrophage-Derived NO Is an Important Mediator of MDCK Cell Apoptosis but Is Not Implicated in the Inhibition of MDCK Cell Proliferation

Previous data indicate that macrophage-derived NO is involved in the cytotoxicity of cytokine-activated macrophages toward tumor cells[34] and glomerular mesangial cells.[18] We therefore performed co-cultures with macrophages derived from either iNOS wild-type or iNOS knockout mice. Co-cultures of activated iNOS wild-type macrophages and MDCK cells exhibited a 3.5-fold higher level of MDCK cell apoptosis compared to co-cultures of MDCK cells with activated iNOS knockout macrophages (Figure 2A; 4.6 ± 0.9% versus 1.14 ± 0.4% apoptosis; activated co-cultures with iNOS wild-type macrophages versus activated co-cultures with iNOS knockout macrophages; $P < 0.001$). In addition, cytokine-activated iNOS knockout macrophages did not induce apoptosis above the background level evident in cytokine-treated target cells alone, thereby suggesting a key role for macrophage-derived NO in the induction of MDCK death (1.14 ± 0.4% versus 0.69 ± 0.04% apoptosis; activated co-cultures with iNOS knockout macrophages versus nonactivated co-cultures with iNOS knockout macrophages; $P > 0.05$). Furthermore, the cytotoxic effect of activated iNOS wild-type macrophages was completely abrogated by the inclusion of the non-competitive NOS inhibitor *N*-nitro-L-arginine methyl ester (L-NAME, 200 μmol/L) thereby reinforcing the importance of NO as a death effector in cytokine-activated co-cultures (Figure 2A; 0.92 ± 0.1% versus 4.6 ± 0.9% apoptosis; activated co-culture with L-NAME versus activated co-culture; $P < 0.001$). Importantly, inclusion of the control isomer *N*-nitro-D-arginine methyl ester (D-NAME, 200 μmol/L) did not prevent the cytotoxic action of cytokine-activated iNOS wild-type macrophages (Fig-

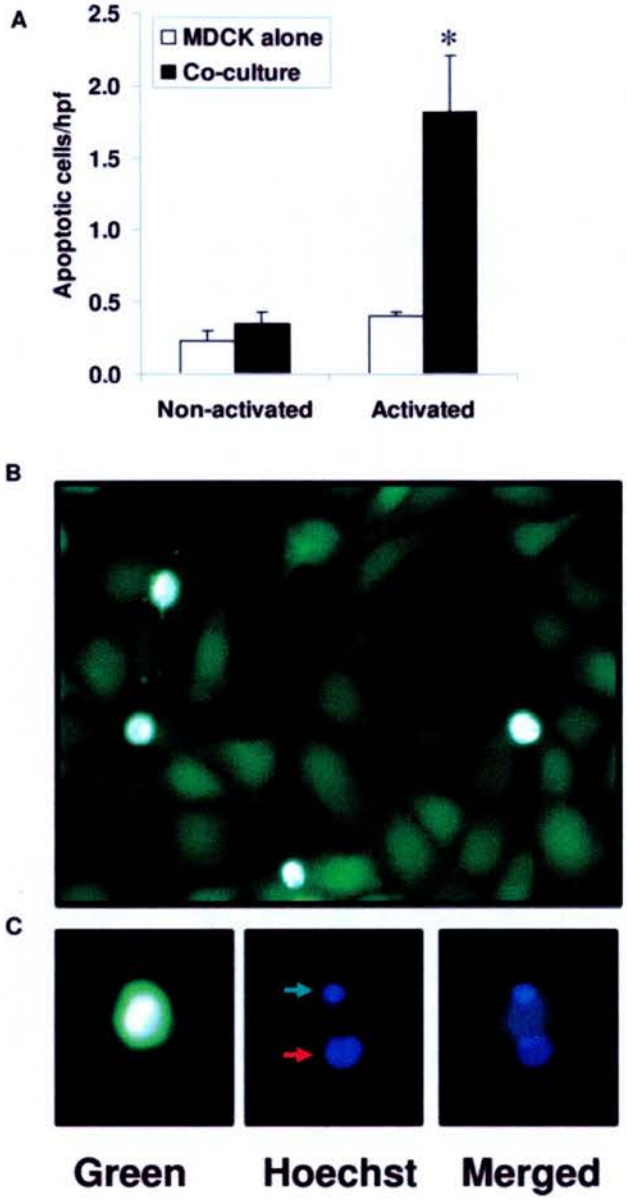

Figure 1. Cytokine-activated macrophages induce MDCK cell apoptosis. **A:** MDCK cells were cultured alone or in the presence of mature murine bone marrow-derived macrophages in the presence or absence of LPS and IFN-γ. After a 24-hour incubation the level of MDCK cell apoptosis is determined by *in situ* fixation of cultures with formaldehyde and fluorescence microscopy after staining with Hoechst. Cytokine-activated macrophages induce significant MDCK cell death. $^*P < 0.001$ versus nonactivated co-culture (data from experiments with macrophages from four different mice). **B:** Low-power view of cytokine-activated co-culture of macrophages (unlabeled) and CellTracker green-labeled MDCK cells after 24 hours. Apoptotic MDCK cells are visible as bright cells exhibiting cytoplasmic condensation. **C:** The bright rounded apoptotic MDCK cell exhibits nuclear pyknosis (**green arrow**); a classical feature of apoptosis. The nucleus of an adjacent unlabeled macrophage is also evident (**red arrow**). The merged image demonstrates the proximity of the macrophage to the MDCK cell.

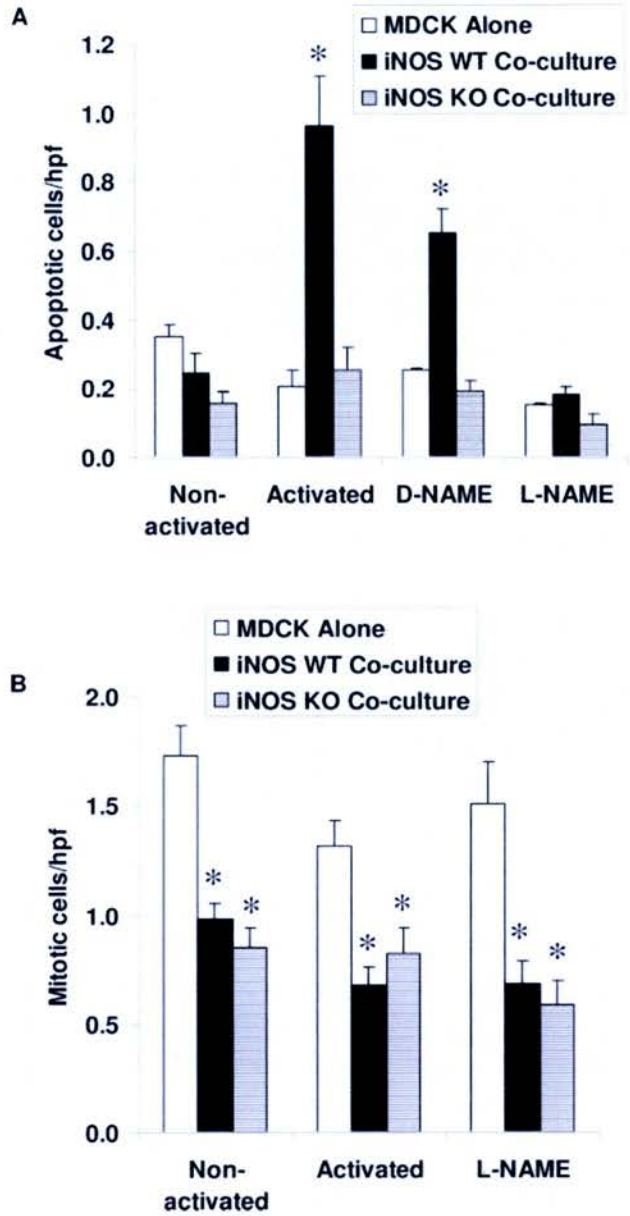

Figure 2. Macrophage-derived NO is an important mediator of MDCK cell apoptosis but is not involved in the inhibition of MDCK cell proliferation. **A:** MDCK cells were cultured alone or in the presence of bone marrow-derived macrophages derived from either iNOS wild-type (WT) or knockout (KO) mice. Cultures were activated with LPS and IFN-γ in the presence or absence of the NOS inhibitor L-NAME (200 μmol/L) or control D-NAME (200 μmol/L). iNOS knockout macrophages are not cytotoxic under any conditions whereas the cytotoxicity of iNOS wild-type macrophages is completely abrogated by pharmacological inhibition of NO production. $^*P < 0.05$ versus nonactivated iNOS wild-type macrophage co-cultures (data from experiments with macrophages from three different mice). **B:** MDCK cells were cultured alone or in the presence of mature bone marrow-derived macrophages derived from either iNOS wild-type or knockout mice. Cultures were activated with LPS and IFN-γ in the presence or absence of the NOS inhibitor L-NAME. Inhibition of MDCK cell proliferation by macrophages is independent of cytokine activation, macrophage genotype, or pharmacological inhibition of NO production. $^*P < 0.05$ versus MDCK cells alone (data from experiments with macrophages from three different mice).

ure 2A; 4.4 ± 0.3% versus 4.6 ± 0.9% apoptosis; activated co-cultures with D-NAME versus activated co-cultures; $P > 0.05$).

MDCK cell proliferation was significantly inhibited by co-culture with macrophages, with the anti-proliferative effect being independent of macrophage activation by LPS and IFN-γ (Figure 2B). Furthermore, this anti-proliferative effect was unaffected by the inclusion of the NOS inhibitor L-NAME in the co-culture or the use of iNOS wild-type and knockout macrophages (Figure 2B). This indicates, in contrast to previous work using mesangial

cells,[18] that NO was not involved in the modulation of MDCK cell proliferation. No difference was evident in total cell number in these experiments (data not shown).

Macrophage-Derived NO Induces Apoptosis in Murine PTE Cells

Although MDCK cells are a well-established tubular cell line, they are of canine origin and may therefore not be susceptible to other putative murine macrophage-derived death effectors such as FasL and TNF-α. We therefore determined whether cytokine-activated macrophages exerted similar effects on murine PTE cells. Treatment of PTE cells with LPS and IFN-γ did not induce significant apoptosis (Figure 3A). Cytokine activation of co-cultures induced a significant threefold increase in PTE cell apoptosis compared to nonactivated co-cultures (Figure 3A; 5.28 ± 0.7% versus 1.08 ± 0.3% apoptosis; activated co-cultures versus nonactivated co-cultures; $P < 0.001$). In addition, inclusion of the NOS inhibitor L-NAME reduced tubular cell death to baseline levels (Figure 3A; 5.28 ± 0.7% versus 1.47 ± 0.3% apoptosis; activated co-cultures versus activated co-cultures treated with L-NAME; $P < 0.001$). Furthermore, although iNOS wild-type macrophages were significantly cytotoxic (Figure 3B; 3.26 ± 0.4% versus 0.72 ± 0.3% apoptosis; activated co-cultures with iNOS wild-type macrophages versus nonactivated co-cultures with iNOS wild-type macrophages; $P < 0.001$), cytokine-activated iNOS knockout macrophages did not induce significant apoptosis of PTE cells (Figure 3B; 0.57 ± 0.4% versus 0.33 ± 0.1% apoptosis; activated co-cultures with iNOS knockout macrophages versus nonactivated co-cultures with iNOS knockout macrophages; $P > 0.05$).

In contrast to MDCK cells, incubation of PTE cells with macrophages in the presence or absence of LPS and IFN-γ had no effect on the level of PTE cell proliferation (data not shown). It should, however, be noted that PTE cells exhibit a low level of proliferation compared to MDCK cells. Although there was a trend to a reduced total cell number in activated co-cultures, this did not reach statistical significance (data not shown). We also noted evidence of phagocytosis of apoptotic PTE cells by macrophages in this primary cell co-culture system (Figure 3C) unlike co-cultures of macrophages with MDCK cells. The effect of phagocytosis would be predicted to reduce the levels of free apoptotic cells evident, and this may explain why a lower level of apoptotic PTE cells was detected compared to MDCK cells. Interestingly, in accordance with the increased level of PTE cell apoptosis in activated co-cultures of iNOS wild-type macrophages compared to iNOS knockout macrophages, we noted an increased percentage of macrophages containing phagocytosed apoptotic PTE cells (1.2 ± 0.79 macrophages/high-power field versus 0.3 ± 0.25 macrophages/high-power field: iNOS wild-type macrophages versus iNOS knockout macrophages). In these studies we did not find any significant difference between experiments involving the co-culture of C57BL/6 PTE cells with either allogeneic FVB/N macrophages or syngeneic C57BL/6 macrophages (0.58 ± 0.1 apoptotic cells per high-power field versus 0.42 ± 0.06 apoptotic cells per high-power field; activated co-cultures with C57BL/6 PTE cells and FVB/N macrophages versus activated co-cultures with C57BL/6 PTE cells and C57BL/6 macrophages; $P > 0.05$).

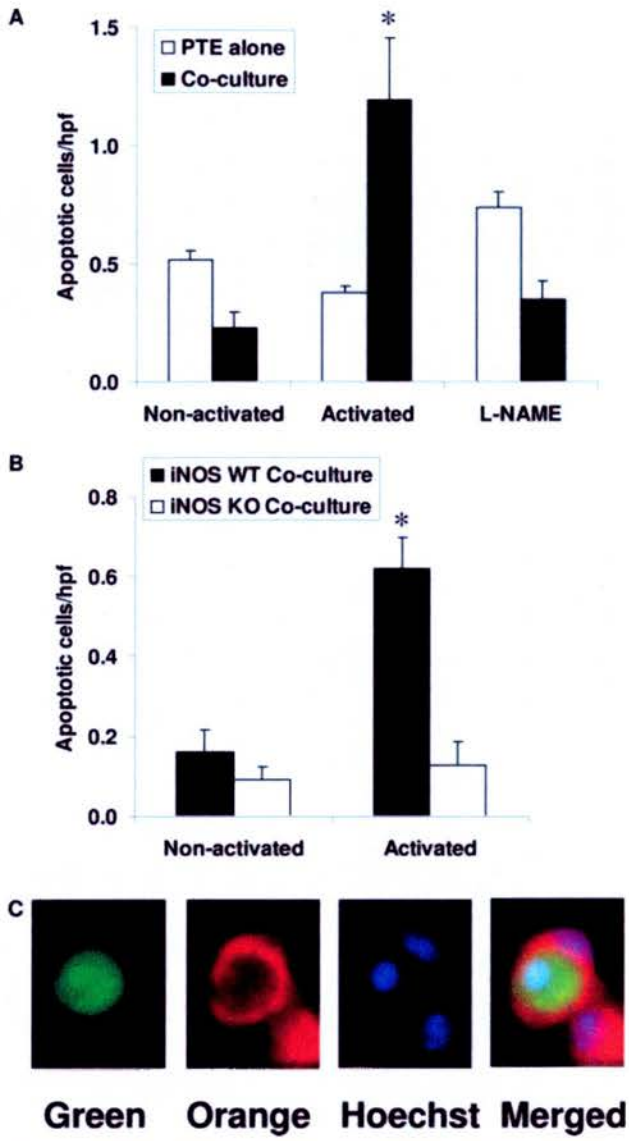

Figure 3. Cytokine-activated macrophages induce apoptosis in primary murine tubular epithelial cells (PTEs). **A:** PTE cells were cultured in the presence of mature murine bone marrow-derived macrophages. Selected cell cultures were activated with LPS and IFN-γ in the presence or absence of the NOS inhibitor L-NAME (200 μmol/L). $^*P < 0.05$ versus activated co-cultures in the presence or absence of L-NAME (data from experiments with cells from three different mice). **B:** PTE cells were cultured in the presence of mature bone marrow-derived macrophages derived from either iNOS wild-type or knockout mice. Selected cell cultures were activated with LPS and IFN-γ. Cytokine activation of iNOS wild-type macrophages induced PTE cell apoptosis whereas activated iNOS knockout macrophages were noncytotoxic. $^*P < 0.05$ versus nonactivated co-culture (data from experiments with cells from five different mice). **C:** Photomicrographs from a co-culture of fluorescently labeled macrophages (CellTracker orange) and PTE cells (CellTracker green) demonstrating evidence of macrophage recognition and phagocytosis of apoptotic tubular cells. The merged image demonstrates a condensed green apoptotic tubular cell with a pyknotic nucleus that has been ingested by a CellTracker orange-labeled macrophage.

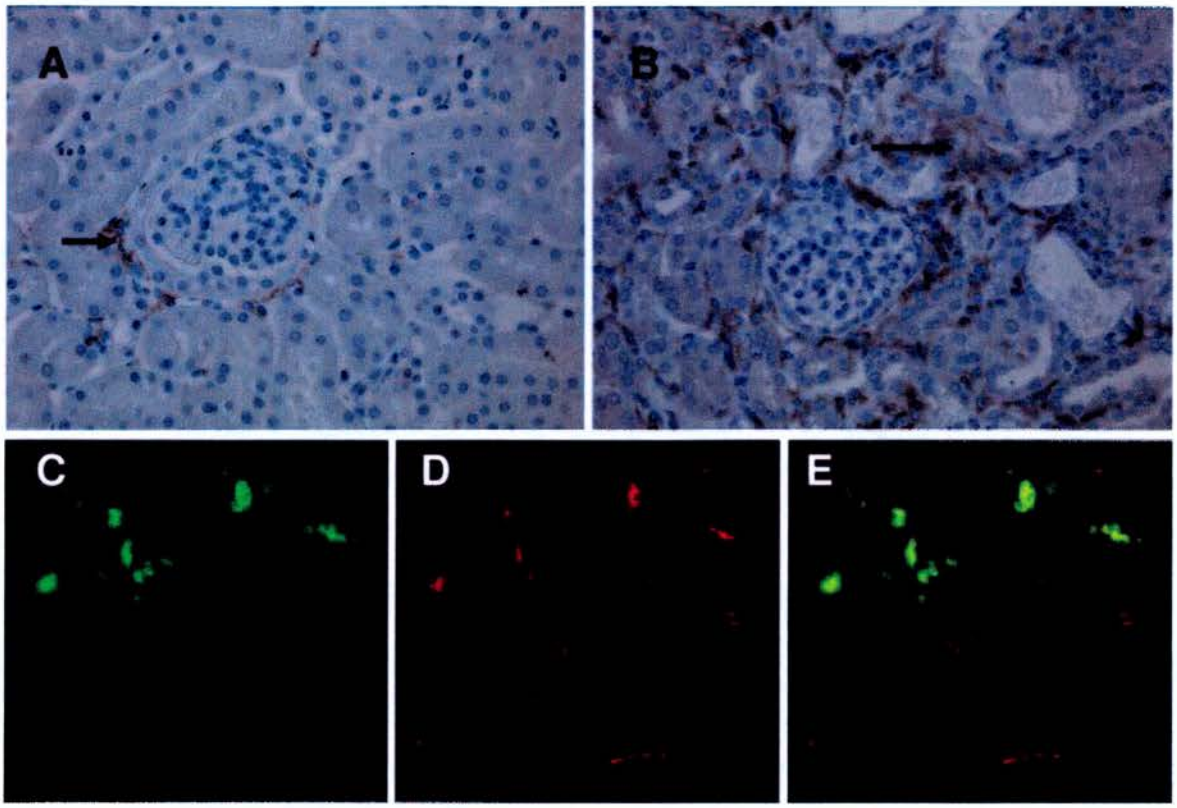

Figure 4. Obstructed kidneys exhibit tubulointerstitial infiltration with macrophages and iNOS-positive cells. Tissue sections were immunostained for the macrophage marker F4/80 and/or iNOS. **A:** Normal nonmanipulated kidneys exhibit occasional F4/80-positive resident macrophages (**arrow**). **B:** In contrast, obstructed kidneys exhibit a prominent interstitial population of infiltrating F4/80-positive macrophages (**arrow**). **C–E:** Fluorescent photomicrographs showing double-immunofluorescent staining of iNOS and F4/80 in day 7 obstructed kidney: iNOS-positive cells stained green (**C**), F4/80-positive interstitial macrophages stained red (**D**), and merged image demonstrating co-localization (yellow) of iNOS and F4/80 indicating the presence of infiltrating macrophages expressing iNOS (**E**).

Pharmacological Blockade of iNOS by L-NIL Reduces Tubular Epithelial Cell Apoptosis in Experimental Hydronephrosis

We then sought a role for iNOS-derived NO in the tubular cell apoptosis evident during tubulointerstitial inflammation *in vivo*. We used L-NIL, a specific irreversible iNOS inhibitor, to pharmacologically inhibit the enzyme iNOS in the model of experimental hydronephrosis, a model characterized by marked tubulointerstitial macrophage infiltration and tubular epithelial cell death.[22,35] We induced experimental hydronephrosis in FVB/N mice and administered L-NIL in the drinking water[27,28] between day 5 and day 7, at which time the obstructed kidneys were removed for histological analysis. Administration of the inactive isomer D-NIL served as control. Normal kidneys exhibited occasional scattered F4/80-positive resident macrophages whereas obstructed kidneys developed a prominent macrophage infiltrate in the tubulointerstitium (Figure 4, A and B; 0.32 ± 0.04% versus 3.9 ± 0.9% F4/80-positive surface area; normal kidney versus day 7 obstructed kidney; $P < 0.001$). In addition, iNOS-positive macrophages were evident within the tubulointerstitium (Figure 4, C–E). Pharmacological inhibition of iNOS did not have any significant effect on the level of macrophage infiltration (3.2 ± 0.7% versus 3.9 ± 0.9% F4/80-positive surface area; L-NIL versus control; $P > 0.05$). Tubular cell apoptosis and proliferation was determined by TUNEL and PAS staining, respectively (Figure 5). Administration of L-NIL significantly reduced the level of tubular epithelial cell apoptosis compared to controls (Figure 6A). In contrast, the administration of L-NIL did not affect the level of tubular cell proliferation in obstructed kidneys (Figure 6B).

Pharmacological Blockade of iNOS by L-NIL Reduces Interstitial Cell Apoptosis and Increases Tubulointerstitial Fibrosis in Experimental Hydronephrosis

Interstitial cell apoptosis and proliferation were determined by TUNEL and PAS staining, respectively (Figure 5). The administration of L-NIL also resulted in a significant reduction in the level of interstitial cell apoptosis (Figure 7A) with no effect on interstitial cell proliferation being evident (Figure 7B). Tubulointerstitial fibrosis was assessed by immunohistochemical staining for collagen III, which is deposited by fibroblasts and is a representative collagen of the scarred and injured tubulointerstitium.[36] Careful morphometric analysis of collagen III immunostaining indicated that pharmacological blockade of the enzyme iNOS resulted in increased collagen III deposition (Figure 8). We stained sections for α-smooth

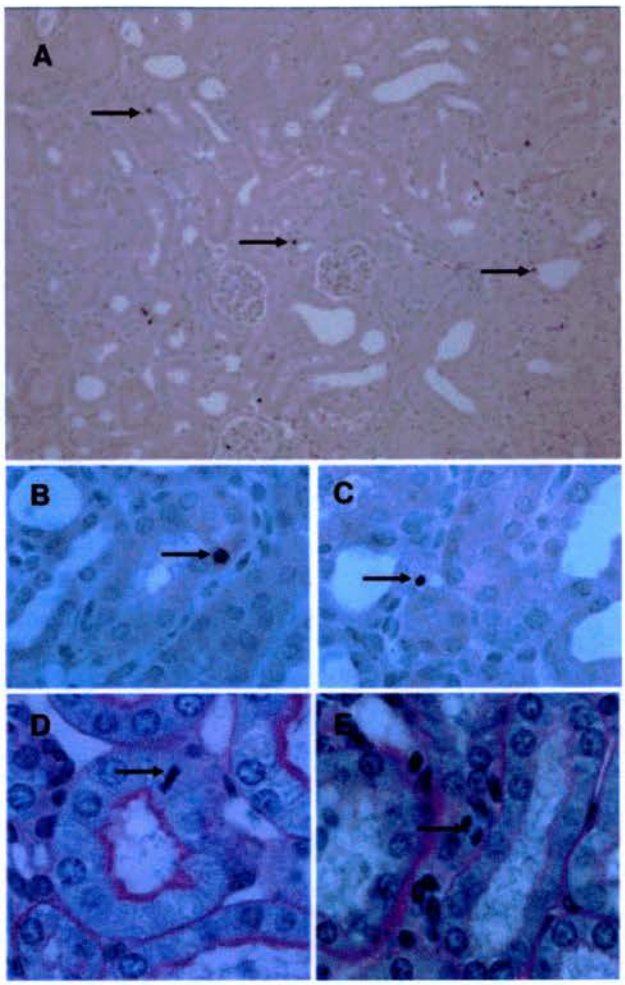

Figure 5. Obstructed kidneys exhibit apoptosis and proliferation of tubular epithelial and interstitial cells. Tissue sections underwent TUNEL staining to detect apoptotic cells whereas cells undergoing mitosis were identified on PAS-stained tissue sections. **A:** Low-power view of obstructed kidneys demonstrating scattered TUNEL-positive apoptotic cells (**arrows**). **B:** High-power view of a TUNEL-positive apoptotic tubular epithelial cell (**arrow**). **C:** High-power view of a TUNEL-positive apoptotic interstitial cell (**arrow**). **D:** High-power view of a tubular epithelial cell undergoing mitosis (**arrow**). **E:** High-power view of an interstitial cell undergoing mitosis (**arrow**). Original magnifications: ×200 (**A**); ×1000 (**B–E**).

muscle actin, which is expressed by tubulointerstitial myofibroblasts.[26] The area of the renal tubulointerstitium occupied by α-smooth muscle actin staining was assessed morphometrically as an indirect measure of the tubulointerstitial myofibroblast population. This analysis indicated no significant difference in α-smooth muscle actin staining after short-term blockade of iNOS (3.1 ± 0.4% versus 2.8 ± 0.6% α-smooth muscle actin staining; L-NIL treatment versus control; $P > 0.05$).

Discussion

The main finding of this study is that, despite the fact that inflammatory macrophages may produce myriad pro-apoptotic mediators,[18–20] NO is the key mediator of macrophage-induced tubular epithelial cell apoptosis *in vitro* and plays a prominent role *in vivo* during tubulointerstitial

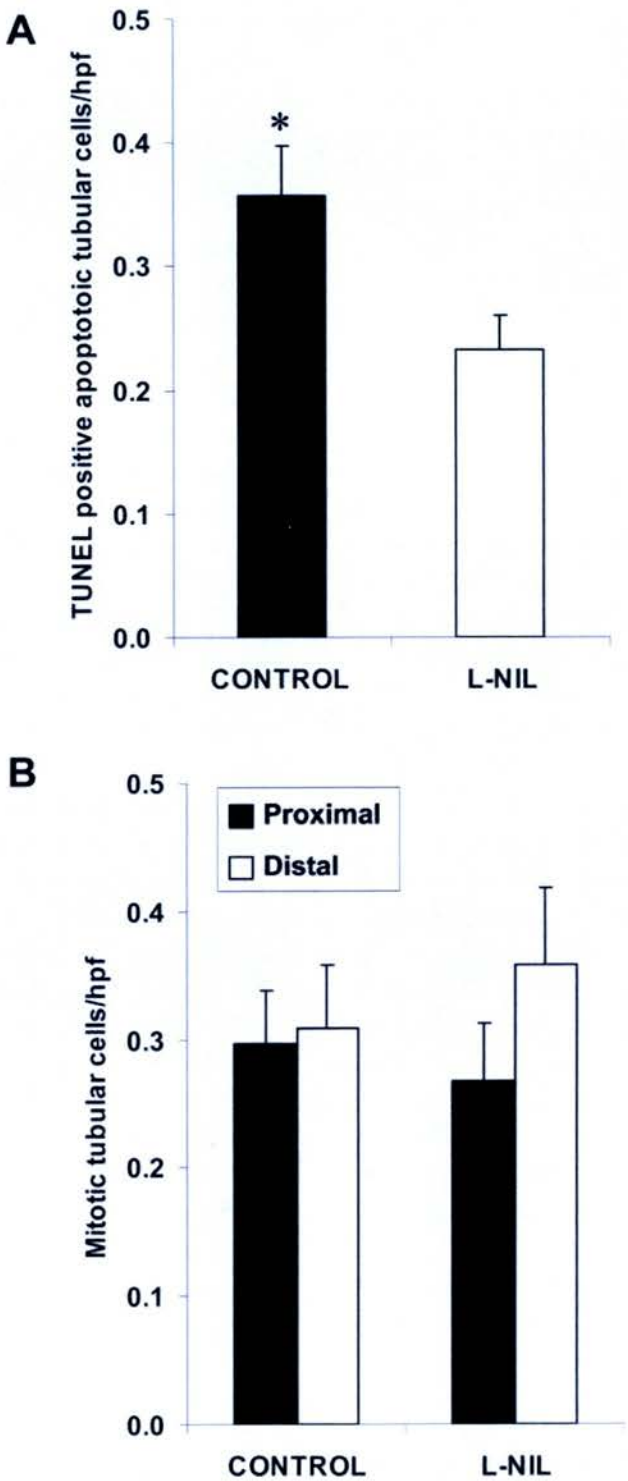

Figure 6. Pharmacological blockade of iNOS reduces tubular cell apoptosis but does not affect tubular cell proliferation after ureteric obstruction. Mice were administered L-NIL, an irreversible pharmacological inhibitor of the enzyme iNOS, or the isomeric control D-NIL, and the obstructed kidneys were removed at day 7. **A:** The level of tubular cell apoptosis in obstructed kidneys is significantly reduced after the administration of L-NIL. $^*P < 0.05$ versus control (eight mice per group). **B:** The level of tubular cell proliferation in obstructed kidneys is unaffected after the administration of L-NIL (n = seven to eight mice per group).

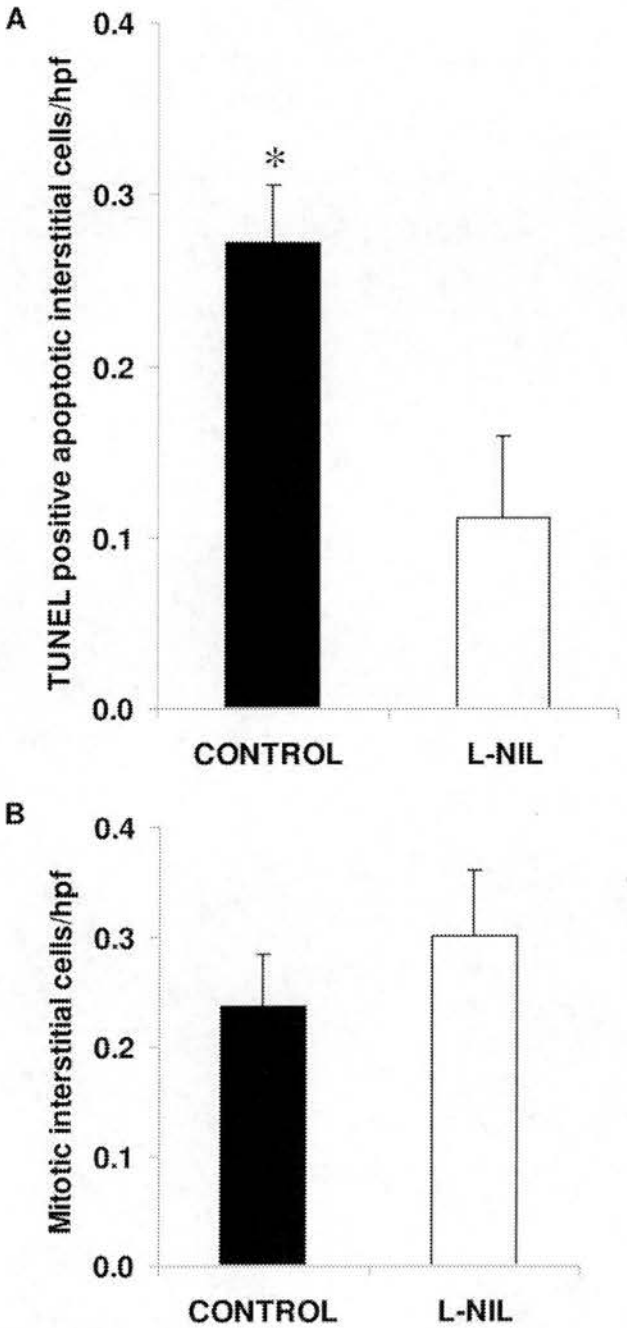

Figure 7. Pharmacological blockade of iNOS reduces interstitial cell apoptosis but does not affect interstitial cell proliferation after ureteric obstruction. Mice were administered L-NIL, an irreversible pharmacological inhibitor of the enzyme iNOS, or the isomeric control D-NIL, and the obstructed kidneys were removed at day 7. **A:** The level of interstitial cell apoptosis in obstructed kidneys is significantly reduced after the administration of L-NIL. $^{*}P < 0.05$ versus control (eight mice per group). **B:** The level of interstitial cell proliferation in obstructed kidneys is unaffected after the administration of L-NIL (n = seven to eight mice per group).

inflammation. Our data indicates that nonactivated macrophages per se are not inherently cytotoxic whereas cytokine-activated macrophages induce significant apoptosis of MDCK cells, a well-characterized renal tubular cell line. Studies using both pharmacological inhibitors of NO production and macrophages derived from either iNOS knockout or wild-type mice indicate that macrophage cytotoxicity *in vitro* is markedly dependent on iNOS-derived NO. Importantly, similar results were obtained in an entirely primary cell co-culture system using murine primary renal tubular epithelial cells. These data are in accordance with previous work indicating that NO is an important mediator of macrophage cytotoxicity toward renal mesangial cells and tumor cells.[18,34] Interestingly, we noted that the level of PTE cell apoptosis evident in these studies was less than the level of MDCK cell apoptosis. Although this may reflect a variety of factors including the different species of origin and the proliferation status of the cells, our data suggest that macrophage phagocytosis of apoptotic PTE cells but not MDCK cells may be at least partly responsible because apoptotic cells may be rapidly recognized, ingested, and degraded.[37]

Despite the fact that previous work has indicated the involvement of NO in the macrophage induced apoptosis of mesangial cells[18] and vascular smooth muscle cells,[38] other death effectors such as TNF-α[12,19,39]; and FasL[35,38,40] have also been implicated. In our study, however, pharmacological inhibition of NO production or the use of iNOS-deficient macrophages resulted in a complete abrogation of tubular cell apoptosis compared to control co-cultures, thereby suggesting that NO is the dominant mediator of tubular epithelial cell death induced by cytokine-activated macrophages *in vitro*. This suggests that the presence of significant additional *in vitro* proapoptotic mechanisms is unlikely and that macrophage generation of NO is critically important. Previous *in vitro* studies have suggested macrophage production of a soluble proapoptotic factor capable of inducing tubular cell death,[11,12,21] and this may reflect the use of different cells and assays in these studies.

The effect of macrophages on the level of target cell proliferation varied according to the nature of the target cell. The proliferation of MDCK cells was reduced by incubation with nonactivated or cytokine-activated macrophages. Bone marrow-derived macrophages secrete significant levels of transforming growth factor-β and this cytokine has been documented to inhibit MDCK cell proliferation.[24,41] In contrast, bone marrow-derived macrophages exerted no significant effects on PTE cell proliferation although this may reflect the lower level of proliferation of these primary cells.

Because *in vitro* studies suggested a key role for macrophage-derived NO, we examined the effects of pharmacological inhibition of iNOS on tubular cell death during renal inflammation *in vivo*. We used the neutrophil- and lymphocyte-independent model of experimental hydronephrosis that is characterized by prominent macrophage infiltration and significant tubular cell apoptosis.[22,26] Importantly, the administration of the specific iNOS inhibitor L-NIL did not result in any confounding effects on the level of interstitial macrophage infiltration. However, L-NIL treatment did significantly reduce the level of tubular cell apoptosis compared to the control group but had no effect on tubular cell proliferation, in accord with our *in vitro* experiments using primary murine tubular epithelial cells.

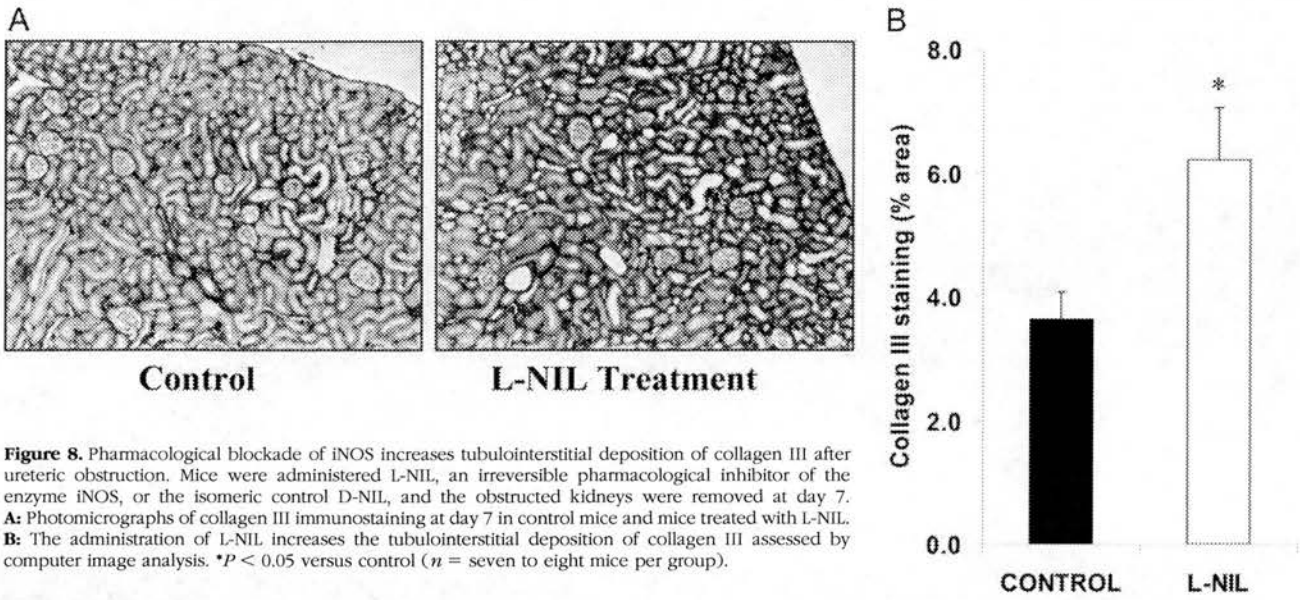

Figure 8. Pharmacological blockade of iNOS increases tubulointerstitial deposition of collagen III after ureteric obstruction. Mice were administered L-NIL, an irreversible pharmacological inhibitor of the enzyme iNOS, or the isomeric control D-NIL, and the obstructed kidneys were removed at day 7. **A:** Photomicrographs of collagen III immunostaining at day 7 in control mice and mice treated with L-NIL. **B:** The administration of L-NIL increases the tubulointerstitial deposition of collagen III assessed by computer image analysis. $^{*}P < 0.05$ versus control (n = seven to eight mice per group).

It should also be noted that additional mechanisms have been suggested for macrophage-mediated tubular cell apoptosis *in vivo*. A study of a murine model of Alport syndrome suggested that macrophage production of matrix metalloproteinases may result in degradation of tubular basement membrane and resultant tubular cell apoptosis by anoikis.[42,43] In addition, Misseri and colleagues[44] suggested a role for TNF-α in the induction of tubular cell death in experimental hydronephrosis in the rat. In this study, the obstructed kidneys exhibited up-regulation of both TNF-α and FasL expression with systemic administration of a pegylated form of soluble TNF receptor type 1, significantly inhibiting tubular cell apoptosis. Macrophage infiltration, however, was not determined, and it is therefore unclear whether blocking the action of TNF-α may have modulated macrophage infiltration, a key factor in determining the level of tubular cell apoptosis during tubulointerstitial infiltration.[14] However, because L-NIL administration resulted in a partial inhibition of tubular cell apoptosis, additional proapoptotic mediators may be used by infiltrating inflammatory macrophages to induce tubular cell death during tubulointerstitial inflammation *in vivo*.

Our study does, however, reinforce the critically important role of infiltrating macrophages during tubulointerstitial inflammation. A body of evidence indicates that macrophages are implicated in the deleterious induction of tubular cell apoptosis *in vivo*. For example, the induction of renal inflammation in mice exhibiting defective tubulointerstitial macrophage recruitment is characterized by significantly reduced levels of tubular cell apoptosis.[11–13] Also, we recently used the transgenic CD11b-DTR conditional ablation mouse[45] to examine the role of macrophages in progressive renal inflammation during nephrotoxic nephritis. The ablation of macrophages between days 15 and 20 of nephrotoxic nephritis improves renal function and significantly reduced the level of tubular cell apoptosis[14] thereby reinforcing a direct role for macrophages in the induction of tubular cell death. Our data indicate that the pharmacological blockade of the production of proapoptotic NO by iNOS can inhibit tubular epithelial cell death without affecting the level of macrophage infiltration and stresses the importance of macrophage phenotype as well as macrophage numbers during renal inflammation. Our data resonate with the work of Anders and colleagues[46] who noted that blockade of the chemokine CCL5/RANTES in glomerulonephritis successfully inhibited macrophage infiltration but resulted in increased macrophage expression of iNOS and increased tissue injury as a result.

It is also of interest that L-NIL treatment significantly reduced the level of interstitial cell apoptosis. Previous work has established that the vast majority of TUNEL-positive apoptotic cells detected within the tubulointerstitium of the kidney have actually been phagocytosed and are located within viable nonapoptotic cells.[47] We were therefore unable to use double staining for α-smooth muscle actin and TUNEL to determine whether the apoptotic tubulointerstitial cells were dying myofibroblasts. Despite the reduction in interstitial cell apoptosis, we found no significant difference in the tubulointerstitial population of myofibroblasts assessed by morphometric analysis of α-smooth muscle actin immunostaining. This may be attributable to the fact that the period of pharmacological blockade of iNOS was relatively short. Despite the absence of a significant difference in tubulointerstitial α-smooth muscle actin expression, we found that L-NIL treatment significantly increased the tubulointerstitial deposition of collagen III that is characteristically found in renal injury and scarring. This suggests that iNOS-derived NO may also be involved in limiting tubulointerstitial renal scarring and it is therefore of interest that iNOS knockout mice develop increased levels of tubulointerstitial fibrosis after ureteric obstruction.[48] Our data indicating that pharmacological blockade of iNOS-derived NO ameliorates the level of tubular cell apoptosis is not in accordance with previous work because NO has been

implicated as a protective factor in the induction of tubular cell apoptosis by mechanical stretch *in vitro* and *in vivo* in ureteric obstruction.[49] The reasons for this are unclear, although strain differences may be important because this can significantly affect the amount of NO generated by macrophages.[50] Although beyond the scope of this study, it would be interesting to perform ureteric obstruction in irradiated iNOS wild-type mice reconstituted with bone marrow derived from iNOS knockout mice because this would localize the defective expression of iNOS to the infiltrating leukocyte population. It should be noted, however, that double immunolabeling revealed F4/80-positive macrophages that were strongly iNOS-positive within the tubulointerstitium of obstructed kidneys, indicating that infiltrating macrophages may express iNOS.

Lastly, it is apparent from this and other studies that a significant level of macrophage-independent tubular cell death occurs in this model and it is undoubtedly the case that additional proapoptotic stimuli including mechanical stretch, hypoxia, ischemia, and so forth, also play a major role in the apoptosis of tubular epithelial cells.[51–53] In conclusion, our work indicates that iNOS-derived NO is an important mediator of macrophage-induced tubular epithelial cell apoptosis *in vitro* and plays an important role in tubular epithelial cell apoptosis and tubulointerstitial fibrosis *in vivo*.

References

1. Gordon S: Macrophage-restricted molecules: role in differentiation and activation. Immunol Lett 1999, 65:5–8
2. Leibovich SJ, Ross R: The role of the macrophage in wound repair. A study with hydrocortisone and antimacrophage serum. Am J Pathol 1975, 78:71–100
3. Gouon-Evans V, Rothenberg ME, Pollard JW: Postnatal mammary gland development requires macrophages and eosinophils. Development 2000, 127:2269–2282
4. Lang RA, Bishop JM: Macrophages are required for cell death and tissue remodeling in the developing mouse eye. Cell 1993, 74:453–462
5. Savill J, Dransfield I, Gregory C, Haslett C: A blast from the past: clearance of apoptotic cells regulates immune responses. Nat Rev Immunol 2002, 2:965–975
6. Diez-Roux G, Argilla M, Makarenkova H, Ko K, Lang RA: Macrophages kill capillary cells in G1 phase of the cell cycle during programmed vascular regression. Development 1999, 126:2141–2147
7. Lang R, Lustig M, Francois F, Sellinger M, Plesken H: Apoptosis during macrophage-dependent ocular tissue remodelling. Development 1994, 120:3395–3403
8. Kluth DC, Erwig L-P, Rees AJ: Multiple facets of macrophages in renal injury. Kidney Int 2004, 66:542–557
9. Kipari TMJ, Hughes J: Macrophage-mediated renal cell death. Kidney Int 2002, 61:760–761
10. Nikolic-Paterson DJ: A role for macrophages in mediating tubular cell apoptosis? Kidney Int 2003, 63:1582–1583
11. Tesch GH, Schwarting A, Kinoshita K, Lan HY, Rollins BJ, Kelley VR: Monocyte chemoattractant protein-1 promotes macrophage-mediated tubular injury, but not glomerular injury, in nephrotoxic serum nephritis. J Clin Invest 1999, 103:73–80
12. Lenda DM, Kikawada E, Stanley ER, Kelley VR: Reduced macrophage recruitment, proliferation, and activation in colony-stimulating factor-1-deficient mice results in decreased tubular apoptosis during renal inflammation. J Immunol 2003, 170:3254–3262
13. Lange-Sperandio B, Cachat F, Thornhill BA, Chevalier RL: Selectins mediate macrophage infiltration in obstructive nephropathy in newborn mice. Kidney Int 2002, 61:516–524
14. Duffield JS, Tipping PG, Kipari T, Cailhier JF, Clay S, Lang R, Bonventre JV, Hughes J: Conditional ablation of macrophages halts progression of crescentic glomerulonephritis. Am J Pathol 2005, 165:1207–1219
15. Gobe GC, Axelsen RA: Genesis of renal tubular atrophy in experimental hydronephrosis in the rat. Role of apoptosis. Lab Invest 1987, 56:273–281
16. Bohle A, Wehrmann M, Mackensen-Haen S, Gise H, Mickeler E, Xiao TC, Muller C, Muller GA: Pathogenesis of chronic renal failure in primary glomerulopathies. Nephrol Dial Transplant 1994, 9:4–12
17. Bohle A, Muller GA, Wehrmann M, Mackensen-Haen S, Xiao JC: Pathogenesis of chronic renal failure in the primary glomerulopathies, renal vasculopathies, and chronic interstitial nephritides. Kidney Int Suppl 1996, 54:S2–S9
18. Duffield JS, Erwig L-P, Wei X-Q, Liew FY, Rees AJ, Savill JS: Activated macrophages direct apoptosis and suppress mitosis of mesangial cells. J Immunol 2000, 164:2110–2119
19. Duffield JS, Ware CF, Ryffel B, Savill J: Suppression by apoptotic cells defines tumor necrosis factor-mediated induction of glomerular mesangial cell apoptosis by activated macrophages. Am J Pathol 2001, 159:1397–1404
20. Brown SB, Savill J: Phagocytosis triggers macrophage release of Fas ligand and induces apoptosis of bystander leukocytes. J Immunol 1999, 162:480–485
21. Lange-Sperandio B, Fulda S, Vandewalle A, Chevalier RL: Macrophages induce apoptosis in proximal tubule cells. Pediatr Nephrol 2003, 18:335–341
22. Diamond JR: Macrophages and progressive renal disease in experimental hydronephrosis. Am J Kidney Dis 1995, 26:133–140
23. Wei XQ, Charles IG, Smith A, Ure J, Feng GJ, Huang FP, Xu D, Muller W, Moncada S, Liew FY: Altered immune responses in mice lacking inducible nitric oxide synthase. Nature 1995, 375:408–411
24. Yang YL, Guh JY, Yang ML, Lai YH, Tsai JH, Hung WC, Chang CC, Chuang LY: Interaction between high glucose and TGF-beta in cell cycle protein regulations in MDCK cells. J Am Soc Nephrol 1998, 9:182–193
25. Sato M, Muragaki Y, Saika S, Roberts AB, Ooshima A: Targeted disruption of TGF-{beta}1/Smad3 signaling protects against renal tubulointerstitial fibrosis induced by unilateral ureteral obstruction. J Clin Invest 2003, 112:1486–1494
26. Hughes J, Brown P, Shankland SJ: Cyclin kinase inhibitor p21CIP1/WAF1 limits interstitial cell proliferation following ureteric obstruction. Am J Physiol 1999, 277:F948–F956
27. Westenfeld R, Gawlik A, de Heer E, Kitahara M, Abou-Rebyeh F, Floege J, Ketteler M: Selective inhibition of inducible nitric oxide synthase enhances intraglomerular coagulation in chronic anti-Thy 1 nephritis. Kidney Int 2002, 61:834–838
28. Reilly CM, Farrelly LW, Viti D, Redmond ST, Hutchison F, Ruiz P, Manning P, Connor J, Gilkeson GS: Modulation of renal disease in MRL/lpr mice by pharmacologic inhibition of inducible nitric oxide synthase. Kidney Int 2002, 61:839–846
29. Hunter MG, Hurwitz S, Bellamy CO, Duffield JS: Quantitative morphometry of lupus nephritis: the significance of collagen, tubular space, and inflammatory infiltrate. Kidney Int 2005, 67:94–102
30. Duffield JS, Forbes SJ, Constandinou CM, Clay S, Partolina M, Vuthoori S, Wu S, Lang R, Iredale JP: Selective depletion of macrophages reveals distinct, opposing roles during liver injury and repair. J Clin Invest 2005, 115:56–65
31. Ophascharoensuk V, Giachelli CM, Gordon K, Hughes J, Pichler R, Brown P, Liaw L, Schmidt R, Shankland SJ, Alpers CE, Couser WG, Johnson RJ: Obstructive uropathy in the mouse: role of osteopontin in interstitial fibrosis and apoptosis. Kidney Int 1999, 56:571–580
32. Baker AJ, Mooney A, Hughes J, Lombardi D, Johnson RJ, Savill J: Mesangial cell apoptosis: the major mechanism for resolution of glomerular hypercellularity in experimental mesangial proliferative nephritis. J Clin Invest 1994, 94:2105–2116
33. Hughes J, Johnson RJ: Role of Fas (CD95) in tubulointerstitial disease induced by unilateral ureteric ligation (UUO). Am J Physiol 1999, 277:F26–F32
34. Cui S, Reichner JS, Mateo RB, Albina JE: Activated murine macrophages induce apoptosis in tumor cells through nitric oxide-dependent or -independent mechanisms. Cancer Res 1994, 54:2462–2467
35. Hughes J, Johnson RJ: Role of Fas (CD95) in tubulointerstitial disease induced by unilateral ureteric obstruction. Am J Physiol 1999, 277:F26–F32

36. Mazzali M, Jefferson JA, Ni Z, Vaziri ND, Johnson RJ: Microvascular and tubulointerstitial injury associated with chronic hypoxia-induced hypertension. Kidney Int 2003, 63:2088–2093
37. Barres B, Hart IK, Coles HSR, Burne JF, Voyvodic JT, Richardson WD, Raff MC: Cell death and control of cell survival in the oligodendrocyte lineage. Cell 1992, 70:31–46
38. Boyle JJ, Weissberg PL, Bennett MR: Human macrophage-induced vascular smooth muscle cell apoptosis requires NO enhancement of Fas/Fas-L interactions. Arterioscler Thromb Vasc Biol 2002, 22:1624–1630
39. Boyle JJ, Weissberg PL, Bennett MR: Tumor necrosis factor-alpha promotes macrophage-induced vascular smooth muscle cell apoptosis by direct and autocrine mechanisms. Arterioscler Thromb Vasc Biol 2003, 23:1553–1558
40. Boyle JJ, Bowyer DE, Weissberg PL, Bennett MR: Human blood-derived macrophages induce apoptosis in human plaque-derived vascular smooth muscle cells by Fas-ligand/Fas interactions. Arterioscler Thromb Vasc Biol 2001, 21:1402–1407
41. Nicolas FJ, Lehmann K, Warne PH, Hill CS, Downward J: Epithelial to mesenchymal transition in Madin-Darby canine kidney cells is accompanied by down-regulation of Smad3 expression, leading to resistance to transforming growth factor-beta-induced growth arrest. J Biol Chem 2003, 278:3251–3256
42. Rodgers KD, Rao V, Meehan DT, Fager N, Gotwals P, Ryan ST, Koteliansky V, Nemori R, Cosgrove D: Monocytes may promote myofibroblast accumulation and apoptosis in Alport renal fibrosis. Kidney Int 2003, 63:1338–1355
43. Frisch SM, Francis H: Disruption of epithelial cell-matrix interactions induces apoptosis. J Cell Biol 1994, 124:619–626
44. Misseri R, Meldrum DR, Dinarello CA, Dagher P, Hile KL, Rink RC, Meldrum KK: TNF-alpha mediates obstruction-induced renal tubular cell apoptosis and proapoptotic signaling. Am J Physiol 2005, 288:F406–F411
45. Cailhier JF, Partolina M, Vuthoori S, Wu S, Ko K, Watson S, Savill JS, Lang RA, Hughes J: Conditional macrophage ablation demonstrates that resident macrophages initiate acute peritoneal inflammation. J Immunol 2005, 174:2336–2342
46. Anders HJ, Frink M, Linde Y, Banas B, Wornle M, Cohen C, Vielhauer V, Nelson PJ, Grone HJ, Schlondorff D: CC chemokine ligand 5/RANTES chemokine antagonists aggravate glomerulonephritis despite reduction of glomerular leukocyte infiltration. J Immunol 2003, 170:5658–5666
47. Coles HS, Burne JF, Raff MC: Large-scale normal cell death in the developing rat kidney and its reduction by epidermal growth factor. Development 1993, 118:777–784
48. Hochberg D, Johnson CW, Chen J, Cohen D, Stern J, Vaughan EDJ, Poppas D, Felsen D: Interstitial fibrosis of unilateral ureteral obstruction is exacerbated in kidneys of mice lacking the gene for inducible nitric oxide synthase. Lab Invest 2000, 80:1721–1728
49. Miyajima A, Chen J, Poppas DP, Vaughan EDJ, Felsen D: Role of nitric oxide in renal tubular apoptosis of unilateral ureteral obstruction. Kidney Int 2001, 59:1290–1303
50. Mills CD, Kincaid K, Alt JM, Heilman MJ, Hill AM: M-1/M-2 macrophages and the Th1/Th2 paradigm. J Immunol 2000, 164: 6166–6173
51. Kiley SC, Thornhill BA, Belyea BC, Neale K, Forbes MS, Luetteke NC, Lee DC, Chevalier RL: Epidermal growth factor potentiates renal cell death in hydronephrotic neonatal mice, but cell survival in rats. Kidney Int 2005, 68:504–514
52. Cachat F, Lange-Sperandio B, Chang AY, Kiley SC, Thornhill BA, Forbes MS, Chevalier RL: Ureteral obstruction in neonatal mice elicits segment-specific tubular cell responses leading to nephron loss. Kidney Int 2003, 63:564–575
53. Fine LG, Orphanides C, Norman JT: Progressive renal disease: the chronic hypoxia hypothesis. Kidney Int Suppl 1998, 65:S74–S78